

Aus dem Institut für Immunologie

Geschäftsführender Direktor Prof. Dr. Stefan Bauer

des Fachbereichs Medizin der Philipps-Universität Marburg

**The effect of pattern recognition receptor RIG-I variant expression
during mammalian- or avian-adapted influenza A infection and
adaptation in the mouse.**

Inaugural-Dissertation

zur Erlangung des Doktorgrades der Naturwissenschaften

dem Fachbereich Medizin der Philipps-Universität Marburg vorgelegt von

Benjamin Rupf, geboren Kandziora

aus Karl-Marx-Stadt, heute Chemnitz

Marburg, 2023

Originaldokument gespeichert auf dem Publikationsserver der Philipps-Universität Marburg
<http://archiv.ub.uni-marburg.de>

Dieses Werk ist durch eine Lizenz des Typs CC BY-NC-SA 4.0 Deutschland geschützt.



Angenommen vom Fachbereich Medizin der Philipps-Universität Marburg am 06.09.2023

Gedruckt mit Genehmigung des Fachbereichs Medizin.

Dekanin Frau Prof. Dr. Denise Hilfiker-Kleiner

Referent Herr Prof. Dr. Stefan Bauer

1. Korreferentin Frau Prof. Dr. Eva Friebertshäuser

Der größte Feind des Wissens ist nicht Unwissenheit, sondern die Illusion, wissend zu sein.

-Stephen Hawking

Index

Index	I
Abbreviations	VI
List of Figures	XI
List of Tables.....	XIV
1. Introduction	1
1.1. The influenza A viruses	1
1.1.1. History	1
1.1.2. Clinical aspects of IAV	1
1.1.3. General aspects of IAV.....	2
1.1.4. IAV infection, replication cycle and antiviral defense	6
1.2. Antiviral immunity	10
1.2.1. General interaction between immune cells.....	10
1.2.2. Antiviral activities of pattern recognition receptors	11
1.2.3. The cytoplasmic pattern recognition receptor RIG-I.....	13
1.2.4. IFN signaling and stimulated genes	18
1.2.5. The OAS-RNaseL system as IFN downstream target	20
1.2.6. IAV evasion and adaptation strategies for RIG-I	23
1.3. Mouse models for the understanding of human pathologies	28
1.4. Aims of this study	28
2. Material.....	30
2.1. Consumables	30
2.2. Laboratory hardware	31
2.3. Stimuli.....	33
2.4. Buffers	34
2.5. Media, agar and components.....	38
2.6. Cell lines and bacteria.....	40
2.7. Mouse lines	40

2.8.	Virus strains	41
2.9.	Reagents	41
2.10.	Kits.....	42
2.11.	Plasmids.....	43
2.12.	Antibodies	43
2.13.	Software	46
3.	Methods	47
3.1.	Generation of mouse lines with RIG-I variants	47
3.2.	RIG-I mouse genotyping	48
3.3.	Sanger-sequencing	49
3.4.	The amplification of IAV/PR/8 Δ NS1 virus in chicken eggs	51
3.5.	Extraction of primary mouse cells	51
3.6.	In vitro generation and treatment of bone marrow derived macrophages.....	52
3.7.	ELISA.....	53
3.8.	BCA	54
3.9.	Western blotting	55
3.10.	WB signal semi-quantification	56
3.11.	Murine embryonal fibroblasts	56
3.12.	Generation of recombinant IAV.....	57
3.12.1.	A plasmid system for the generation of recombinant virus.....	57
3.12.2.	Virus assembly.....	62
3.12.3.	Virus multiplication.....	62
3.13.	The validation of the recombinant IAV PB2 stock quality.....	63
3.13.1.	The validation of the IAV PB2-627 codon with Sanger-sequencing	63
3.13.2.	Virus titration with a single cell infection assay	66
3.13.3.	Virus titration with a hem-agglutination test	67
3.13.4.	Virus titration with a plaque assay	68
3.13.5.	IAV M protein semi-quantification with Western blotting	68

3.13.6.	Competitive infection assay in MEF	69
3.14.	The mouse study plan.....	70
3.15.	The mouse infection procedure.....	71
3.16.	The analysis of RIG-I variant effects on main infection parameters	73
3.16.1.	Analysis of weight loss and body temperature upon IAV infection	73
3.16.2.	Virus titer quantification in the BALF	73
3.16.3.	Virus detection in the lung tissue with immune histochemistry.....	73
3.16.4.	Histological staining with H&E and PAS	75
3.16.5.	The FITC-albumin lavage to serum ratio as indicator for altered lung barrier integrity	76
3.17.	The analysis of RIG-I variant effects on innate immune signaling.....	77
3.17.1.	The determination of IFN levels in the BALF with ELISA	77
3.17.2.	The analysis of inflammatory cytokine concentrations in the BALF with a multiplex cytokine assay	78
3.18.	The IAV PB2 nt 1879 genotyping in the BALF	78
3.19.	Statistical analysis.....	79
3.19.1.	Histogram	79
3.19.2.	Box plot.....	79
3.19.3.	Stacked bar plot.....	79
3.19.4.	Superimposed symbol plot	79
3.19.5.	Outlier analysis	80
3.19.6.	Normal distribution	80
3.19.7.	T-test	80
3.19.8.	2-Way ANOVA.....	80
4.	Results	82
4.1.	The establishment of a RIG-I WT, PM and KO mouse line	82
4.1.1.	Homozygous RIG-I PM and KO mice do not develop a burdening phenotype	83
4.2.	Mouse line RIG-I functionality tests.....	83
4.2.1.	mRIG-I protein expression is detectable with Western blotting in primary cells from RIG-I WT and PM mice, but not RIG-I KO mice	83

4.2.2.	RIG-I-mediated signaling in RIG-I PM and KO mouse derived BmdMΦ is abolished, while the signaling via other PRRs is not altered	86
4.2.3.	Summary: Innate immune signaling in the established RIG-I variant mouse lines.....	99
4.2.4.	Validation of murine embryonal fibroblast cell lines	100
4.3.	Generation and characterization of recombinant IAV/PR/8 PB2-627K and IAV/PR/8 PB2-627E strains.....	101
4.3.1.	The generation of a plasmid encoding for the PB2-627E variant with primer-mediated mutagenesis	101
4.3.2.	A recombinant IAV/PR/8 PB2-627E strain does not replicate in mammalian cell lines without adaptive mutations, in comparison to an IAV PB2-627K variant.....	102
4.3.3.	Characterization of recombinant virus strains generated in DF-1 cells.....	104
4.3.4.	Competitive infection of RIG-I WT, PM and KO MEF cells with both IAV PB2-627K and -627E strains suggests slight, but not significant effects of differential RIG-I expression on virus replication	108
4.3.5.	The recombinant IAV PB2-627K and IAV PB2-627E virus strains seem to be genetically stable in regard to the PB2 RNA gene	111
4.3.6.	Summary: Generation and characterization of recombinant IAV strains	113
4.4.	Mouse infection study.....	113
4.4.1.	Comparison of primary influenza infection parameters in dependence of the RIG-I genotype.....	113
4.4.2.	Summary: Primary infection parameters do not markedly differ in dependence of RIG-I variant expression	133
4.4.3.	IAV PB2-627K, but not IAV PB2-627E infection causes an induction of IFN-β in RIG-I WT mice, which is reduced in RIG-I PM and KO mice	134
4.4.4.	Proinflammatory and antiinflammatory cytokine expression is enhanced in response to IAV PB2-627K and IAV PB2-627E infection and slightly altered by RIG-I variant expression ..	135
4.4.5.	The genetic stability of the IAV PB2-627E strain during mouse lung infection is dependent of RIG-I variant expression.....	148
5.	Discussion.....	151
5.1.	Current knowledge and aims of the project	151
5.2.	RIG-I WT, PM and KO mouse lines are not burdened and their immune cells functional corresponding to the genotype.....	151
5.3.	The insufficiency of IAV PB2-627E replication in mammalian cells without adaptive mutations highlights the importance of the IAV PB2-627K polymerase adaptation	153

5.4. Both the recombinant IAV PB2-627K and IAV PB2-627E strain from DF-1 chicken cells are genetically stable.....	154
5.5. Competitive infection of MEF cells with both the IAV PB2-627K and IAV PB2-627E strain suggests a slight effect of RIG-I variant expression on virus replication.....	155
5.6. The IAV PB2-627E genotype is not stable during mouse infection and its rate of back mutation is dependent on RIG-I variant expression.....	156
5.6.1. RIG-I mediates a selective pressure on the IAV PB2-627 codon	156
5.6.2. RIG-I blocks the access to the panhandle structures for the IAV PB2-627E polymerase.....	158
5.7. The investigation of cytokine expression upon IAV PB2-627K and IAV PB2-627E infection suggests a differential induction of chemokines and IFN- γ depending on RIG-I variant expression	160
5.7.1. The infections with the mammalian-adapted IAV PB2-627K strain	160
5.7.2. The infections with the avian-adapted IAV PB2-627E strain.....	161
5.7.3. IFN- γ may be alternatively induced by a RIG-I dependent positive feedback loop.....	163
5.8. RIG-I as pharmaceutical target	163
5.9. Conclusion	164
5.10. Outlook.....	165
6. Summary	167
7. Zusammenfassung.....	169
8. List of citations	171
9. Supplementary Figures.....	178
Lebenslauf.....	i
Persönliche Daten	i
Ausbildung.....	i
Verzeichnis der akademischen Lehrer.....	ii
Danksagung.....	iii

Abbreviations

5'ppp	5' triphosphate
A	adenine
aa	amino acid
AGE	agarose-gel-electrophoresis
AMP	adenosine monophosphate
AP-1	activator protein 1
APC	antigen presenting cell
approx.	approximately
ARDS	acute respiratory distress syndrome
AUC	area under the curve
BALF	bronchoalveolar lavage fluid
B-cell	B-lymphocyte
Bio-Rad	Bio-Rad Laboratories Inc.
BmdMΦ	bone marrow derived macrophages
BSA	bovine serum albumin
C	cytosine
CARD	caspase recruitment domain
c. c.	compare chapter
CD	cluster of differentiation
cDNA	complementary DNA
cGAS	cyclic GMP-AMP synthase
comp.	complete
CTD	C-terminal domain
d	day
DAMPs	damage-associated molecular pattern
DC	dendritic cell
DNA	desoxy-ribonucleic acid
ds	double-strand
E. Coli	Escherichia coli
e.g.	for example (<i>lat. exempli gratia</i>)
ELISA	enzyme-linked immunosorbent assay
EMCV	encephalomyocarditis virus
ER	endoplasmic reticulum
eRL	endogenous RIG-I ligand

EtOH	ethanol
f.	and the following chapter
ff.	and the following chapters
FCS	fetal calf serum
FFU	focal forming units
FITC	fluorescein-5-isothiocyanate
Fwd.	forward
G	guanine
GMP	guanosine monophosphate
h	hour
HA	IAV hem-agglutinin
HAU	hem agglutinating units
H&E	hematoxylin and eosin
hRIG-I	human RIG-I
HRP	horseradish peroxidase
IAV	influenza A virus
IBV	influenza B virus
IFITM3	IFN-induced transmembrane protein 3
IFN	interferon
IFN-1	type 1 interferon
IFNAR	IFN-1 receptor
IHC	immunohistochemistry
IL	interleukin
IL-1R	interleukin-1 receptor
IM	infection medium
IHC	immune histochemistry
IRF	interferon regulatory factor
ISG	interferon-stimulated gene
ITS2	internal transcribed spacer 2 region of 45S rRNA
IVC	individually ventilated cages
JAK	Janus kinase
kDa	kilo Dalton
KO	knockout
LGP2	Laboratory of Genetics and Physiology 2
LPS	lipopolysaccharide

MAVS	mitochondrial antiviral signaling protein
MDA5	melanoma differentiation-associated gene 5
MDCK	Madin-darby canine kidney
MEF	murine embryonal fibroblasts
MHC	major histocompatibility complex
MHC-1	MHC class 1
MHC-2	MHC class 2
mIFN- α	murine IFN- α
mIL-6	murine Interleukin 6
min	minutes
mM-CSF	murine Macrophage-colony stimulating factor
mock	only treated with the respective negative control procedure
M protein	IAV matrix-protein
mRNA	messenger RNA
MX1	MX dynamin like GTPase-1
NA	IAV neuraminidase
NEMO	NF- κ B essential modulator
NFAT	nuclear factor of activated T-cells
NF- κ B	nuclear factor- κ B
NK cells	natural killer cells
NLS	nuclear localisation signal
NLRP3	NOD-like receptor family, pyrin domain containing-3
NP	IAV nucleoprotein
ns	negative-strand
NS1 and 2	IAV nonstructural proteins 1 and 2
nt	nucleotide
OA	2'-5'-oligoadenylate
OAS	2'-5'-oligoadenylate-synthetase
o. n.	over night
OPD	o-phenylenediamine dihydrochloride
PA	IAV polymerase subunit A
PAMPs	pathogen-associated molecular pattern
PAS	periodic acid-Schiff
PB1	IAV polymerase subunit B1
PB2	IAV polymerase subunit B2

PBS	phosphate buffered saline
PCR	polymerase chain reaction
PDE12	2'phosphodiesterase 12
PFA	paraformaldehyde
PFU	plaque forming units
p.i.	post infection
pl:C	polyinosinic:polycytidylic acid
PKR	protein kinase R
PM	K271A point mutation
PRR	pattern recognition receptor
ps	positive-strand
P/S	Penicillin/Streptomycin
Q	Glutamine
3R	reduction, refinement, replacement
RCF	relative centrifugal force
Rev.	reverse
RNA	ribonucleic acid
rRNA	ribosomal RNA
ROUT	robust regression and outlier removal
RT	room temperature
SA	sialic acid
SCIA	single cell infection assay
SDS-PAGE	sodium-dodecyl-sulfate-polyacrylamide gel electrophoresis
siRNA	small interfering ribonucleic acid
SOCS	suppressor of cytokine signaling
SPF	specific pathogen free
SRP	signal-recognition-particles
ss	single strand
STAT	signal transducers and activators of transcription
STING	stimulator of interferon genes
T	thymine
T-cell	T-lymphocyte
Thermo	Thermo scientific
TIR	Toll interleukin-1 receptor
TLR	toll-like receptor

TMD	transmembrane domain
TNF	tumor necrosis factor
TRAF-6	TNF-receptor associated factor-6
TRIM25	E3-ligase tripartite-motif containing 25
tRNA	transfer RNA
TYK2	tyrosine kinase 2
up water	ultrapurified water
vRNP	viral ribonucleoprotein
WB	Western blotting
WHO	World Health Organization
WT	wild type

List of Figures

Figure 1: Schematic depiction of an IAV vRNP.	3
Figure 2: Schematic depiction of an IAV particle.	4
Figure 3: Domain structure of the PRR RIG-I.	15
Figure 4: Overview of the expected RIG-I–IAV strain interactions.	29
Figure 5: Overview of the IAV PB2-627 codon.....	60
Figure 6: A Schematic depiction of the primer-mediated mutagenesis strategy.....	61
Figure 7: Overview about the endpoint schedule.	71
Figure 8: Examples for a representative RIG-I WT, PM and KO genotyping.	82
Figure 9: RIG-I protein is detectable in primary cells from RIG-I WT and PM mice, but not in primary cells from RIG-I KO mice.....	84
Figure 10: RIG-I protein expression in cells from RIG-I KO mice, but not in cells from RIG-I PM mice, is significantly altered in comparison to expression in cells from RIG-I WT mice.	85
Figure 11: The effect of specific RIG-I ligands to enhance mIFN- α production is abolished in BmdM Φ from RIG-I PM and KO mice, in contrast to RIG-I WT cells.....	87
Figure 12: A recombinant IAV strain with functional NS1 protein does not induce mIFN- α production in BmdM Φ	89
Figure 13: The majority of mIFN- α induction upon infection with a recombinant IAV strain lacking the NS1 protein in BmdM Φ is dependent on RIG-I.	90
Figure 14: Sendai virus infection triggers the induction of mIFN- α and mIL-6 in BmdM Φ , which is dependent on RIG-I.	92
Figure 15: TLR9 activation by CpG 2216 in BmdM Φ significantly enhances mIFN- α and mIL-6 levels and is not effected by expression of RIG-I variants.	94
Figure 16: TLR4 activation by LPS or TLR1/2 activation by Pam3Cys enhances mIL-6 production in BmdM Φ , which is not effected by a lack of RIG-I functionality.....	96
Figure 17: Alternative RIG-I variant expression does not affect mIFN- α induction by DNA-activated cGAS/STING signaling in BmdM Φ	98
Figure 18: MEF cells derived from the established RIG-I mouse lines express the correct RIG-I variants.	101
Figure 19: The Sanger-sequencing of the IAV PB2 plasmid coding for the 627E version.....	102
Figure 20: The recombinant IAV PB2-627E strain does not propagate in mammalian cell lines without adaptive mutations.	103
Figure 21: The infectious titer of both recombinant IAV PB2-627K and -627E virus strains generated in DF-1 chicken cells is similar.	105

Figure 22: The IAV PB2-627E virus strain carries more M-protein than the IAV PB2-627K virus strain.	107
Figure 23: IAV PB2-627K has a replication advantage compared to IAV PB2-627E in RIG-I WT and PM MEFs, which is slightly lower in RIG-I KO MEFs.	110
Figure 24: The validation of the genetic stability of the IAV PB2-627 codon in the mammalian- and the avian-adapted strain by Sanger-sequencing.....	112
Figure 25: The infection of RIG-I WT, PM and KO mice with a recombinant IAV PB2-627K or -627E strain causes a significant weight loss, slightly dependent on the RIG-I genotype in the IAV PB2-627E infections.....	117
Figure 26: The BALF infectious virus titer shows high variation between mouse individuals upon infection with recombinant IAV strains.	119
Figure 27: The detection of IAV NP protein at different time points p.i. in lung tissue from female mice infected with IAV PB2-627K or -627E visualizes the course of the infection.....	122
Figure 28: The semi-quantification of viral load in the lung tissue of IAV PB2-627K- and -627E-infected RIG-I WT, PM and KO mice suggests a questionable effect of RIG-I signaling deficiency on the IAV PB2-627E virus titer.....	124
Figure 29: Mononuclear immune cell infiltration of RIG-I WT, PM and KO mouse lungs infected with IAV PB2-627K or -627E results in formation of cellular exudates.....	127
Figure 30: RIG-I WT, PM and KO mice infected with IAV PB2-627K or -627E suffer from an acute lung infection without mucus production and basal membrane damage.....	130
Figure 31: IAV PB2-627K and -627E infections mediate lung damage formation, independent of RIG-I variant expression.	133
Figure 32: IAV PB2-627K mouse infection causes a significant induction of IFN- β , which is slightly dependent on RIG-I variant expression.	135
Figure 33: RIG-I variant expression affects the induction of chemokines in an IAV PB2-627K infection and the expression of IFN- γ in an IAV PB2-627E infection.	148
Figure 34: RIG-I variant expression influences the PB2 nucleotide 1879 G back mutation to A in mice infected with an IAV PB2-627E strain.	150

Supplementary Figure 1: A RIG-I PM and RIG-I KO mouse line, generated with CRISPR/Cas9 and homozygous for the respective RIG-I variant, do not develop a burdening phenotype.	179
Supplementary Figure 2: The infection of RIG-I WT, PM and KO mice with a recombinant IAV PB2-627K or -627E strain causes a significant drop of the body temperature.	181
Supplementary Figure 3: The detection of IAV NP protein at different time points p.i. in lung tissue from mice infected with IAV PB2-627K or -627E visualizes the course of the infection.	183
Supplementary Figure 4: Mononuclear immune cell infiltration of RIG-I WT, PM and KO mouse lungs infected with IAV PB2-627K or -627E results in formation of cellular exudates.	185
Supplementary Figure 5: RIG-I WT, PM and KO mice infected with IAV PB2-627K or -627E suffer from an acute lung infection without mucus production and basal membrane damage.	187
Supplementary Figure 6: IAV PB2-627E, but not -627K infection-induced cytokine expression varies between the RIG-I mouse lines.	194

List of Tables

Table 1: IAV proteins and their functions.	25
Table 2: Consumables.	30
Table 3: Laboratory hardware.	31
Table 4: Cell culture stimuli.	33
Table 5: Buffers.	34
Table 6: Media, agar and components.	38
Table 7: Cell lines and bacteria.	40
Table 8: Mouse lines.	40
Table 9: Virus strains.	41
Table 10: Reagents.	41
Table 11: Kits.	42
Table 12: Plasmids.	43
Table 13: Antibodies.	43
Table 14: Software.	46
Table 15: The primer used in the RIG-I genotyping procedure.	48
Table 16: DreamTaq Green PCR composition.	49
Table 17: Cyclor program for RIG-I genotyping PCR.	49
Table 18: The master mix used for Sanger-sequencing.	50
Table 19: The RIG-I genotype variants of the three mouse lines.	50
Table 20: Summary of the treatment conditions for the BmdMΦ.	53
Table 21: The primer required for primer-mediated mutagenesis of the pHW2000-PB2 plasmid.	59
Table 22: The master mix used for the PCR reactions.	59
Table 23: The cyclor program used for the PCR reactions.	60
Table 24: The master mix for the restriction reactions.	61
Table 25: The ligation reaction.	62
Table 26: Primer used for the IAV PB2 sequencing process.	64
Table 27: The master mix used for the cDNA synthesis.	64

Table 28: The cycler program used for the cDNA synthesis.	64
Table 29: The master mix used for the PCR.....	65
Table 30: The cycler program used for the PCR reactions.	65
Table 31: The primer used for the complete PB2 Sanger-sequencing.....	66
Table 32: The different infection and control groups of the mouse study.	71
Table 33: The QuPath algorithm settings for the determination of IAV positive lung cells.....	75
Table 34: The settings for fluorescence measurement with the Tecan i control device.	77
Table 35: A summary of the results derived from the ELISA analyses.....	100
Table 36: A recombinant IAV/PR/8 PB2-627E strain does not replicate in mammalian cell lines without adaptive mutations, in contrast to an IAV PB2-627K variant.	104
Table 37: Results of the hem-agglutination test.....	105
Table 38: Semi-quantification of IAV M-protein indicates an approximately 3.5-fold higher amount of viral particles in the IAV PB2-627E stocks compared to the IAV PB2-627K stocks.....	107
Table 39: A summary of the results derived from the multiplex cytokine assay.	137
Table 40: Variations between avian- and mammalian-adapted IAV PB2 RNA genes.	158

1. Introduction

1.1. *The influenza A viruses*

1.1.1. *History*

Influenza A viruses (IAV) cause an infectious disease known as the flu, which is common all over the world today. The flu is responsible for several great epidemic and pandemic outbreaks worldwide, with the first pandemic documented as the Russian flu in 1889. In modern history, IAV pandemics occurred repeatedly after approximately (approx.) 30 years until today. The most severe outbreaks resulted in the pandemics of 1918 (Spanish flu), 1957 (Asian flu), 1968 (Hong Kong flu), 1977 (19th century Russian flu) and 2009 (swine flu). Among those, the Spanish flu, affecting approx. one third of the human population, was the most severe IAV pandemic ever known. It caused a huge death toll of at least 50 million people in one year, due to lack of therapeutics and supported by ongoing circumstances of the first world war, with massive troop movements and bad life conditions driving virus spread and susceptibility of the people. At least for the soldiers, it is known that in lethal cases most often secondary bacterial infections were present. There are also reports about different other outbreaks, which did not result in whole pandemics, but major epidemics (e.g. 1947 pseudo-pandemic; 1976 swine flu) (Kilbourne E. D. 2006; Peteranderl C. 2016).

1.1.2. *Clinical aspects of IAV*

1.1.2.1. *Flu as disease*

The flu comes with a two to eight day (d) short, but often severe acute phase including headache, cough, extremity pain, chills, fever, myalgia, malaise and in some cases also gastrointestinal illness with diarrhea and vomiting. In general, healthy individuals can handle IAV infections and need no therapy, while it might become life-threatening for individuals of the so called risk group, containing people with immune suppression, severe comorbidities, severe respiratory diseases, pregnant women, women with baby and in general individuals younger than two years and older than 65 years. Especially people linked to the risk group may develop severe pneumonia, acute respiratory distress syndrome (ARDS) and acute respiratory failure. Also remarkable, the flu often weakens the respiratory tract of infected individuals, enabling other viruses or bacteria to cause secondary infections, which can be a threat for the life of the infected individual. Most common secondary infections are based on *Streptococcus pneumoniae* and *Staphylococcus aureus* (Peteranderl C. 2016).

1.1.2.2. Flu prevention and therapy

Today, only a few reliable therapeutics are known, which are only efficient in early stages of the disease. Hence, the early recognition and a fast initiation is the primary goal in influenza therapy, because enduring lung infections can do severe and irreparable tissue damage. Standard therapeutics are the Neuraminidase (NA) inhibitors Oseltamivir, Zanamivir and Peramivir, while M2 proton channel inhibitors are not recommended anymore due to high prevalence of resistant flu strains. Among the NA inhibitors, Oseltamivir/Tamiflu is not recommended in some countries because of high occurrence of side effects. Direct antiviral therapeutics may be combined with artificial respiration in cases of severe respiratory dysfunction. New therapeutics in clinical studies of different stages target sialic acid (SA) residues on the cell surface or the viral proteins M2, HA and PB1 and are based on antibodies, small interfering ribonucleic acid (siRNA) or small molecular inhibitors, among others. Improving host immunity and controlling overshooting inflammation are in special focus, as well as the support of lung regeneration after severe infections, e.g. with stem cell based approaches (Peteranderl C. 2016).

A big approach in modern medicine is the annually updated flu vaccination, depending on presently circulating virus strains, which are monitored by the World Health Organization (WHO). Currently approved vaccines are based on antigenic subunits from inactivated virus grown in chicken eggs or cell culture (for intramuscular injection) or living, attenuated virus (intranasal application for children, adapted to 25 °C to limit spread in host). Actual trivalent or quadrivalent injection vaccines contain antigens of IAV H1N1, H3N2 and Influenza B virus (IBV) Yamagata and/or Victoria strains (Peteranderl C. 2016).

1.1.3. General aspects of IAV

1.1.3.1. Influenza virus nomenclature

IVs are divided into the classes A, B, C and D depending on their viral ribonucleoprotein (vRNP) antigens. Additionally, the strains are identified by place of first isolation, strain number, year of isolation and HA and NA surface antigen subtype. All known influenza strains are classified in the influenza nomenclature today:

[Virus type/vRNP]/[location of virus isolation]/[number of strain]/[year of isolation]([subtypes])
(Chanock R. H. 1972),

Example: A/Puerto Rico/8/1934(H1N1).

1.1.3.2. Molecular biology of IAV

The IAVs belong to the family of *orthomyxoviridae*. The RNA genome consists of eight single-stranded (ss) RNA genes with negative orientation, coding for ten viral proteins and other accessory proteins depending on the strain (Dou D. 2018). In the virus particles, those RNAs form vRNPs, mainly with the viral Nucleoprotein (NP). The 5' and 3' ends of all eight IAV RNAs are conserved and show partial complementarity, resulting in the formation of a double strand (ds) like RNA structure known as the IAV panhandle. This structure is recognized by the viral polymerase (pol.), which is a heterotrimer formed by the viral proteins PB1, PB2 and PA. A schematic depiction of the vRNP is shown in Figure 1 (Weber M. 2015; Dou D. 2018). The vRNP-complexes are surrounded by the viral envelope, formed from membrane remains of the previous host cell. At its inner side, M1 proteins are supporting the envelope, while M2 proton channels as well as the glycoproteins neuraminidase (NA) and hemagglutinin (HA) cover its outer side and are important for virus-target cell adhesion and entry in the host cells. HA and NA are also important antigens. The schematic of an IAV particle is shown in Figure 2 (Weber M. 2015).

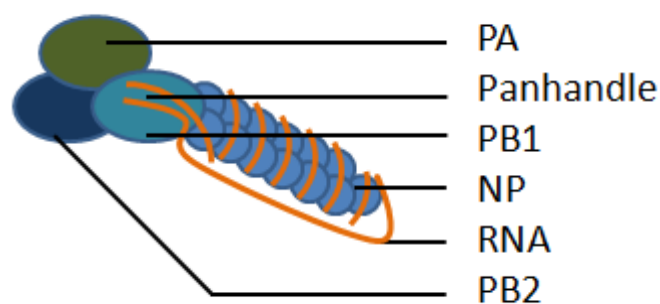


Figure 1: Schematic depiction of an IAV vRNP.

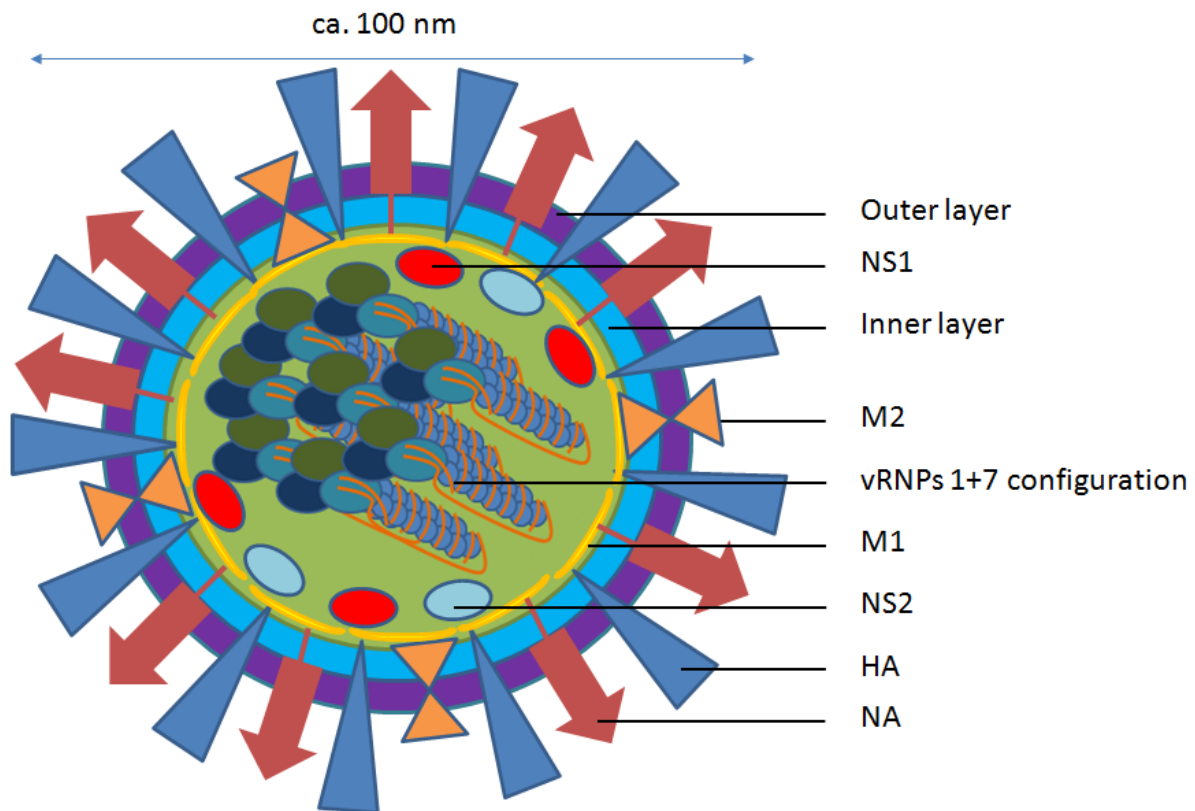


Figure 2: Schematic depiction of an IAV particle.

1.1.3.3. *Natural influenza reservoirs*

While the influenza B virus (IBV) strains Victoria and Yamagata only circulate in humans, just a few IAV strains do so (H1N1 and H3N2), while additional large reservoirs in wild and domesticated animals like birds, waterfowl and swine exist (e.g. H5N1 and H7N9 avian types) (Barber M. R. W. 2010; Peteranderl C. 2016; Dou D. 2018). Those strains usually cause asymptomatic infections in their natural hosts, but by new mutations, they might also cause their death (Barber M. R. W. 2010). Due to this natural IAV reservoir, there is ongoing risk that virus jumps over to domesticated and less resistant animals. For example, IAV strains from wild birds are often lethal for domesticated chickens, because they lack the important antiviral protein RIG-I as baseline defense initiator (Barber M. R. W. 2010). There is also a risk that strains from the natural reservoir acquire new mutations and jump over to humans, resulting in a zoonotic infection. In rare cases, this may lead to an epidemic or even a pandemic. Of special note are swine here, because they carry IAV receptors compatible to human and avian-adapted strains in their respiratory tract. This makes them ideal hosts for reassortment of human, swine and avian IAV strains, which happened in the 2009 swine flu pandemic (Peteranderl C. 2016).

1.1.3.4. Virus adaptation and the zoonotic sword of Damocles

The main reason for influenza being a threat to human health lies in its potential to acquire new mutations and hence host adaptations very fast, which enables it to challenge the mammalian immune systems. This potential originates from two molecular features of IAV. First, the IAV polymerases have a very high error rate (1:2000-10000 per bp), which leads to multiple slight changes in proteins and hence to formation of slightly different virus particles. This leads to a high number of mistakes in virus particles, but a few of those may have advantages in the host compared to the original virus particles, which is the key to sustainable virus circulation in populations. This is a reason why IAV is able to adapt to a host very fast (Weber-Gerlach M. 2016b). The polymerase may create a mistake during viral replication, which leads to the mutation of an antigenic protein. This may not cause a loss of its functionality, but may enable the virus to bypass a host immunity, which was established during previous infections (antigenic drift) (Dou D. 2018). Secondly, if an individual is infected with two different virus strains, single cells may get infected with virus particles from both strains. Due to the segmented RNA genome of IAV, a genetic recombination between two or even more virus strains is possible, resulting in new strains with the strongest features of both original strains combined (antigenic shift, reassortment). Those recombined strains have a huge potential in bypassing established immune defenses of a host population, may also have enhanced infection potential and are responsible for the more severe epidemics and pandemics of influenza studied in the last decades (Weber M. 2014; Peteranderl C. 2016; Dou D. 2018).

Today, the bird virus strains H5N1 and H7N9 are linked to the highest risk to cause a severe flu course during a zoonotic infection, if they get an adaptive mutation. In such a case, the resulting flu can easily become dangerous, with reported mortalities of approx. 50 % for H5N1 and 40 % for H7N9. By this reason, it is very important that those cases are recognized and quarantined, to stop the spread of new strains as fast as possible, limiting the chance for a new pandemic. Enhanced risk appears where humans and domestic animals live in close proximity with limited care for disease transmissions, like on the big animal markets in Asia (among others). It stays important that we learn from history and see with open eyes in current pandemics like COVID19 and, most important, spread this knowledge in society. Infectious virus diseases have to be taken serious and prevention strategies as well as alert plans have to be examined and executed to reduce the risk of new pandemics as much as possible. Especially today, with still rising human population and international fluctuation, big pandemics are more dangerous than in the past, even with the huge approaches in modern medicine. Worldwide, IAV infects approx. 1 billion people per year, of which approx. 290-650 thousand people die (Frank K. 2020). The economic burden by IAV caused disease in the USA, resulting in prevented working days, delayed production and capital needed for therapies, is

estimated 26 billion US-dollars per annum, an incredibly high number which would be worth in many regards to put time and resources in to reduce it, all over the world. By those reasons, it stays important to deepen the knowledge about disease and host responses on clinical, molecular biological and pharmaceutical level to find more versatile, reliable and diverse therapeutics and treatment strategies to prevent and treat flu waves (Peteranderl C. 2016).

1.1.4. IAV infection, replication cycle and antiviral defense

1.1.4.1. Entry in body and first line defense mechanisms

IAV is mainly transmitted by droplet infection between individuals of the same or different species. Droplets containing virus particles enter the organism mainly through open mouth and through nostrils. After entering the nose and the throat, they face the first row of the host innate immune system. The surface of the respiratory tract is covered with a surface epithelium producing mucus, which contains mucins with glycans and SA residues, to which IAV particles bind, leading to their (temporary) neutralization (Dou D. 2018). Additionally, the mucus contains antibodies of the immune globulin (Ig) A type, which can mediate neutralization of pathogens directly by agglutination and indirectly by opsonization or complement activation. The epithelial cells further form a barrier with tight junctions, not letting pass most substances and particles uncontrolled. Nevertheless, some virus particles may manage to enter cells of the mucosa of nasal cavity, throat or even trachea, dependent on the integrity of the innate immune barrier and the amount of incoming virus particles.

1.1.4.2. Entry

If virus particles are not neutralized by the first line defense and reach a cell surface, the HA proteins can bind to terminal SA residues of glycoproteins (attachment). Since there are many different SA containing glycoproteins and not all are sufficient entry receptors for IAV, the particles have to "search" for a sufficient receptor. The viral NA cleaves the terminal SA residues of the surface glycoproteins and, by this, enables the virus to bind to other SA-glycoproteins of the cell. The "right" SA-glycoprotein is currently expected to differ between IAV strains and it is possible that there is more than one that is sufficient. If an IAV particle binds to its sufficient SA-glycoprotein, the process of endocytosis is triggered by clathrin-dependent pathways or macropinocytosis, mediating uptake of the virus particle inside an endosome (entry) (Dou D. 2018).

1.1.4.3. Uncoating

After uptake, the endosomal pH-value is decreased by the influx of protons from the cytosol. This physiological process triggers the conformational switch of the viral HA protein, which brings both virus surface and endosome wall in close proximity. Now it is important that at some point HA was cleaved by a Serine-protease like TMPRSS2 or Trypsin. If HA was cleft, its membrane fusion domain is exposed now, mediating membrane fusion. Additionally, the acidic pH-value activates the M2 proton channel, leading to decrease in pH-value of the inside of the virus, which causes a conformational change of the M1 protein. This causes the release of the vRNPs, which can now enter the cytoplasm of the attacked cell (uncoating) (Dou D. 2018).

1.1.4.4. vRNP nuclear translocation

In the cytoplasm, vRNP transport to the nucleus can differ dependent on host cell types, but the best-described mechanism uses the importin- α/β import pathway. The viral RNAs are associated with viral NP proteins and the polymerase subunits, which expose nuclear localization signals (NLS). Those attract binding of importin- α and hence recruitment of the transport receptor protein importin- β , which mediates transport of the vRNP-importin-complex to the nuclear pores and nuclear translocation. While it takes approx. 1 hour (h) from virus particle adhesion until arrival of vRNPs in the nucleus, uncoating takes approx. 10 minutes (min) and the transport to nucleus the remaining time. Since high efficiency in importin system activation is crucial for successful IAV infections, NP adaptations to host importin machinery are very important (Dou D. 2018).

1.1.4.5. Replication and mRNA transcription

In the nucleus, IAV negative strand (ns) RNAs have to be transcribed into positive-strand (ps) RNAs. This works with an unprimed transcription, in which the first two nucleotides have to bind randomly to the 3' ends of viral RNAs, to start elongation. The complete ps RNA is then released and complexes with viral NPs and one copy of viral polymerase, resulting in the formation of a complementary vRNP. The priming mechanism of ps RNA transcription back to ns RNA is not completely solved yet, but it is expected to happen similar to ns RNA transcription into ps RNA, with an unprimed transcription (replication) (Dou D. 2018).

The mRNA-transcription from ns RNA and ps RNA is different as well as more efficient than replication and it starts earlier (Weber M. 2015; Dou D. 2018). It is a primed mechanism, which uses host cell mRNA 5' caps. The PB2 subunit of the IAV polymerase binds 5' ends of cellular mRNAs,

which are complementary to the ends of IAV RNAs. The PA subunit endonuclease activity then cleaves the host-mRNA ends 10-13 nt downstream. After a rotation of the PB2 subunit, those 10-13-mers bind to the ends of the IAV RNAs and serve as primer for mRNA transcription, in the PB1 subunit. At the end, the polymerase adds a poly-adenin (poly-A) tail to the mRNA by a process called "reiterative stuttering", resulting in capped and poly-adenylated RNAs. In higher eukaryotes, the mRNAs are 5'-capped and have a poly-A tail, which enhances their stability and prevents them from recognition and degradation by cellular defense mechanisms. Hence, the viral RNAs with the stolen modifications also become completely masked for antiviral defense mechanisms. Further, IAV mRNAs have splicing sites like host mRNAs, resulting in alternate expression of NS (NS1 and NS2) and M (M1 and M2) proteins (Dou D. 2018).

1.1.4.6. Synthesis and modification of viral proteins

Followed to synthesis in the nucleus, viral mRNAs are exported to the cytoplasm and translated either at cytoplasmic ribosomes (PB1, PB2, PA, NP, NS1, NS2, M1) or endoplasmic reticulum (ER) ribosomes (membrane proteins HA, NA, M2). The viral proteins NP, PA, PB1, PB2, NS1, NS2 and M1 all carry NLS and translocate into the nucleus, where they support viral replication and translation or support vRNP export to the cytoplasm, among other individual functions. In the cytoplasm, vRNPs with masked NLS bind to Rab11 mediated by PB2, leading to transport to the cellular membrane with the microtubule system. The future surface proteins HA, NA and M2, synthesized by the ER-ribosomes, carry hydrophobic targeting sequences, which are recognized by the signal recognition particles (SRP) of the ER and hence translocate into it. In the ER, the translocon mediates organization of HA, NA and M2 into membranes in dependence of their respective transmembrane domains (TMD). Further, HA and NA receive multiple N-linked glycans, whose amount and position can differ between IAV strains and subtypes. The glycans are important for the recruitment of the lectin-chaperones calnexin and calreticulin, mediating correct protein folding, as well as the oxidoreductase ERp57, which drives intramolecular and intermolecular disulfide-bonding. Intermolecular disulfide-bonds are important for M2- and NA-homotetramerization and HA-homotrimer and homooligomerization. The different oligomerizations require high protein synthesis rates in the ER to achieve local proximity of the monomers, which drives the risk of triggering the ER unfolded protein stress response (Dou D. 2018).

To achieve full functionality, HA needs to undergo a cleavage. Depending on IAV strain, it carries a monobasic (most mammalian-adapted strains) or multibasic (high pathogenic avian-adapted strains) cleavage sites. The cleavage has to occur at a time point between synthesis and start of uncoating and has no effect until HA conformation is changed by low pH-milieu. In avian, the serine-protease

furin in the trans-golgi, expressed ubiquitously, is cleaving multibasic HA sites. In mammals, airway-epithelial-cell serine-transmembrane-protease TMPRSS2, trypsin-like protease HAT of upper airway-epithelium, or eventually TMPRSS4, all targeting monobasic HA cleavage sites, do the job. This is suggested as a major reason why mammalian flu is restricted to the respiratory tract, while it can replicate in the gastrointestinal tract of birds additionally (Dou D. 2018).

1.1.4.7. Assembly

Since the envelopes of IAV carry enriched amounts of sphingolipids and cholesterol, compared to the average of cell membranes, it is suggested that new IAV particles bud from lipid raft areas of their host cells, which are linked to exocytosis (Salaün C. 2004). To deliver the newly synthesized IAV components to those membrane regions, the components need special labels. For example, HA gets lipid modifications at its C-terminal cysteine residues, while NA gets lipid modifications in its TMD. Those modifications are key signals for the cellular transport mechanisms and determine the target location. M1 and M2 proteins are expected to be complexed with cytoplasmic domains of HA and NA in the golgi membranes and reach budding locations via hitchhiking. The vRNPs are transported to the budding regions by Rab11 and bind to M1 (assembly) (Dou D. 2018; Noda K. 2018).

1.1.4.8. Budding

In the last step of the IAV replication cycle, the newly assembled virus components need to get packed into the virus envelope and exit the host cell. For this process, IAV uses different mechanisms known from the process of exocytosis. To achieve membrane curving or protrusions, cells can attach curved proteins to a membrane, form protein clusters in one side of a bilayer, use the cytoskeleton, as well as concentrate cone-shaped lipids like lysophosphatidylcholine or lysophosphatidic acid at the outer side or inverted cone-shaped lipids like phosphatidic acid, diacylglycerine, phosphatidylethanolamine and cholesterol at the inner side of the membrane. While the process of exiting the cell is not solved for IAV in detail, the current opinion is that IAV uses a mix of the mentioned mechanisms to achieve that aim. The oligomerized surface proteins HA and NA enrich in the outer membrane layer of lipid rafts, with the effect of membrane curving. At the inner layer, incoming M1 oligomerizes, leading to formation of curved structures, bending the membrane from the inner side. M2 also has membrane-shaping abilities. Additionally, the IAV proteins have affinity to membrane-shaping lipids, which suggests a recruitment potential. In the next steps, the vRNPs bind to M1. In detail, the different vRNP segments group in a characteristic 1+7 configuration (one vRNP in the middle is surrounded by the other seven, compare Figure 2), hypothetically through structure-based specific interaction. In contrast, the nonstructural (NS) proteins NS1 and NS2 are packed into

the forming structure in low amounts, suggesting that this may happen by chance and that it is sufficient that they are newly synthesized after infection of new cells. By those processes, membrane protrusion enhances while more proteins assemble to the complex until a last bottleneck remains, which is cut by M1, completely separating virus particle and host cell (budding) (Dou D. 2018).

1.1.4.9. Release

Finally, the IAV is in a similar position as in its adhesion stage, with HA-molecules eventually bound to surface SA-glycoproteins. The NA can cut those remaining connections to the host cell (or to SA-residues on NA and HA of other IAV particles) to dislodge the new virus particle, which sets it on track for the infection of other cells (release) (Dou D. 2018).

1.2. Antiviral immunity

1.2.1. General interaction between immune cells

1.2.1.1. Cellular virus responses in the lung

In the IAV infected lung, airway and lung epithelial cells are the primary target of IAV. As response, the epithelial cells detect viral antigens via pattern recognition receptors (PRR). In the following, innate antiviral responses via IFNs and cytokines are initiated, as well as antigen presentation via major histocompatibility complex class I (MHC-I) proteins. Apoptotic cells and virus particles are taken up by resident alveolar macrophages via phagocytosis and antigens are presented to cluster of differentiation (CD)4+ T-lymphocytes (T-cells) or CD8+ cytotoxic T-cells, which in turn activate B-lymphocytes (B-cells) or drive infected tissue cells into apoptosis. Natural killer cells (NK cells) support the eradication of infected cells via apoptosis, if those cells fail to present self-antigens, have IgG antibodies bound to their surface and/or if they secrete a lot of cytokines. Chemokine release by infected cells and resident macrophages attracts neutrophilic granulocytes, dendritic cells (DCs) and monocytes from blood vessels and surrounding tissue to the spot of infection. These cells enhance virus neutralization, eradication of infected cells and antigen presentation after differentiation and maturation, eventually at the cost of tissue damage during ongoing inflammation. DCs are the most versatile professional antigen presenting cells and are able to migrate to local lymph nodes upon antigen uptake, to stimulate large amounts of CD4+ and CD8+ T-cells. CD4+ T-cells can be activated by antigen presentation via MHC-II, which is mediated by DCs, macrophages or B-cells. The activated CD4+ T-cells in turn can activate B-cells, leading to B-plasma cell maturation and big-scale production of specific antibodies. High amounts of specific antibodies usually lead to clearance of the infection.

Additionally, activated T-cells and B-cells can become memory cells, which can circulate in the body for years and shorten the establishment of a humoral immune response in case of a re-infection with known antigens significantly. In case of a virus infection, key for an efficient immune response is a fast recognition of foreign antigens by innate PRRs and to bring all the important antiviral components in line fast. This enables to achieve a rapid clearance of the virus and the re-establishment of tissue barriers, before follow-up-infections occur. If this fails, enduring activation especially of innate immune cells can lead to irreparable lung damage, secondary bacteria infections and hence to the severe syndromes like ARDS and acute respiratory failure (Akira S. 2006; Peteranderl C. 2016; Eiz-Vesper B. 2020; Frank K. 2020).

1.2.2. *Antiviral activities of pattern recognition receptors*

1.2.2.1. *Detection of IAV by PRRs*

Main actors of the innate immune system are the PRRs, a diverse family of membrane bound or cytoplasmic receptors, which can detect a broad range of different ligands that are usually components of pathogens. IAV is detected by at least five PRRs: RIG-I, TLR3, TLR7, TLR8 and NLRP3. Depending on the cell type, expression of those can vary and they may play different roles in activation of downstream signaling pathways. In human macrophages and dendritic cells, for example, NLRP3 and TLR7 detect viral genomic RNA, while in human lung epithelial cells, mainly RIG-I, TLR3 and NLRP3 are involved. In both, the ligand recognition by PRRs activates innate immune signaling pathways containing the transcription factors nuclear factor- κ B (NF- κ B), interferon regulatory factors (IRF), activator protein 1 (AP-1), signal transducers and activators of transcription (STAT) or nuclear factor of activated T-cells (NFAT). These transcription factors control the expression of components of the innate immune system, like IFN-1, proinflammatory cytokines and also induce further signaling cascades like IL-12 and IL-18, which lead to the induction of IFN- γ and the activation of the components of the adaptive immune system (Pothlichet J. 2013; Almatrouk S. 2021).

1.2.2.2. *Toll-like receptors - overview*

Toll-like receptors (TLR) are membrane-bound PRRs. Today, 13 different TLRs are known in mammals, which all differ in expression, antigen specificity and downstream signaling, sometimes even between different mammals. Overall, the cell surface bound TLR1, 2, 4, 5, 6 and 10 are known, as well as the endosomal TLR3, 7, 8, 9, 11, 12 and 13. Humans possess the TLRs 1 to 10, while mice also have the TLRs 11, 12 and 13, while lacking TLR10. Additionally, some of the ligands recognized by the TLRs differ between humans and mice (Akira S. 2006; Malik G. 2020). TLRs are evolutionarily very

old structures highly conserved from nematodes to mammals, which even exist in insects. They are integral membrane glycoproteins with a cytoplasmic signaling domain and detect extracellular pathogens or those trapped in endosomes. They are broadly expressed on different immune cell types like antigen presenting dendritic cells and macrophages, as well as on different non-immune cells like epithelial cells and fibroblasts. TLRs represent a broad pattern recognition spectrum, which closes gaps well with the other PRRs to identify the very most of relevant extra-and intracellular pathogens (Akira S. 2006).

1.2.2.3. Toll-like receptor signaling

Binding of a ligand to a TLR leads to homo- or heterodimerization, followed by recruitment of TIR-domain adaptor proteins (MyD88, TIRAP, TRIF or TRAM) to the cytosolic domains of the receptor. The bound TLR ligand affects binding of the respective adaptor and can also lead to variation in downstream signaling. Like for the IL-1 receptor (IL-1R), the kinase IRAK4 is crucial for TLR signaling. Recruited IRAK4 phosphorylates IRAK1, which associates with TNF-receptor-associated factor 6 (TRAF-6). TRAF-6 associates with an ubiquitinylation complex, leading to self-ubiquitinylation and ubiquitinylation of NF- κ B essential modulator (NEMO). This process results in recruitment of the TAK1 complex and phosphorylation of IKK- β , Mitogen-activated protein kinase 8 and p38, which activate the transcription factor AP-1. pIKK- β is needed to inactivate I κ B, resulting in the activation of NF- κ B. TRAF-6 further activates the transcription factor IRF-5, which controls cytokine genes. Taken together, the transcription factors IRF-5, AP-1 and NF- κ B, controlling cytokine and chemokine genes, can be activated after TLR stimulation. TLR3, 4, 7 and 9 activation can result in TRAM/TRIF recruitment. In the following, TRIF can activate RIP1, leading to NF- κ B activation, and TBK1, which further supports NF- κ B activation and IRF-3 and IRF-7 phosphorylation, leading to IFN type 1 (IFN-1, mainly IFN- α and IFN- β) expression (Akira S. 2006).

1.2.2.4. NOD-LRR receptors and the NLRP3 inflammasome

The Nucleotide-binding oligomerization domain leucine-rich repeat (NOD-LRR) receptor family is a group of cytoplasmic PRRs, which detect a broad range of damage-associated molecular patterns (DAMPs) and pathogen-associated molecular patterns (PAMPs). Their signaling contains NF- κ B and the expression of cytokines (Akira S. 2006). The closely related PRR NOD-like receptor family, pyrin domain containing 3 (NLRP3) is special because this PRR alone has a very broad spectrum of ligands. Those include DAMPs like crystallized molecules, cyclic guanosine monophosphate- adenosine monophosphate (cGMP-AMP), neutrophilic extracellular traps, alum and nanoparticles as well as PAMPs of viral, bacterial and fungal origin like lipopolysaccharide (LPS), ds RNA and mannan. Upon

ligand binding, NLRP3 can form a mammalian inflammasome with ASC and Caspase 1, enabling Caspase 1 autocatalysis activation and hence the cleavage of pro-IL-1 β and pro-IL-18 to the mature and active variants IL-1 β and IL-18 (Dinarello C. A. 2018; Swanson K. V. 2019).

1.2.2.5. *cGAS-STING*

The cGMP-AMP synthase (cGAS) is another innate PRR detecting cytosolic desoxy-ribonucleic acid (DNA). Upon DNA binding, it gets activated and produces cGMP-AMP, the ligand of stimulator of IFN genes (STING). Activated STING mediates phosphorylation and activation of IRF-3 and IRF-7 and hence IFN signaling (Schneider W. M. 2014).

1.2.2.6. *RIG-like receptors*

The family of the cytoplasmic RIG-like receptors contains retinoic acid inducible gene I (RIG-I/DDX58/ISG56), melanoma differentiation-associated gene 5 (MDA5) and Laboratory of Genetics and Physiology 2 (LGP2) (Kolakofsky D. 2012). RIG-I and MDA5 play important roles in RNA detection. MDA5 is the main detector of polyinosinic:polycytidylic acid (pI:C) (next to RIG-I and TLR3) and also detects long ds RNA fragments, e.g. of picornaviruses, leading to activation of the mitochondrial antiviral signaling protein (MAVS). LGP2 seems to be a positive regulator of MDA5 and a negative regulator of RIG-I (Barber M. R. W. 2010; Weber-Gerlach M. 2016a).

1.2.3. *The cytoplasmic pattern recognition receptor RIG-I*

1.2.3.1. *RIG-I: general aspects*

An important antiviral protein of basal innate immunity is RIG-I, which consists of 925 amino acids (aa). It is expressed in the cytoplasm of most mammalian cell types on a low level and remains mostly in an inactive state of auto-inhibition. Its basal character is also reflected by its very primal origin: it is conserved among invertebrates like sponges and nematodes, as well as vertebrates (Kolakofsky D. 2012). Since it is not described in other organisms but *metazoa* and of those also in sponges, its evolutionary origin seems to be somewhere between 500 - 600 million years ago, before sponges separated from other *animalia* and in relative close proximity to the Cambrian explosion of species (Nettersheim B. J. 2019).

1.2.3.2. *Variation of RIG-I expression in birds*

The red jungle fowl (*Gallus gallus, galliformes*), from which modern domesticated chicken lines descend, is very special in its feature to have no genes encoding for a RIG-I analogue, while the closely related ducks (*Anas platyrhynchos, anseriformes*) express it (van Tuinen M. 2001; Barber M. R. W. 2010). There is also no RIG-I in the DF-1 chicken fibroblast cell line, which responds weakly to IAV due to this deficiency, but restoring RIG-I expression with a duck variant can replenish immune responses. The RIG-I analogue of *Anas platyrhynchos* differs from human RIG-I by 53 % and from zebra finch RIG-I by 78 %, but they all show the conserved functional domains known from the well-investigated human RIG-I. Nevertheless, not all amino acids (aa) crucial for different RIG-I mechanisms are conserved (Barber M. R. W. 2010). Chickens compensate their lack of RIG-I, at least partially, by MDA5 adaptations, enabling MDA5-STING-mediated recognition of viral RNAs during later stages of IAV infections, but this signaling is also inhibited by MAVS-targeting viral counter mechanisms, like in RIG-I signaling (Weber-Gerlach M. 2016b).

1.2.3.3. *RIG-I ligands*

Like the other RIG-like receptors, RIG-I is localized in the cytoplasm. Most affine ligands of RIG-I are ds or ds-like RNA structures with 5' triphosphates (5'ppp) (Weber M. 2014). A ds-like RNA structure is a ss RNA which has partial self-complementarity, leading to the formation of partial ds structures. An example are the IAV RNA genome panhandle structures (similar to stem-loop structures), formed by 5'/3' end self-complementarity of the eight IAV genome segments. Minimum requirement for a RIG-I ligand is a blunt-ended 10-20 nucleotide (nt) 5'ppp ds RNA, but also longer RNAs of about 200 base pairs (bp), even without blunt ends or 5'ppp, are recognized. Further, RIG-I is able to directly bind the viral RNAs even if they are present as vRNP, so it is able to bind them right after viral entry, before start of viral transcription and replication (Weber M. 2013; Weber M. 2015). In summary, natural RIG-I ligands are functional, viral genomes associated with vRNPs (especially A/U rich regions in 3' untranslated regions), defective viral genomes, virus replication products and RNase A or L cleavage products with a 2',3'-cyclic phosphate and a G-quadruplex containing sequence motif (Kolakofsky D. 2012; Weber M. 2014; Weber-Gerlach M. 2016b; Jung S. 2020). Such RNA structures exist in influenza, vesicular stomatitis, Ebola, Rift Valley fever, measles and hepatitis C viruses or are generated upon RNaseA and OAS/RNaseL system activation. Reports about ss RNAs to be RIG-I ligands remain controversial and may result from ds RNA side products of ss RNA synthesis (Kolakofsky D. 2012).

1.2.3.4. Specificity of RIG-I to detect foreign RNA

While RIG-I detects different kinds of foreign RNA and is localized in the cytoplasm, expressing cells need to mask their own RNAs like ribosomal RNA (rRNA) and messenger RNA (mRNA). It is expected that this is realized due to cellular RNA modifications, which some viruses can mimic. Host cell 7-methyl-guanosine caps do not alter RNA recognition by RIG-I, which is important for translation. In contrast, 2' O-methylation of the first and/or second base of an RNA significantly reduces its affinity to RIG-I, most likely due to interference with RIG-I 830H. This modification also reduces RIG-I ATPase activity. 2' O methylations are generated by 2' O-methyltransferases and some viruses like Ebola, yellow fever and Marburg evolved methods to modify their RNAs, by hijacking host methyltransferase or coding their own ones (Devarkar S. C. 2016). The masking can be overcome by cleavage of self-RNAs by RNases during pathologic conditions, resulting in production of potent RIG-I ligands (Jung S. 2020; Steinberg J. 2021).

1.2.3.5. RIG-I structure

The N-terminus of RIG-I carries two caspase recruitment domains (CARDs), which are important for the interaction with signaling partners upon activation. The center is a DExD/H-box RNA helicase domain (two functional helicase motifs in two subdomains and one nonfunctional helicase motif, Hel2i), which enables RIG-I to bind RNA. The first helicase subdomain also carries an ATPase domain, which plays a significant role in ligand-dependent conformational switch. The C-terminal domain (CTD) carries a zinc ion and is important for 5'ppp binding, like depicted in Figure 3 (Takahashi K. 2008; Kolakofsky D. 2012).

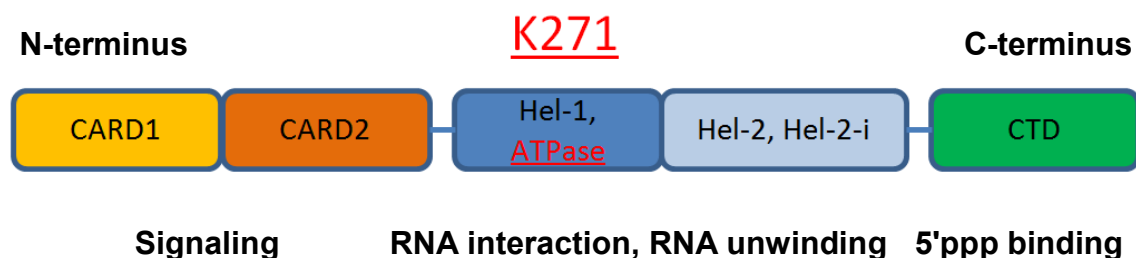


Figure 3: Domain structure of the PRR RIG-I.

1.2.3.6. *RIG-I mediated IFN induction upon RNA binding*

The best-investigated antiviral function of RIG-I is its ability to enhance IFN-1 production after binding of RNA ligands. In inactive state, the CARDS are interacting with the Hel2i motif and no signaling occurs. If a 5'ppp RNA is bound by the CTD, it leads the structure to the helicase domain, which surrounds the RNA structure (Kolakovsky D. 2012). In case of IAV, RIG-I interacts with the panhandle structure (Weber M. 2013; Weber-Gerlach M. 2016a). The RNA binding leads to a conformational switch, significantly enhanced by ATP binding at the ATPase domain, resulting in dissociation of the CARDS. This process can be completely inhibited by the point mutation hRIG-I K270A (and accordingly murine K271A), resulting in RIG-I insufficiency to activate downstream IFN-1 production upon ligand binding (Yoneyama M. 2004). Importantly, other mutations in the RIG-I gene do also inactivate RIG-I-mediated signaling, e.g. the RIG-I S183I mutation, which prevents separation of the CARD domains, resulting in a similar effect (Pothlichet J. 2013). Additionally, but not essentially, if the bound RNA has a 3' overhang >5 nt, the Helicase domain can unwind the RNA under consumption of ATP, but this effect is not correlating with immunogenicity of the ligand (Takahashi K. 2008). After dissociation, the CARDS can interact with E3-ligase tripartite-motif containing 25 (TRIM25), which passes K63 bound ubiquitin to K172 of the CARDS (Gack M. U. 2007). By this, the CARDS of four RIG-I molecules can become linked via polyubiquitylation, leading to RIG-I tetramerization. The mitochondrial membrane chaperone 14-3-3 ϵ now directs the complex to mitochondria, where the CARDS can interact with MAVS, which leads to MAVS aggregation (Kolakovsky D. 2012). In the following, MAVS aggregates activate the kinases IKK-i and TBK1, which phosphorylate and activate the transcription factors IRF-3, IRF-7 and NF- κ B. Those control the expression of the IFN-1 group and the expression of inflammatory cytokines (Kolakovsky D. 2012; Schneider W. M. 2014).

1.2.3.7. *RIG-I can block the access to the IAV panhandle for the viral polymerase*

A second and less investigated antiviral mechanism of RIG-I is its ability to block the IAV panhandle. Despite it is well known that RIG-I binds the panhandle structure, this was not seen as direct antiviral action until described by Michaela Weber-Gerlach and Friedemann Weber *in vitro* (Weber-Gerlach M. 2016a). RIG-I has the potential to bind the panhandle directly after virus entry and can even disassemble polymerase subunits from it, leading to inhibition of viral replication before other antiviral mechanisms take action. The effect is further supported by the ability of RIG-I to bind to all three viral polymerase subunits, so it has always close proximity to the panhandle, even if not binding to it directly at first (Weber-Gerlach M. 2016a). This effect depends on the PB2 polymerase

genotype: While the PB2-627E polymerase variant, common in avian, is outcompeted by RIG-I, it fails to outcompete the PB2-627K variant, common in mammals (Weber M. 2015). So far, the relevance of this effect has not been confirmed *in vivo*.

1.2.3.8. *RIG-I can recruit the mammalian inflammasome*

The third antiviral function of RIG-I is its ability to contribute to the activation of the mammalian inflammasome. RIG-I, MAVS, CARD9 and Bcl10 together stimulate NF- κ B-mediated expression of pro-IL-1 β , which can also be induced by IFN-1 signaling. Further, RIG-I contributes to a complex containing the adaptor protein ASC and Caspase-1, to form the inflammasome, similar to NLRP3. In this complex, Caspase-1 autocatalysis is enabled, leading to its activation and hence the cleavage and activation of pro-IL-1 β to IL-1 β as well as the activation of IL-18 in a similar manner. IL-1 β is secreted rapidly from the cell by different mechanisms containing exocytosis, pyroptosis and inflammatory cytokine release. Since mice lacking important inflammasome components show enhanced weakness to IAV infection, recruitment of the inflammasome is another important antiviral function of RIG-I. Importantly, since the activation of the inflammasome by RIG-I requires its signaling capabilities, the RIG-I K271A variant should be deficient for both the described variants to contribute to IL-1 β production (Pothlichet J. 2013; Weber-Gerlach M. 2016a; Dinarello C. A. 2018).

1.2.3.9. *IL-1 β signaling*

IL-1 β signaling works similar to TLR signaling. IL-1 β is a member of the IL-1 cytokine family and a key factor of innate immunity, which binds to an IL-1R1/3 heterodimeric receptor to mediate proinflammatory signaling or to an IL-1R2/3 heterodimeric receptor to mediate antiinflammatory signaling. The IL-1 receptors share structural similarity with the TLRs, both using so-called Toll interleukin-1 receptor (TIR) domains, which mediate the activation of MyD88 (compare chapter (c. c.) 1.2.2.3). Thus, IL-1 receptor and TLR signaling activate similar downstream elements of innate immunity like the expression of cytokines, chemokines or nitric oxide production. IL-1 β serves as signaling molecule between epithelial cells and monocytes during establishment of early inflammation and it also plays a role in establishment of the adaptive immune response. Additionally, IL-1 β induction is linked to pyroptosis, a variant of lytic programmed cell death. Epithelial cells secrete IL-1 β to stimulate surrounding cells to produce direct antiviral factors for inhibition of virus replication and to produce CXCL8, an attractant for neutrophilic granulocytes and mediator of inflammation. As a downside, IL-1 β is a mediator of chronic inflammatory processes like atherosclerosis and contributes to the development of some cancer types. Besides the mentioned

effects upon virus infections, IL-1 β may also have effects on epithelial tissue homeostasis (Pothlichet J. 2013; Dinarello C. A. 2018).

1.2.3.10. RIG-I as tumor suppressor and therapeutic target

A less-investigated function of RIG-I is its role in tumor suppression. Upon foreign RNA detection, besides activation of MAVS, RIG-I can interact with Caspase-9, a potent inducer of apoptosis. Some recent experimental approaches in the development of new cancer therapeutics used 5'ppp siRNAs. One of those 5'ppp siRNAs targets the apoptosis inhibitor BCL2, leading to solid induction of apoptosis in melanoma cells *in vitro* and *in vivo*. Those effects are caused by RIG-I-mediated Caspase-9 activation, reduced block of apoptosis by BCL2 and additional induction of IFN-1 expression and inflammation, leading to innate immune activation at the site of the tumor. A second 5'ppp siRNA against TGF- β 1, which has an important role in pancreatic cancer development, was used in mouse models to significantly induce tumor cell apoptosis, IFN-1 production and CD8+ T-cell recruitment. Further, selective induction of apoptosis by classic RIG-I ligands like 5'ppp RNA or replication-deficient virus particles was observed for cells of prostate cancer, mammary carcinoma, lung cancer and glioblastoma, while nonmalignant cells seem to be widely spared from RIG-I ligand induced apoptosis, interestingly. Reversely, RIG-I deficiency mediates predisposition of hepatocytes to hepatocellular carcinoma development and RIG-I knockout (KO) mice often developed myeloproliferative disorders, which could be rescued by restoration of IRF-8 expression (Li X.-Y. 2014). Taken together, those approaches show a huge potential for new RNA-based therapeutics, especially in combination with new approaches in RNA delivery systems.

Some different and even less studied functions of RIG-I are also remarkable. First, RIG-I is important for phagocytosis of bacteria and immune cell migration, both independent of viral RNA but dependent on interaction with the cytoskeleton. Second, the PxxP motif upstream of the first Helicase domain of RIG-I interacts with Src in an inactivating and STAT1 in an activating manner. Those interactions happen in inactive conformation to mediate antitumorigenic effects (Li X.-Y. 2014). Third, RIG-I seems important for the control of granulocyte maturation, since RIG-I-deficient mice tend to develop a progressive myeloproliferative disorder and RIG-I is upregulated in proliferating myeloid cells (Zhang N.-N. 2008).

1.2.4. IFN signaling and stimulated genes

IFNs belong to the group of cytokines, which are a core element of innate immune signaling and can be separated in three major classes, IFN-1, -2 and -3. The IFN-2 group consists of IFN- γ , which binds

to a receptor consisting of the IFNGR subunits 1 and 2. The IFN-3 group, containing IFN- λ 1 - 3 and IFNL4, binds to a receptor consisting of the IL-10R β and IL-28R α subunits (Wang H. 2017).

The largest class of IFNs, namely type 1, contains the IFNs - α , - β , - ϵ , - κ , - ω , - δ and - τ , amongst IFN- α and - β are dominant. IFN- α can be divided into IFN- α 1 - 13, of which IFN- α 1 and 2 can be divided into even more subtypes. Nevertheless, all IFN-1 cytokines bind to the IFN-1 receptor (IFNAR), which is a heterodimer consistent of an IFNAR1 and an IFNAR2 subunit and located at the cell surface. With only a few exceptions, most body cells can produce IFN- α and - β , but during infections, plasmacytoid dendritic cells produce the majority of them per cell. The general effects of IFN-1 are antiviral, antiproliferative and immunomodulatory and they play, next to induction of antiviral effects in virus-invaded cells themselves, a very important role in inducing similar antiviral responses in neighboring cells via IFNAR/Janus kinase (JAK)/STAT signaling and in the recruitment of immune cells upon secretion (Schneider W. M. 2014; Li X.-Y. 2014; Wang H. 2017).

After IFN-1 binding to IFNAR, receptor-associated JAK1 and Tyrosine kinase 2 (TYK2) get activated and phosphorylate multiple receptor-tyrosine-residues, leading to phosphorylation of STAT proteins (STAT1-4, 5a and 5b, 6) proteins, which heterodimerize (STAT1 and 2 in majority). In the following, they complex with IRF-9, translocate into the nucleus and drive the expression of IFN-stimulated genes (ISGs) (Schneider W. M. 2014). This large group of genes is responsible for the activation of the antiviral state of the expressing cell, containing chemokine signaling components, immune regulatory proteins, driver proteins for apoptosis, as well as antiviral, antibacterial and antiparasitic proteins. Remarkably, a lot of the PRRs and their downstream signaling components are also ISGs, leading to self-induction upon initial activation and hence multiplication of innate immune signaling capacity. In addition to JAK/STAT signaling, IFNs can also activate NF- κ B and AP-1 signaling. The signaling of IFN-2 and IFN-3 receptors works similarly to the IFN-1 receptor signaling, but all pathways contain variations, as well as subsets of the target genes can vary. In general, IFNs mediate innate antiviral effects, where the IFN-1 and IFN-3 groups are inducers of first line responses. IFN-2 is also a mediator of cell-mediated responses and contributes to the initiation of an adaptive immune response. Here is also to mention that RIG-I/MDA5 downstream signaling elements, containing IFN-1 signaling, are shared between TLR, NOD-LRR and RLR pathways, leading to comparable innate immune responses which are activated in synergy upon recognition of PAMPs (Akira S. 2006; Kolakofsky D. 2012; Weber M. 2013; Schneider W. M. 2014; Weber-Gerlach M. 2016b; Wang H. 2017; Kopitar-Jerala N. 2017).

The most potent antiviral ISGs are MX dynamin like GTPase 1 (MX1), IFN-induced transmembrane protein 3 (IFITM3), protein kinase R (PKR), RIG-I and the 2'-5'-oligoadenylate-synthetase

(OAS)/RNaseL system. Mx1 binds to IAV NP together with UAP56 and URH49, leading to a block of vRNP access to the nucleus and hence a block of viral replication and transcription of the bound vRNPs, but NP binding can be inhibited by some NP mutations. Other proteins of the Mx family are expected to mediate separation of viral PB2 and NP proteins from vRNPs, also leading to inhibition of viral replication and transcription. IFITM3 is enriched in endosomes and can inhibit the fusion of virus and host cell membrane, preventing virus entry, which makes it a mediator for IFN-1-induced protection of neighboring cells. The ds RNA binding PKR can inhibit virus RNA translation and activates NF- κ B. Additionally, ISG15 should be mentioned, one of the strongest induced ISGs. It is comparable to ubiquitin and can be linked covalently to different proteins, of which a lot are also ISGs. ISG15 linkage, also known as ISGylation, can enhance or reduce protein half-life and even block protein function. Hence, it contributes to sustained innate immune signaling after linkage to proteins like TRIM25 and IRF-3 or halt of the cell cycle by mediating degradation of cyclin D1 (Schneider W. M. 2014; Weber-Gerlach M. 2016b).

1.2.5. *The OAS-RNaseL system as IFN downstream target*

1.2.5.1. *The OAS-RNaseL system*

OAS has three different variants, OAS1, 2 and 3. All variants are induced by IFN- β and produce 2'-5'-oligoadenylate (OA) oligomers from ATP after activation by ds RNA, but they differ in the synthesis rate and the amount of monomers they put together. RNaseL is constitutively expressed in the cytoplasm, but inactive without its ligand OA. Upon ligand binding, RNaseL monomers dimerize. Active RNaseL dimers cleave ss RNAs downstream of UU and UA sequences, leaving small and often duplexed fragments with 3'-phosphoryl groups, which can form cyclic phosphate groups by release of water (Malathi K. 2007). During IAV infection, RNaseL cleaves mostly the PA, PB1 and PB2 segments among the IAV RNA genome, which are the largest ones. Among the cellular RNAs, RNaseL cleaves ribosomal RNAs (rRNAs), transfer RNAs (tRNAs) and messenger RNAs (mRNAs), but remarkably not the mRNAs of IFN-1 and IFN-3, as well as ISGs. This leads to a switch between standard metabolism and an antiviral state of the cell: The expression of housekeeping and viral proteins is reduced, while the expression of antiviral proteins is highly enhanced (Cooper D. A. 2015; Chitrakar A. 2018).

1.2.5.2. *The RIG-I IFN-1 OAS/RNaseL positive feedback loop*

The activation of RIG-I induces IFN-1 production and hence activation of the OAS/RNaseL system, which in turn cleaves RNAs with the result of producing more RIG-I ligands. Hence, RIG-I OAS/RNaseL signaling is a positive feedback loop. It enhances the IFN-1 production during viral infection

significantly, establishes an antiviral metabolic state and boosts ISG production (Malathi K. 2007; Chitrakar A. 2018). This loop is negatively regulated by the OA-degrading 2'phosphodiesterase 12 (PDE12), LGP2 and the ubiquitin ligase RNF125. It can also get interrupted by suppressor of cytokine signaling (SOCS) 1 and 3 (Pothlichet J. 2013). Additionally, RIG-I is an ISG itself (Schoggins J. W. 2011; Xu L. 2017). The finding that RIG-I activation correlates with the amount of viral replication (Weber M. 2015) suggests that this positive feedback loop may serve organisms to quantify virus infections and scale their grade of antiviral response.

1.2.5.3. The nature of a self-RNA derived RIG-I ligand

Remarkably, RNaseL cleaves viral RNA as well as the endogenous RNA. Among those viral and also cellular RNA fragments, there are different RIG-I ligands, which are known for their ability to enhance IFN-1 production (Malathi K. 2007). The detailed nature of the RIG-I ligand of cellular origin has long been unsolved. Recently, the structure and function of an endogenic RIG-I ligand (eRL), which is generated as a result of RNase activation, has been unraveled. The ligand is a guanosine-derivative binding aptamer, which originates from the internal transcribed spacer 2 region (ITS2) of the 45S pre rRNA. The cleavage of the ITS2 by either RNaseL or RNaseA creates a G-rich ss 72mer RNA fragment with a 5' hydroxyl group and a 3' phosphoryl group, which can form a cyclic phosphate. The 72mer forms a complex stem-loop structure, characteristic for RIG-I ligands, which enhances the half-life of the molecule. Less characteristic for RIG-I ligands is the lack of a 5'ppp residue and the occurrence of a cyclic phosphate, which was found to be important for an immunostimulative potential (c. c. 1.2.3.3). In the end, it was found that the 72mer carries a guanosine-quadruplex containing sequence motif, enabling the fragment to bind GMP, GDP and GTP, with GTP resulting in a substitute for the missing 5'ppp residue. Among guanosine derivatives, GTP is the most prominent in the cell, leading to the conclusion that the 72mer-GTP complex is majority, which mediates RIG-I activation. This connection depicts a sensor for RNA degradation and enhanced rRNA processing (Jung S. 2020). In a recent study, it was shown that the eRL is formed in cells upon IAV infection and has a significant effect on IFN-1 induction next to direct sensing of vRNPs, independent of apoptosis-mediated RNA degradation. Despite identification of this eRL, there are hints for additional, different RIG-I ligands generated from cellular RNA (Steinberg J. 2021).

1.2.5.4. New approaches in IAV vaccination

Current research on this area aims to find the ideal combinations of vaccine and adjuvant to maximize safety and immune protection, which is challenging due to a high variety in human immune stimulation. Hence, it is of great importance to gain detailed knowledge about impact and crosstalk

of PRR-mediated immune signaling, immune cell interaction and their individual variation. With the aim to reduce vaccination side effects as much as possible, virus subunit vaccines got more and more popular. The drawback of those vaccines is the weakness of the resulting immunogenicity. Thus, vaccination adjuvants are commonly used to boost the immune reactions triggered by the vaccine itself. In the last decades, Aluminium hydroxide (alum) based adjuvants have been used intensively.

Since alum based adjuvants boost T-helper 2 supported IgG1 production, alum adjuvants are no reasonable choice for boosting production of antibodies targeting intracellular pathogens, which is supported by T-helper 1 cells. A newer approach in vaccination vs. intracellular pathogens aimed to trigger different TLRs in dendritic cells to stimulate T-helper 1 cells, with success vs. human papilloma virus. Since activation of nucleic acid receptors like cGAS and RIG-I induce strong immune responses, those receptors are further interesting targets for the development of modern adjuvants. A very challenging aspect in finding the correct adjuvant is that it requires fitting in the gap between too low and too high immune responses. pl:C is a very good inducer of innate immune signaling, because it activates TLR3, MDA5 as well as RIG-I, resulting in antigen presenting cell (APC), T-helper 1 and cytotoxic CD8+ cell activation, but it is not a safe adjuvant because it can cause a cytokine burst as side effect, which may be lethal (Ziegler A. 2017).

So far, ss RNA was not investigated intensively for its potential as adjuvant. This may be due to low durability in comparison with other molecules and the lack of sufficient pharmacodelivery in the body cells, which changed in the last years. In a recent study, a 547 nt uncapped, noncoding ss RNA, in complex with disulfide-crosslinked cationic peptides, namely RNAdjuvant, was shown to have promising abilities as an adjuvant. In combination with the IAV subunit vaccine Influvac, RNAdjuvant significantly enhances the survival of mice infected with IAV, comparable to pl:C and with significantly lower cytokine production. Further, the RNAdjuvant effect was depending on MAVS and MyD88. The combination stimulated T-helper 1 and 2 cells, following virus-specific IgG 1, 2b and 2c antibody production, showing that RNA based adjuvants are able to boost induction of humoral immune responses targeting intracellular pathogens (Ziegler A. 2017).

In this context, it seems reasonable and important to enhance understanding of the RIG-I functions in the immune system, to ease investigation of new RNA-based vaccines and adjuvants and to predict and understand possible occurring side effects. Additionally, the mentioned RNaseA and RNaseL derived RIG-I ligand may be a potential candidate for a new vaccination adjuvant.

1.2.6. *IAV evasion and adaptation strategies for RIG-I*

After millions of years, in which viruses and their hosts evolved and adapted to each other, both developed a huge arsenal of pathogenicity factors and defense mechanisms. Still, after millions of years, with a huge difference in complexity between viruses and vertebrates, it is astonishing that a system composed of eight vRNPs encapsulated in a membrane, combined with a handful of structural proteins, is able to challenge and eventually overcome huge organism systems. Thus, it is no surprise that all components of the IAV have more than just one function helping to invade and abuse potential hosts for their own propagation. Hence, it is hardly possible to go into detail with all known IAV protein functions, but some examples with relevance for this study should be explained. Nevertheless, many known IAV protein functions are listed in a table at the end of the chapter (compare Table 1).

1.2.6.1. *Adaptations in IAV replication*

Because of the disadvantage of facing RIG-I in the cytoplasm, vRNPs evolved to translocate into the nucleus and replicate there. The IAV polymerase, next to its replication function, also has an endonuclease function, which enables it to cleave host capped mRNAs and use it as primer for own replication. This endonuclease function is also suggested to cause significant reduction in host cell protein production (Dou D. 2018). To hinder RIG-I binding, there is a tight balance for bp mismatches in the viral panhandle structures, leading to selection of the perfect possible balance between lowest RIG-I detection and efficient binding of own polymerase depending on the current host. Besides the already mentioned functions of the viral polymerase, their components are also able to interact with MAVS and inhibit its function. As already mentioned above, most of the viral proteins expose NLS, translocate into the nucleus and support nuclear export of vRNPs (Weber M. 2014; Weber-Gerlach M. 2016a, 2016b; Dou D. 2018).

1.2.6.2. *The PB2-627 polymorphism: bird-human adaptation*

An important example for IAV host adaptation is the before mentioned PB2 aa 627 polymorphism (c. 1.2.3.7). While in avian-adapted IAV strains, the PB2-627E genotype is most frequent (32 % PB2-627K in H5N1 and H7N9 strains) (Peteranderl C. 2016), in mammals usually the variant PB2-627K is predominant. Today, two different factors are known, which cause this diversity. First, IAV PB2-627K has a higher affinity to viral NP and the panhandle than IAV PB2-627E in mammals, enabling it to compete with RIG-I binding affinity to this structure. This leads to reduced RIG-I-mediated signaling and higher replication rates during IAV PB2-627K infections (Weber M. 2015). Secondly, the

IAV PB2-627E genotype has an advantage in avian due to interaction with ANP32A, leading to stabilization of the viral polymerase and increased functionality, while some avian like chickens even have no RIG-I (Barber M. R. W. 2010; Long J. S. 2016; Mistry B. 2020). By those reasons, RIG-I is treated as one of the host factors that cause this diversity (Weber M. 2015), and so is ANP32A.

1.2.6.3. The Swiss knife of IAV: nonstructural protein NS1

The seemingly most versatile IAV component is the NS1. It is remarkable, because it has even more different functions than the average IAV proteins, supporting the virus and antagonizing host responses. It is expected to form homodimers, which is crucial to unfold the full potential, and even able to form oligomers when high concentrations are achieved in a cell (Hale B. G. 2014). NS1 is packed in low numbers in virus particles and can for example inhibit RIG-I-mediated IFN-1 induction by blocking of TRIM25, PACT and Riplet, by repressing IRF3/NFκB-mediated gene expression and also by inhibition of host antiviral proteins via direct interaction (e.g. the OAS/RNaseL system and PKR) (Weber-Gerlach M. 2016a, 2016b; Ji Z.-X. 2021). To study IFN responses upon IAV infection, virus variants lacking functional NS1 may be sufficient, depending on the experimental setting.

1.2.6.4. Nonstructural proteins on alternate reading frames

In addition to the IAV standard components HA, NA, M1, M2, PB1, PB2, PA, NP, NS1 and NS2, some IAV strains can express further nonstructural proteins. Those factors are only mentioned briefly and for completion of the overview. An alternate reading frame on the PA gene encodes for PA-X, an RNA-endonuclease that functions as an inhibitor of innate immune signaling by cleaving host mRNAs. Another accessory protein deriving from an alternate reading frame is the PB1-F2 protein, which interacts with MAVS, leading to mitochondrial membrane potential decrease and hence insufficient IFN induction (Weber-Gerlach M. 2016b).

1.2.6.5. The evolutionary tradeoff of evasion strategies

A study passaging IAV on IFN signaling-deficient cells with subsequent virus sequencing shows mutations in all viral RNA genes, leading to reduction of antiviral functions and/or enhanced ability to induce IFN production (Pérez-Cidoncha M. 2014). This shows that the interaction of multiple antiviral functions and immune evasion strategies of the virus are required to overcome the complex host antiviral defense mechanisms. The many different existing and circulating virus genotypes and defense settings suggest that there is always a tradeoff between defense, speed and proliferation,

which is under consequent and never-ending adaption and re-adjustment, leading to constant coevolution.

1.2.6.6. *Known IAV proteins and their different functions*

As an overview, known effects of all IAV proteins are catalogized in Table 1.

Table 1: IAV proteins and their functions.

Virus protein	Known functions	Sources
HA	Binding of SA residues on cell surfaces	(Dou D. 2018)
	Closing range between virus and host cell membrane (conformational switch)	(Dou D. 2018)
	Induction of virus and host cell membrane fusion (fusion peptide)	(Dou D. 2018)
	Support of budding by membrane shaping	(Dou D. 2018)
	Outer domains can mutate for immune evasion	(Dou D. 2018)
	SRP target sequence for ER uptake	(Dou D. 2018)
	Serine protease cleavage site	(Dou D. 2018)
	Lipid modifications for targeted delivery to lipid rafts	(Dou D. 2018)
	Suppresses STING-mediated IFN-1 signaling	(Weber-Gerlach M. 2016b)
	Mediates IFNAR degradation	(Weber-Gerlach M. 2016b)
NA	Cleavage of terminal SA residues on surface glycoproteins	(Dou D. 2018)
	Driver of budding by membrane shaping	(Dou D. 2018)
	Outer domains can mutate for immune evasion	(Dou D. 2018)
	SRP target sequence for ER uptake	(Dou D. 2018)
	Lipid modifications for targeted delivery to lipid rafts	(Dou D. 2018)

M1	Adaptor between surface proteins and vRNPs	(Dou D. 2018)
	Curved protein, drives budding	(Dou D. 2018)
	Cuts budded virus particle from cell membrane	(Dou D. 2018)
	Changes conformation in acidic pH to unleash vRNPs	(Dou D. 2018)
	NLS for nuclear translocation	(Dou D. 2018)
	Masks NLS in vRNP complexes	(Dou D. 2018)
	Links vRNPs to nuclear export proteins	(Dou D. 2018)
M2	Supports membrane curving	(Dou D. 2018)
	Ion channel, controls pH during entry phase	(Dou D. 2018)
	SRP target sequence for ER uptake	(Dou D. 2018)
PA	Polymerase subunit: replication and transcription	(Dou D. 2018)
	endonuclease	(Dou D. 2018)
	NLS	(Dou D. 2018)
	Can block access to panhandle for RIG-I (pol.)	(Weber-Gerlach M. 2016b)
	Downregulation of ISGs via DR1/RNA polymerasell	(Weber-Gerlach M. 2016b)
	Can inhibit MAVS	(Weber-Gerlach M. 2016b)
PB1	Polymerase subunit: replication and transcription	(Dou D. 2018)
	NLS	(Dou D. 2018)
	Can block access to panhandle for RIG-I (pol.)	(Weber-Gerlach M. 2016b)
	Downregulation of ISGs via DR1/RNA polymerasell	(Weber-Gerlach M. 2016b)
	Can inhibit MAVS	(Weber-Gerlach M. 2016b)
PB2	Polymerase subunit: replication and transcription	(Dou D. 2018)
	Binding of host mRNA	(Dou D. 2018)

	NLS	(Dou D. 2018)
	Mediates vRNP transport to budding sites via Rab11 binding	(Dou D. 2018)
	Can block access to panhandle for RIG-I (pol.)	(Weber-Gerlach M. 2016b)
	Downregulation of ISGs via DR1/RNA polymerase II	(Weber-Gerlach M. 2016b)
	Can inhibit MAVS (9D genotype)	(Weber-Gerlach M. 2016b)
NP	Binds and masks viral RNA	(Weber-Gerlach M. 2016b)
	NLS	(Dou D. 2018)
NS1	IFN antagonist	(Weber M. 2014; Dou D. 2018)
	Direct RIG-I antagonism	(Pothlichet J. 2013)
	TRIM25 inhibition	(Weber M. 2014)
	ds RNA binding and masking (anti OAS-RNaseL)	(Hale B. G. 2014; Min J.-Y. 2006)
	OAS/RNaseL and PKR inhibition	(Weber-Gerlach M. 2016a)
	Host mRNA transport and processing inhibition	(Weber M. 2014; Noda K. 2018; Min J.-Y. 2006)
	NLS	(Dou D. 2018)
	Links vRNPs to nuclear export proteins	(Dou D. 2018)
	Inhibition of host antiviral gene expression via CPSF30 inhibition	(Hale B. G. 2014)
	Promotion of virus replication via PI3Kinase p85 β isoform	(Hale B. G. 2014)
	Downregulation of IFNAR	(Peteranderl C. 2016)
NS2	NLS	(Dou D. 2018)
	Links vRNPs to nuclear export proteins	(Dou D. 2018)
PA-X	Host mRNA cleavage	(Weber-Gerlach M. 2016b)
PB1-F2	MAVS interaction, IFN signaling repression	(Weber-Gerlach M. 2016b)

1.3. *Mouse models for the understanding of human pathologies*

Mice and humans are both mammals and evolutionary related close enough to allow comparisons. Since mice have, in comparison to other mammals, low requirements for their habitat and reproduce very fast with a high resistance to inbreeding problems, they are an ideal species as mammalian model organism to get new insights in some pathologies, which share similarities with the respective human diseases. Mouse models of acute lung infection are well established and are sufficient to draw conclusions on human pathologies. In the past, they were often used to gain the necessary basic knowledge to develop new therapeutics and also to perform initial tests for their effects and side effects (Graham A. 2021). Intranasal mouse lung infection with IAV causes diffusely-distributed broncho-interstitial pneumonia in single lung lobes. Characteristic pathologic changes in the lung were alveolar necrosis, inflammatory cell infiltration, alveolar edemas as well as hemorrhage in alveoli and interstitium (Dietert K. 2017).

1.4. *Aims of this study*

Since direct effects of the RIG-I panhandle block, enhancement of IL-1 β production and enhancement of IFN production can be investigated well in cell culture, the effect and relevance of those functions in the workflow of the whole immune system cannot be investigated with that ease. The main aim of this study is to validate the impact of the different RIG-I functions in the defense against a mammalian-adapted and an avian-adapted influenza strain. For this, mouse models expressing different RIG-I variants in infection experiments with recombinant IAV strains will be used to screen for differences in the flu-mediated disease courses depending on the mouse RIG-I genotypes, with the aim to draw conclusions on the underlying molecular mechanisms.

The first aim is to generate mouse lines that express (i) wild type (WT) RIG-I, (ii) a RIG-I variant with a K271A point mutation deficient to enhance IFN- α and IL-1 β production, or (iii) no RIG-I. The established mouse lines will be validated for their differential RIG-I expression and altered IFN- α and IL-6 induction in dependence on different ligands of PRRs of the innate immune system.

Second aim of this study is to generate and characterize recombinant IAV strains to determine RIG-I functions in an *in vivo* mouse infection study. Therefore, the mammalian-adapted IAV/PR/8 PB2-627K strain was chosen, which usually causes a well-described course of disease. Additionally, the avian-adapted IAV PB2-627E version of this strain was chosen, which shows a lower potency to compete with RIG-I for the access to the viral panhandle structures, to allow a more detailed study of RIG-I effects on the virus function (c. c. 1.2.3.7).

The final aim is to perform a mouse infection study with the established mouse lines and the characterized recombinant virus strains. The hypothesis is, that RIG-I variant expression in mice affects parameters in the course of a flu infection. Of those, the parameters weight and body temperature will be monitored daily. At the endpoint of the experimental course, whole blood, bronchoalveolar lavage fluid (BALF) and the heart-lung circulation will be harvested for histological analysis. With these samples, parameters like lung barrier integrity, virus titer in the BALF, virus abundance in the lung tissue as well as the expression of IFNs and cytokines in the BALF will be determined. By this, it is aimed to draw conclusions on the impact of the different RIG-I functions in the defense against human- and avian-adapted IAV strains in a complete mammalian organism, as summarized in Figure 4.

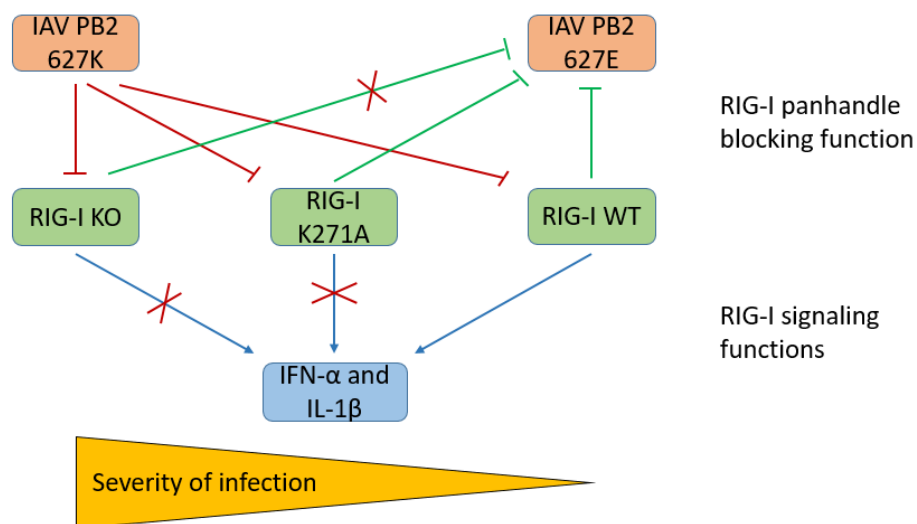


Figure 4: Overview of the expected RIG-I-IAV strain interactions. Supported by the literature, it is expected that RIG-I-mediated IFN- α and IL-1 β induction is dysfunctional in the RIG-I PM and KO mice. The suggested panhandle blocking function is not present in the RIG-I KO mice, but in the RIG-I WT and PM mice. An increased binding affinity of the IAV PB2-627K strain to the viral panhandle structures may prevent binding of RIG-I to this structure. This is not expected for the avian-adapted IAV PB2-627E variant, which should be more susceptible to RIG-I effects. At least on this IAV strain, a RIG-I-mediated block of the viral panhandle structures for the access of the viral polymerase should result in a difference between RIG-I PM and KO mice. In general, the highest severity of infections is expected for the RIG-I KO mice and the lowest for RIG-I WT mice.

2. Material

2.1. Consumables

Table 2: Consumables.

Product	Brand name	Company of origin
1.5 and 2.0 ml reaction container	1.5 and 2.0 ml reaction container	Sarstedt, Nümbrecht, Germany
15 ml reaction container	15 ml reaction container	Greiner Bio-one, Frickenhausen, Germany
50 ml reaction container	50 ml reaction container	Greiner Bio-one
Bacteria container	14 ml culture container round bottom, Falcon	Corning, Corning, USA
Bacteria inoculation loops	Bacteria inoculation loops	Sarstedt
Black 96-well plates	Microlon Fluorotrac 200 F-bottom, half area	Greiner Bio-one
Cell culture dishes coated	cell culture dishes coated, Primaria	Corning
Cell culture dishes non-coated	cell culture dishes non-coated Corning	Corning
Cell culture flasks	TC Flask Standard T25, T75, T175	Sarstedt
Cell strainer 70 µm	Sterile cell strainer	Thermo scientific, Waltham, USA
Cryo container cells	CryoPure 1.6 ml	Sarstedt
Filtertips	ultra point graduated filtertip 10, 100, 1000 µl	Starlab, Hamburg, Germany
PCR stripes	Low-Profile PCR Tubes 8-tube strips clear	Bio-Rad Laboratories Inc., Hercules, USA
PCR stripe lids	Optical Flat 8-Cap Strips for 0.2 ml tube strips	Bio-Rad
Petri dishes for agar	Petri dish 92x 16 mm with cams	Sarstedt
Pipette tips	pipette tips 10, 200, 1000 µl	Sarstedt

SDS-PAGE ready to use gels	Run-Blue SDS Protein Gels 4-12 %	Expedeon, Swavesey, UK
SDS-PAGE ready to use gels alternative	TEO-Tricine Precast Gels RunBlue 4-20 % 12-well	Abcam, Cambridge, UK
Serological pipettes	serological pipettes 5, 10, 25 ml	Sarstedt
Syringe	1 and 5 ml Omnifix	Braun, Melsungen, Germany
Syringe tips	24G and 27G Microlance	Becton Dickinson, Franklin Lakes, Germany
Syringe with hose	21G safety multifly	Sarstedt
Throwaway gloves	Semper Care Premium Latex Powder-free	Sempermed, Vienna, Austria
Trachea katheter	Vasofix Safety 18G vena canule	Braun
Vessels for virus storage	2.0 ml Micro Tube	Sarstedt
WB-membrane	Immobilon-P PVDF membrane	Merck millipore, Darmstadt, Germany
6-well plates cell culture	6-well plates standard F-bottom	Sarstedt
96-well plates cell culture	96-well plates F-bottom	Greiner bio-one
96-well plates ELISA	96-well Immuno plates Nunc	Thermo scientific
96-well plates U-bottom	96-well plates U-bottom	Sarstedt
96-well plates V-bottom	PS-microplate, 96-well, V shape	Greiner bio-one
Whatman paper WB	Whatman paper GB003	Schleicher and Schuell, Keene, USA

2.2. *Laboratory hardware*

Table 3: Laboratory hardware.

Gear	Model	Company of origin
Bacteria clean bench	Integra 2F 120-11 GS	Heraeus, Hanau, Germany
Bacteria Incubator	Cytoperm	Heraeus
Bacteria Shaker/Incubator	innOva 4200	New Brunswick Scientific, Edison, USA

Breeding chamber		Grumbach Brutgeräte GmbH, Aßlar, Germany
Bond III IHC staining system	Leica Biosystems, Wetzlar, Germany	Bond III IHC staining system
Cell culture clean bench	Hera safe	Thermo scientific, Waltham, USA
Cell incubator 5.0 % CO₂	HeraCell 240i	Thermo scientific
Cell incubator 7.5 % CO₂	HeraCell 240	Thermo scientific
ELISA washer	Skan Washer 400	Molecular Devices, San Jose, USA
Gel Imager	GelStick Imager	Intas, Göttingen, Germany
Laboratory centrifuge	Rotanta/RPC	Hettich, Kirchleugern, Germany
Laboratory centrifuge	Multifuge 1 L-R	Heraeus
Laboratory centrifuge	Biofuge stratos	Heraeus
Light microscope	Leitz Labovert	Leica Microsystems GmbH, Wetzlar, Germany
Luminescence imager	ChemiDoc MP	Bio-Rad Laboratories Inc., Hercules, USA
Multimode plate reader for fluorescence measurement	Tecan i control infinite 200 pro	Tecan Trading AG, Männedorf, Switzerland
Multiplex plate analyzer	Bio-plex 200 system	Bio-Rad
Multiplex wash station	Bio-Plex HTF	Bio-Rad
PAA-Electrophoresis chamber	DCX-700 CBS	Thermo scientific
PCR thermal cycler	iCycler	Bio-Rad
Plate photometer	Emax	Molecular Devices
Power unit for AGE	EC 105	Cambridge scientific, Watertown, USA
Power unit for Electrophoresis	PowerPac Basic	Bio-Rad
RNA clean bench	Lamin Air HLB2448	Heraeus
Semi-dry blotter	TE77XP Hoefer	Thermo scientific

Shaker	IKA-Schüttler MTS4	IKA Labortechnik, Staufen, Germany
Slide scanner	Aperio AT2	Leica Biosystems, Wetzlar, Germany
Spectrophotometer	NanoDrop 1000	Thermo scientific
Tabletop centrifuge	Mikro 200R	Hettich

2.3. Stimuli

Table 4: Cell culture stimuli.

Substance	Effect	Concentration stock	Concentration final	Vector reagent	Company of origin
3p-hpRNA	RIG-I agonist	100 ng/ μ l	100; 50; 25 pg/ μ l	Lipofectamine 2000	Invivogen, Toulouse, France
5'ppp dsRNA	RIG-I agonist	200 ng/ μ l	1 ng/ μ l	Lipofectamine 2000	Invivogen
CpG 2216	TLR9 agonist	500 μ M	1 μ M	none	TIB Molbiol, Berlin, Germany
Lipopolysaccharide	TLR4 agonist	1 μ g/ μ l	2 ng/ μ l	none	Bioz Inc., Los Altos, USA
mM-CSF	Macrophage colony stimulating factor	10 μ g/ml	20 ng/ml	none	Peprtech, Hamburg, Germany
Pam3Cys	TLR2 agonist	1 μ g/ μ l	5 ng/ μ l	none	Invivogen
Plasmid-DNA (pcDNA3.1)	cGAS agonist	380 ng/ μ l	5 ng/ μ l	Lipofectamine 2000	in house batch
Universal IFN-α	Innate immunity activator	1000 U/ μ l	1 U/ μ l	none	PBL Assay Science, Piscataway, USA

2.4. Buffers

Table 5: Buffers.

Buffer	Component	Quantity or final concentration	Company of origin
ELISA			
10x PBS	KCl	2.0 g	Carl Roth, Karlsruhe, Germany
	KH ₂ PO ₄	2.0 g	Carl Roth
	NaCl	80.0 g	Carl Roth
	Na ₂ HPO ₄	11.5 g	Carl Roth
	autoclaved water	To 1 L	
ELISA blocking buffer	10x PBS	1x	
	Bovine serum albumin (BSA)		
	Fraction V	1 %	Carl Roth
	Tween 20	0.05 %	Bernd Kraft GmbH, Duisburg, Germany
ELISA substrate buffer	C ₆ H ₈ O ₇	7.3 g	Carl Roth
	Na ₂ HPO ₄ x 2 H ₂ O	11.87 g	Carl Roth
	autoclaved water	To 1 L	
	OPD tablet (30 mg)	1 mg/ml	Sigma-Aldrich, St. Louis, USA
	H ₂ O ₂ 30 %	0.03 %	Carl Roth
ELISA wash buffer	10x PBS	500 ml	
	Tween 20	2.5 ml	Bernd Kraft GmbH
	autoclaved water	Fill to 5 ml	

Others			
Bicarbonate buffer	NaHCO ₃	8.4 g	Carl Roth
	NaOH	Adjust to pH 9.2	Carl Roth
	DEPC-treated water	Fill up to 200 ml	
0.5 M EDTA pH 8.0	EDTA	0.5 M	Carl Roth
	NaOH	To pH 8.0	Carl Roth
	Autoclaved water	Fill up	
Erythrocyte-lysis buffer	NH ₄ Cl	0.8 % (w/v)	Merck, Darmstadt, Germany
	KHCO ₃	10 mM	Carl Roth
	EDTA	0.1 mM	Carl Roth
	autoclaved water	Fill up	
Lavage buffer	DPBS def.	10 ml	PAN biotech, Aidenbach, Germany
	cComplete Mini protease inhibitor	1 tablet	Roche, Basel, Switzerland
	EDTA pH 8.0, 0.5 M	2 mM	
10 % Paraformaldehyde	Paraformaldehyde	10 % (w/v)	Carl Roth
	PBS def.	Fill up	PAN biotech
RNase free water, 2x autoclaved	Diethylidicarbonate (DEPC)	1 ml	Carl Roth
	Autoclaved water	Fill up to 1 L	
50x TAE buffer	TRIS-base	242 g	Thermo scientific, Waltham, USA
	Acetic acid	57.1 g	Carl Roth
	EDTA (pH 8.0), 0.5 M	100 ml	
	autoclaved water	Fill up	

1x TAE buffer AGE	50x TAE buffer autoclaved water	1:50 dilution Fill up	
Tail lysis buffer	Tris pH 8.0, 1 M EDTA pH 8.0, 0.5 M NaCl, 5 M SDS, 10 % Autoclaved water	10 ml 50 ml 20 ml 50 ml Fill to 1 l	
Single cell infection assay			
4 % Paraformaldehyde	Paraformaldehyde DPBS def.	4 % (w/v) Fill up	Carl Roth PAN biotech
SCIA wash buffer	DPBS +/- Tween 20	 0.05 %	PAN biotech
SCIA permeabilization buffer	DPBS +/- Triton X 100 Glycine	 0.3 % 20 mM	PAN biotech Sigma-Aldrich
Western blotting			
1 % Triton X cell lysis buffer	Triton X 100 DPBS def. EDTA pH 8.0, 0.5 M Halt protease-inhibitor 100x Na ₃ VO ₄ 20 mM NaF 0.5 M	1 % Fill up 0.005 M 1x 0.2 mM 0.02 M	Sigma-Aldrich PAN biotech Thermo scientific

6x Lämmli buffer	SDS	12 % (w/v)	Merck
	β-Mercapto-ethanol	12.5 % (w/v)	Carl Roth
	Glycerol	60 % (v/v)	Carl Roth
	Tris Base pH 6.8	375 mM	Sigma-Aldrich
	Autoclaved water	Fill up	
	Adjust to pH 6.8 with HCl		
	Add Brom Phenole blue	0.06 %	Sigma-Aldrich
1x Run Blue buffer	20x RunBlue™ buffer	50 ml	Abcam, Camebridge, UK
	autoclaved water	To 1 L	
Western blot wash buffer	10 x PBS	1 x	
	Tween 20	0.1 %	Bernd Kraft GmbH
Western blot block buffer	10x PBS	1x	
	Tween 20	0.1 %	Bernd Kraft GmbH
	Skim milk powder	5 % (w/v)	Sigma-Aldrich
20x NuPAGE transfer buffer	Bicine	10.2 g	Sigma-Aldrich
	Bis-TRIS	13.1 g	Sigma-Aldrich
	EDTA	0.75 g	ELITechGroup, Zottegem, Belgium
	Ultrapurified water	To 125 ml	Thermo scientific
1x NuPAGE transfer buffer	20x NuPAGE transfer buffer	2.5 ml	
	Methanol (100 %)	5.0 ml	Carl Roth
	Ultrapurified water	Fill to 50 ml	Thermo scientific

2.5. Media, agar and components

Table 6: Media, agar and components.

Medium	Ingredient	Volume/ final concentration	Company of origin
Agarose gel 1 % (w/v)	Agarose LE	1 g	Anprotec, Bruckberg, Germany
	1 x TAE buffer	100 ml	
Deadhesion buffer	FCS	3 %	Anprotec
	EDTA	2 mM	Carl Roth
	DPBS def.	Fill up	PAN biotech, Aidenbach, Germany
DMEM complete (comp.)	DMEM High Glucose	500 ml	PAN biotech
	4.5 g/l		
	FCS	10 %	Anprotec
	Penicillin/Streptomycin	1 %	PAN biotech
	(P/S) 10000 U/ml P 10 mg/ml S		
	L-Glutamine (Q)	1 %	PAN biotech
	200 mM		
DMEM-infection medium (IM)	DMEM High Glucose	500 ml	PAN biotech
	4.5 g/l		
	P/S	1 %	PAN biotech
	Q	1 %	PAN biotech
DPBS w Ca²⁺ Mg²⁺	BSA 35 % in DPBS def.	0.1 %	Sigma-Aldrich, St. Louis, USA
			PAN biotech
DPBS w/o Ca²⁺ Mg²⁺ (DPBS def.)			PAN biotech

LB liquid medium	LB medium Lennox	2 % w/v	Carl Roth
	Ampicillin 100 mg/ml	To 100 µg/ml	Carl Roth
	Autoclaved water	Fill up	
LB solid agar	LB agar Lennox	3.5 % w/v	Carl Roth
	Ampicillin 100 mg/ml	To 100 µg/ml	Carl Roth
	Autoclaved water	Fill up	
Opti-MEM Gibco			Thermo scientific, Waltham, USA
RPMI-comp.	RPMI	500 ml	PAN biotech
	FCS	10 %	Anprotec
	P/S	1 %	PAN biotech
	Q	1 %	PAN biotech
	β-ME	0.1 %	PAN biotech
RPMI freeze medium	FCS	50 %	Anprotec
	RPMI-MEF	40 %	
	DMSO	10 %	Merck, Darmstadt, Germany
RPMI-IM	RPMI	500 ml	PAN biotech
	P/S	1 %	PAN biotech
	Q	1 %	PAN biotech
	BSA 35 % in DPBS def.	0.1 %	Sigma-Aldrich
RPMI-MEF	RPMI	500 ml	PAN biotech
	FCS	10 %	Anprotec
	P/S	1 %	PAN biotech
	Q	1 %	PAN biotech
TPCK-treated Trypsin	1 mg/ml	1 µg/ml	Sigma-Aldrich
1x Trypsin	10x Trypsin-EDTA	1x	PAN biotech
	DPBS def.	Fill up	

2.6. Cell lines and bacteria

Table 7: Cell lines and bacteria.

Cell line/bacteria strain	Original organism	Derived from
Chicken erythrocytes	Chicken whole blood	LDG Laboratory Diagnostics Germany GmbH, Cuxhaven, Germany
DF-1	Immortalized chicken fibroblasts	Friedemann Weber
Escherichia coli DH5 α	Bacteria strain	In house
HEK293	Human embryonic kidney cells	In house
Huh7.5	Human hepatocyte carcinoma	In house
MDCK	Madin-darby canine kidney (dog)	In house
MEF from C57BL/6J RIG-I WT	Murine embryonic fibroblasts	In house
MEF from C57BL/6J RIG-I PM	Murine embryonic fibroblasts	In house
MEF from C57BL/6J RIG-I KO	Murine embryonic fibroblasts	In house

2.7. Mouse lines

Table 8: Mouse lines.

Description	Notes	Company of origin
C57BL/6J RIG-I WT	RIG-I WT	The Jackson Laboratory, Bar Harbor, USA
C57BL/6J RIG-I PM	RIG-I K271A point mutation	Founder mice commercially generated by the Institute of Laboratory Animal Science University of Zurich, Switzerland
C57BL/6J RIG-I KO	RIG-I KO	Founder mice commercially generated by the Institute of Laboratory Animal Science University of Zurich, Switzerland

2.8. *Virus strains*

Table 9: Virus strains.

Virus description	Medium	Origin
IAV/PR/8/H1N1 ΔNS1	chicken egg allantois fluid	Peter Stäheli, Institute of Virology University Hospital Freiburg, Germany
IAV/PR/8/H1N1 recombinant	CaCo2 cell culture supernatant	In house
IAV/PR/8/H1N1 PB2-627K recombinant	DF-1 cell culture supernatant	Generated with 8-plasmid system (Hoffmann E. 2002)
IAV/PR/8/H1N1 PB2-627E recombinant	DF-1 cell culture supernatant	Generated with 8-plasmid system (Hoffmann E. 2002), PB2-627K to -627E mutation generated with primer-mediated mutagenesis
Sendai virus	chicken egg allantois fluid	In house

2.9. *Reagents*

Table 10: Reagents.

Reagent	Company of origin
DOTAP transfection reagent	Carl Roth, Karlsruhe, Germany
Eosin Y solution, alcoholic	Sigma-Aldrich, St. Louis, USA
Fluorescein-5-isothiocyanate (FITC) labeled albumin	Sigma-Aldrich
Forene (Isofluran) 100 % v/v	Abbvie, North Chicago, USA
Isopropanol 100 %	Carl Roth
Ketamin 10 %	bela-pharm GmbH u. Co. KG, Vechta, Germany
Lipofectamine 2000	Thermo scientific, Waltham, USA
NaCl for infusion 0.9 %	B. Braun, Melsungen, Germany
Proteinase K, recombinant, PCR grade	Roche, Basel, Switzerland
Restore PLUS Western blot stripping buffer	Thermo scientific
Rompun 2 %	Bayer, Leverkusen, Germany

2.10. Kits

Table 11: Kits.

Kit	Company of origin
Bio-Plex Pro Mouse Cytokine 23-plex Group I (M60009RDPD)	Bio-Rad Laboratories Inc., Hercules, USA
Bond Polymer Refine Detection Kit	Leica Biosystems, Wetzlar, Germany
cOmplete Mini protease inhibitor	Roche, Basel, Switzerland
DreamTaq Green PCR Master Mix 2x	Thermo scientific, Waltham, USA
EcoRI, cont. buffer R	Thermo scientific
ExtractMe Total RNA kit	Blirt, Danzig, Poland
GeneJET Gel Extraction Kit	Thermo scientific
GeneJET PCR Purification Kit	Thermo scientific
GeneJET Plasmid Miniprep Kit	Thermo scientific
GeneRuler 1 kb DNA ladder	Thermo scientific
KPL TrueBlue Peroxidase Substrate	Sera Care, Milford, USA
Mph1103-I, cont. buffer R	Thermo scientific
Page ruler prestained protein ladder	Thermo scientific
peqGOLD Total RNA kit	VWR International GmbH, Darmstadt, Germany
Phusion Hot Start II HF DNA polymerase	Thermo scientific
Pierce BCA Protein Assay Kit	Thermo scientific
Pierce ECL Western blotting substrate kit	Thermo scientific
RevertAid First Strand cDNA Synthesis kit	Thermo scientific
SuperSignal West Dura kit	Thermo scientific
T4 DNA Ligase kit	Thermo scientific

2.11. Plasmids

Table 12: Plasmids.

Plasmid name	Origin	Used for
pcDNA3.1		Stimulation of cGAS-STING signaling
pHW2000-HA	In house (Hoffmann E. 2002)	Generation of recombinant IAV PR8 strains
pHW2000-NA		
pHW2000-M		
pHW2000-NP		
pHW2000-NS		
pHW2000-PA		
pHW2000-PB1		
pHW2000-PB2 (627K)		
pHW2000-PB2 (627E)	Edited with primer-mediated mutagenesis	Generation of recombinant IAV with PB2-627E mutation

2.12. Antibodies

Table 13: Antibodies.

Antibody	Origin and target	Dilution	Company of origin	Reference number
ELISA mIFN-α				
Capture	Rat anti mouse	1:2000	PBL Assay Science, Piscataway, USA	22100-1
Standard	mIFN- α standard	500 U/mL, 1:2 dilution row	In house	
Detection	Rabbit anti mouse	1:1000	PBL	32100-1
Enzyme conjugate	Goat anti rabbit HRP	1:5000	Jackson Immuno Research, Ely, UK	111-035-045

<i>ELISA mIFN-β</i>				
Capture	Duo Set mouse IFN-β	1:250	R & D systems, Minneapolis, USA	DY 8234-05
Standard		10 ng/ml, 1:2 dilution row		
Detection		1:400		
Enzyme conjugate	Streptavidin HRP	1:5000		
<i>ELISA mL-6</i>				
Capture	Rat anti mouse	1:500	R & D systems	MAB 406
Standard	Murine IL6	10 ng/mL, 1:2 dilution row	R & D systems	406-ML
Detection	Biotin rat anti mouse	1:500	R & D systems	BAF 406
Enzyme conjugate	Streptavidin HRP	1:5000	Roche, Basel, Switzerland	11089153001
<i>Immunohistochemistry</i>				
Primary antibody	Rabbit anti IAV NP polyclonal	1:5000	Thermo scientific, Waltham, USA	PA532242
Secondary antibody (Bond polymer Refine Detection kit)	Polymer anti-rabbit poly-HRP IgG	25 µg/ml	Leica Biosystems, Wetzlar, Germany	DS9800 (kit)
<i>Single cell infection assay</i>				
Primary antibody	Mouse anti NP monoclonal	1:5000	Abcam, Cambridge, UK	43821
Secondary antibody	Goat anti mouse HRP	1:2000	Jackson Immuno Research	115-035-062
<i>Virus M protein semi-quantification</i>				
Primary antibody	HB64 hybridoma cell supernatant anti IAV M	1:25	In house	
Secondary antibody	Goat anti mouse HRP	1:5000	Jackson Immuno Research	115-035-062

Western blot mRIG-I				
Primary antibody	Rat anti mouse	1:500	Enzo Life Sciences, Lörrach, Germany	ALX-804-960-0100 (clone SS1A)
Secondary antibody	Rabbit anti rat HRP	1:5000	Abcam	Ab6734
Western blot h/m β-Actin				
Primary antibody	Mouse anti human	1:1000	Sigma-Aldrich, St. Louis, USA	A2228 (clone AC-74)
Secondary antibody	Goat anti mouse HRP	1:5000	Jackson Immuno Research	115-035-062

2.13. Software

Table 14: Software.

Software	Company of origin
Basic Local Alignment Search Tool (BLAST)	National Institute of Health, Bethesda, USA
BioEdit	Ibis Biosciences, Carlsbad, USA
Bio-plex Manager vers. 6.2	Bio-Rad
ChromatQuantitor	Mullins Lab, University of Washington, Seattle, USA
Google Translate	Alphabet Inc., Mountain View, USA
G*Power v.3.1.9.2	Heinrich Heine University, Düsseldorf, Germany
GraphPad Prism 9	Graphpad Software Inc., San Diego, USA
ImageJ	Wayne Rasband @National Institutes of Health, Bethesda, USA, open source
Image Lab version 6.1	Bio-Rad Laboratories Inc., Hercules, USA
LAS software version 4.12	Leica Microsystems, Wetzlar, Germany
Office 2016 (analysis) and 2007 (writing)	Microsoft, Redmond, USA
Oligo Analyzer	Integrated DNA technologies Inc., Coralville, USA
PONS online dictionary	PONS-Langenscheidt GmbH, Stuttgart, Germany
QuPath version 0.2.2	Open source software, (Bankhead P. 2017)
Reverse complement	Bioinformatics.org
SoftMax Pro v5	Molecular Devices, Sunnyvale, USA
Tecan i-control version 1.10.4.0	Tecan Trading AG, Männedorf, Switzerland

3. Methods

3.1. Generation of mouse lines with RIG-I variants

To validate the RIG-I-mediated blocking function of the viral panhandle structures and to investigate the impact of the different RIG-I-mediated antiviral effects *in vivo*, three mouse lines differing in their RIG-I functionality were generated. While WT RIG-I is able to induce IFN production, IL-1 β production and to block the IAV panhandle structures for the access of the viral polymerase, the murine RIG-I K271A variant (analog to K270A in human) is deficient in signal activation, but may still block the panhandle structures. For RIG-I KO, all described functions are lost.

The generation and propagation of RIG-I PM and KO mice was permitted by the Regierungspräsidium Gießen (reference number G96-2017 for RIG-I PM and G6-2019 for RIG-I KO). The mouse lines were destined to be used for an infection study with recombinant IAV strains. The genetically modified mice were generated on the C57BL/6J strain background in cooperation with the Institute of Laboratory Animal Science of the University of Zurich. To generate founder mice, a plasmid encoding for the guide RNA and the Cas9, together with an oligonucleotide serving as template for the homology directed repair mechanism, were injected into fertilized zygotes. The oligonucleotide carried a RIG-I nt 811 A to G and a 812 A to C substitution (mRNA nt position), replacing the aa K at position 271 with A (AAA lysine --> GCA alanine). Further, it carries additional wobble mutations in the two codons following the codon 271, which do not alter the aa sequence, but prevent the cleavage of the oligonucleotide by Cas9. After the CRISPR/Cas9 application, the zygotes were incubated *o. n.* and injected into pseudo-pregnant female mice, which gave birth to potential founder mice. Biopsies derived from the offspring were genotyped for genetic alterations in the targeted area of the RIG-I gene, as described in the following chapters. By this, a heterozygous RIG-I K271A founder mouse and one with a RIG-I nt 803-807 deletion (mRNA nt position), leading to frameshift and knockout of this gene (RIG-I KO), were generated (the detailed genotypes will also be described in the following chapters).

The founder mice were bred with C57BL/6J WT mice and the resulting offspring was genotyped. The heterozygous mice were interbred and genotyped again in search for homozygous mice. All heterozygous and homozygous mice of the PM and KO line were visually inspected weekly and the weight of a subset of mice was determined and protocolled weekly to investigate a potential burdening by their genotype. Final examinations validating the burden were performed by comparison of weight curves and pub mortality with data from Jackson Lab and in-house averages. Some homozygous RIG-I WT mice resulting from the breeding were used to generate a RIG-I WT line

closely related to the RIG-I PM and KO lines. All mice were bred under specific pathogen free (SPF) conditions in individually ventilated cages (IVC). Mice for the infection experiments were bred from either homozygous RIG-I WT, PM or KO mice and transferred from the highest priority SPF breeding lab to the lower priority SPF S2 laboratory between one day and one week before starting the infection experiments.

3.2. *RIG-I mouse genotyping*

To determine the RIG-I genotype of mice, tail biopsies were harvested and lysed with 0.5 ml of a tail lysis buffer containing proteinase K o. n. at 56 °C. Afterwards, the lysis reaction was vortexed and the reaction was centrifuged at 5000 RCF for 5 min in a tabletop centrifuge to spin down undigested debris. In the following, the supernatant was transferred to 0.5 ml 100 % isopropanol, the reaction was well mixed and put on ice to precipitate genomic DNA. Insoluble DNA was trapped with a pipette and transferred to 100 µl ultrapurified (up) water. After solution of the DNA at room temperature (RT), the DNA concentration was measured with a NanoDrop device (Thermo).

For amplification of the DNA region flanking the RIG-I 271 codon, a polymerase chain reaction (PCR) was performed by using the DreamTaq Green PCR Master Mix (Thermo) and the primer listed in Table 15. The PCR protocol and the cycler program are summarized in Table 16 and Table 17. The resulting PCR product had a size of approx. 400 bp. Afterwards, the PCR reaction was purified with a GeneJET PCR Purification Kit (Thermo) according to the manufacturer's manual. The PCR product was eluted with up water and the DNA concentration was determined with a NanoDrop device. In the following, the DNA was used for Sanger-sequencing, as described in the following chapter.

Table 15: The primer used in the RIG-I genotyping procedure.

Primer	Sequence	Melting temperature
RIG-I fwd.	TGGACAGCGATAAGGAGGGA	57.7 °C
RIG-I rev.	TGCCTGCTGCTCATAGACAG	57.1 °C

Table 16: DreamTaq Green PCR composition.

Component	Quantity
DreamTaq Green Master Mix (2x)	15 µl
Primer RIG-I fwd. (10 µM)	1.5 µl
Primer RIG-I rev. (10 µM)	1.5 µl
Genomic DNA	150 ng
Up water	Fill to 30 µl

Table 17: Cycler program for RIG-I genotyping PCR.

Step	Temperature (°C)	Duration	Cycles
Initial denaturation	95	3 min	1
Denaturation	95	30 s	30
Annealing	57	30 s	
Extension	72	1 min	
Final extension	72	15 min	1
Conservation	10	infinite	

3.3. Sanger-sequencing

To validate the sequence of nucleic acids like genomic DNA or PCR products, the commercially available Sanger-sequencing service of the Microsynth Seqlab GmbH (Göttingen, Germany) was used. The method uses electrophoresis and the incorporation of fluorescence-labelled, strand terminating dideoxy-nucleotides to determine the sequence of a template DNA. While Sanger-sequencing is usually used to validate the sequence of a purified, homogeneity DNA, it can also be used to analyze the heterogeneity of one or more specific positions, because the peak intensities at a specific position can be used to quantify the distribution of each nucleotide (nt). In the following, both applications were used.

In this study, a genomic part adjacent to the RIG-I 271 codon of mice was sequenced, as well as the plasmid sequence or the RNA sequence encoding for the IAV PB2 gene. For the first, the mentioned part of the genomic DNA was amplified with a PCR reaction as described (compare chapter (c. c.) 3.2). For the second, purified plasmid DNA was amplified by PCR. For the latter, isolated viral RNA was reverse-transcribed into cDNA and amplified with a PCR reaction as described later on (c. c. 3.13.1). For all, 80 ng of the respective purified PCR product were sequenced by the Microsynth Seqlab GmbH (Göttingen, Germany) with the respective sequencing primer (compare Table 15 RIG-I fwd. and chapter 3.13.1.1 Table 26 PB2 Seq fwd. or PB2 Seq rev.). The sequencing reaction is described in Table 18. The sequencing results were compared to the RIG-I WT sequence or the IAV/PR/8 PB2 sequence to detect differences in the nucleic acid sequence with a BLAST alignment tool (NIH).

Table 18: The master mix used for Sanger-sequencing.

Component	Quantity
DNA	20 ng per 100 bp
Sequencing primer (10 µM)	3 µl
Up water	Fill to 15 µl

Table 19: The RIG-I genotype variants of the three mouse lines (starting at codon -4 downstream of codon 271 of C57BL/6J RIG-I WT). The codon 271 is marked green. One option of the 5 nt loss in the RIG-I KO mouse is marked red (GTTGT deletion is possible as well). The location where the 5 nt deletion was located in the RIG-I KO mouse is marked blue. The wobble mutations preventing targeting of the repair-oligonucleotide are still found in the RIG-I PM genotype and are marked orange.

Genotype	Sequence
RIG-I WT	AAA GGT TGT GGA AAA ACC TTT GTG
RIG-I PM	AAA GGT TGT GGA GCA ACA TTC GTG
RIG-I KO	AAA GGG AAA AAC CTT TGT G

3.4. *The amplification of IAV/PR/8 Δ NS1 virus in chicken eggs*

An important tool of IAV immune evasion is the NS1 protein. It potently represses innate immune signaling pathways like the IFN-1 response. To study RIG-I-mediated IFN responses due to IAV infection, initial experiments with a recombinant complete IAV strain suggested the requirement of using an IAV strain lacking the NS1 protein (IAV/PR/8 Δ NS1). Since IAV Δ NS1 strains do not replicate well in cell lines with functional innate immune responses, it was required to use a system without mature innate immune response. Hence, chicken eggs were used for virus propagation.

Fertilized eggs from SPF-held chickens (Valo Biomedica GmbH, Osterholz-Scharmbeck, Germany) were incubated at 37 °C for seven days in a breeding chamber (Grumbach), in which eggs were turned around automatically in intervals. An infection of the eggs at day seven is necessary to prevent maturation of important components of the chicken immunity, which is important for the successful generation of the weakened IAV strain lacking the NS1 protein. The eggs were checked with a Schier-lamp for the presence of an embryo and eggs without embryos were removed. Eggs with an embryo were turned upside-down, a hole was drilled into the air chamber of the egg and 1000 FFU of virus diluted in 100 μ l of DPBS def. were injected into the allantois cave. Infected eggs were bred for further 2 d at 37 °C in a cell culture incubator and then incubated at 4 °C o. n. The next day, the eggs were opened and the allantois fluid from infected eggs was harvested and batched into 1 ml aliquots. The batches were stored at -80 °C and the virus load was determined with a single cell infection assay (SCIA) as described later on (c. c. 3.13.2).

3.5. *Extraction of primary mouse cells*

For the validation, if the RIG-I mutations are sufficient to inactivate the different functions of the protein, initial experiments with primary cells derived from the homozygous mouse lines were performed. Bone marrow derived cells were differentiated to macrophages *in vitro* and treated with different innate PRR agonists to investigate alterations in the respective signaling pathways.

RIG-I WT, PM and KO mice were sacrificed by cervical dislocation, fixed back down and disinfected with 70 % Ethanol (EtOH). Femur and tibia were extracted from the mice and transferred to a 10 cm dish on ice. The bone caves were opened at both sides carefully, the bone marrow was rinsed out with 10 ml RPMI cont. 10 % FCS, 1 % P/S, 1 % Q and 0.1 % β -Mercapto-ethanol (RPMI comp.). Following, the bone marrow cells were separated by rinsing with medium, transferred to a 50 ml container and centrifuged at 500 RCF in a laboratory centrifuge for 7 min. The medium was removed and then the cells were suspended in 3 ml erythrocyte-lysis buffer (compare Table 5) for 5 min.

Afterwards, the reaction was stopped by addition of RPMI comp. and the suspension was centrifuged at 500 RCF for 7 min. The medium was removed and the cells were suspended in 10 ml RPMI comp., mixed 1:2 with eosin and counted in a Neubauer-chamber. At least two big corner quadrates were counted and the mean cell count was calculated. The cell count per μl was calculated by multiplying mean cell count with the dilution factor 2 and by 10 to derive cells per μl (compare Formula 1). In general, 30 to 60 x 10⁶ cells per mouse can be expected.

Formula 1: Calculation of the cell count per μl with a Neubauer-chamber.

$$\text{mean cell count} = \frac{\text{sum of counts in corner quadrates}}{\text{number of used corner quadrates}}$$

$$\text{cells per } \mu\text{l} = \text{mean cell count} * 20$$

3.6. *In vitro generation and treatment of bone marrow derived macrophages*

To generate bone marrow derived macrophages (BmdM Φ) from bone marrow cells *in vitro*, 5 x 10⁶ bone marrow cells extracted from the mice were seeded in 10 ml RPMI comp. containing 20 ng/ml murine macrophage-colony stimulating factor (mM-CSF, Peprotech) in 10 cm dishes without coating to prevent strong adhesion (Corning). The cells were incubated for 5 d at 37 °C and 5 % CO₂ and the same dose of mM-CSF was added again at day 3 after the first stimulation. After 5 days, the medium was removed, the cells were washed with DPBS def. and then incubated for a minimum of 15 min at 37 °C with 5 ml deadhesion buffer (DPBS def. containing 3 % FCS and 2 mM EDTA, also compare Table 5). Afterwards, the cells were rinsed with a 1 ml pipette from the plate and transferred to a 50 ml container containing RPMI comp. The cells were centrifuged at 500 RCF for 7 min at 4 °C in a laboratory centrifuge, medium was substituted with 10 ml RPMI comp. and a sample of the cells was diluted 1:2 with eosin. The cell concentration was determined in a Neubauer-chamber as described (compare Formula 1).

BmdM Φ were seeded 0.1 x 10⁶ per well in 96-well plates with flat bottom (Greiner) and incubated for 1 h at 37 °C. Afterwards, the cells were stimulated with different ligands of innate PRRs, were infected with a recombinant WT IAV/PR/8/1934 (H1N1) strain, an IAV/PR/8/1934 Δ NS1 strain from chicken eggs or a Sendai virus strain from chicken eggs (compare Table 4 for cell culture stimuli, compare Table 9 for virus strains, all ligands and virus strains are additionally summarized in Table 20). Appropriate negative controls for the respective treatment conditions with vector reagents or

for infections were chosen as well. After the treatment, the cells were incubated for 16 h at 37 °C and 5 % CO₂. In the following, the cell culture supernatant was transferred to 96-well U-bottom plates (Sarstedt) and stored at -80 °C until further processing. The medium was analyzed for its concentration of murine IFN- α (mIFN- α) and murine Interleukin 6 (mIL-6) by ELISA.

Table 20: Summary of the treatment conditions for the BmdM Φ .

Ligand/virus strain	Used concentrations	Vector/ 0 ctrl.	Function
CpG 2216	1 μ M	None/ medium	TLR9 agonist
LPS	2 ng/ μ l	None/ medium	TLR4 agonist
Pam3Cys	5 ng/ μ l	None/ medium	TLR1/2 agonist
Plasmid DNA	5; 1; 0.2 ng/ μ l	Lipofectamine	cGAS/STING agonsit
5'ppp-dsRNA	1 ng/ μ l	Lipofectamine	RIG-I agonist
3p-hpRNA	100; 50; 25 pg/ μ l	Lipofectamine	RIG-I agonist
IAV/PR/8 complete	9; 3; 0.6 MOI	None/ medium	IFN induction
IAV/PR/8 ΔNS1	9; 3; 0.6 MOI	None/ allantois fluid	IFN induction
Sendai virus	9; 3; 0.6 MOI	None/ allantois fluid	IFN/IL-6 induction

3.7. ELISA

For the investigation of differences in PRR activation depending on RIG-I variant expression, the IFN- α and/or IL-6 level in cell culture supernatant of treated or infected BmdM Φ was determined with a respective enzyme-linked immunosorbent assay (ELISA). Similarly, the level of IFN- α and IFN- β was measured in the BALF of IAV infected mice.

For murine IFN- α , IFN- β and mIL-6 ELISA, 96-well ELISA plates (Thermo) were coated with the respective antibody (compare Table 13) in DPBS def. o. n. at 4 °C. Afterwards, the antibody dilution was removed and the plates were blocked with 250 μ l ELISA blocking buffer (compare Table 5) for 1 h at RT. Following, the buffer was removed, plates were washed with ELISA washing buffer (compare Table 5) in an ELISA washer (Molecular Devices), standards were added in 50 μ l ELISA blocking buffer and 50 μ l samples were added (mIFN- α and β) or diluted 1:5 in ELISA blocking buffer (mIL-6) (compare Table 5). After 1 h (IFN- β) or 1.5 h (IFN- α and IL-6) of incubation at RT the samples and standards were removed and the plates were washed with ELISA washing buffer in the washer. If the

samples potentially contained infectious virus particles, the samples were manually removed and the following wash step was performed manually, too. Afterwards, the respective detection antibodies were added in 50 μ l ELISA blocking buffer and incubated for 1 h (IL-1 β) or 1.5 h (IFN- α and IL-6) at RT. In the following, the dilutions were removed, the plates washed with ELISA washing buffer in the washer and the respective conjugate or antibody carrying a horseradish peroxidase (HRP) enzyme was added in 50 μ l ELISA blocking buffer. After 1 h (IFN- α and β) or 30 min (IL-6) incubation at RT, the dilutions were removed and the plates were washed with ELISA washing buffer in the washer. 50 μ l ELISA substrate buffer containing 1 mg/ml (w/v) o-phenylenediamine dihydrochloride (OPD) and 0.03 % H₂O₂ (compare Table 5) were added and the plates were incubated for 10 to 20 min in the dark. When the standards were well developed, the reactions were stopped with 2 M H₂SO₄ and the absorption at 490 nm was measured against a reference absorption of 650 nm with an EMax plate photometer (Molecular Devices). The result processing was performed with the SoftMax Pro v5 software (Molecular Devices), MS Excel (Microsoft) and GraphPad Prism 9 (Graphpad Software Inc.).

3.8. *BCA*

To quantify protein in cell lysates to adjust the input for Western blots (WB), a BCA assay was performed. For the generation of cell lysates, 10⁷ cells were suspended in 1.5 ml RPMI comp. containing 1 U/ μ l universal IFN- α (PBL, compare Table 4) and seeded in 6-well plates (Sarstedt). The following day, medium was removed carefully and the cells were harvested in 150 μ l triton X cell lysis buffer (DPBS def. containing protease inhibitor, NaF, Na₃VO₄, EDTA and 1 % Triton X 100; compare Table 5). The cells were harvested with help of a 1 ml syringe plug; then the cell suspension was transferred to a 1.5 ml container and incubated by overhead rotation for 30 min at 4 °C. The protein concentration was determined with a Pierce BCA Protein Assay Kit (Thermo) according to the manufacturer's manual. The absorption by the dye complex at a wavelength of 490 nm was measured with an EMax photometer (Molecular Devices) and the Soft Max Pro v5 software (Molecular Devices).

3.9. *Western blotting*

Proteins can be blotted on membranes via electrophoresis and specific proteins can be detected with a primary antibody. The resulting complex can be visualized by detection with a secondary antibody, labelled with an enzyme like HRP. By the addition of a substrate dilution, the HRP-mediated chemiluminescence can be detected on the membrane and marks the location of the detected protein. By comparison with a marker, the size of the protein can be determined.

For WB, 20-30 µg protein were diluted in 20 µl DPBS def. and mixed with 4 µl 6x Lämmli sample buffer (compare Table 5). The samples were heated 10 min at 95 °C and put on a sodium-dodecyl-sulfate-polyacrylamide gel electrophoresis (SDS-PAGE) ready-to-use gel (Expedeon or Abcam) with 1x RunBlue™ buffer (Abcam). SDS-PAGE was started with 80 mV for 20 min and performed with 110 mV until the smallest marker of the buffer reached the lower end of the gel. Afterwards, the borders of the gel were cut and it was washed in 1x WB transfer buffer (compare Table 5). Three Whatman papers (Schleicher and Schuell) were soaked with 1x WB transfer buffer and stacked on a semi-dry WB aperture (Thermo). An Immobilon-P PVDF membrane (Merck) was activated in 100 % methanol (MeOH, Roth), washed in 1x WB transfer buffer and stacked on the Whatman papers. The gel was now stacked on top, as well as 3 additional soaked Whatman papers. It had been taken care that a sufficient amount of 1x WB transfer buffer was in between the layers and that potential air inclusions were removed. The blotting process was performed at 39 mA for 1h and 10 min. After blotting, the membrane was blocked with WB block buffer (compare Table 5) for 1 h. After blocking, the membrane was put upside down on a glass plate covered with 2 ml WB block buffer containing the respective primary antibody (compare Table 13), in a humid chamber. The reaction was incubated o. n. at 4 °C. The next day, the membrane was washed with WB wash buffer (compare Table 5) three times and then incubated in 9 ml WB block buffer containing the secondary antibody (compare Table 13). After 1.5 h, the membrane was washed again three times in WB wash buffer and transferred into DPBS. For development, 2 ml Super signal west ECL or Dura (Thermo) substrate solution were prepared referring to the respective manufacturer's manual and added to the blot. Afterwards, the membrane was covered with a transparent foil and the development of chemiluminescence was detected with a ChemiDoc imaging system and the Image Lab software (Bio-Rad). If the chemiluminescence signal after application of the ECL solution was too low, the membrane was washed with DPBS and the Dura solution was added, enabling a detection with higher sensitivity. After chemiluminescence detection, a colorimetric picture of the ladder was taken, both images were merged with the Image Lab software (Bio-Rad).

Afterwards, the membrane was washed with DPBS and then stripped with the Restore PLUS Western blot stripping buffer (Thermo). After 15 min incubation at RT, the membrane was blocked again with WB block buffer. The membrane was then incubated for 1 h at RT with 9 ml WB block buffer containing anti human/mouse β -actin antibody in a 1:1000 dilution (compare Table 13). After washing 3 times with WB wash buffer, the membrane was incubated with 9 ml WB block buffer containing anti-mouse antibody conjugated with HRP in a 1:5000 dilution for 1 h at RT. After three times washing with WB wash buffer, the membrane was put into DPBS, treated with Super Signal West ECL (Thermo) and chemiluminescence was analyzed with a ChemiDoc imaging system and the Image Lab software, as described. Pictures from chemiluminescence and colorimetric were merged again and saved as JPEG file.

3.10. *WB signal semi-quantification*

To get a more detailed result from a WB, the resulting band intensity can be semi-quantified with an area under the curve (AUC) determination. This method was applied by using the open source ImageJ software (NIH). Using this approach, the band intensity of the mRIG-I WBs and respective β -actin WBs was semi-quantified to compare the RIG-I and β -actin band intensity between RIG-I WT, PM and KO mouse derived cells. The mean band intensities of three independently performed experiments were calculated and analyzed with a t-test for significant differences. The t-test was performed with the software GraphPad Prism9 (Graphpad Software Inc.) (also c. c. 3.19.7).

3.11. *Murine embryonal fibroblasts*

To perform initial *in vitro* experiments with recombinant IAV strains to test their compatibility with the mice, murine embryonal fibroblasts (MEF) were generated as non-immortal cell lines. The lines were generated in house from homozygous RIG-I WT, PM and KO mouse lines by Prof. Dr. Stefan Bauer. Mouse embryonal tissue was digested with 1x Trypsin for 20 min at 37 °C. The suspension was well mixed afterwards to separate the cells from each other. The digestion was stopped by addition of RPMI-MEF medium (compare Table 6). The cell suspension was additionally passed through a 70 μ m sterile cell strainer (Thermo) afterwards and centrifuged at 500 RCF for 5 min. The supernatant was removed and the cells were resuspended in RPMI-MEF medium. Afterwards, the cells were seeded in T75 cell culture flasks and incubated at 37 °C in a 7.5 % CO₂ atmosphere. The next day, the cells were investigated for viability by light microscopy and samples from the cells were separated for genotyping as well as protein analysis. Afterwards, the cells were splitted 1:2 to a new T75 flask. When they densely covered the flasks, the cells were harvested, suspended in freeze medium (50 % FCS, 40 % RPMI-IM, 10 % DMSO, compare Table 6) and stored in liquid nitrogen at -196 °C.

3.12. Generation of recombinant IAV

3.12.1. A plasmid system for the generation of recombinant virus

For IAV infection experiments with the established mouse lines, recombinant IAV strains with well-known characteristics and protein sequences were generated. Therefore, the eight plasmid system introduced by Hoffmann *et al.* (Hoffmann E. 2000), modified like described by Czudai-Matwich *et al.* (Czudai-Matwich V. 2013) to code for IAV/PR/8/1934 (H1N1), was used. The eight pHW2000 vector based plasmids each code for one of the eight IAV RNA genes (HA, NA, NP, M, PA, PB1, PB2 and NS, compare also Table 12). The original PB2 plasmid codes for the amino acid (aa) 627K variant. The method of primer-mediated mutagenesis was used for sequence-editing to generate a plasmid variant coding for the aa 627E variant instead of 627K, which reflects a sequence common in avian IAV strains (c. c. 1.2.6.2). This can be achieved by substitution of the nt 1879 from A to G, leading to a switch of the aa 627 from K to E.

The desired mutation was achieved in two PCR steps. In the first one, the pHW2000-PB2 plasmid was used as template. Two different reactions were performed in parallel (primer A and B; C and D, compare Table 21 primer, Table 22 master mix and Table 23 cyclor program), with primer A and D carrying the target sites for a restriction enzyme (A: Mph 1103-I and D: EcoRI). Both enzymes cut the PB2 gene and the vector only at one site. The primer B and C are completely complementary to each other and cover the location where the mutation needs to be placed. Additionally, both primer contain a single nucleotide mismatch to the pHW2000-PB2 vector, which is the equivalent to the PB2 nt 1879 G., changing the codon PB2-627 from AAG (aa K) to GAG (aa E) (compare Figure 5). The resulting PCR products were analyzed by agarose-gel electrophoresis (AGE) using 1 % agarose gels, 1 x TAE buffer and the GeneRuler 1 kb DNA ladder (Thermo) (compare Table 6 gel and Table 11 marker). Bands with the correct size of 607 bp (A + B) and 398 bp (C + D) were excised and purified with a gel purification kit (Thermo) (gel image not shown). For the second PCR step, the two purified PCR products from the first PCR step were mixed in an equal ratio and were used as template. The PCR was performed with the two primer carrying the target sites for restriction enzymes (primer A and D), to get the completely covered sequence amplified. The PCR product was analyzed again by AGE, the band with the correct size of 980 bp was excised and purified with a gel purification kit as described (gel image not shown). The complete process is simplified in Figure 6.

In the next step, the original pHW2000-PB2 vector was cleft with the restriction enzymes Mph1103-I and EcoRI (Thermo) in a restriction reaction with the buffer R (Thermo) at 37 °C o. n. (compare Table 24) and also analyzed by AGE (image not shown). The restricted plasmid was excised from the gel

and purified as described. Similarly, the purified PCR product was cleft with Mph 1103-I and EcoRI at 37 °C o. n. Afterwards, it was purified from the restriction components with a PCR purification kit (Thermo). Both the purified restricted plasmid and the PCR product were set into a ligation reaction using a T4 DNA Ligase kit (Thermo), which was incubated for 10 min at 25 °C (compare Table 25). In the following, the ligation reaction was used to transform *Escherichia coli* (*E. Coli*) DH-5 α (compare Table 7 for the bacteria strain). For this, bacteria were unfrozen on ice, mixed with the complete ligation reaction and incubated 30 min on ice. Afterwards, the bacteria were heat-shocked for 20 sec at 42 °C and incubated another 2 min on ice. The transformed bacteria were transferred to a LB-agar plate containing 100 μ g/ml ampicillin (compare Table 6) and spread over the plate in three sectors to achieve different growth densities. As a negative control, untransformed bacteria were spread on an additional plate. The plates were incubated at 37 °C until single bacteria colonies were detectable. Six colonies were picked separately and transferred to 3 ml liquid LB medium containing 100 μ g/ml ampicillin in bacteria containers (Corning). The liquid cultures were incubated at 37 °C o. n. while shaking. The next day, containers were spun at 500 RCF for 5 min at RT in a laboratory centrifuge (Hettich), the supernatant was removed and the plasmid DNA from the bacteria was extracted with a GeneJET Plasmid Miniprep kit (Thermo) according to the manufacturer's manual. The plasmid DNA was eluted with 40 μ l up water. The plasmid DNA concentration was determined with a NanoDrop device (Thermo).

Table 21: The primer required for primer-mediated mutagenesis of the pHW2000-PB2 plasmid. The primer were derived from the Metabion GmbH (Planegg, Germany).

Primer name	Sequence	Melting temperature (°C)	Function
PB2-627E_A	TCCTATGCATCAACTTTTAAGACATTTTCAGA	57.0	Contains Mph1103-I restriction site
PB2-627E_B	CATTCTACTTTGCTCTGGTGGAGCG	59.6	Contains mutation
PB2-627E_C	CGCTCCACCAGAGCAAAGTAGAATG	59.6	Contains mutation
PB2-627E_D	TCCGAATTCTTTTGGTCGCTGT	57.1	Contains EcoRI restriction site
PB2 Seq fwd.	CAGTGGTCCCAGAACCCTAC	57.0	For sequencing
PB2 Seq rev.	CGCAAGGTTGCTCAGTTCATTG	57.0	For sequencing

Table 22: The master mix used for the PCR reactions.

Component	Quantity
Phusion HF buffer (5x)	10 µl
Primer fwd. (10 µM)	2.5 µl
Primer rev. (10 µM)	2.5 µl
dNTPs (10 mM)	1 µl
DNA template	250 ng
Phusion polymerase	0.5 µl
Up water	Fill to 50 µl

Table 23: The cycler program used for the PCR reactions.

Step	Temperature (°C)	Duration	Cycles
Initial denaturation	98	30 sec	1
Denaturation	98	10 s	25
Annealing	60	30 s	
Extension	72	1 min	
Final extension	72	10 min	1
Conservation	4	infinite	

Codon PB2 627K



Codon PB2 627E



nt 1879

Figure 5: Overview of the IAV PB2-627 codon. The first nucleotide (1879) of the IAV PB2-627K codon was changed from A to G with primer-mediated mutagenesis to generate the IAV PB2-627E variant.

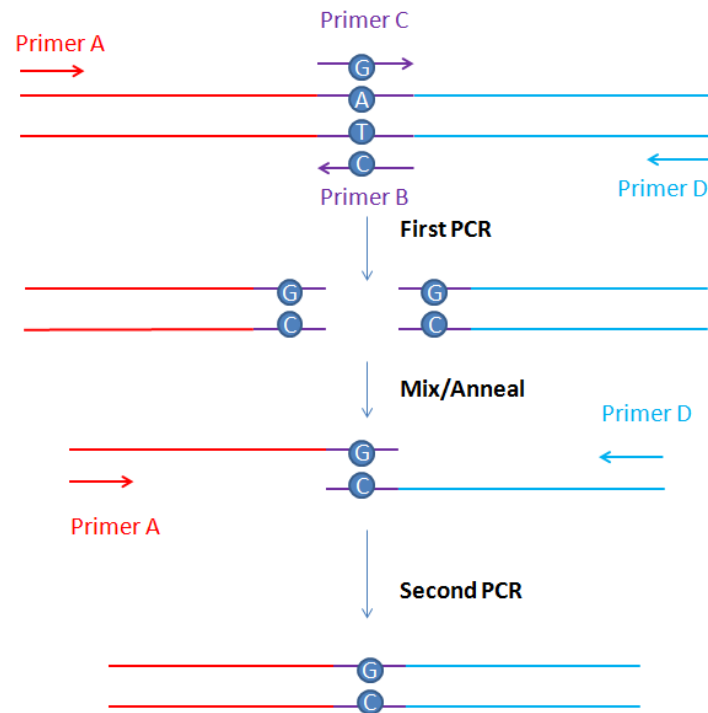


Figure 6: A Schematic depiction of the primer-mediated mutagenesis strategy. The primer B and C carry the PB2 nt 1879 mutations for the PB2 codon 627K to 627E mutation and are depicted violet. The amplicons generated in the first PCR step are depicted red and blue (with primer A + B and C + D). Both the red and the blue amplicons are mixed and anneal by complementarity of the violet areas. In the second PCR step, the annealed amplicons are completed and multiplied with the primer A and D, which also contain target sites for the restriction enzymes Mph1103-I and EcoRI (not depicted), with which the complete PCR products can be inserted into an opened pHW2000-PB2 plasmid.

Table 24: The master mix for the restriction reactions.

Component	Quantity
Buffer R (10x)	3 μ l
Mph1103-I	1 μ l
EcoRI	1 μ l
DNA	2 μ l pHW2000-PB2 or 25 μ l insert
Up water	Fill to 30 μ l if required

Table 25: The ligation reaction.

Component	Stock concentration	Final concentration
Ligation buffer	10x	1x
T4 DNA ligase	1 Weiss U/ μ l	0.05 Weiss U/ μ l
Restricted pHW2000 PB2		50 ng
Restricted PCR insert		Fill to 20 μ l

3.12.2. *Virus assembly*

To assemble virus particles, HEK293 cells (compare Table 7) were transfected with the eight plasmids coding for the IAV proteins. Therefore, 3×10^6 HEK293 cells were seeded in T25 flasks and incubated o. n. at 37 °C at 7.5 % CO₂. The transfection mix consisted of 1 μ g from each of the eight different plasmids in 1 ml OptiMEM containing Lipofectamine 2000 (Thermo) 1:20, which were incubated 20 min at RT together. Before transfection, the cells were washed with DPBS def. and then 4 ml OptiMEM and the transfection mix were added. After an incubation of 6 h at 37 °C, medium was substituted with 4 ml DMEM-IM (containing 0.1 % BSA, 1 % Pen/Strep and 1 % Glutamine, compare Table 6). Cells were incubated for further 72 h while 7.5 % bicarbonate buffer was added if the medium turned towards yellow, to prevent a conformation change of the HA. After 72 h, the medium was harvested and cell debris was removed by a 10 min centrifugation at 500 RCF and 4 °C in a laboratory centrifuge. The supernatant was batched in 1 ml aliquots, 1 μ g/ml TPCK-Trypsin (Sigma-Aldrich) was added and the aliquots were incubated 1 h at 37 °C before storage at -80 °C.

3.12.3. *Virus multiplication*

To enrich the virus particles assembled in HEK293 cells, the Trypsin-treated cell culture supernatants were used to infect different mammalian cell lines. Of those, only DF-1 chicken cells turned out to be sufficient host cells for the IAV PB2-627E strain, while the IAV PB2-627K strain replicated efficiently in all cell lines tested.

For the enrichment of both the IAV PB2-627K and -627E strain, 1×10^6 DF-1 immortalized chicken fibroblast cells were seeded in T25 flasks and incubated o. n. at 37 °C in a 7.5 % CO₂ containing atmosphere. HEK293 supernatants were mixed with 4 ml DMEM-IM, 50 μ l 7.5 % Bicarbonate buffer and TPCK-Trypsin to a concentration of 1 μ g/ml. Cells were washed with DPBS +/- and the infection

mix was added. The cells were incubated for 72 h at 37 °C and 7.5 % CO₂, until medium was harvested and processed as described in the previous chapter.

To quantify the amount of virus particles in the supernatant, it was determined with a SCIA, which will be described later on (c. c. 3.13.2). To validate enrichment of the correct virus particles, the PB2 codon 627 sequence was analyzed by Sanger-sequencing (c. c. 3.3 and 3.13.1).

In a second multiplication step, 7×10^6 DF-1 cells were seeded in different T175 flasks, incubated o. n. and the cell amount of one flask was counted in a Neubauer-chamber (compare Formula 1). After washing with DPBS +/+, the cells were infected with recombinant IAV PB2-627K and -627E strain candidates from DF-1 cells of a 0.001 multiple of infection (MOI, 0.001 virus particles per cell in the flask) in 25 ml DMEM-IM containing 70 µl 7.5 % Bicarbonate buffer and TPCK-Trypsin (1 µg/ml). After 30 h, a cytopathic effect was visible and cell culture supernatants were harvested, batched in 10 ml aliquots and processed as described above (c. c. 3.12.2). The digested 10 ml aliquots were pooled again and batched in 2 ml virus containers with screw top. Afterwards, the aliquots were frozen and stored at -80 °C. The recombinant virus stocks were analyzed and compared for different quality criteria as described in the following chapters.

3.13. The validation of the recombinant IAV PB2 stock quality

3.13.1. The validation of the IAV PB2-627 codon with Sanger-sequencing

3.13.1.1. Basic procedure

As mentioned before, also the sequence of the IAV PB2-627 codon was validated by Sanger-sequencing (c. c. 3.3). Therefore, 300 µl culture supernatant of the infected DF-1 cells were used for RNA isolation with an ExtractMe easy RNA kit (Blirt), which was executed as indicated in the manufacturer's manual. The isolated RNA was used for a reverse-transcription with a Revert Aid first strand cDNA kit (Thermo) and a primer complementary to the IAV RNA-genome segments (Hoffmann E. 2001), for a more selective reaction (compare Table 26 primer, Table 27 master mix and Table 28 cycler program). Afterwards, the PB2 cDNA was amplified with a DreamTaq Green PCR Master Mix (Thermo) (compare Table 26 primer, Table 29 master mix and Table 30 cycler program). Finally, the PCR products were purified with a PCR purification kit (Thermo), the DNA concentration in the samples was measured with a NanoDrop device as described and Sanger-sequencing was performed by the Microsynth Seqlab GmbH (Göttingen, Germany) as described before (c. c. 3.3).

Table 26: Primer used for the IAV PB2 sequencing process. The primer were derived from the Microsynth Seqlab GmbH (Göttingen, Germany).

Primer	Sequence	Function	Melting T (°C)
IAV RT primer	AGCAAAAGCAGG	Complementary to IAV RNA gene segments	
IAV PB2 Seq fwd.	CAGTGGTCCCAGAACCCTAC	PCR and sequencing	57.0
IAV PB2 Seq rev.	CGCAAGGTTGCTCAGTTCATTG	PCR	57.0

Table 27: The master mix used for the cDNA synthesis.

Component	Quantity
RT buffer (5x)	4 µl
IAV RT primer (10 µM)	4 µl
dNTP	2 µl
RiboLock RNase Inhibitor	1 µl
Reverse transcriptase	1 µl
Eluted RNA	8 µl

Table 28: The cyler program used for the cDNA synthesis.

Step	Temperature (°C)	Duration
Annealing	65	5 min
Initialization	25	5 min
Reverse-transcription	42	1 h
Termination	70	5 min
Conservation	10	infinite

Table 29: The master mix used for the PCR.

Component	Quantity
DreamTaq Green Master Mix (2x)	12.5 µl
Primer PB2 Seq fwd. (10 µM)	0.5 µl
Primer PB2 Seq rev. (10 µM)	0.5 µl
cDNA	3.5 µl (undiluted)
Up water	Fill to 25 µl

Table 30: The cycler program used for the PCR reactions.

Step	Temperature (°C)	Duration	Cycles
Initial denaturation	95	3 min	1
Denaturation	95	30 s	40
Annealing	60	30 s	
Extension	72	1 min	
Final extension	72	10 min	1
Conservation	10	infinite	

3.13.1.2. Complete PB2 gene sequencing

To prove the genetic stability of the complete IAV PB2 RNA gene segment, its sequence was analyzed by a combination of Sanger-sequencing reactions. This procedure was used to validate the PB2 sequence of the recombinant IAV PB2-627K and -627E strains in the P1 and P2 stages during stock generation. For further analysis, only the PB2-627 codon containing area was analyzed, as described in the previous chapters.

The isolation of virus RNA from cell culture supernatant and cDNA synthesis was performed as described in the previous chapter. The amplification of the cDNA in a PCR reaction was performed in two pieces. The first half was amplified with the primer 5' UTR fwd. and quart 2 rev. and the second half with the primer 941 fwd. and 3' UTR rev. (compare Table 31 primer, compare also chapter

3.13.1.1). Next, the PCR reactions were purified with a PCR purification kit (Thermo). The first half was Sanger-sequenced with the primer 5' UTR fwd., 401 rev. and 717 fwd. The second half was Sanger-sequenced with the primer 941 fwd. and PB2 Seq fwd. The Sanger-sequencing was ordered at the Microsynth Seqlab GmbH as described (c. c. 3.3 and Table 31). The sequence data were analyzed with BioEdit (Ibis Biosciences) and ChromatQuantitator (University of Washington).

Table 31: The primer used for the complete PB2 Sanger-sequencing.

Primer	Sequence	Use	Melting T (°C)
PB2 5' UTR fwd.	GGGAGCGAAAGCAGGTCAAT	PCR and sequencing	57.9
PB2 401 rev.	GCCAAAGGTTCCATGCTTTAGC	sequencing	57.1
PB2 717 fwd.	GACTCAAGGAACATGCTGGG	sequencing	55.9
PB2 941 fwd.	ATATGCAAGGCTGCAATGGG	PCR and sequencing	56.1
PB2 quart 2 rev.	GGCCACAATTATTGCTTCGGC	PCR and sequencing	57.4
PB2 Seq fwd.	CAGTGGTCCCAGAACCCTAC	sequencing	57.1
PB2 3' UTR rev.	GTAGAAACAAGGTCGTTTTTAAAC	PCR and sequencing	50.8

3.13.2. *Virus titration with a single cell infection assay*

For controlled virus infections, a virus titration is required. With a SCIA, the infectious virus particles in a sample can be quantified.

Therefore, Madin-Darby canine kidney cells (MDCK) were seeded by a quantity of 25×10^3 cells per well in a 96-well plate and were incubated o. n. at 37 °C and 7.5 % CO₂. The next day, virus samples were diluted 1:10 in DMEM-IM in a 96-well U-bottom plate and a 1:10 dilution row for 3 to 7 additional dilutions was prepared, depending on the expected virus load in the respective samples. A previously analyzed virus sample was prepared similarly and used as a positive control. The medium from the MDCK cells was substituted with the prepared sample dilutions or with IM without virus as a negative control. Infected cells were incubated for 1 h at 37 °C before the inoculum was substituted with DMEM-IM again. The cells were incubated for 16-18 h until medium was removed and cells were fixated with 100 µl DPBS def. containing 4 % paraformaldehyde (PFA) at 4 °C for 30 min. Afterwards, the PFA was removed and cells were washed with DPBS +/- . In the next step, 100 µl SCIA permeabilization buffer (DPBS +/- containing 0.3 % Triton-X 100 and 20 mM glycine, compare Table

5) were added for 30 min at RT to permeabilize the cell membranes of the fixated cells. Afterwards, the solution was removed and cells were washed with SCIA wash buffer (DPBS +/- containing 0.05 % Tween 20, compare Table 5). In the next step, 50 µl SCIA wash buffer containing an anti-NP antibody in a 1:5000 dilution (Abcam, compare Table 13) were added to the cells. Afterwards, the cells were incubated for 1.5 h at RT while shaking, the dilution was removed and the cells were washed with SCIA wash buffer. Next, 50 µl SCIA wash buffer containing a goat-anti mouse antibody coupled to HRP in a 1:2000 dilution was added (compare Table 13). Following, the cells were incubated for 1.5 h at RT while shaking, the dilution was removed and cells were washed twice with SCIA wash buffer. Afterwards, 50 µl True Blue substrate (KPL) containing extra 30 % H₂O₂ in a dilution of 1:1000 were added and the emerge of the staining was investigated with a light microscope (Leica Microsystems GmbH). After establishment of a dark blue staining in the positive control samples, the substrate was removed and the cells were washed once with autoclaved and deionized water to conserve the dye complexes. Following, the plates were stored protected from light. The next day, blue-stained cells in wells with a reasonable amount of positive cells were counted, the means of the technical replicates were calculated and the focal forming units per ml (FFU/ml) were calculated (compare Formula 2).

Formula 2: Calculation of focal forming units per ml.

$$\text{Focal forming units per ml} \left(\frac{\text{FFU}}{\text{ml}} \right) \\ = \text{mean of positive cells in technical replicates} * \text{well dilution} * 10$$

3.13.3. Virus titration with a hem-agglutination test

A quantification of the virus load in samples is also possible by the determination of the agglutination of erythrocytes by the viral HA protein. This titration variant is indicated as hem-agglutinating units per ml (HAU/ml).

For a hem-agglutination test, chicken erythrocytes were derived from the LDG Laboratory Diagnostics Germany GmbH (Cuxhaven, Germany). First, a 1 % (v/v) chicken erythrocyte suspension in DPBS def. was generated. Second, 25 µl DPBS def. were filled in a 96-well V-bottom plate (Greiner). In the next step, 25 µl of virus containing samples were added to the first row and 1:2 dilution rows were prepared, as technical duplicates. A previously analyzed IAV strain was used as positive control and DPBS without virus was used as negative control. Following, 25 µl of the 1 % erythrocyte dilution was

added to the wells, the plate was covered with foil and incubated for 45 min at RT in an area protected from tremor. Finally, the wells were analyzed for erythrocyte agglutination and the last well with detectable agglutination was used for the determination of the HAU titer per ml, as described in Formula 3. This titration variant was only done once because it did not deliver significantly required additional information.

Formula 3: The calculation of the HAU titer.

$$\frac{HAU}{ml} = \text{well dilution factor} * 40$$

3.13.4. *Virus titration with a plaque assay*

A plaque assay can be used to determine the amount of virus particles in a sample, which are able to replicate. In combination with other titration methods, the amount of defective virus particles can be assessed.

To quantify the replicating virus particles in the DF-1 virus stocks, a plaque assay on MDCK cells was kindly performed by the group of Prof. Dr. Eva Friebertshäuser, at the Institute for Virology of the Philipps-University Marburg. The results were indicated as plaque forming units per ml (PFU/ml).

3.13.5. *IAV M protein semi-quantification with Western blotting*

To investigate the amount of defective particles in the generated IAV strains, the IAV M protein was semi-quantified. Therefore, a volume containing one, two or four mio. FFU of the respective virus strain was centrifuged at 8×10^4 RCF in a laboratory centrifuge (Heraeus). The supernatant was removed up to a remain of 30 μ l. 6 μ l of 6x Lämmli buffer (compare Table 5) were added to the samples, which were well suspended and heated for 5 min at 95 °C afterwards. Detection of viral M-protein with WB was performed as described previously (c. c. 3.9), with the respective antibodies (compare Table 13). The semi-quantification of the band intensities was achieved with an AUC size determination procedure, as described previously (c. c. 3.10). The ratio between the size AUC of the IAV PB2-627E strain and -627K strain was calculated for the amount of set virus particles separately. In the end, the mean of the ratios for 1×10^6 and 2×10^6 FFU were calculated. The experiment was only performed once because it does not deliver significantly important additional information.

3.13.6. *Competitive infection assay in MEF*

For the purpose of comparing replication efficiency between the recombinant IAV PB2-627K and -627E strain in MEF lines differing in their RIG-I expression, a competitive infection assay was performed. Therefore, cells were infected with different mixing ratios of both virus strains. The virus particles in the infection mixes prior to infection, as well as the virus particles in the cell culture supernatants at the endpoint, were Sanger-sequenced, to investigate a change of the ratio between both virus strains.

RIG-I WT, PM and KO MEF cells were seeded 6.5×10^5 cells per well in a 6-well plate (Sarstedt) in RPMI-MEF medium one day prior to infection. The next day, the recombinant IAV PB2-627K and -627E strain generated in DF-1 chicken cells under similar conditions were mixed in RPMI-IM to different ratios: 100 % to 0 %, 75 % to 25 %, 50 % to 50 %, 25 % to 75 % and 0 % to 100 % (% IAV PB2-627K to % -627E), to achieve a MOI of 0.5 in complete. A sample from each infection mix was stored for sequencing at 4 °C. Afterwards, the medium was removed from the MEF cells, they were washed with DPBS ++ and the infection mixes were added for infection. The inoculum was substituted with RPMI-IM one h post infection. The infected cells were incubated for 4 d before the cell culture supernatant was harvested. The virus particles in the supernatants were concentrated in 300 μ l by centrifugation at 8×10^4 RCF for 45 min in a laboratory centrifuge (Heraeus) before the viral RNA was extracted with an ExtractMe Total RNA kit (Blirt). The RNA was reverse-transcribed into cDNA and used in a PCR reaction to amplify the regions flanking the PB2-627 codon as described (c. c. 3.13.1.1). The PCR reaction was purified with a PCR purification kit following the manufacturer's manual (Thermo). Afterwards, the concentration of the purified PCR reaction was measured with a NanoDrop device and Sanger-sequencing was ordered at Microsynth Seqlab as described (c. c. 3.3). The nt distribution at the position 1879 of the viral PB2 gene was read out with the ChromatQuantitator open-source web tool (University of Washington) and the percentage nt distribution was calculated. The nt 1879 of the viral PB2 gene is the first nt in the PB2 aa 627. An nt A at the position results in the codon AAG, coding for the aa 627K (mammalian adaptation), while a nt G at the position results in the codon GAG, coding for the aa 627E (avian adaptation) (compare Figure 5). For the generation of the avian-adapted strain, the nt 1879 A was substituted with G via primer-mediated mutagenesis. The means of three independent experiments were calculated and depicted as mean nucleotide percentage distribution in a stacked bar plot with the respective standard deviation (for a description of the stacked bar plot, c. c. 3.19.3). For statistical analysis, only the samples from cells infected with both virus strains were compared for differences in the nucleotide G percentage abundance, as indicated in the respective result figure. Therefore, a 2-Way ANOVA was used to indicate significant effects of the factors "RIG-I genotype" (and "infection mix

ratio") on the variable "PB2 nt 1879 G abundance" (for a more detailed ANOVA description c. c. 3.19.8).

Additionally, MEF cells were infected with either the IAV PB2-627K or -627E virus strain alone (100 % to 0 %; 0 % to 100 %). These were analyzed as negative controls, since no competition should occur in these settings, indicated by no differences between the nucleotide distribution in the infection mixes and the cell culture supernatants. These samples were also used for the validation of the absence of a possible contamination of the virus stock preparations with the opposite virus strain or for the occurrence of (back) mutations, which were found during propagation of the IAV PB2-627E strain in mammalian cell lines (c. c. 4.3.2). Therefore, it was expected that a contamination or back mutation in the avian-adapted IAV PB2-627E strain to the mammalian-adapted IAV PB2-627K strain would result in overgrowth of the first by the latter, indicated by a change in the nt 1879 distribution in the favor of A.

3.14. *The mouse study plan*

The mouse infection study was permitted by the Regierungspräsidium Gießen (reference number G7-2019). The aim of the study was to investigate the effect of the different RIG-I functions in the defense vs. IAV. Therefore, mouse lines expressing functional RIG-I (WT), signaling inactive RIG-I (PM) or no RIG-I (KO) should be infected with either an IAV PB2-627K strain, an IAV PB2-627E strain or treated with PBS only. Since the impact of RIG-I on the virus is dependent on different factors like virus strain, mouse line or time post infection, its effect on different infection parameters was hard to predict. Consequently, it was decided to initiate the investigation with an orientation study containing low n numbers but a high diversity of infection groups, to have the opportunity to compare the impact of many different factors on the infection parameters. In a possible second part of the investigation, it was aimed to investigate tendencies or small effects more detailed with an adapted study concept. This track was also chosen to respect the guideline of reduction, refinement and replacement (3R) (Russell W. M. S. 1959) to limit animal experiments to the minimum necessary extend.

The study groups contained two female and two male mice for any infection condition. Using the open source software G*Power (Heinrich Heine University, Düsseldorf, Germany) (Faul F. 2007), this group size was calculated to be sufficient to determine significant differences with a t-test between two independent means, at a significance level of 0.05 and a power of 80 %.

RIG-I WT, PM and KO mice were infected with either 1×10^2 IAV PB2-627K, 8.3×10^4 IAV PB2-627E or were treated with PBS. The endpoints were set at 4, 7, 10 or 14 days post infection (p.i.) and an additional group with 0 d p.i. was done for mock treated mice, as a reference. All groups are summarized in Figure 7 and described more detailed in Table 32. In total, 156 mice were used for the generation of the data sets. The day 0 groups were used to validate direct effects of the infection procedure and were not used for further analysis.

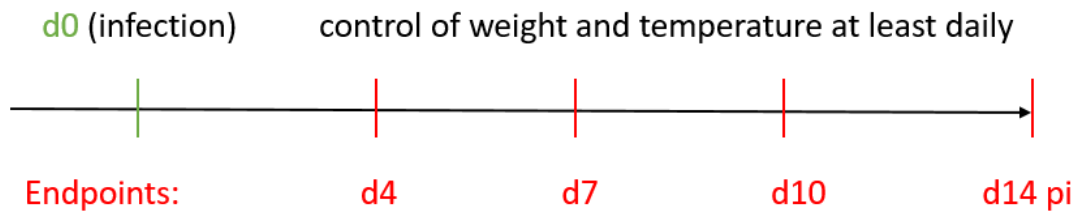


Figure 7: Overview about the endpoint schedule.

Table 32: The different infection and control groups of the mouse study.

Mouse line	RIG-I WT, PM and KO					
Infection	Endpoint					Sum
	d 0	d 4	d 7	d 10	d 14	
IAV PB2-627K	0	4	4	4	4	52 of each genotype
IAV PB2-627E	0	4	4	4	4	
PBS mock	4	4	4	4	4	

3.15. *The mouse infection procedure*

For the infection experiments, mice of an age between three and four months were used. The mice chosen for infection experiments were held in a laboratory permitted for animal keeping and S2 safety conditions. For the course of infection, it was prioritized to have two mice in one cage to respect the appropriate keeping standards, if possible. For all the different infection groups, two female and two male mice were chosen and analyzed for the respective parameters.

At day 0, the parameters weight and body temperature were determined prior to infection. Afterwards, the mice were anaesthetized with a 5 % Isoflurane/air mix derived from a vaporizer. The anaesthetized mice were fixated in the neck to establish a straight track between nose, trachea and the lungs. 35 μ l of DPBS def. pure (mock infection), containing 1×10^2 PFU IAV PB2-627K or 8.3×10^4 PFU IAV PB2-627E were applied into the mouse nostrils for infection. Afterwards, the mice were replaced to the cage and regain of consciousness was observed. From day 0 to the day of the endpoint, body weight and temperature were determined and documented daily and mice were checked up to two times daily for the fulfillment of abortive criteria to minimize animal suffering. To prevent rapid weight loss due to reduced hunger and dehydration during infection, up to 250 μ l of 0.9 % sodium chloride infusion dilution were injected subcutaneous up to four times daily to mice suffering from markedly weight loss.

At the day of the endpoint, the mice were taken from their cage and fixed in a fixation unit. The tail was exposed to a red-light lamp to enhance blood supply and 100 μ l fluorescein-5-isothiocyanate (FITC)-labeled albumin (1 mg/ml) was injected into one of the tail veins of the mouse with a 27G syringe tip. Approx. one h after FITC application, the mice received a lethal injection of 240 mg/kg body weight Ketamine and 30 mg/kg Rompun in sterile NaCl infusion dilution (this represents a three-fold overdose), which was applied intraperitoneal with a 24G syringe tip. After the loss of consciousness and the pain reflex in the legs, mice were sacrificed by bleeding of the left *angulus venosus*. The blood was collected in a 1.5 ml container and stored on ice. Mice were fixed on a preparation fixture, disinfected with ethanol, and then skin and thorax were opened. The trachea was punctuated and a Braun 18G trachea catheter was inserted. Following, the lungs were rinsed once with 1 ml lavage buffer (compare Table 5) and then rinsed again two times with an additional 1 ml of lavage buffer. Both were pooled and stored on ice. Afterwards, a 21G Safety Multifly (Sarstedt) was inserted into the heart to rinse the heart-lung circulation with 5 ml DPBS def. Following, 1 ml 4 % PFA were injected into the lung via the trachea catheter, the trachea was closed with a yarn and the heart-lung complex was excised from the mice and transferred to 14 ml of 4 % PFA in a 15 ml container. Finally, a tail tip biopsy was taken from the sacrificed mouse for validation of the correct genotype.

3.16. The analysis of RIG-I variant effects on main infection parameters

3.16.1. Analysis of weight loss and body temperature upon IAV infection

As described in the previous chapter, the body temperature and body weight of RIG-I WT, PM and KO mice were determined prior to infection or treatment and afterwards at least once daily until the mice were sacrificed. In regard to the body temperature, the data was analyzed without normalization. Concerning the body weight, the mean body weight of individual mice was calculated from data points protocolled before the first weight drop in response to the infection or treatment. For the calculation of the percentage remaining body weight, all individual weight data points were divided by the mean body weight prior to weight drop and multiplied with 100. For both the body temperature and body weight, all available data for the respective infection group and timepoint p.i. were used to calculate the mean body temperature and the mean percentage remaining body weight (d0-4: n = 16; d5-7: n = 12; d8-10: n = 8; d11-14: n = 4). The data was depicted as superimposed symbol plots (c. c. 3.19.4) with the respective standard deviations. The consideration of all available data was used to enhance the robustness of the analyses with a 2-Way ANOVA (c. c. 3.19.8), which was used to investigate significant effects of the factors "days p.i." and "RIG-I genotype", as well as their interaction, on the variable "body temperature" or "remaining body weight", respectively.

3.16.2. Virus titer quantification in the BALF

For the quantification of the IAV titer in the BALF of the study mice, a SCIA was used. The virus quantification was performed as described previously (c. c. 3.13.2). The data was analyzed with a 2-Way ANOVA to indicate significant effects of the factors "days p.i." and "RIG-I genotype", as well as their interaction, on the variable "BALF virus titer".

3.16.3. Virus detection in the lung tissue with immune histochemistry

For the validation of successful lung tissue infection with the IAV PB2-627K and -627E strain, as well as absence of unwanted contaminations with virus in the PBS treated mice, the abundance of IAV NP in the lung tissue of infected and mock-infected mice was investigated with an immune histochemical (IHC) staining. Therefore, the heart-lung circulation system was harvested at the endpoint and was fixated in 4 % PFA. By the Neuropathology department of the UKGM, the tissue was embedded in paraffine and slices were prepared on slides for histological stainings.

The IHC detection of viral NP was achieved with an automated protocol in a Bond III IHC staining system (Leica Biosystems) with a Bond Polymer Refine Detection Kit (Leica Biosystems). The protocol starts with a dewaxing, a peroxide block and NP detection with a polyclonal primary antibody (Thermo), interrupted by washing steps. It continues with the application of a polymer- and HRP-coupled secondary antibody, the addition of a DAB substrate and finishes with a hematoxylin counterstaining, again interrupted by washing steps (compare Table 13 antibodies and Table 11 detection kit). The staining was performed and validated by Dr. Frederik Helmprobst and Prof. Dr. Axel Pagenstecher at the Neuropathology department of the UKGM. The stained slides were scanned with a Aperio slide scanner (Leica Biosystems) with 20-fold magnification and transformed into a digital format. The picture files were analyzed with the open source software QuPath (Bankhead P. 2017), representative sectors of the lung tissue from one female and one male individual were chosen in an additional five-fold magnification as image examples. Additionally, the percentage amount of cells with positive NP detection was determined in the complete lung tissue on the slides. Therefore, a threshold-based semi-quantification algorithm was applied as indicated with QuPath (compare Table 33). The mean lung tissue virus titers were calculated for the respective infection groups with $n=4$ and were depicted as histograms with the respective standard deviation. The variable "virus abundance in the lung tissue" was investigated for significant differences in dependence of the factors "days p.i." and "RIG-I genotype" with a 2-Way ANOVA (c. c. 3.19.8).

Table 33: The QuPath algorithm settings for the determination of IAV positive lung cells.

Detection image	Hematoxylin OD
Requested pixel size	0.5 μm
Background radius	8 μm
Median titer radius	0 μm
Sigma	1.5 μm
Minimum area	10 μm^2
Maximum area	400 μm^2
Threshold	0.1
Max background intensity	2
Cell expansion	5 μm
Score compartment	Nucleus DAB OD mean
Threshold 1+	0.2
Threshold 2+	0.4
Threshold 3+	0.6
Additional settings	
Split by shape	
Include cell nucleus	
Smooth boundaries	
Make measurements	
Singe threshold	

3.16.4. *Histological staining with H&E and PAS*

The histological staining of lung slices with a hematoxylin and eosin (H&E) and a periodic acid-Schiff (PAS) protocol, as well as method validation, was performed by Dr. Frederik Helmprobst and Prof. Dr. Axel Pagenstecher at the Neuropathology department of the UKGM. Later, the slides were analyzed with a light microscope (Leica Microsystems GmbH) at 50-fold magnification. Representative sectors

of tissue from one female and one male individual of any infection group were chosen and a picture was taken in 50-fold magnification with the LAS software (Leica).

3.16.5. *The FITC-albumin lavage to serum ratio as indicator for altered lung barrier integrity*

The lung barrier, formed by tightly connected lung epithelial cells, enables the exchange of O₂ and CO₂ between air and blood, while it prevents the uncontrolled leakage of liquids. If its function is altered, liquid may enter the alveolar lumen uncontrolled. After introduction of FITC-labeled albumin into the blood circulation, it is possible to detect alterations in the lung barrier function depending on factors. Therefore, the FITC-albumin abundance in the BALF and the serum is determined by measurement of the fluorescence production in these samples.

BALF and full blood of IAV infected or mock treated mice was harvested approx. one h after FITC-albumin application via a tail vein. Full blood was stored at 4 °C for complete coagulation until centrifugation at 4000 RCF for 5 min in a table-top centrifuge. The serum was separated from the samples and transferred to a new reaction container. The BALF was centrifuged at 4000 RCF for 5 min as well, the supernatant was separated from the cells and transferred to a new container. 0.5 ml of the BALF were separated and stored at 4 °C for RNA isolation at the following day, as described elsewhere. Both the serum and BALF samples were stored at -80 °C.

For the determination of the FITC-albumin lavage to serum ratio, serum was diluted 1:10. Therefore, lavage buffer and 10 % PFA were added to achieve a final serum dilution of 1:10 and a PFA concentration of 4 %. For the purpose of virus neutralization, 10 % PFA was added to the BALF as well, to achieve a final concentration of 4 % in the samples. This makes a dilution factor of 10 for the serum samples and 1.2 for the lavage samples. The fluorescence emission in the BALF and serum samples, as well as the blank, were measured as duplicates at 520 nm after excitation at 485 nm in a half area Microlon Fluorotrac 200 96-well plate (Greiner) with a Tecan i control fluorimeter (Tecan Trading AG). The used settings are summarized in Table 34. The FITC-albumin lavage to serum ratio was calculated as shown in Formula 4. The mean of the ratios of four mice per infection group was calculated and depicted as histograms with the respective standard deviation. An increase of the ratio indicates a disruption of the lung barrier integrity. Last, significant effects of the factors "days p.i." and "RIG-I genotype" on the variable "FITC-albumin lavage to serum ratio" were analyzed by application of a 2-Way ANOVA (c. c. 3.19.8).

Table 34: The settings for fluorescence measurement with the Tecan i control device.

Parameter	Setting
Mode	Fluorescence Top Reading
Emission wavelength start	516 nm
Emission wavelength end	526 nm
Emission wavelength step size	2 nm
Emission scan number	6
Excitation wavelength	485 nm
Gain	100 Manual
Number of flashes	25
Integration time	20 μ s
Lag time	0 μ s
Settle time	0 ms
Z-position (Manual)	20000 μ m

Formula 4: The calculation of the FITC-albumin lavage to serum ratio.

$$FITC - albumin \text{ lavage to serum ratio} = \frac{\text{fluorescence lavage} * 1.2}{\text{fluorescence serum} * 10}$$

3.17. The analysis of RIG-I variant effects on innate immune signaling

3.17.1. The determination of IFN levels in the BALF with ELISA

To investigate IFN- α and β production in response to virus lung infection in dependence on RIG-I variant expression, the abundance of the IFNs was measured with ELISA in the BALF of infected mice. The procedures were described in detail previously (c. c. 3.7).

3.17.2. The analysis of inflammatory cytokine concentrations in the BALF with a multiplex cytokine assay

To quantify the concentration of 23 inflammatory cytokines, a Pro Mouse Cytokine 23-plex cytokine assay (M60009RDPD, Bio-Rad) was performed. The detection system of the assay works with phycoerythrin-mediated fluorescence, which is compatible with remaining FITC-albumin in the samples (emission maximum of PE 575 nm and of FITC 514 nm). For the assay, the BALF of two female mice as well as two male mice per infection group, were mixed to equal parts and 35 % BSA was added to achieve a final concentration of 0.5 %. 50 µl of the samples were analyzed for cytokine concentrations as duplicates with the multiplex cytokine assay, guided by Dr. Thomas Butterbrodt from Bio-Rad with a Bio-plex 200 device connected to a HTF wash station (Bio-Rad), according to the manufacturer's manual. The standard reference values were set as indicated in the assay kits. The raw data was processed with the Bio-plex Manager software (Bio-Rad). Of all measured cytokines, the ones with a solid detection level at least at one time point were used for further analysis. The mean of the two female sample replicates and the two male sample replicates were calculated and depicted as histograms, with the respective standard deviations. A 2-Way ANOVA was used to determine significant effects of the factors "days p.i." and "RIG-I genotype" on the variable "cytokine concentration", for each of the analyzed cytokines (c. c. 3.19.8).

3.18. The IAV PB2 nt 1879 genotyping in the BALF

The IAV PB2-627E strain turned out to be genetically unstable for the PB2-627E mutation in mammalian cell lines, while this genotype was stable in DF-1 chicken cells. To validate the genetic stability of the IAV PB2-627E strain during the course of mouse infection, the viral PB2 RNA in the BALF was analyzed with Sanger-sequencing. Therefore, 500 µl of cell-free BALF were centrifuged at 8×10^4 RCF for 45 min in a laboratory centrifuge (Heraeus) to concentrate the virus particles in a volume of 300 µl. The RNA isolation, cDNA synthesis and PCR were performed as described previously (c. c. 3.13.1) and the Sanger-sequencing was ordered at the Microsynth Seqlab GmbH as described before (c. c. 3.3). The PB2 nt 1879 percentage distributions were calculated for the individual mice as described for the competitive infection assay (c. c. 3.13.6). The mean percentage PB2 nt 1879 distributions was calculated for every infection group of the study and depicted as stacked bar plot with the respective standard deviations. For statistical analysis, only the percentage abundance of the PB2 nt 1879 G was used. Significant effects of the factors "days p.i." and "RIG-I genotype" on the variable "percentage PB2 nt 1879 G abundance" were detected with a 2-Way ANOVA (c. c. 3.19.8).

3.19. *Statistical analysis*

All statistical analysis and most of the data evaluation and depiction was performed with GraphPad Prism 9 (Graphpad Software Inc.), if not indicated differently.

3.19.1. *Histogram*

For the result mean depiction of experiments with low n numbers and/or low data variation, the histogram was chosen to give an overview about the data. All histograms in this study show the mean and standard deviation of the respective results.

3.19.2. *Box plot*

For the depiction of results from experiments with high n numbers and high data variation, box plots were chosen to give an overview about the data variation. In all depicted box plots, whiskers indicate the lowest and the highest values, box borders indicate the 25th and the 75th percentile and the mid indicates the median.

3.19.3. *Stacked bar plot*

To show the percentage distribution of the four possible nucleotides at the PB2 nt 1879 position, which is the first one of the IAV PB2-627 codon, a depiction as stacked bar plot was chosen to visualize differences in the nt distribution in dependence of factors. In all of the depicted stacked bar plots, the mean percentage nt 1879 distribution is depicted with the respective standard deviation for the four possible nt options (the complete lack of a signal for single nt is possible).

Importantly, for statistical analysis by ANOVA, only the mean percentage abundance of the nt G for the respective infection condition or infection group was used to determine significant differences. The data groups used for the calculations are indicated in the respective figures.

3.19.4. *Superimposed symbol plot*

For the depiction of dependent data derived from repeated measurement of body weight and temperature of the mice, the superimposed symbol plot was chosen. This depiction directly indicates the dependency of the data and depicts the high amount of data in a clear structure.

3.19.5. *Outlier analysis*

Outliers highly differ from the gross of the data and can disturb the identification of significant differences by statistical tests or even cause wrong positive indications. In this study, all data groups were analyzed with a robust regression and outlier removal (ROUT) test before further analysis. In the results, it is only mentioned if outliers were indicated by the analysis and removed from the data set. Most of the data groups were free from outliers, only three outliers were removed from the 3p-hpRNA data (c. c. 4.2.2.1).

3.19.6. *Normal distribution*

The ideal for the analysis with a t-test or an ANOVA of any kind is a normal distribution of the data in a set. In general, it can be assumed that data samples derived from measurements in biologic systems follow a normal distribution, if the amount of n-numbers is sufficient. Nevertheless, if the method of measurement is inaccurate and/or the n-number not sufficient for a robust data set, the statistical analysis may create inaccurate results. Hence, the normal distribution of the data should be validated before application of a statistic test. This can be achieved with different tests for a normal/ Gaussian distribution. In this study, the data sets were analyzed with both the Shapiro-Wilk and the Kolmogorov-Smirnov test, since these tests can analyze small data groups, too. Most of the compared data groups showed normal distribution, but in some cases small groups failed the validation. Those are indicated in the results section and suggest that important findings need to be validated with a sufficient amount of biological replicates.

3.19.7. *T-test*

For the determination of significant differences between low amounts of data groups, usually t-tests were used. All data sets analyzed with t-tests were analyzed for normal distribution before application of the t-test. In this study, the p-values indicating significant differences between the compared groups are shown at bars indicating the compared data groups in the respective diagrams.

3.19.8. *2-Way ANOVA*

To determine significant effects of different factors on a variable, a 2-Way ANOVA is a useful tool. This algorithm delivers three different p-values: the first one indicates a significant interaction between the two factors in their effects, the second indicates a significant effect of the first factor on the variable and the third indicates a significant effect of the second factor on the variable. The interaction can be either a synergistic effect or an inhibitory effect, which would result in a significant

interaction. If one or both factors mediate no effect or both factors mediate an effect independent of each other, the ANOVA would not indicate a significant interaction. An insignificant interaction can also indicate that a factor is not sufficient to completely abolish an effect by the other factor on the variable. The 2-Way ANOVA is an interesting tool for the analysis of more complex effects and tendencies in big data sets with different factors. Further, it can be used to reduce a big amount of t-tests. For experiments, in which different quantities of a factor were used to effect a variable, the ANOVA is more reliable than a t-test in correctly identifying significant effects of the factors on the variable.

In this study, a special focus was put on effects of RIG-I variant expression on different variables. Therefore, the RIG-I WT, PM and KO data sets were compared separately with one another, to derive the most detailed information possible.

4. Results

4.1. The establishment of a RIG-I WT, PM and KO mouse line

Potential founder mice derived from genetically engineered oocytes in Zurich were genotyped for a RIG-I PM or KO genotype with Sanger-sequencing (compare chapter (c. c.) 3.2 f.). Heterozygous mice were bred to generate homozygous mice. Later on, homozygous individuals were used for further breeding. A homozygous RIG-I WT mouse line was received from heterozygous mice of the RIG-I KO line. An example for every genotype sequencing result aligned with the RIG-I WT genotype is shown in Figure 8.

A RIG-I WT

Sequence ID: Query_2099Length: 339Number of Matches: 1
Range 1: 186 to 339[Graphics](#) Next Match Previous Match

Alignment statistics for match #1

	Score	Expect	Identities	Gaps	Strand
	274 bits(148)	2e-78	151/154(98%)	0/154(0%)	Plus/Plus
Query	1		tttttttttcttttttCTTCCCTACTAAAAGGTTGTGGAAAAACCTTTGTGTCGCTTCTT		60
Sbjct	186		TTTTTTTTTCTTTTTTCTTCCCTACTAAAAGGTTGTGGAAAAACCTTTGTGTCNCCTTCTT		245

B RIG-I PM

Sequence ID: Query_18461Length: 143Number of Matches: 1
Range 1: 1 to 142[Graphics](#) Next Match Previous Match

Alignment statistics for match #1

	Score	Expect	Identities	Gaps	Strand
	241 bits(130)	6e-69	138/142(97%)	0/142(0%)	Plus/Plus
Query	17		tttttttttcttttttCTTCCCTACTAAAAGGTTGTGGAAAAACCTTTGTGTCGCTTCTT		76
Sbjct	1		TTTTTTTTTCTTTTTTCTTCCCTACTAAAAGGTTGTGGAGCAACATTCGTGTCGCTTCTT		60

C RIG-I KO

Sequence ID: Query_31181Length: 326Number of Matches: 1
Range 1: 190 to 326[Graphics](#) Next Match Previous Match

Alignment statistics for match #1

	Score	Expect	Identities	Gaps	Strand
	219 bits(118)	8e-62	134/142(94%)	5/142(3%)	Plus/Plus
Query	1		tttttttttcttttttCTTCCCTACTAAAAGGTTGTGGAAAAACCTTTGTGTCGCTTCTT		60
Sbjct	190		TTTTTTTTTCTTTTTTCTTCCCTACTAAAAG-----GGAAAAACCTTTGTGTCNCCTTCTT		244

Figure 8: Examples for a representative RIG-I WT, PM and KO genotyping. An example for the result of a RIG-I WT (A), PM (B) and KO (C) mouse Sanger-sequencing was aligned with the RIG-I WT genomic sequence, with the NCBI BLAST web tool. The RIG-I codon 271 is marked **yellow**. The two additionally introduced mutations at wobble positions in the RIG-I PM mouse are marked **green**. The position where the five nt are lost in the RIG-I KO mouse is marked **red**.

4.1.1. Homozygous RIG-I PM and KO mice do not develop a burdening phenotype

To determine if the generated RIG-I PM and KO mouse lines are burdened by their genotype, nine batches of RIG-I PM and twenty batches of RIG-I KO mice were analyzed for their newborn loss. Additionally, 13 individuals of the RIG-I PM and 37 individuals of the RIG-I KO line were analyzed for their weight gain and phenotypic alterations once per week, over a course of 24 weeks.

The average of lost newborns with 7.04 % of the RIG-I PM and with 17.8 % of the RIG-I KO batches did not extend the expectations of newborn loss in the animal facility of the BMFZ in Marburg. In those batches, no young mice died during the window of seven days post-partum and the weaning after 21 days post-partum. The weight determination and comparison with RIG-I WT mouse data deriving from Jackson Labs for the C57BL/6J line (data access 2019/08/11) showed a negligible difference of 7.9 % for male RIG-I PM mice and of 7.0 % of male RIG-I KO mice after 20 weeks. Since this difference was similar for a few investigated RIG-I WT mice in the animal facility of the institute (data not shown), the differences to the data deriving from Jackson Labs most likely appear due to deviations in the diet. The weight difference of female mice to the Jackson Lab data was lower, with 3.4 % for RIG-I PM and 1.7 % for RIG-I KO mice after twenty weeks. Further, there was no increased susceptibility for diseases or enhanced mortality of the RIG-I PM and KO mice detectable. The results were interpreted as no burden of the RIG-I genotype for the mice in a final examination of the respective mouse line, confirmed by the responsible department at the Regierungspräsidium Gießen, which permitted the propagation of the mouse lines (compare Supplementary Figure 1).

4.2. Mouse line RIG-I functionality tests

4.2.1. mRIG-I protein expression is detectable with Western blotting in primary cells from RIG-I WT and PM mice, but not RIG-I KO mice

To determine RIG-I protein integrity in the established mouse lines, primary cells were extracted from the bone marrow of RIG-I WT, PM and KO mice (c. c. 3.5). RIG-I expression was induced by IFN- α treatment. With Western blotting (WB), either RIG-I or β -actin expression was detected in the cell lysates (c. c. 3.8 f.).

The results of the WB showed that RIG-I was detectable in RIG-I WT and PM mouse derived cells, but not in RIG-I KO mouse derived cells. In contrast, β -actin was detectable in all cell lysates with a comparable quantity (compare Figure 9). The result that the RIG-I PM band ran slightly faster in the gel most likely results from the substitution of the amino acid (aa) lysine with alanine, which changes

the molar mass and the charge of the protein and may lead to the loss of a site for post-translational modification of the protein, since the additional amino group of lysine is a common residue for acetylation, methylation, SUMOylation or ubiquitylation (Kontaxi C. 2017).

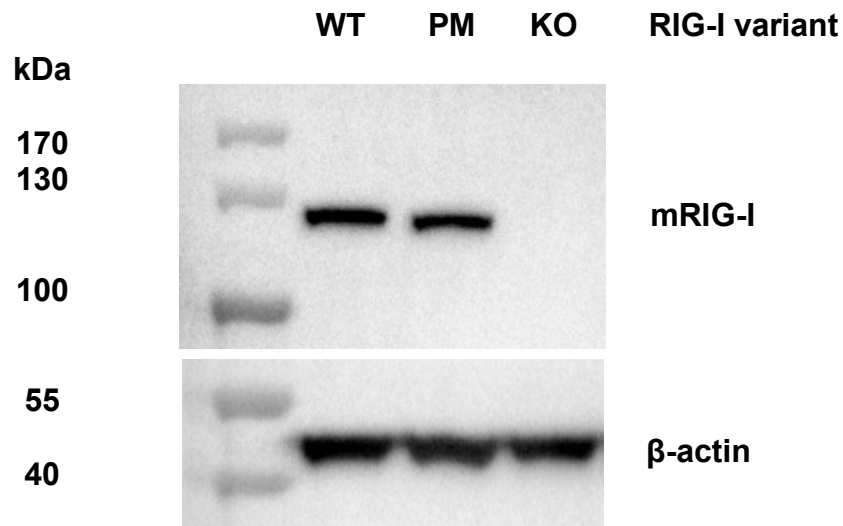


Figure 9: RIG-I protein is detectable in primary cells from RIG-I WT and PM mice, but not in primary cells from RIG-I KO mice. Murine bone marrow cells were treated with IFN- α , WB was performed with an anti-mRIG-I antibody (Enzo ALX-804-960-0100) or anti- β -actin antibody (Sigma-Aldrich A2228) as loading control. The result of one out of three independently performed WB is shown as example.

For statistical analysis, the WB signals were semi-quantified. For this, the images of the blots were analyzed for band size intensity with the software ImageJ (c. c. 3.10). The mean area under the curve (AUC) of three independent experiments were calculated and depicted as histograms, with the respective standard deviation (compare Figure 10). An unpaired t-test was used to indicate significant differences in RIG-I and β -actin expression. For RIG-I detection, the t-tests indicated no significant difference in RIG-I expression between RIG-I WT and PM mouse derived cells ($p = 0.47$), but a significant difference between RIG-I WT and KO mouse derived cells ($p = 0.01$) (compare Figure 10 A). For β -actin detection, the t-tests indicated no significant difference between RIG-I WT and PM mouse derived cells ($p = 0.37$) and no significant difference between RIG-I WT and KO mouse derived cells ($p = 0.28$) (compare Figure 10 B).

Taken together, these results suggest that the CRISPR/Cas9 application for the generation of the RIG-I PM mouse did not cause additional mutations leading to frameshift and protein loss. The band size and intensity do not differ markedly, compared to the RIG-I band from the RIG-I WT mouse derived cells. For the RIG-I KO mouse line, the lack of a RIG-I band indicates that the five nucleotide

(nt) deletion in the RIG-I gene is indeed resulting in a RIG-I knockout, as expected. The lack of a significant difference in β -actin expression shows the similarity of the protein concentration and integrity in all three cell lysates.

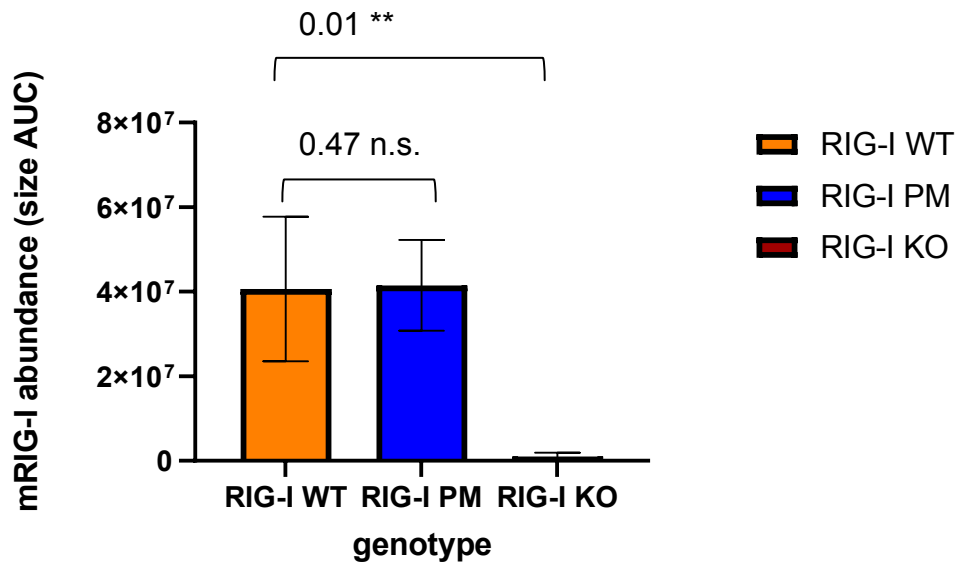
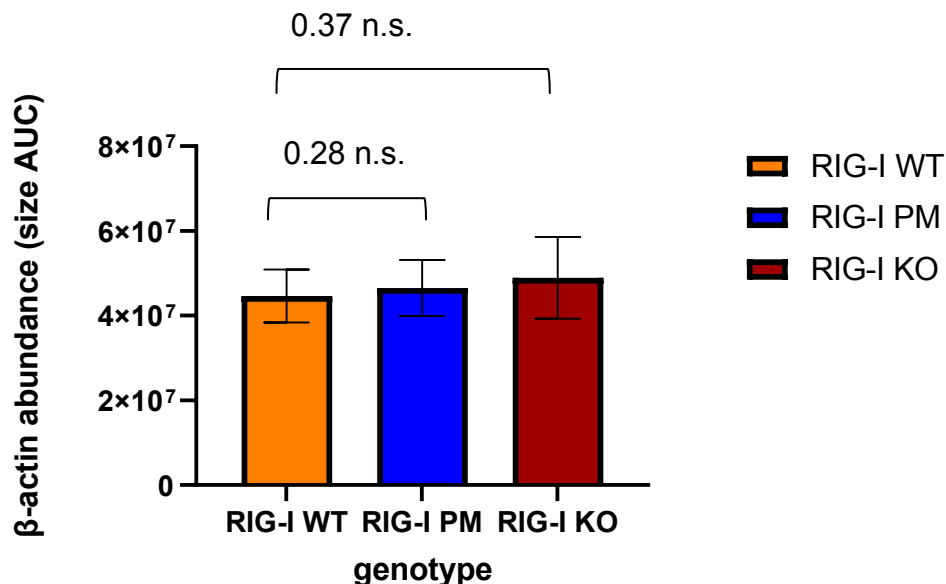
A**B**

Figure 10: RIG-I protein expression in cells from RIG-I KO mice, but not in cells from RIG-I PM mice, is significantly altered in comparison to expression in cells from RIG-I WT mice. RIG-I (A) or β -actin (B) protein expression was detected in primary bone marrow cells from RIG-I WT, PM or KO mice, by WB. The WB images of three independent experiments were semi-quantified with the ImageJ software, means of the areas under the curve (AUC) from band signals were calculated and depicted in histograms with the respective standard deviations. Unpaired t-tests were used to detect significant differences in RIG-I or β -actin protein expression of cells from RIG-I PM and KO mice, in comparison to cells from RIG-I WT mice.

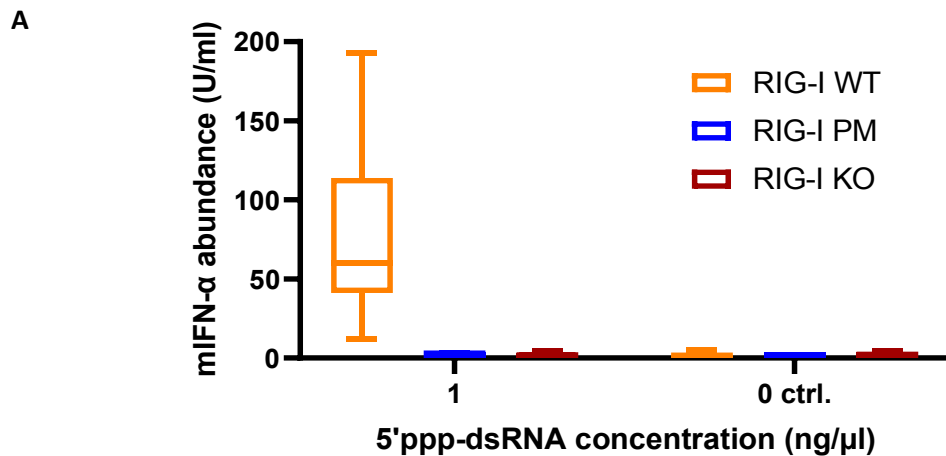
4.2.2. RIG-I-mediated signaling in RIG-I PM and KO mouse derived BmdMΦ is abolished, while the signaling via other PRRs is not altered

To validate the functionality of the generated mouse lines, RIG-I-mediated IFN- α induction was investigated, in BmdM Φ in response to different specific RIG-I ligands, IAV infections and Sendai virus infection. Additionally, the cells were analyzed for potential direct side effects of the genetic engineering using CRISPR/Cas9 or compensatory changes in the signaling of different PRRs of the innate immune system in response to expression of signaling-deficient RIG-I or a RIG-I loss.

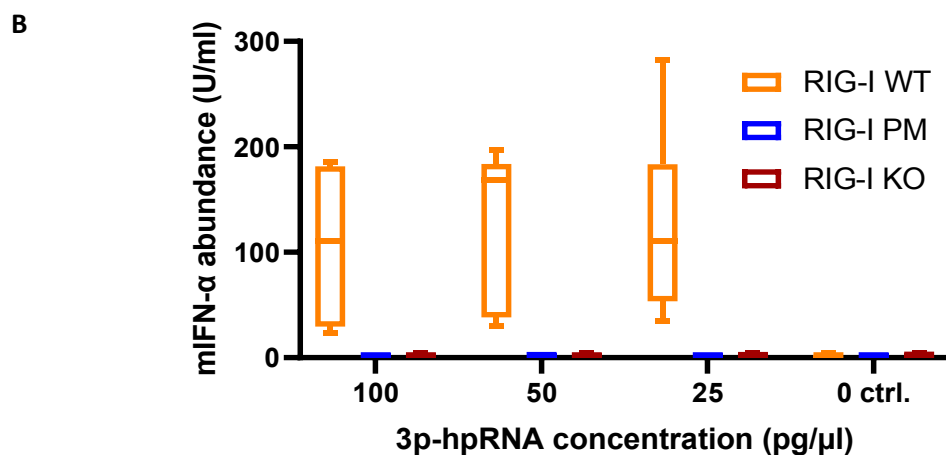
4.2.2.1. RIG-I signaling is altered in RIG-I PM and KO mouse derived BmdMΦ, but not in RIG-I WT mouse derived BmdMΦ

To investigate alterations in RIG-I-mediated mIFN- α expression, bone marrow cells were extracted from RIG-I WT, PM and KO mice. The cells were differentiated into M Φ *in vitro* and then treated with specific RIG-I ligands. Therefore, cells were transfected with 5'ppp-dsRNA, three different concentrations of 3p-hpRNA or the transfection reagent only. An ELISA detecting mIFN- α in the medium from the treated cells was performed (c. c. 3.5 ff.). The results of at least five independent experiments were depicted as box plots (compare Figure 11). The data set of 3p-hpRNA was analyzed with ROUT outlier identification (compare 3.19.5) and three outliers were identified (100 pg/ μ L 726.7 U/mL; 50 pg/ μ L 766.7 U/mL; 25 pg/ μ L 425.0 pg/ μ L). Those values were excluded from the data set before further calculations. To indicate significant effects of the factors "5'ppp-dsRNA concentration" or "3p-hpRNA concentration" on the variable "mIFN- α abundance", a 2-Way ANOVA was performed (c. c. 3.19.8).

The results show that both the factors "5'ppp-dsRNA concentration" and "3p-hpRNA concentration" significantly enhance the IFN- α expression in BmdM Φ from RIG-I WT mice but not from PM and KO mice. This is indicated by a significant effect of these factors on the variable in the comparisons including RIG-I WT cells (p at least 0.0046 for 5'ppp-dsRNA and p at least 0,0086 for 3p-hpRNA) and a lack of a significant effect in the comparison between RIG-I PM and KO cells. The induction of IFN- α is abolished due to RIG-I PM and KO expression, indicated by a significant effect of the factor "RIG-I genotype" on the variable (p at least 0.0054 for 5'ppp-dsRNA and p < 0.0001 for 3p-hpRNA) and a significant interaction between the factors (p at least 0.0052 for 5'ppp-dsRNA and p at least 0.0084 for 3p-hpRNA) in the comparisons including RIG-I WT cells. The results also show that the RIG-I K271A mutation is sufficient to completely inactivate RIG-I-mediated IFN- α induction, indicated by no significant effect of the RIG-I genotype on the variable and no significant interaction between the factors in the comparison between RIG-I PM and KO cells (compare Figure 11 A and B).



2-Way ANOVA	RIG-I WT vs. PM		RIG-I WT vs. KO		RIG-I PM vs. KO	
source of variation	p value	p value summary	p value	p value summary	p value	p value summary
interaction	0.0052	**	0.0048	**	0.4849	ns
5'ppp-dsRNA	0.0046	**	0.0050	**	0.6446	ns
RIG-I genotype	0.0051	**	0.0054	**	0.5795	ns



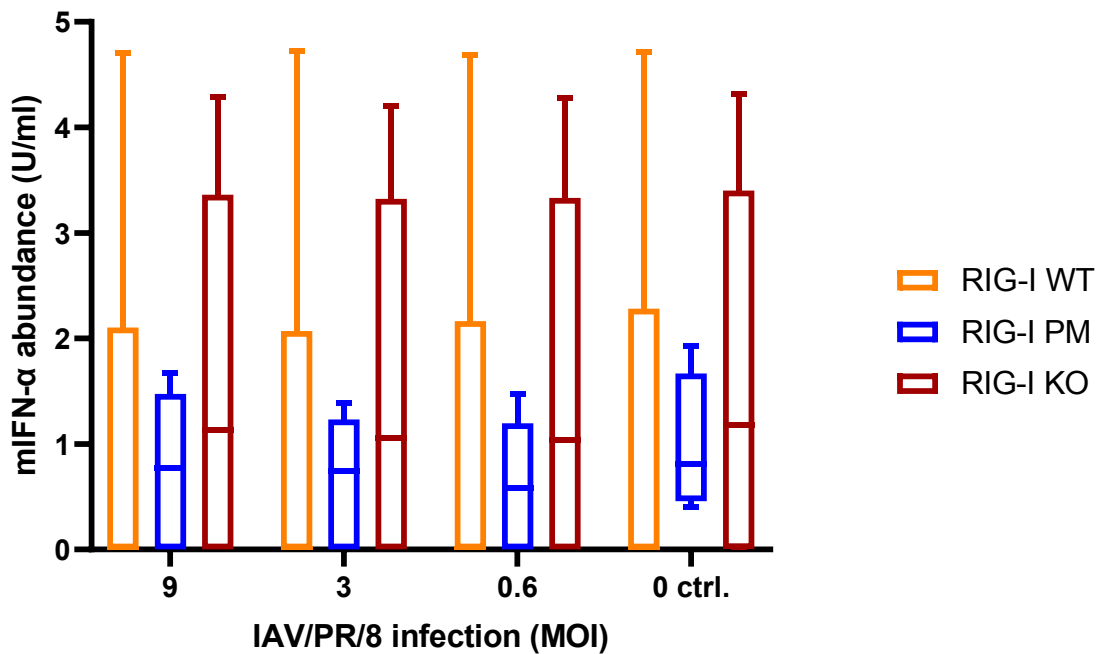
2-Way ANOVA	RIG-I WT vs. PM		RIG-I WT vs. KO		RIG-I PM vs. KO	
source of variation	p value	p value summary	p value	p value summary	p value	p value summary
interaction	0.0084	**	0.0070	**	0.9969	ns
3p-hpRNA	0.0086	**	0.0072	**	0.9466	ns
RIG-I genotype	<0.0001	****	<0.0001	****	0.0738	ns

Figure 11: The effect of specific RIG-I ligands to enhance mIFN- α production is abolished in BmdM Φ from RIG-I PM and KO mice, in contrast to RIG-I WT cells. Bone marrow cells were extracted from RIG-I WT, PM and KO mice. The cells were differentiated into M Φ *in vitro* and then transfected with the specific RIG-I ligands 5'ppp-dsRNA (1 ng/ μ l), 3p-hpRNA (100, 50 or 25 pg/ μ l), or the transfection reagent only (0 ctrl.). An ELISA detecting mIFN- α in cell culture supernatant from treated cells was performed. The results of at least five independent experiments are depicted as box plots (whiskers indicate lowest and highest value, box borders indicate 25th and 75th percentile, mid indicates the median). A 2-Way ANOVA was used to show significant effects of the factors "5'ppp-dsRNA concentration" and "RIG-I genotype" on the variable "mIFN- α abundance" (A), or the factors "3p-hpRNA concentration" and "RIG-I genotype" on the variable "mIFN- α abundance" (B). The results of the ANOVAs are depicted in the table.

4.2.2.2. A recombinant IAV/PR/8 strain lacking the NS1 protein significantly induces mIFN- α expression in dependence of RIG-I variant expression, while a strain with functional NS1 protein does not

To investigate, if IAV infection-triggered mIFN- α production differs between the mouse lines, bone marrow cells were extracted from RIG-I WT, PM and KO mice. The cells were differentiated into M Φ *in vitro* and then infected with different MOI of either a recombinant IAV/PR/8 strain with functional NS1 or a recombinant IAV/PR/8 strain lacking the NS1 protein (Δ NS1). An ELISA detecting mIFN- α in the supernatant from infected cells was performed (c. c. 3.5 ff.).

For the IAV strain with functional NS1 expression, the results of at least six independent experiments are depicted as box plots (compare Figure 12). A 2-Way ANOVA was used to indicate significant effects of the factors "MOI IAV infection" and "RIG-I genotype", as well as their interaction, on the variable "mIFN- α abundance". In general, the measured IFN- α abundance was very low compared to induction by specific RIG-I ligands (compare previous chapter). Hence, a detection at the border to the detection limit is expected. The results indicate no significant effect of the factor "MOI IAV infection" on the variable, for all comparisons between the groups. This and the lack of a significant interaction between the factors suggests that the measured IFN- α levels are background noise of the ELISA. Hence, specific effects of the factor "RIG-I genotype" on the variable suggested by the ANOVA analyses appear most likely due to differences in the background noise intensity, which is dependent on the incubation time during ELISA development. Taken together, the results suggest that the used IAV strain is poorly inducing mIFN- α production in the BmdM Φ . This is most likely due to the function of the viral NS1 protein, which is a potent inhibitor of IFN-1 signaling. Hence, an IAV strain lacking the NS1 protein was used in another experiment to investigate RIG-I-mediated IFN- α induction in response to infection.



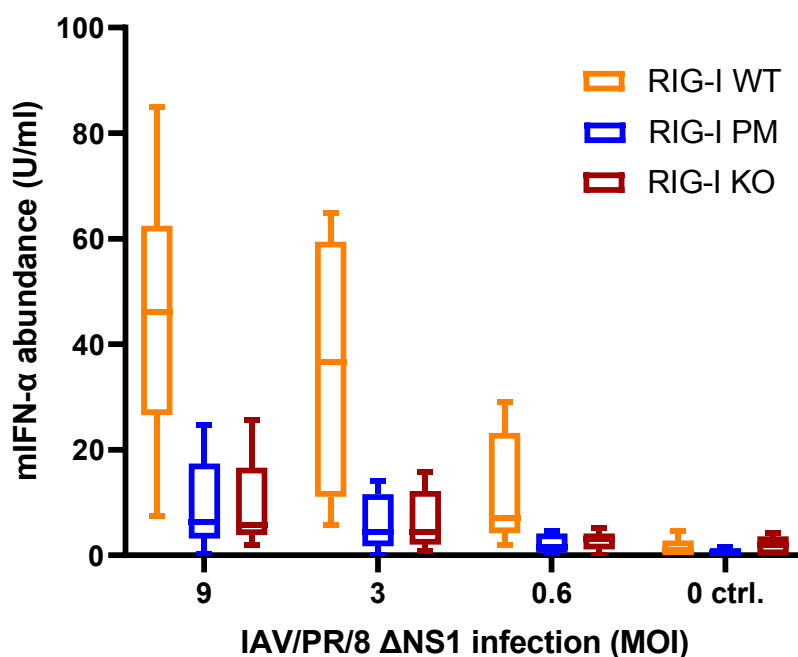
2-Way ANOVA source of variation	RIG-I WT vs. PM		RIG-I WT vs. KO		RIG-I PM vs. KO	
	p value	p value summary	p value	p value summary	p value	p value summary
interaction	0.9875	ns	>0.9999	ns	0.9931	ns
MOI IAV	0.9861	ns	>0.9999	ns	0.9790	ns
RIG-I genotype	0.2036	ns	0.5355	ns	0.0448	*

Figure 12: A recombinant IAV strain with functional NS1 protein does not induce mIFN- α production in BmdM Φ . Bone marrow cells were extracted from RIG-I WT, PM and KO mice. The cells were differentiated into M Φ *in vitro* and then infected with different MOI of a recombinant IAV/PR/8 strain (9; 3; 0.6 MOI) or mock (0 ctrl.). An ELISA detecting mIFN- α in cell culture supernatant was performed. The results of at least six independent experiments are depicted as box plots (whiskers indicate lowest and highest value, box borders indicate 25th and 75th percentile, mid indicates the median), a 2-Way ANOVA was used to indicate significant effects of the factors "MOI IAV" and "RIG-I genotype", as well as their interaction, on the variable "mIFN- α abundance". The results of the ANOVAs are depicted in the table.

The results of at least five independent experiments using an IAV strain lacking the NS1 protein to infect BmdM Φ are depicted as box plots (compare Figure 13). A 2-Way ANOVA was used to indicate significant effects of the factors "MOI IAV Δ NS1 infection" and "RIG-I genotype", as well as their interaction, on the variable "mIFN- α abundance".

At first, the data confirm that the assumption about the suppression of IFN- α induction by the NS1 protein was correct. In detail, the results showed a similar IFN- α induction pattern as the results from the assays with the specific RIG-I ligands. The infection induces IFN- α production in RIG-I WT mouse derived BmdM Φ , which is much lower, but not completely abolished, in RIG-I PM and KO mouse derived cells (unlike for specific RIG-I ligands, compare previous chapter). This is indicated by a significant effect of the factor "MOI IAV Δ NS1 infection" on the variable in all comparisons between

the groups (p at least 0.0090) and a significant effect of the factor "RIG-I genotype" on the variable in the comparisons including RIG-I WT cells (p at least 0.0001), as well as a significant interaction between the factors in the same comparisons (p at least 0.0208). Further, the results indicate that the RIG-I PM is sufficient to completely inhibit RIG-I-mediated IFN- α induction, indicated by no significant effect of the factor "RIG-I genotype" on the variable and no significant interaction between the factors in the comparison between the RIG-I PM and KO mouse derived cells, comparable with the results of the previous chapter. Interestingly, despite of RIG-I signaling deficiency or KO, the virus was significantly inducing IFN- α production, indicating that this is also mediated by other PRRs, but to a much lower extend (compare Figure 13).



2-Way ANOVA	RIG-I WT vs. PM		RIG-I WT vs. KO		RIG-I PM vs. KO	
source of variation	p value	p value summary	p value	p value summary	p value	p value summary
interaction	0.0208	*	0.0165	*	0.9944	ns
MOI IAV Δ NS1	0.0003	***	0.0004	***	0.0090	**
RIG-I genotype	<0.0001	****	0.0001	***	0.7797	ns

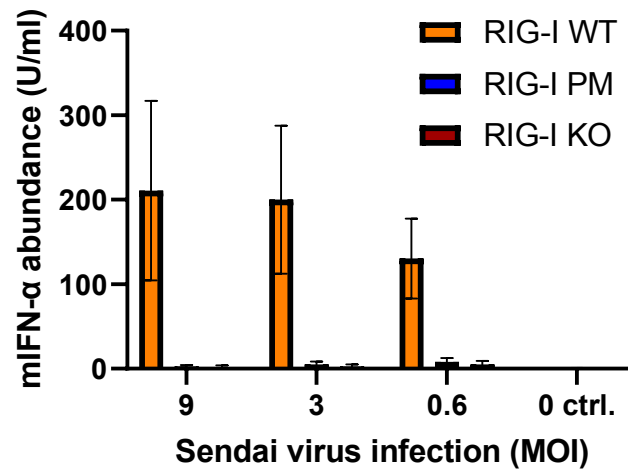
Figure 13: The majority of mIFN- α induction upon infection with a recombinant IAV strain lacking the NS1 protein in BmdM Φ is dependent on RIG-I. Bone marrow cells were extracted from RIG-I WT, PM and KO mice. The cells were differentiated into M Φ *in vitro* and then infected with different MOI of a recombinant IAV/PR/8 strain lacking the NS1 protein (9; 3; 0.6 MOI) or mock (0 ctrl.). An ELISA detecting mIFN- α in cell culture supernatant was performed. The results of at least five independent experiments are depicted as box plots (whiskers indicate lowest and highest value, box borders indicate 25th and 75th percentile, mid indicates the median). A 2-Way ANOVA was used to indicate significant effects of the factors "MOI IAV Δ NS1" and "RIG-I genotype", as well as their interaction, on the variable "mIFN- α abundance". The results of the ANOVAs are depicted in the table.

4.2.2.3. Sendai virus infection-mediated induction of mIFN- α and mIL-6 is significantly dependent on RIG-I in BmdM Φ

To investigate, if mIFN- α and mIL-6 production in response to Sendai virus infection differs between the mouse lines, bone marrow cells were extracted from RIG-I WT, PM and KO mice. The cells were differentiated into M Φ *in vitro* and then infected with different MOI of a Sendai virus strain. An ELISA detecting mIFN- α (A) or mIL-6 (B) in the cell culture supernatant was performed (c. c. 3.5 ff.).

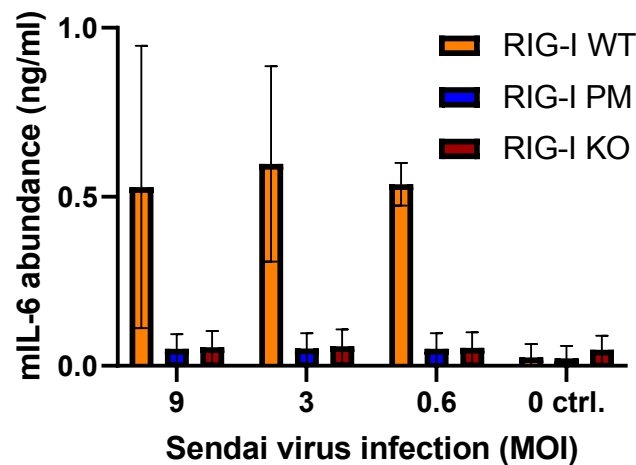
The results of at least three independent experiments detecting mIFN- α or mIL-6 are depicted as box plots (compare Figure 14). A 2-Way ANOVA was used to indicate significant effects of the factors "MOI Sendai infection" and "RIG-I genotype", as well as their interaction, on the variable "mIFN- α abundance" or "mIL-6 abundance". The outcome of both the investigations was similar, but in case of mIFN- α , the ANOVA analyses suggest that the induction of the cytokine was not only dependent on RIG-I, unlike mIL-6. Additionally, the results of the mIFN- α analysis was very similar to the one of the IAV Δ NS1 infection experiment and the outcome of the mIL-6 very similar to the one of the specific RIG-I ligands. In detail, the ANOVA analyses indicate a significant effect of the factor "MOI Sendai virus infection" on the variable "mIFN- α abundance", in all of the comparisons between the data groups (p at least 0.0092), showing that the expression of the cytokine is enhanced in all BmdM Φ in response to infection. For mIL-6, the variable is only affected significantly/shows a tendency to significant values by the factor "MOI Sendai virus infection" in the comparisons including WT cells ($p = 0.0400/p = 0.0504$, very close to a significant difference). For the factor "RIG-I genotype", the data indicate a significant effect on the variable "mIFN- α abundance" or "mIL-6 abundance" in the comparisons including RIG-I WT cells ($p < 0.0001$ for mIFN- α and p at least 0.0002 for mIL-6), showing that cytokine induction is significantly reduced in RIG-I PM and KO cells compared to WT cells. This is further supported by the indication of a significant interaction between the factors for mIFN- α (p at least 0.0110) and a similar tendency for mIL-6 (p at least 0.0726), in the comparisons including RIG-I WT cells. The factor "RIG-I genotype" had no significant effect in the comparison between RIG-I PM and KO cells for both cytokines, showing again that RIG-I PM is sufficient to repress the complete potential of the protein to enhance mIFN- α and additionally mIL-6 production (compare Figure 14 A and B).

A



2-Way ANOVA	RIG-I WT vs. PM		RIG-I WT vs. KO		RIG-I PM vs. KO	
	p value	p value summary	p value	p value summary	p value	p value summary
interaction	0.0110	*	0.0104	*	0.8417	ns
MOI Sendai	0.0087	**	0.0092	**	0.0077	**
RIG-I genotype	<0.0001	****	<0.0001	****	0.1485	ns

B



2-Way ANOVA	RIG-I WT vs. PM		RIG-I WT vs. KO		RIG-I PM vs. KO	
	p value	p value summary	p value	p value summary	p value	p value summary
interaction	0.0726	ns	0.0595	ns	0.9660	ns
MOI Sendai	0.0400	*	0.0504	ns	0.8535	ns
RIG-I genotype	0.0001	***	0.0002	***	0.5991	ns

Figure 14: Sendai virus infection triggers the induction of mIFN- α and mL-6 in BmdM Φ , which is dependent on RIG-I. Bone marrow cells were extracted from RIG-I WT, PM and KO mice. The cells were differentiated into M Φ *in vitro* and then infected with different MOI of a recombinant Sendai virus strain (9; 3; 0.6 MOI), or mock (0 ctrl.). An ELISA detecting mIFN- α (A) or mL-6 (B) in cell culture supernatant was performed. The results of three independent experiments are depicted as box plots (whiskers indicate lowest and highest value, box borders indicate 25th and 75th percentile, mid indicates the median). A 2-Way ANOVA was used to indicate significant effects of the factors "MOI Sendai virus" and "RIG-I genotype", as well as their interaction, on the variables "mIFN- α abundance" (A) or "mL-6 abundance" (B). The results of the ANOVAs are depicted in the respective tables.

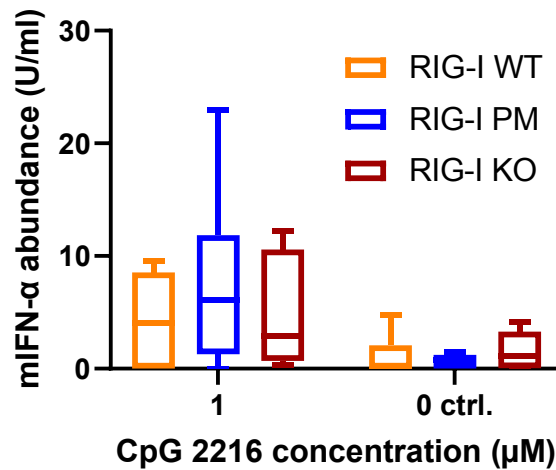
4.2.2.4. *TLR signaling does not differ between RIG-I WT, PM and KO mice*

For the investigation of altered TLR signaling, bone marrow cells were extracted from RIG-I WT, PM and KO mice. The cells were differentiated into M Φ *in vitro* and then treated with either the agonists CpG 2216 (TLR9), LPS (TLR4), Pam3Cys (TLR1 and 2) or mock. An ELISA detecting mIFN- α and/or mL-6 in cell culture supernatant from treated cells was performed (c. c. 3.5 ff.).

For the analysis of TLR9 signaling, the results of at least six independent experiments detecting mIFN- α (compare Figure 15 A) or seven independent experiments detecting mL-6 (compare Figure 15 B), using the ligand CpG 2216, are depicted as box plots. A 2-Way ANOVA was used to show significant effects of the factors "CpG 2216 treatment" and "RIG-I genotype", as well as their interaction, on the variables "mIFN- α abundance" or "mL-6 abundance".

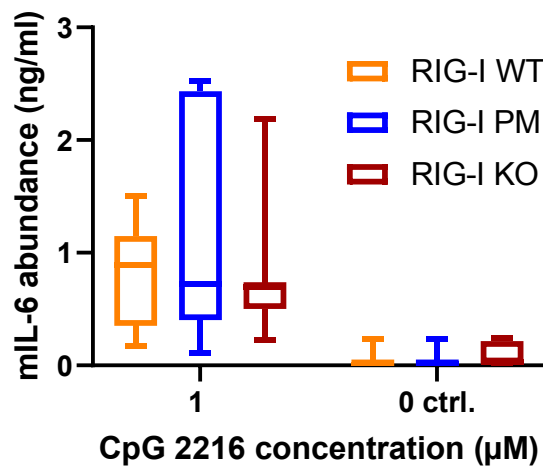
The data demonstrate that the factor "CpG 2216 treatment" significantly increased the variables "mIFN- α abundance" (p at least 0.0270) and "mL-6 abundance" (p at least 0.0005) in all comparisons between the BmdM Φ . This induction was not significantly dependent on the factor "RIG-I genotype" and no significant interaction between the factors was indicated, in all comparisons between the data groups. Nevertheless, there seemed to be a slightly higher induction of IFN- α and mL-6 in RIG-I PM mouse derived cells (compare Figure 15).

A



2-Way ANOVA	RIG-I WT vs. PM		RIG-I WT vs. KO		RIG-I PM vs. KO	
source of variation	p value	p value summary	p value	p value summary	p value	p value summary
interaction	0.2965	ns	0.9178	ns	0.3911	ns
CpG 2216	0.0114	*	0.0270	*	0.0207	*
RIG-I genotype	0.4585	ns	0.7281	ns	0.6685	ns

B



2-Way ANOVA	RIG-I WT vs. PM		RIG-I WT vs. KO		RIG-I PM vs. KO	
source of variation	p value	p value summary	p value	p value summary	p value	p value summary
interaction	0.4561	ns	0.8092	ns	0.4215	ns
CpG 2216	<0.0001	****	<0.0001	****	0.0005	***
RIG-I genotype	0.4417	ns	0.8943	ns	0.5581	ns

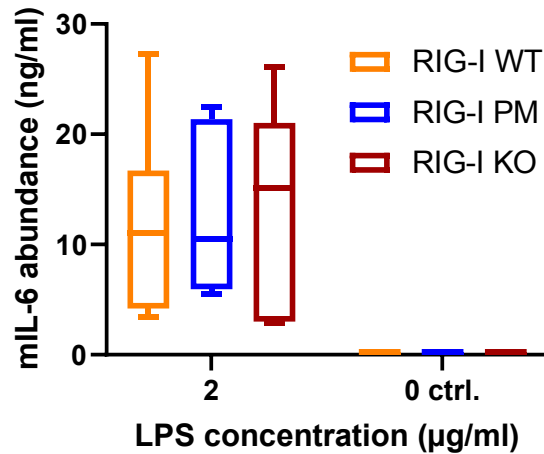
Figure 15: TLR9 activation by CpG 2216 in BmdMΦ significantly enhances mIFN-α and mL-6 levels and is not effected by expression of RIG-I variants. Bone marrow cells were extracted from RIG-I WT, PM and KO mice. The cells were differentiated into MΦ *in vitro* and then treated with 1 μM CpG 2216 or left untreated (0 ctrl.). An ELISA detecting mIFN-α (A) or mL-6 (B) in cell culture supernatant was performed. The results of at least six (A) or seven (B) independent experiments are depicted as box plots (whiskers indicate lowest and highest value, box borders indicate 25th and 75th percentile, mid indicates the median). A 2-Way ANOVA was used to indicate significant effects of the factors "CpG 2216 treatment" and "RIG-I genotype", as well as their interaction, on the variable "mIFN-α abundance" (A) or "mL-6 abundance" (B). The results of the ANOVAs are depicted in the respective tables.

The results of at least seven independent experiments using the ligand LPS to show TLR4-mediated mIL-6 expression or Pam3Cys to show TLR1/TLR2-mediated mIL-6 expression are depicted as box plots (compare Figure 16). A 2-Way ANOVA was used to show significant effects of the factors "LPS treatment" or "Pam3Cys treatment" and "RIG-I genotype", as well as their interaction, on the variable "mIL-6 abundance".

Concerning LPS, the data show that the variable "mIL-6 abundance" was significantly increased by the factor "LPS treatment" in all comparisons ($p < 0.0001$). Further, there was no significant effect of the factor "RIG-I genotype" on the variable and no significant interaction between the factors detectable in all comparisons between the data groups (compare Figure 16 A).

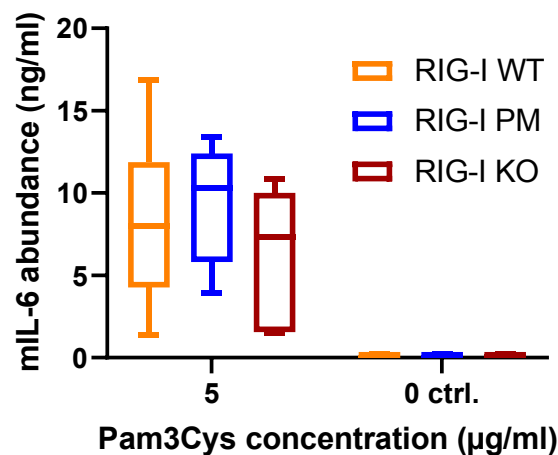
Concerning Pam3Cys, the results show that the variable "mIL-6 abundance" was significantly enhanced by the factor "Pam3Cys treatment" ($p < 0.0001$), but there was no significant effect of the factor "RIG-I genotype" and no significant interaction between the factors detectable, for all comparisons between the data groups. Comparable to the CpG 2216 treatment, there was a tendency to slightly higher mIL-6 abundance in the RIG-I PM mouse derived BmdM Φ (compare Figure 16 B).

A



2-Way ANOVA	RIG-I WT vs. PM		RIG-I WT vs. KO		RIG-I PM vs. KO	
	p value	p value summary	p value	p value summary	p value	p value summary
interaction	0.7874	ns	0.8530	ns	0.9573	ns
LPS	<0.0001	****	<0.0001	****	<0.0001	****
RIG-I genotype	0.7856	ns	0.8343	ns	0.9751	ns

B



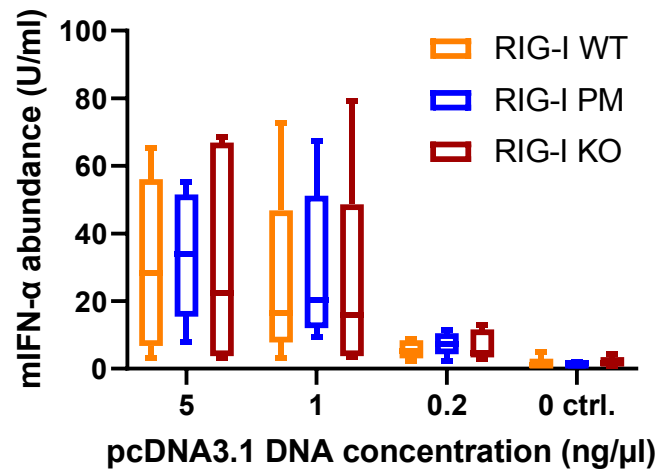
2-Way ANOVA	RIG-I WT vs. PM		RIG-I WT vs. KO		RIG-I PM vs. KO	
	p value	p value summary	p value	p value summary	p value	p value summary
interaction	0.6487	ns	0.3608	ns	0.1263	Ns
Pam3Cys	<0.0001	****	<0.0001	****	<0.0001	****
RIG-I genotype	0.6457	ns	0.3845	ns	0.1377	Ns

Figure 16: TLR4 activation by LPS or TLR1/2 activation by Pam3Cys enhances mL-6 production in BmdMΦ, which is not effected by a lack of RIG-I functionality. Bone marrow cells were extracted from RIG-I WT, PM and KO mice. The cells were differentiated into MΦ *in vitro* and then treated with either 2 µg/ml LPS (A), 5 µg/ml Pam3Cys (B) or were left untreated (respective 0 ctrl.). An ELISA detecting mL-6 in cell culture supernatant was performed. The results of at least seven independent experiments are depicted as box plots (whiskers indicate lowest and highest value, box borders indicate 25th and 75th percentile, mid indicates the median). A 2-Way ANOVA was used to indicate significant effects of the factors "LPS treatment" or "Pam3Cys treatment" and "RIG-I genotype", as well as their interaction, on the variable "mL-6 abundance". The results of the ANOVAs are depicted in the respective table.

4.2.2.5. *cGAS-STING* signaling is not different in RIG-I WT, PM and KO mice

To investigate differences in cGAS-STING-signaling in the mouse lines, bone marrow cells were extracted from RIG-I WT, PM and KO mice. The cells were differentiated into M Φ *in vitro* and then transfected with different concentrations of plasmid-DNA (pcDNA3.1, empty vector) or left untreated. An ELISA detecting mIFN- α in the cell culture supernatant was performed (c. c. 3.5 ff.). The results of at least five independent experiments were depicted as box plots (compare Figure 17). A 2-Way ANOVA was used to show significant effects of the factors "DNA concentration" and "RIG-I genotype", as well as their interaction, on the variable "mIFN- α abundance".

The results show that activation of cGAS/STING upon DNA treatment led to mIFN- α production, which is similar in all BmdM Φ . This is indicated by the finding that the factor "DNA concentration" had a significant effect on the variable in all comparisons between the groups (p at least 0.0012) and that the factor "RIG-I genotype" had no significant effect on the variable, as well as there was no significant interaction between the factors, in all the comparisons between the groups. Despite of a slightly higher mIFN- α abundance in RIG-I PM mouse derived cells, no significant alterations in the cGAS/STING system based on side effects of the CRISPR/Cas9 application or compensatory upregulations in response to RIG-I function loss were detectable (compare Figure 17).



2-Way ANOVA	RIG-I WT vs. PM		RIG-I WT vs. KO		RIG-I PM vs. KO	
	p value	p value summary	p value	p value summary	p value	p value summary
interaction	0.9944	ns	>0.9999	ns	0.9948	ns
DNA	0.0001	***	0.0012	**	0.0009	***
RIG-I genotype	0.7277	ns	0.9407	ns	0.8172	ns

Figure 17: Alternative RIG-I variant expression does not affect mIFN- α induction by DNA-activated cGAS/STING signaling in BmdM Φ . Bone marrow cells were extracted from RIG-I WT, PM and KO mice. The cells were differentiated into M Φ *in vitro* and then transfected with different concentrations of plasmid DNA (pcDNA3.1: 5; 1; 0.2 ng/ μ l) or the transfection reagent only (0 ctrl.). An ELISA detecting mIFN- α in cell culture supernatant was performed. The results of at least five independent experiments are depicted as box plots (whiskers indicate lowest and highest value, box borders indicate 25th and 75th percentile, mid indicates the median). A 2-Way ANOVA was used to indicate significant effects of the factors "DNA concentration" and "RIG-I genotype", as well as their interaction, on the variable "mIFN- α abundance". The results of the ANOVAs are depicted in the table.

4.2.3. Summary: Innate immune signaling in the established RIG-I variant mouse lines

To sum up the investigation of innate immune signaling in BmdM Φ derived from RIG-I WT, PM and KO mice, all observed RIG-I-mediated effects are depicted in one table (compare Table 35). The experiments show that WT RIG-I-mediated mIFN- α and mL-6 release in response to IAV Δ NS1 and Sendai virus infections, as well as treatment with specific RIG-I ligands, is abolished in the RIG-I K271A point mutation and the RIG-I KO mouse derived BmdM Φ . Since TLR1; 2; 4 and 9 signaling, as well as STING signaling, do not significantly differ between the RIG-I WT, PM and KO BmdM Φ , there seem to be no off-target effects by the CRISPR/Cas9-mediated genetic engineering, or significant changes in PRR expression as compensation for lacking or defective RIG-I expression. Remarkably, there might be some slight differences in PRR expression in the RIG-I PM mouse derived cells, which show slightly but insignificantly higher mIFN- α or mL-6 release after stimulation with CpG 2216, Pam3Cys or plasmid DNA, in comparison to RIG-I WT and KO cells. Nevertheless, the findings validate the established mouse lines as useful model for the investigation of RIG-I-mediated effects in innate immunity.

Table 35: A summary of the results derived from the ELISA analyses. The significant differences between the compared BmdMΦ in regard to the effect of the factor RIG-I genotype on the respective cytokine abundance is summarized. In all cases despite of IAV/PR/8 (in brackets), a significant induction of the respective cytokine had been achieved with the used stimulus.

Treatment	Cytokine	RIG-I genotype		
		WT vs. PM	WT vs. KO	PM vs. KO
5'ppp-dsRNA	IFN- α	**	**	ns
3p-hpRNA	IFN- α	****	****	ns
(IAV/PR/8)	IFN- α	ns	ns	*
IAV/PR/8 Δ NS1	IFN- α	****	***	ns
Sendai virus	IFN- α	****	****	ns
Sendai virus	IL-6	***	***	ns
CpG 2216	IFN- α	ns	ns	ns
CpG 2216	IL-6	ns	ns	ns
Pam3Cys	IL-6	ns	ns	ns
LPS	IL-6	ns	ns	ns
Plasmid DNA	IFN- α	ns	ns	ns

4.2.4. Validation of murine embryonal fibroblast cell lines

To perform *in vitro* infection experiments with recombinant IAV strains, MEF cell lines were established from the generated RIG-I WT, PM and KO mouse lines (c. c. 3.11). Genomic DNA was extracted from the cells to validate their RIG-I genotype with Sanger-sequencing (c. c. 3.2). With the aim to validate their correct RIG-I phenotype, the expression of the protein was induced with IFN- α (compare Table 4). Afterwards, the RIG-I and β -actin expression in the cell lysates were analyzed with WB (c. c. 3.8 f.). Since the analysis was a validation of previous findings using primary bone marrow cells from the mouse lines, the experiments were performed only once (c. c. 4.2.1).

The results of the RIG-I genotyping with Sanger-sequencing showed the expected genotypes for the RIG-I WT, PM and KO MEF lines (data not shown, similar as depicted in chapter 4.1). The WB detecting mRIG-I shows that RIG-I protein expression was detectable in the RIG-I WT and PM MEF

lines, but not in the RIG-I KO MEF line, while β -actin was detectable in comparable amounts in all three MEF lines (compare Figure 18). These results were similar to the results of the protein detection in primary bone marrow cells derived from the mouse lines (c. c. 4.2.1) and validate, that the different MEF-lines expressed the expected RIG-I variants and could be used for downstream experiments.

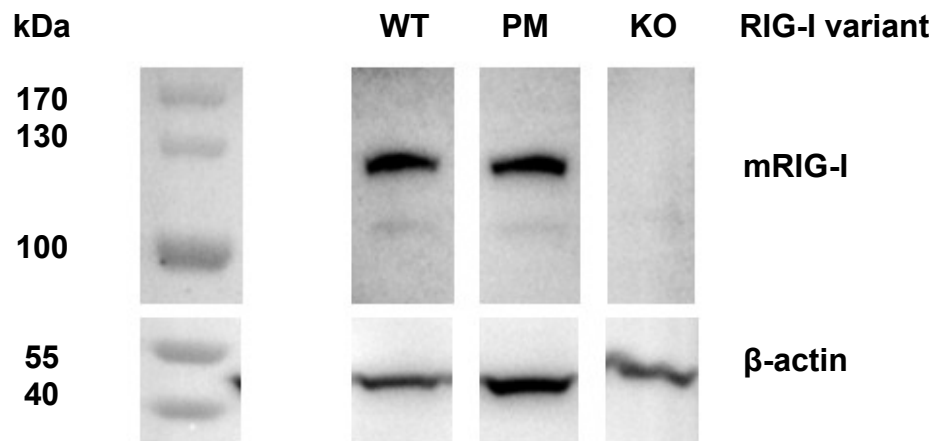


Figure 18: MEF cells derived from the established RIG-I mouse lines express the correct RIG-I variants. MEF cells derived from the established RIG-I WT, PM and KO mouse lines were treated with IFN- α to induce RIG-I. The cells were lysed and WB was performed with a mRIG-I targeting antibody (Enzo ALX-804-960-0100) or a β -actin targeting antibody (Sigma-Aldrich A2228).

4.3. Generation and characterization of recombinant IAV/PR/8 PB2-627K and IAV/PR/8 PB2-627E strains

4.3.1. The generation of a plasmid encoding for the PB2-627E variant with primer-mediated mutagenesis

A pHW2000 plasmid encoding for the IAV PB2 RNA gene was genetically engineered with primer-mediated mutagenesis to substitute the nt 1879 A with G, which changes the aa 627 from a mammalian adaptation (K) to an avian adaptation (E). *E. coli* DH5 α clones potentially expressing the engineered plasmids were picked from LB agar plates and propagated in LB liquid medium o. n. Afterwards, the plasmid DNA was purified with a plasmid purification kit (Thermo), the engineered DNA part was amplified with a PCR and purified with a PCR purification kit (c. c. 3.12.1). In the end, the DNA sequence was analyzed by Sanger-sequencing (c. c. 3.3). The correct plasmid sequence was confirmed in different clones, one example for a sequencing result of the PB2-627 codon complementary strand is depicted in Figure 19. The clear peaks indicate a homogeneous genotype.

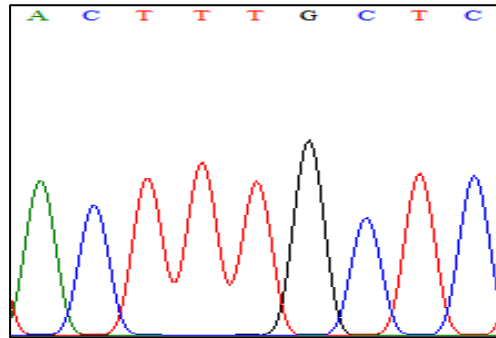


Figure 19: The Sanger-sequencing of the IAV PB2 plasmid coding for the 627E version. The original plasmid coding for the IAV PB2 gene carried the 627K genotype. The first nt of this codon was changed from A to G using a primer-mediated mutagenesis technique to derive the PB2-627E version. *E. coli* DH5 α were transformed with the altered plasmid and the propagated vector was purified. The DNA sequence of the vector was Sanger-sequenced to validate the genotype. The output of the sequencing chromatogram for the three nt of the PB2-627 codon is depicted with two additional codons upstream (the sequence of the complementary strand is depicted).

4.3.2. A recombinant IAV/PR/8 PB2-627E strain does not replicate in mammalian cell lines without adaptive mutations, in comparison to an IAV PB2-627K variant

With the aim to generate a recombinant IAV/PR/8 PB2-627K and -627E strain for mouse infection experiments, which share comparable stock qualities, different mammalian cell lines were investigated as virus hosts. Virus assembly was achieved in HEK293 cells. In passage 1, HEK293 cell culture supernatants containing the desired virus were used to infect MDCK, Huh7.5 RIG-I KO, CaCo2 or MEF RIG-I KO cells (c. c. 3.12.2 ff.). After one infection cycle, the resulting cell culture supernatants were analyzed for infectious virus particles with a MDCK cell line based single cell infection assay (SCIA) (c. c. 3.13.2) and virus RNA was Sanger-sequenced after reverse-transcription into cDNA (c. c. 3.3). Remarkably, no IAV PB2-627E strain without mutations was generated on the different mammalian cell lines, indicating that this virus variant is insufficient to replicate under these conditions. All results are summarized in Table 36 and examples for codons indicating mutations found by Sanger-sequencing are depicted in Figure 20.

To overcome the insufficient replication of the IAV PB2-627E virus in mammalian cells, DF-1 chicken cells were used as virus hosts. Replication of both virus strains was achieved in this cell line, with no adaptive mutations in the PB2 RNA gene of both strains. This shows that the IAV PB2-627E strain could be rescued completely in DF-1 chicken cells, while the IAV PB2-627K strain replicates similar in DF-1 and mammalian cell lines.

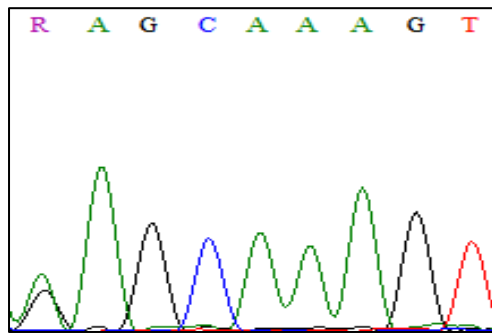
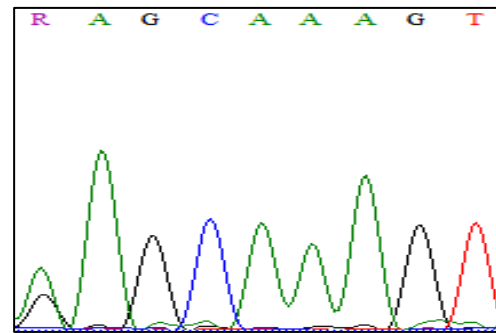
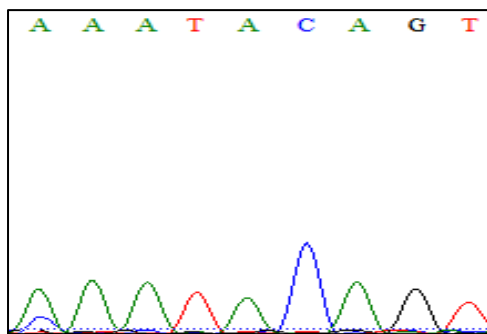
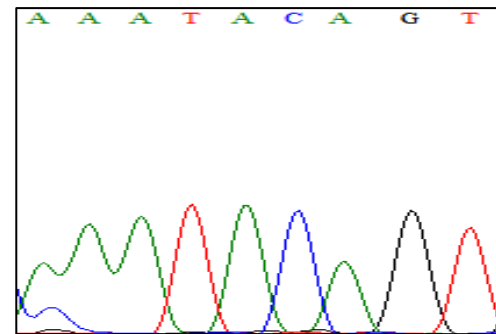
A MDCK cells PB2 627**Sequencing 1****Sequencing 2****B CaCo2 cells PB2 591****Sequencing 1****Sequencing 2**

Figure 20: The recombinant IAV PB2-627E strain does not propagate in mammalian cell lines without adaptive mutations. HEK293 cells were transfected with the eight plasmids encoding for the different IAV RNA genes to assemble the virus. The resulting cell culture supernatants were used to infect MDCK or CaCo2 cells. The sequence of the PB2 gene was Sanger-sequenced in the resulting cell culture supernatants to validate the genotype. The output of the sequencing chromatogram for the three nt of the PB2-627 codon and two codons downstream in the strain from the MDCK cells (A) or of the PB2-591 codon and two additional codons downstream in the strain from the CaCo2 cells (B) are depicted. Both mutations result in an alteration of the amino acid.

Table 36: A recombinant IAV/PR/8 PB2-627E strain does not replicate in mammalian cell lines without adaptive mutations, in contrast to an IAV PB2-627K variant.

Cell line	Replication of IAV PB2-627K	Replication of IAV PB2-627E
MDCK	yes	Only with PB2 E627K back mutation
Huh7.5 RIG-I KO	yes	Only with PB2 E627K back mutation
CaCo2	yes	Only with PB2 E627K or PB2 Q591K mutation
MEF RIG-I KO	yes	Only with a high infection titer (0.5 MOI compared to 0.001 MOI)
DF-1 (chicken)	yes	yes

4.3.3. Characterization of recombinant virus strains generated in DF-1 cells

After generation of the second passage of recombinant IAV PB2-627K and -627E virus in DF-1 cells, recombinant virus stocks were generated (c. c. 3.12.2 f.). To secure a similar quality, the stocks were compared for different features.

4.3.3.1. The virus titration with SCIA indicates a comparable infection potential for the IAV PB2-627K and IAV PB2-627E virus stocks

At first, the infectious virus particles were quantified with a MDCK based SCIA in the recombinant virus stocks derived from DF-1 cells. Two aliquots of each stock were analyzed per assay and three assays were performed, hence six stocks per virus strain were analyzed in total (n=6). The amount of stained cells was counted in two wells of each technical replicate and the values were multiplied with the respective dilution factors to receive FFU/ml (c. c. 3.13.2). The mean count of the technical replicates was calculated. The mean of the six biological replicates was calculated for each of the investigated stocks and depicted as box plot (compare Figure 21). An unpaired t-test was used to indicate significant differences between the virus titers of both recombinant virus stocks. The result indicates no significant difference between the infectious titer of both stocks ($p = 0.97$).

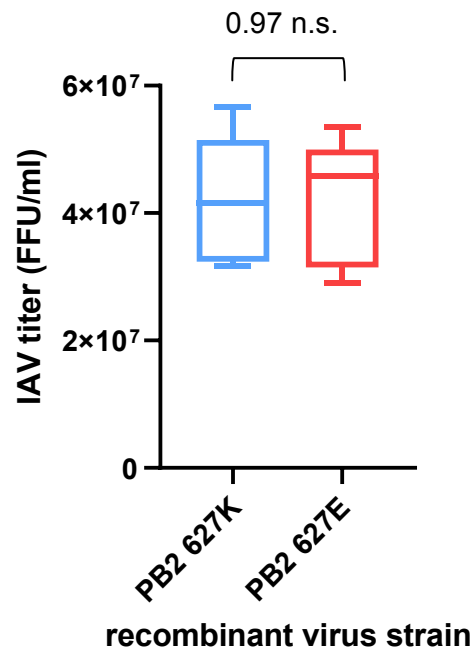


Figure 21: The infectious titer of both recombinant IAV PB2-627K and -627E virus strains generated in DF-1 chicken cells is similar. Recombinant virus stocks generated in DF-1 chicken cells were analyzed for infectious particles with a MDCK based single cell infection assay. The mean count of stained cells of the technical replicates was multiplied by the respective dilution factor, the means of the technical replicates were calculated. The means of six biological replicates are depicted as box plots (whiskers indicate lowest and highest value, box borders indicate 25th and 75th percentile, mid indicates the median). An unpaired t-test was used to indicate a significant difference between the mean FFU/ml of the two analyzed virus strains.

4.3.3.2. A hem-agglutination test indicates similar amounts of HA protein expression in both virus stocks

To compare the amount of HA protein expression in the recombinant virus stocks, a hem-agglutination test was performed. Two biological replicates of the recombinant virus stocks were analyzed as duplicates for their ability to agglutinate chicken erythrocytes (compare 3.13.3). The mean of the duplicates was calculated and listed in Table 37. There was no difference between the technical replicates, so no standard deviation is indicated.

Table 37: Results of the hem-agglutination test.

	IAV PB2-627K	IAV PB2-627E
Hem-agglutination	320 HAU/ml	320 HAU/ml

4.3.3.3. A plaque assay indicates similar amounts of virus particles able to replicate for an IAV PB2-627K and -627E strain, but a reduced spread of IAV PB2-627E particles

A plaque assay for the detection of replicating virus particles in the recombinant virus strains was kindly performed by the group of Prof. Dr. Friebertshäuser, at the Institute for Virology in Marburg. They reported similar amounts of foci for both the IAV PB2-627K (1.1×10^7 PFU/ml) and IAV PB2-627E (9.5×10^6 PFU/ml) strains on MDCK cells, but a diameter of approx. 3 mm for the IAV PB2-627K virus-mediated foci vs. a diameter of approx. 1 mm for the IAV PB2-627E-mediated foci.

This finding indicates a similar amount of infectious virus particles with the ability to replicate for both strains. On the other hand, it shows that the IAV PB2-627E virus particles did replicate less efficient in MDCK cells than IAV PB2-627K particles. This finding is in line with the result that the IAV PB2-627E strain was insufficient to replicate in mammalian cell lines (c. c. 4.3.2). The titers of replicating virus particles (PFU/ml) were approx. four-fold less than the titers of infecting particles (FFU/ml). This suggests that a portion of the virus particles was defective, but to a similar extend in both stocks. For the adjustment of infection doses for the mouse infection study, the titers of infectious particles (PFU/ml and not FFU/ml) were chosen, for the reason of a better comparability between data and experience from the literature and other groups (Reppe K. 2015; Dietert K. 2017; Lu J. 2018).

4.3.3.4. The semi-quantification of recombinant virus stock M-protein suggests that IAV PB2-627E virus stocks carry more virus particles than IAV PB2-627K stocks

For an additional analysis of defective virus particles, viral M-protein expression was analyzed in the IAV PB2-627K and -627E virus stocks. One, two or four million FFU virus were lysed and investigated by WB (c. c. 3.9, also compare Figure 22).

For direct comparison, the WB signals were semi-quantified. Therefore, the images of the blots were analyzed for band size intensity with the software ImageJ. The sizes of the AUC were calculated for the different virus amounts and are shown in Table 38. The values of the samples containing four million virus particles were excluded from further analysis because of signal saturation. In the next step, the ratio between the size AUC of the IAV PB2-627E and -627K strains was calculated for the amount virus particles. In the end, the mean of the ratios for 1×10^6 and 2×10^6 virus particles were calculated (c. c. 3.10 and 3.13.5 for the procedures and Table 38 for the results).

Taken together, these results suggest that the IAV PB2-627E stocks contain an approximately 3.5-fold higher amount of virus particles than the IAV PB2-627K stocks. This finding was not expected in regard to the previous findings, but may be explained with replication disadvantages of the IAV PB2-627E strain in MDCK cells, which masks the true amount of virus particles. This disadvantage should not affect the outcome of the hem-agglutination test, so it is surprising that no differences in the titer were found in this assay (c. c. 4.3.3.2). An explanation for this difference may be the lower precision of the hem-agglutination test, which might fail to detect a 3.5-fold difference.

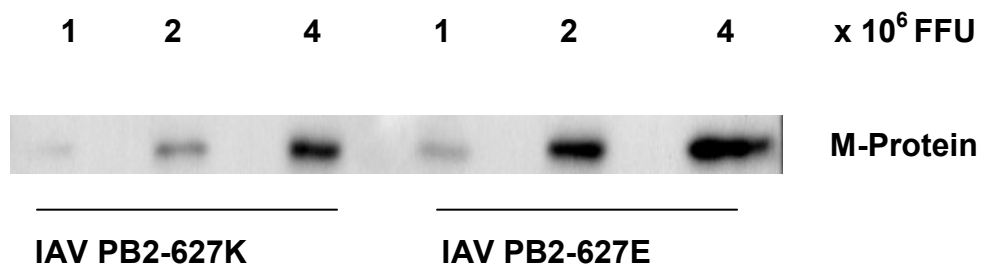


Figure 22: The IAV PB2-627E virus strain carries more M-protein than the IAV PB2-627K virus strain. IAV M-protein was detected with WB using an in house made antibody, in virus stock lysates containing 1, 2 or 4 million infectious virus particles (FFU).

Table 38: Semi-quantification of IAV M-protein indicates an approximately 3.5-fold higher amount of viral particles in the IAV PB2-627E stocks compared to the IAV PB2-627K stocks.

Stock	FFU x 10 ⁶	Size of the area under the curve (AUC)
IAV PB2-627K	1	4,143,004
IAV PB2-627K	2	23,612,602
IAV PB2-627E	1	16,093,773
IAV PB2-627E	2	75,242,208
IAV PB2-627E/-627K 1 x 10 ⁶	IAV PB2-627E/-627K 2 x 10 ⁶	Mean ratio size AUC
3.88	3.19	IAV PB2-627E/-627K
		3.54

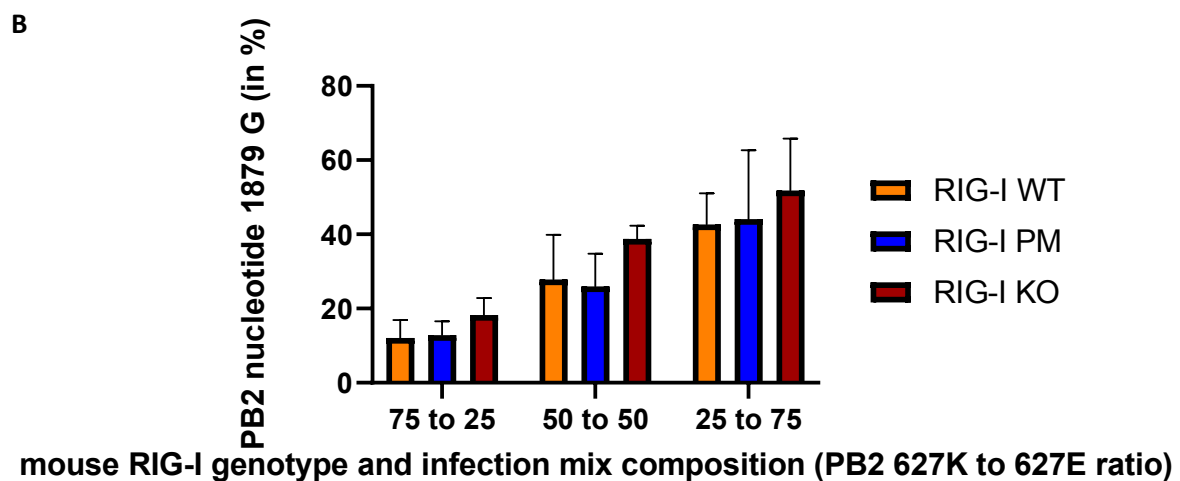
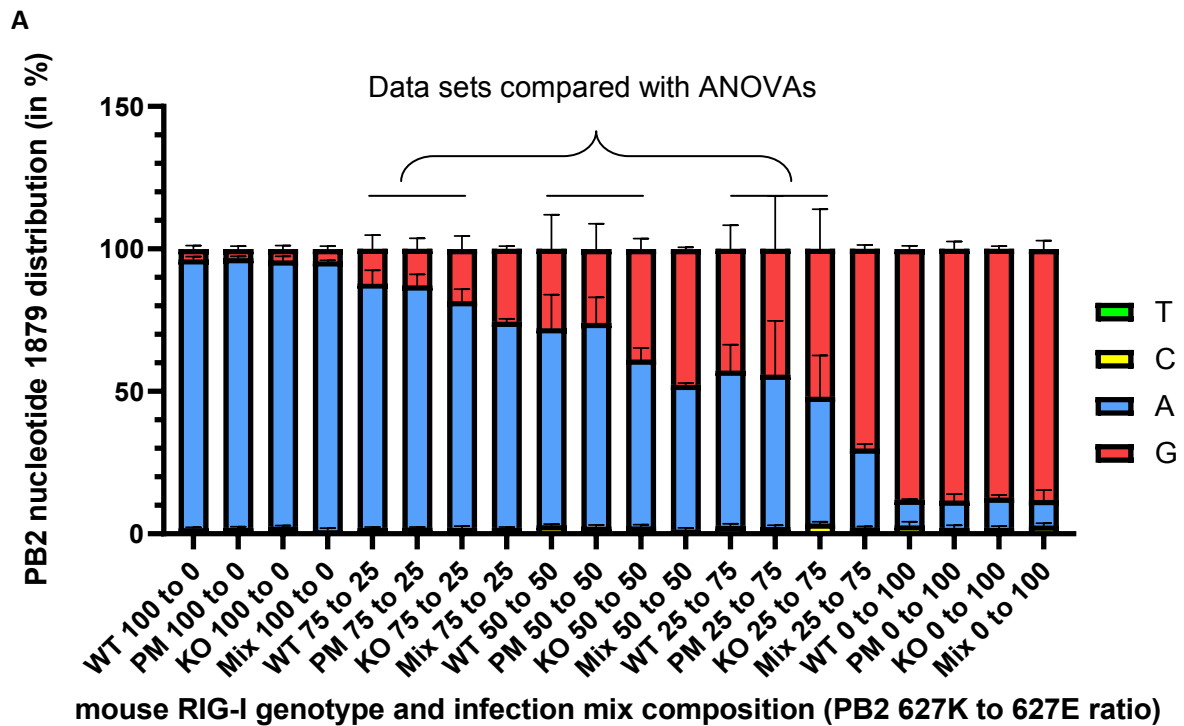
4.3.4. Competitive infection of RIG-I WT, PM and KO MEF cells with both IAV PB2-627K and -627E strains suggests slight, but not significant effects of differential RIG-I expression on virus replication

To compare the replication of both the IAV PB2-627K and -627E strains, a competitive infection experiment was performed. RIG-I WT, PM and KO MEF cells were infected at a total of 0.5 MOI for four days with a variable ratio of either both strains or one strain only (IAV PB2-627K to -627E mix ratios: 100 % to 0 %; 75 % to 25 %; 50 % to 50 %; 25 % to 75 %; 0 % to 100 %). The cell culture supernatants from infected cells were harvested and the viral RNA was analyzed by Sanger-sequencing after reverse-transcription into cDNA to determine the PB2 nt 1879 percentage distribution (c. c. 3.13.6). The mean of three independently performed experiments is depicted with the respective standard deviation as stacked bar plot (compare Figure 23 A and chapter 3.19.3). The depicted nt is the first of the IAV PB2-627 codon and can be used to differentiate IAV PB2-627K (nt A) from -627E (nt G). To determine significant differences in the replication efficiency between both the IAV PB2-627K and -627E strain in the respective subset of the data (compare Figure 23 B, only samples from cells infected with both virus strains were compared), the variable "PB2 nt 1879 G abundance" was analyzed for effects by the factors "infection mix composition" and "RIG-I genotype" with a 2-Way ANOVA.

For the experiments, the infection mix ratio was only adjusted by infectious particle titration and did not depend on a previous infection mix ratio sequencing result. Hence, the results suggest a low variation between the IAV PB2-627K and -627E virus stocks, indicated by the finding that the calculated virus ratios closely mirror the nt distribution ratios in the infection mixes (compare Figure 23 "Mix" samples).

Further, the results suggest that the abundance of PB2 nt 1879 G is markedly reduced in all samples compared to the infection mixes, indicating again that the nt 1879 A/aa 627K variant did replicate stronger in mammalian cell lines than the nt 1879 G/aa 627E variant. The finding that the factor "infection mix composition" significantly affected the variable shows that the replication advantage of the IAV PB2-627K variant was not strong enough to completely overgrow the IAV PB2-627E variant in MEF cells in four days with 0.5 MOI infectious dose. However, the replication advantage might be higher than the results suggest, since the PB2-627K polymerase may also amplify the PB2-627E variant in the cells with both virus types present. Most importantly, the factor "RIG-I genotype" showed a tendency to affect the variable "PB2 nt 1879 G abundance", but was not reaching significance in the comparison between RIG-I KO and both WT and PM MEFs ($p = 0.0559$ and $p = 0.1064$). This finding suggests, that RIG-I might be a factor that mediates positive selection of the IAV

PB2-627K genotype over the -627E genotype, but not the only one. The suggestion is underlined by the finding that the loss of RIG-I was not sufficient to abolish the replication advantage of the PB2-627K genotype over the -627E genotype. This is indicated by a difference between the nt distribution in the infection mix and the RIG-I KO samples, still in favor of the PB2-627K genotype. Hence, there seems to be at least one more factor driving positive selection of the PB2-627K genotype, which might be a replication advantage by the enhanced binding affinity of the PB2-627K polymerase to the viral panhandle structures itself (c. c. 1.2.6.2).



2-Way ANOVA	RIG-I WT vs. PM		RIG-I WT vs. KO		RIG-I PM vs. KO	
source of variation	p value	p value summary	p value	p value summary	p value	p value summary
interaction	0.9602	ns	0.8959	ns	0.8272	ns
inf. mix composition	0.0010	**	0.0001	***	0.0007	***
RIG-I genotype	0.9795	ns	0.0559	ns	0.1064	ns

Figure 23: IAV PB2-627K has a replication advantage compared to IAV PB2-627E in RIG-I WT and PM MEFs, which is slightly lower in RIG-I KO MEFs. Different IAV PB2-627K to -627E infection mixes were prepared (% of mix ratios IAV PB2-627K to -627E: 100 to 0 %, 75 to 25 %, 50 to 50 %, 25 to 75 % and 0 to 100 %). A part of the infection mixes was directly stored for analysis by Sanger-sequencing (Mix). The remaining infection mixes were used to infect either RIG-I WT, PM or KO MEFs with 0.5 MOI in total. After four days, cell culture supernatants were harvested from infected cells and the samples were prepared for RNA analysis by Sanger-sequencing. The mean percentage PB2 nt 1879 distribution with the respective standard deviations of three independently performed experiments is depicted as stacked bar plot (A). A 2-Way ANOVA was used to indicate significant differences between the indicated subset values of "PB2 nt 1879 G abundance" as variable, in dependence of the factors "infection mix composition" and "RIG-I genotype" (B).

4.3.5. The recombinant IAV PB2-627K and IAV PB2-627E virus strains seem to be genetically stable in regard to the PB2 RNA gene

Due to the finding that the IAV PB2-627E strain only replicated in mammalian cells after acquiring an adaptive mutation, which happened frequently (c. c. 4.3.2), the genetic stability of the virus stocks generated in DF-1 cells was validated. Therefore, the complete PB2 RNA gene sequence of the IAV PB2-627K and -627E stocks from passage one and two in DF-1 cells was analyzed by Sanger-sequencing (c. c. 3.13.1.2). Of note, no mutations in the complete PB2 gene in both passages of the strains were found, which were above background levels (the complete sequencing is not shown, compare Figure 24 A for passages 1 and 2 of the IAV PB2 627K strain and Figure 24 B for passages 1 and 2 of the IAV PB2 627E strain). Static background signals are commonly found for most nt's in Sanger-sequencing and result from inaccuracy of the method. The results are supported by further sequencing of the viral PB2 RNA gene sequence flanking the codon 627 several times before and after an additional infection cycle using different cell lines in competitive infection assays (as shown for the PB2 nt 1879 percentage distribution in MEF cells, compare Figure 23 A 100 to 0 % and 0 to 100 % samples in the previous chapter; similar for A549 cell lines, data not shown). In these results, no marked change of the ratio between the nt G and A was found, compared to the infection mix, if the cells were only infected with one of the virus strains. Additionally, the abundance of the nt A was not higher than the average background noise in Sanger-sequencing, for the IAV PB2-627E strain. Since a fast overgrowth of the PB2-627E genotype by PB2-627K was found in early attempts to generate an IAV PB2-627E stock in mammalian cell lines, it is assumed that a small amount of PB2-627K genotype would overgrow the PB2-627E genotype very fast. Based on this assumption and the finding that no overgrowth of the PB2-627E strain by PB2-627K (or vice versa) occurred during three tracked passages, both the recombinant virus strains were validated as genetically stable for their respective PB2 RNA sequence.

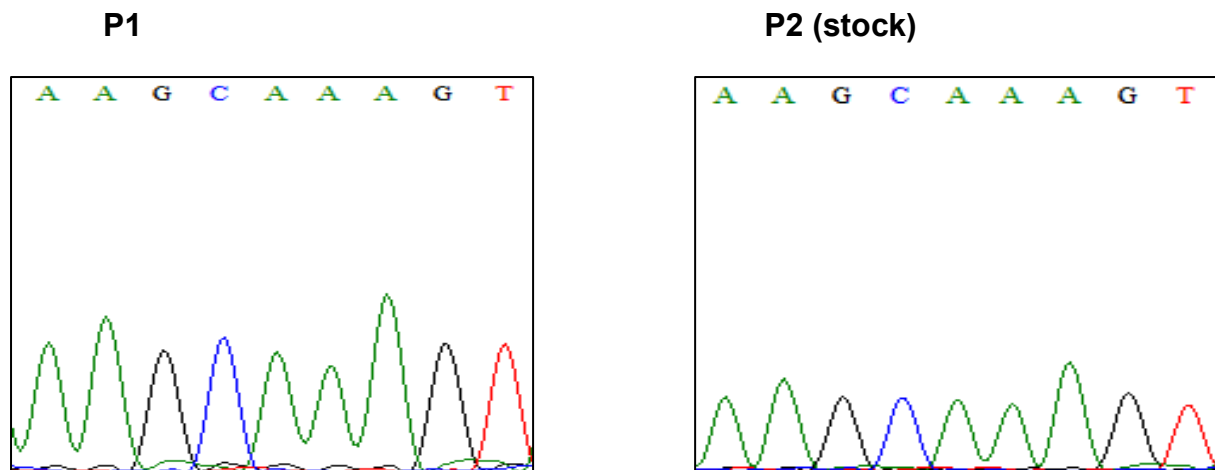
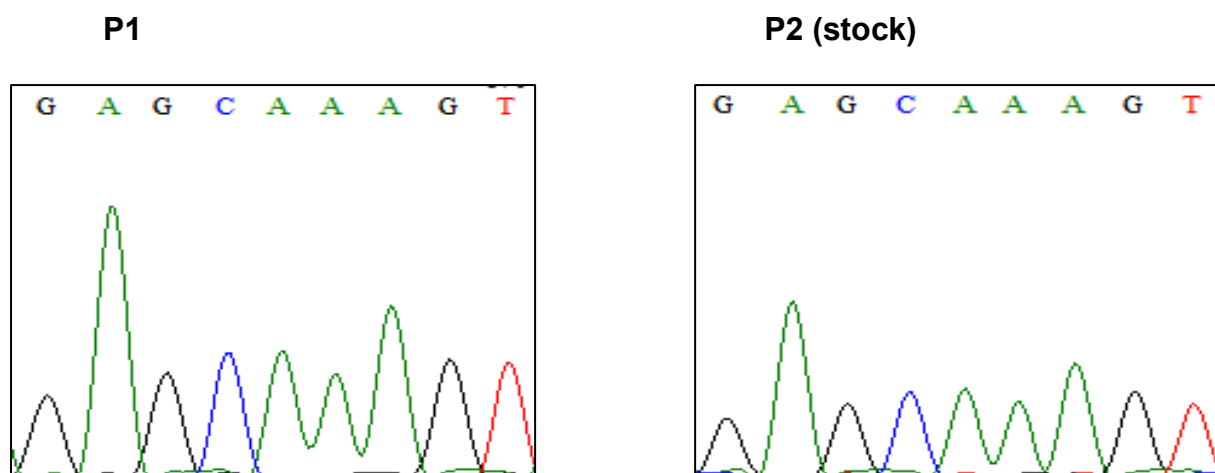
A IAV PB2-627K**B IAV PB2-627E**

Figure 24: The validation of the genetic stability of the IAV PB2-627 codon in the mammalian- and the avian-adapted strain by Sanger-sequencing. HEK293 cells were transfected with the respective eight plasmids encoding for the different IAV RNA genes to assemble either the IAV PB2-627K or -627E strain. The resulting cell culture supernatants were used to infect DF-1 cells. The sequence of the PB2 gene was Sanger-sequenced in the resulting cell culture supernatants to validate the genotype after the first passage. The output of the sequencing chromatogram for the three nt of the PB2-627 codon and two additional codons downstream are depicted for the mammalian-adapted strain (A, P1) and the avian-adapted strain (B, P1). The same cell culture supernatants were used to infect DF-1 cells for a second passage of the virus, to propagate the virus. The procedure of sequencing in the resulting cell culture supernatants was performed similarly. The output of the sequencing chromatogram for the three nt of the PB2-627 codon and two additional codons downstream are depicted for the mammalian-adapted strain (A, P2) and the avian-adapted strain (B, P2).

4.3.6. Summary: Generation and characterization of recombinant IAV strains

A recombinant IAV PB2-627K and -627E strain were generated successfully in DF-1 chicken cells. Of those, the latter did replicate weaker in mammalian cells than the first, indicated by failure of stock generation in mammalian cell lines, the results of a plaque assay and a competitive infection assay. Nevertheless, the analysis of the virus titers by SCIA, hem-agglutination test and plaque assay showed that both strains have a similar virus titer. The analysis of viral M-protein expression by WB semi-quantification suggests that the IAV PB2-627E strain had approx. 3.5 fold more defective particles than the IAV PB2-627K strain. Validation of the genetic stability of the PB2 RNA area carrying the codon 627 in three subsequent virus passages suggests that both virus strains are genetically stable and free of mutations. Hence, despite the expected differences in the potential to replicate in mammalian cells, it is concluded that both IAV strains are comparable and suitable for mouse infection studies.

4.4. Mouse infection study

4.4.1. Comparison of primary influenza infection parameters in dependence of the RIG-I genotype

To investigate the importance of the different antiviral functions of RIG-I in the context of an organism, a mouse infection study with the established mouse lines and recombinant IAV strains was performed. The RIG-I WT, PM and KO mice were infected with either IAV PB2-627K, -627E or were treated with PBS only and monitored for 4, 7, 10 or 14 days. At the last day of the infection course, FITC-albumin was injected into a tail vein and the mice were sacrificed one h thereafter. Whole blood, BALF, the lungs and the spleen were harvested and stored until further preparation (c. c. 3.14 f.).

In mice, the sex can affect the susceptibility for and outcome of IAV infections (Celestino I. 2018; Vermillion M. S. 2018; Sabikunnahar B. 2022). Initially, it was considered to differentiate between female and male individuals for data analysis. After the generation of all data, it was found that most of the experimental readouts included higher individual variation than assumed during the planning phase. Hence, female and male groups were pooled to enhance the robustness of the analyses.

4.4.1.1. More IAV PB2-627E virus than IAV PB2-627K virus is required to achieve comparable infection parameters in mouse lung infection experiments

In a first setting, 2.5×10^3 PFU in 35 μ l DPBS of one or the other virus strain was applied intranasal to achieve a moderate lung infection. During these infections, it was found that the dose is too high for the IAV PB2-627K virus, indicated by rapid weight loss. Additionally, the dose was too low for the IAV PB2-627E virus, indicated by no marked weight loss during the course of infection and no detectable virus titers in the BALF (data not shown). Hence, the doses were adjusted to 1×10^2 PFU for the IAV PB2-627K strain and to 8.3×10^4 PFU for the IAV PB2-627E strain, which resulted in comparable infections. This is a factor difference of 8.3×10^2 , but in regard to the weak replication of the IAV PB2-627E strain in all used mammalian cell lines, it was not surprising.

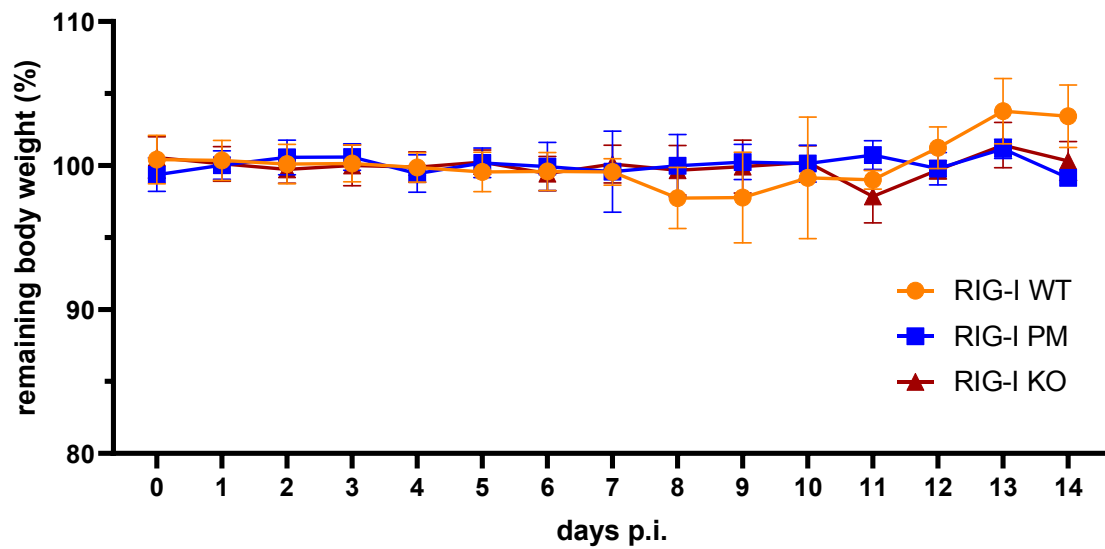
4.4.1.2. Weight loss during IAV PB2-627K and IAV PB2-627E infections in mice

To track the course of IAV lung infection, the weight of mice infected with either IAV PB2-627K, -627E or treated with PBS was measured at least once daily, starting at the day of infection and ending at the day of sacrifice. All weight data points for the indicated day p.i. of mice included in the study were used to calculate the mean for the respective time point (d0-4: n = 16; d5-7: n = 12; d8-10: n = 8; d11-14: n = 4) to enhance the robustness of the data. The mean of the percentage remaining weight was depicted in a superimposed symbol plot with connecting lines, with the respective standard deviation (c. c. 3.19.4). The data from PBS-treated, IAV PB2-627K infected and -627E infected mice were depicted in separate graphs (compare Figure 25 A-C). A 2-Way ANOVA was used to determine significant effects of the factors "days p.i." and "RIG-I genotype" on the variable "remaining body weight".

Taken together, the data indicates a characteristic and significant weight loss of all mouse lines infected with either the IAV PB2-627K or -627E strain, which reaches its maximum at day 7 p.i. in the IAV PB2-627K infections and day 8 p.i. in the IAV PB2-627E infections. This is indicated by a significant effect of the factor "days p.i." on the variable in all comparisons between the groups ($p < 0.0001$). The weight drop indicates an ongoing infection, of which mice start to recover from after reaching the maximum. The weight loss is not observed in the PBS treated groups, as expected. The indication of significant effects in this data set suggested by the ANOVA analyses are probably due to differences in the weight variation of the WT mice in comparison to the nearly constant weight measurements of the PM and KO mice. This may result from some individual feeding behavior of the WT mice and cannot be explained by unwanted infections, indicated by the lack of detectable virus

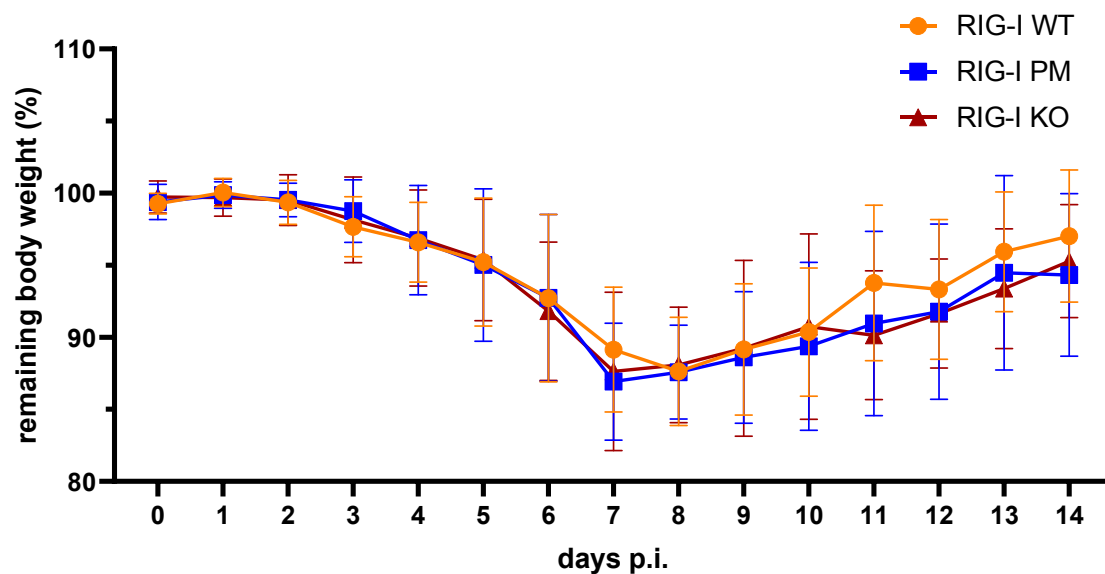
particles in BALF and lung tissue of this group (c. c. 4.4.1.4 and 4.4.1.5). Concerning the factor "RIG-I genotype", the ANOVA analyses indicate no significant effect on the variable in the IAV PB2-627K context. In contrast, a significant effect in the comparison between RIG-I WT and KO mice ($p = 0.0061$) and a similar tendency in the comparison between RIG-I WT and PM mice ($p = 0.0572$) was found in the IAV PB2-627E context. Remarkably, also the average highest weight loss in RIG-I WT mice was at day 8 p.i., in contrast to day 7 p.i. for RIG-I PM and KO mice, in the IAV PB2-627K infections. For both virus infections, no significant interaction between the factors was detectable, indicating that the effect by the RIG-I variant expression is not very strong. As final remark, the data presentation with decreasing numbers of mice in direction of the late time points seems not optimal, but was chosen to account to all data and to minimize the impact of individual variation at early time points.

A PBS mock treatment



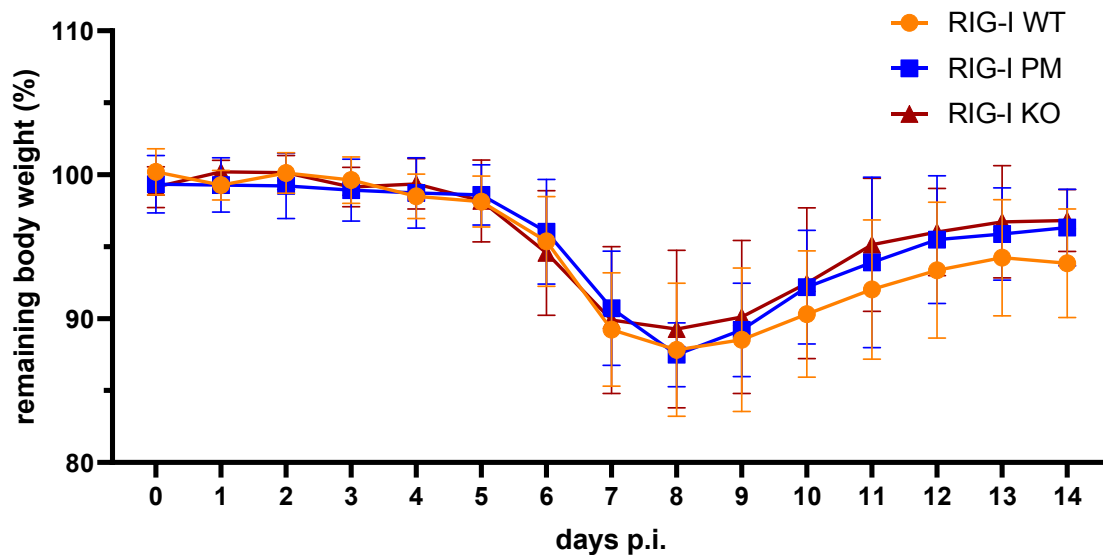
2-Way ANOVA source of variation	RIG-I WT vs. PM		RIG-I WT vs. KO		RIG-I PM vs. KO	
	p value	significance	p value	significance	p value	significance
interaction	<0.0001	****	0.0034	**	0.0323	*
days p.i.	<0.0001	****	<0.0001	****	0.2724	ns
genotype	0.8024	ns	0.4168	ns	0.5254	ns

B IAV PB2-627K infection



2-Way ANOVA source of variation	RIG-I WT vs. PM		RIG-I WT vs. KO		RIG-I PM vs. KO	
	p value	significance	p value	significance	p value	significance
interaction	0.9749	ns	0.9785	ns	>0.9999	ns
days p.i.	<0.0001	****	<0.0001	****	<0.0001	****
genotype	0.1249	ns	0.1686	ns	0.8670	ns

C IAV PB2-627E infection



2-Way ANOVA	RIG-I WT vs. PM		RIG-I WT vs. KO		RIG-I PM vs. KO	
	p value	significance	p value	significance	p value	significance
interaction	0.7986	ns	0.6612	ns	0.9756	ns
days p.i.	<0.0001	****	<0.0001	****	<0.0001	****
genotype	0.0572	ns	0.0061	**	0.3313	ns

Figure 25: The infection of RIG-I WT, PM and KO mice with a recombinant IAV PB2-627K or -627E strain causes a significant weight loss, slightly dependent on the RIG-I genotype in the IAV PB2-627E infections. RIG-I WT, PM and KO mice were PBS-treated (A) or infected intranasal with a recombinant IAV PB2-627K (B) or -627E (C) strain and monitored for a maximum of 14 days p.i. All weight data points for the indicated day p.i. of mice included in the study were used to calculate the mean percentage remaining body weight at the respective time point (d0-4: n = 16; d5-7: n = 12; d8-10: n = 8; d11-14: n = 4). The data was depicted as superimposed symbol plots with the respective standard deviation. A 2-Way ANOVA was used to indicate significant effects of the factors "days p.i." and "RIG-I genotype" on the variable "remaining body weight", as well as their interaction.

4.4.1.3. The body temperature of mice drops after infection with IAV PB2-627K and IAV PB2-627E

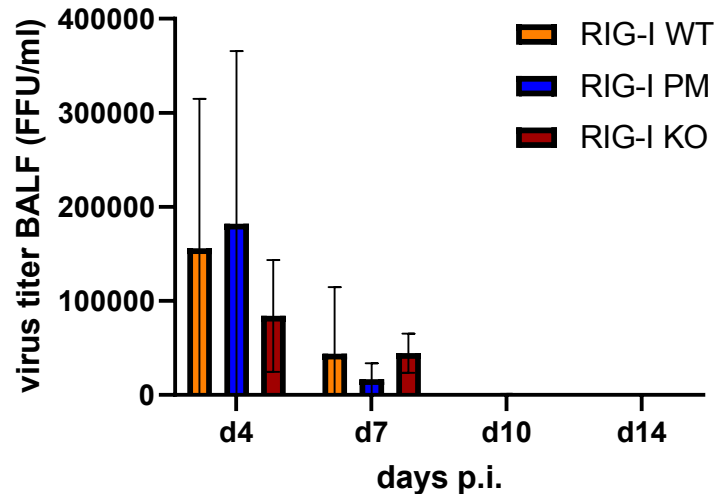
As a second variable to track the course of IAV lung infection, the body temperature of mice infected with either recombinant IAV PB2-627K, -627E or treated with PBS only was measured rectal at least once daily. The resulting data showed high inaccuracy of the measurement, making statistical analysis unreliable. The results are depicted in the Supplementary Figure 2.

4.4.1.4. Infectious virus particles are detectable in the BALF of IAV PB2-627K- and IAV PB2-627E-infected mice

To compare the virus titers in the lungs of mice infected with IAV PB2-627K, -627E or treated with PBS only, the infectious particles were determined with a SCIA in BALF harvested at the endpoint of the time course (c. c. 3.13.2). Infectious virus particles were only detectable at day 4 and day 7 p.i., but not anymore at day 10 and 14 p.i. Further, no virus particles were detectable in PBS-treated mice (data not shown). The mean SCIA virus titer of four mice per infection group are depicted as histograms for the infections with IAV PB2-627K and -627E separately (compare Figure 26 A and B). A 2-Way ANOVA was used to indicate significant effects of the factors "days p.i." and "RIG-I genotype" on the variable "virus titer".

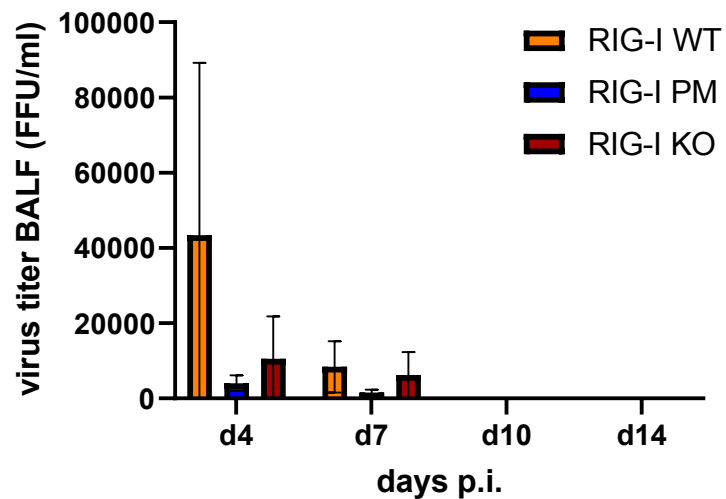
Since there is a broad variation in the BALF virus titer data, indicated by high error bars and a failed confirmation of a normal distribution in the RIG-I WT data, the limited data set with four mice per infection group seems not to be sufficient to draw reliable conclusions based on the BALF virus titer data. However, the results show that the detectable virus titer reached highest values in the early stages of the infections at day 4 p.i., well detectable in the BALF of IAV PB2-627K-infected mice. This is also indicated by a significant effect of the factor "days p.i." on the variable, in all comparisons between the groups, in the IAV PB2-627K and -627E infections. The BALF virus titers are more than four-fold higher in the IAV PB2-627K infections than in the IAV PB2-627E infections, but since an unequal infection dose was required (1×10^2 PFU IAV PB2-627K and 8.3×10^4 PFU IAV PB2-627E), a direct comparison is difficult. Nevertheless, a lower detectable virus titer of IAV PB2-627E compared to -627K is remarkable, in contrast to a much higher infection titer of IAV PB2-627E, compared to -627K. In regard to the effect of the factor "RIG-I genotype" on the variable, the interpretation is more difficult. In case of the IAV PB2-627K infections, the ANOVA analyses indicate no significant effect of the factor "RIG-I genotype" on the variable, and no significant interaction between the factors was detectable, in all comparisons between the data groups. This suggests no effect of RIG-I variant expression on the BALF virus titer. In contrast, for the IAV PB2-627E infections, the ANOVA analyses indicate tendencies to significant effects of the factor "RIG-I genotype" on the variable and tendencies to significant interactions between the factors, in all comparisons between the data groups (compare Figure 26). These indications seem to come from a very high BALF virus titer in RIG-I WT mice at day 4 p.i. and lower BALF virus titers in RIG-I PM mice and were not expected. If a reasonable explanation for this pattern can be found, it needs to be validated with further experiments.

A IAV PB2 627K infection



2-Way ANOVA source of variation	RIG-I WT vs. PM		RIG-I WT vs. KO		RIG-I PM vs. KO	
	p value	significance	p value	significance	p value	significance
interaction	0,9494	ns	0,6142	ns	0,3031	ns
days p.i.	0,0023	**	0,0033	**	0,0019	**
genotype	0,9959	ns	0,4484	ns	0,4759	ns

B IAV PB2 627E infection



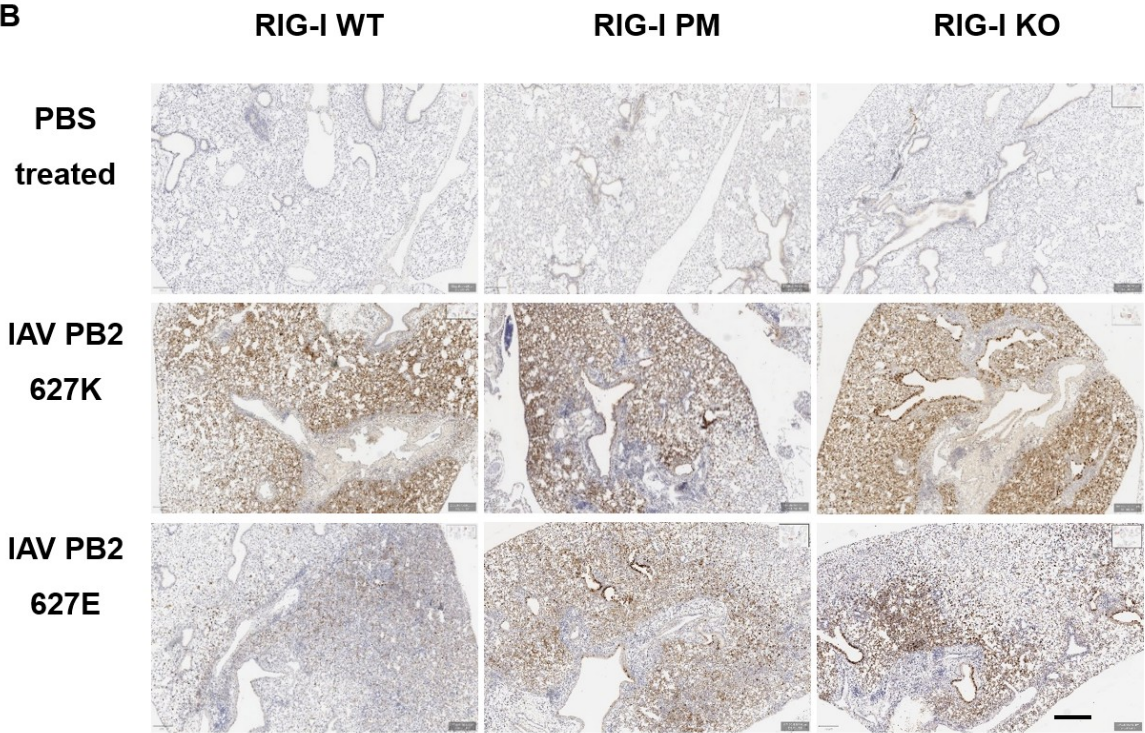
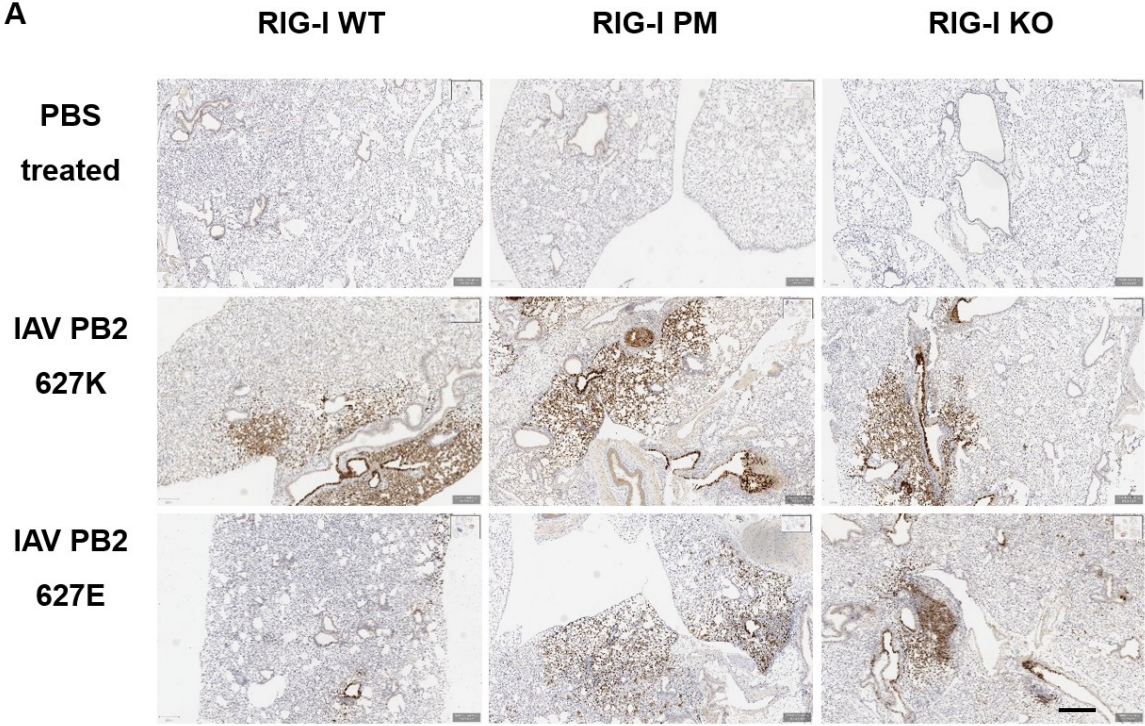
2-Way ANOVA source of variation	RIG-I WT vs. PM		RIG-I WT vs. KO		RIG-I PM vs. KO	
	p value	significance	p value	significance	p value	significance
interaction	0.0724	ns	0.1737	ns	0.3997	ns
days p.i.	0.0232	*	0.0121	*	0.0108	*
genotype	0.0575	ns	0.1570	ns	0.1006	ns

Figure 26: The BALF infectious virus titer shows high variation between mouse individuals upon infection with recombinant IAV strains. RIG-I WT, PM and KO mice were infected with recombinant IAV PB2-627K (A) and -627E (B) strains. At the indicated day p.i. endpoint, the mice were sacrificed and BALF was harvested and analyzed for infectious virus particles with a SCIA. The means and standard deviations of the SCIA virus titer of four mice per infection group are depicted as histograms. A 2-Way ANOVA was used to determine significant effects of the factors "days p.i." and "RIG-I genotype" on the variable "virus titer", as well as their interaction.

4.4.1.5. IAV is detectable in mouse lungs following infection with recombinant IAV PB2-627K and IAV PB2-627E strains, independent of RIG-I variant expression, and is cleared between 10 and 14 days p.i.

To validate the virus load in RIG-I WT, PM and KO mice infected with recombinant IAV PB2-627K, -627E or treated with PBS only, lungs were harvested and the tissue was prepared for histological studies. For immune histochemical (IHC) detection, IAV NP protein was targeted with a primary antibody and stained with a polymer labeled to a secondary antibody and HRP. Finally, the tissue slides were counter stained with hematoxylin. The stained slides were scanned and sectors were selected in 100-fold magnification (c. c. 3.16.3). One sector of a stained slide of a female and a male individual was chosen as an example for the respective infection group. The nine representative sectors for a day p.i. are shown in the same panel (compare Figure 27 day 4 p.i. (A), day 7 p.i. (B), day 10 p.i. (C) or day 14 p.i. (D), female mice; Supplementary Figure 3 A-D, male mice).

The slides from PBS-treated control mice showed very low unspecific staining, as expected. In slides from IAV PB2-627K- and -627E-infected mice, viral NP was already detectable at day 4 p.i., while huge infection spots were detectable at day 7 p.i. At day 10 p.i., the infection spots started to vanish, while virus particles were still detectable. At day 14 p.i., most of the virus particles and infected cells were eradicated, while immune cells were still present in the lung tissue, indicated by clusters of hematoxylin-positive cells. This finding suggests that an ongoing healing process is not finished at this time point. The observations were similar for all three mouse lines and independent of the infection with IAV PB2-627K or -627E strain. However, the infections with the IAV PB2-627K strain caused more virus load in the lungs (compare Figure 27 A-D and Supplementary Figure 3 A-D).



400 μ m

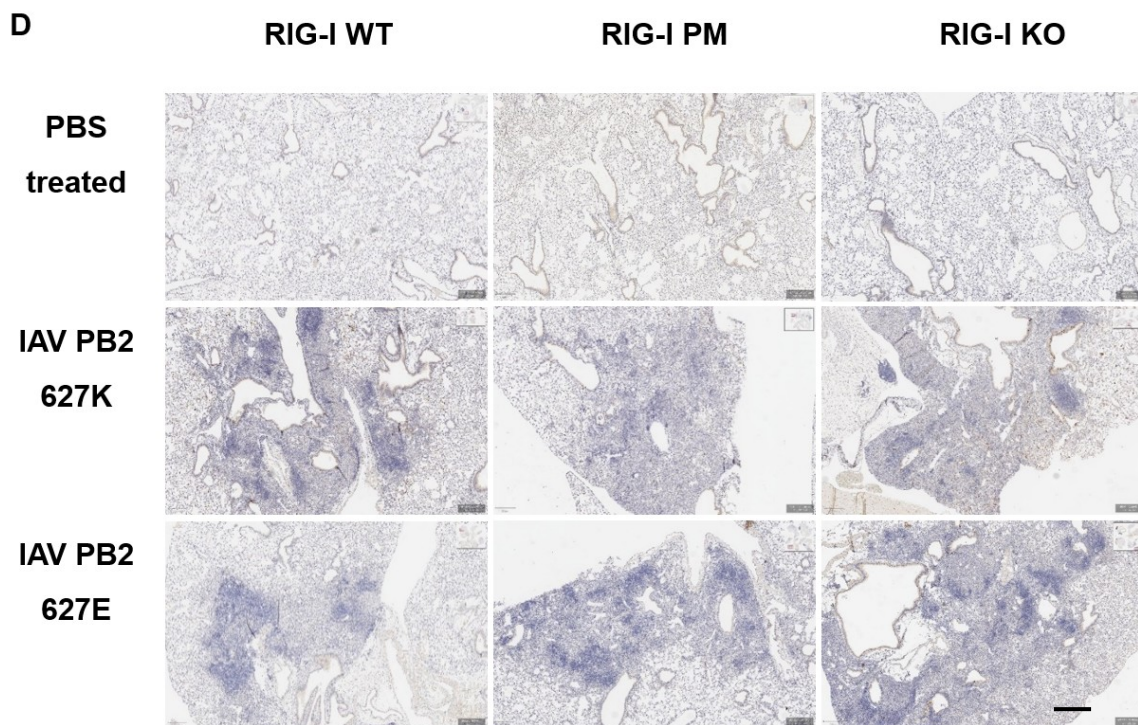
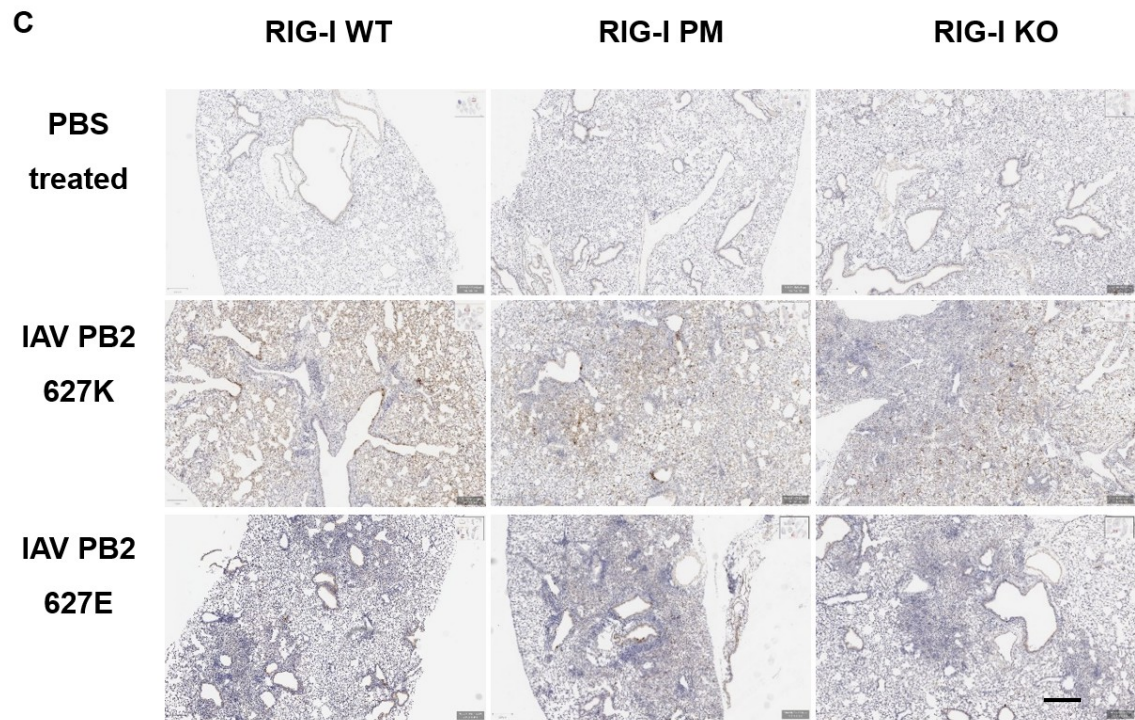
400 μ m

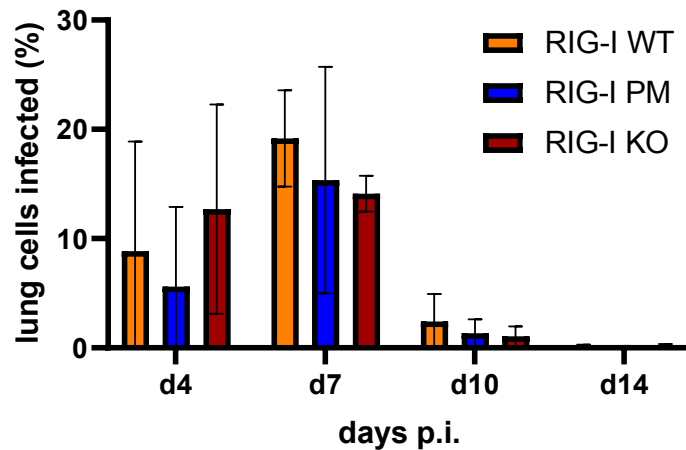
Figure 27: The detection of IAV NP protein at different time points p.i. in lung tissue from female mice infected with IAV PB2-627K or -627E visualizes the course of the infection. RIG-I WT, PM and KO mice were infected with recombinant IAV PB2-627K, -627E or treated with PBS, for 4 (A), 7 (B), 10 (C) or 14 (D) days. At the indicated day p.i., the mice were sacrificed, the lung was fixated and immunohistochemically stained using an antibody detecting IAV NP (Thermo scientific, PA532242) and a HRP- and polymer-labeled secondary antibody construct. Finally, the slides were counterstained with hematoxylin. One sector of a slide from a female individual was chosen as an example for every infection group, the pictures were taken in 100-fold magnification.

For statistical analysis of differences between the virus loads in the lungs, in dependence of the days p.i. and the RIG-I genotype, the IHC detection of viral NP in all the lung cells of one stained slide per mouse was semi-quantified with the QuPath software. The mean percentage of positive cell counts of all mouse individuals per infection group was calculated and is depicted with the respective standard deviation as histograms, separated by the infection condition (compare Figure 28). A 2-Way ANOVA was used to identify significant effects of the factors "days p.i." and "RIG-I genotype" on the variable "lung cells infected" (c. c. 3.16.3).

In slides from PBS-treated control mice, some amount of staining artifacts was visible, but no characteristic IAV NP-positively stained cells could be detected. In summary, no significant differences between the mouse lines were detectable for the control mice (data not shown).

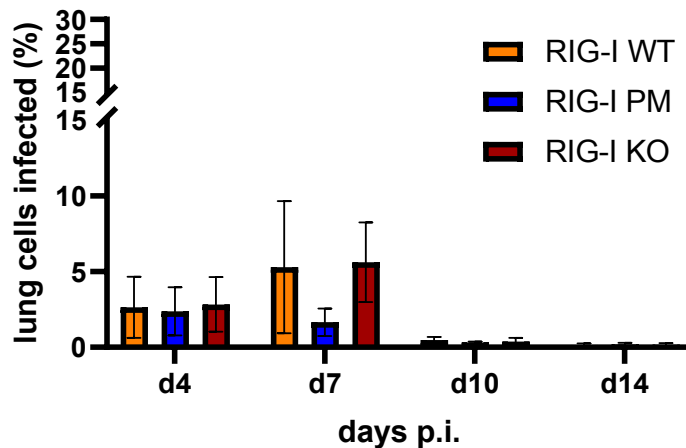
The results show an approx. fourfold higher amount of infected cells in the lungs of the IAV PB2-627K-infected mice than in the -627E-infected mice. Additionally, the amount of infected lung cells increased upon day 7 p.i. and decreased afterwards, due to effects of the immune response. The finding is indicated by a significant effect of the factor "days p.i." on the variable "lung cells infected" in all comparisons between the groups, in both the IAV PB2-627K and -627E infections (p at least 0.0027). Further, the ANOVA analyses indicate no significant effect of the factor "RIG-I genotype" on the variable, as well as no significant interactions between the factors in all comparisons in the IAV PB2-627K infections. This suggests that RIG-I variant expression has no significant effect on the virus spread in an IAV PB2-627K infection. In the IAV PB2-627E infections, the ANOVA analyses indicate a significant effect of the factor "RIG-I genotype" in the comparison between RIG-I PM and KO mice ($p = 0.0249$) and a similar tendency in the comparison between RIG-I PM and WT mice ($p = 0.1300$), with a significant interaction between the factors in the first comparison ($p = 0.0148$) and a tendency in the latter ($p = 0.1630$) (compare Figure 28). This result is based on a lower amount of infected cells detectable in the lungs of RIG-I PM mice compared to WT and KO mice. In contrast, in the comparison between RIG-I WT and KO mice, no significant effect of the factor "RIG-I genotype" is observed. If this unexpected difference pattern is based on a real RIG-I-mediated effect or an infection artifact, needs to be further clarified. All in all, the results of the virus titration with semi-quantification are comparable to the results of the BALF virus titration, but the IHC detection and semi-quantification seems more sensitive, detecting virus until day 14 p.i. and also shows less intensive variation in the infection groups, compared to the detection with the SCIA (also compare previous chapter).

A IAV PB2-627K



2-Way ANOVA	RIG-I WT vs. PM		RIG-I WT vs. KO		RIG-I PM vs. KO	
source of variation	p value	significance	p value	significance	p value	significance
interaction	0.9130	ns	0.4219	ns	0.4534	ns
days p.i.	<0.0001	****	<0.0001	****	<0.0001	****
genotype	0.3449	ns	0.7357	ns	0.4887	ns

B IAV PB2-627E

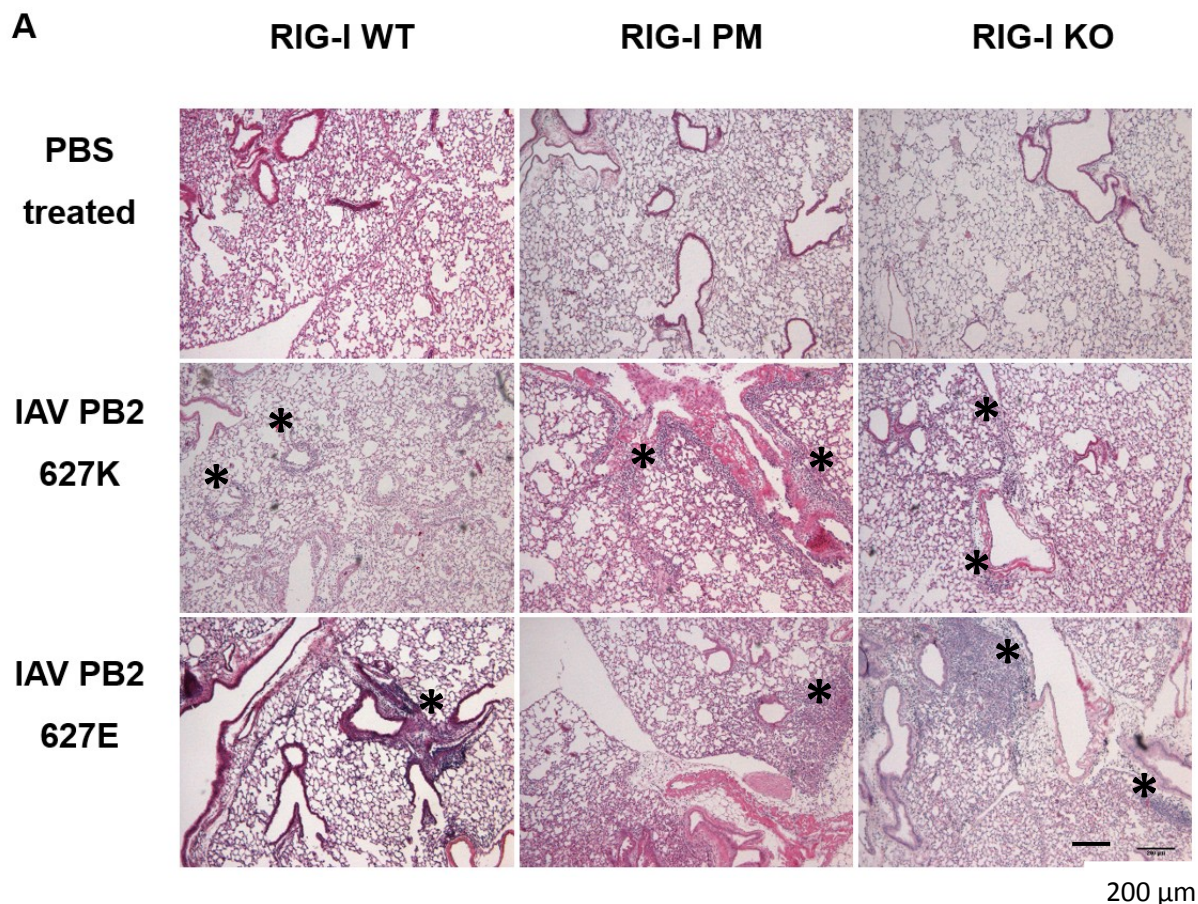


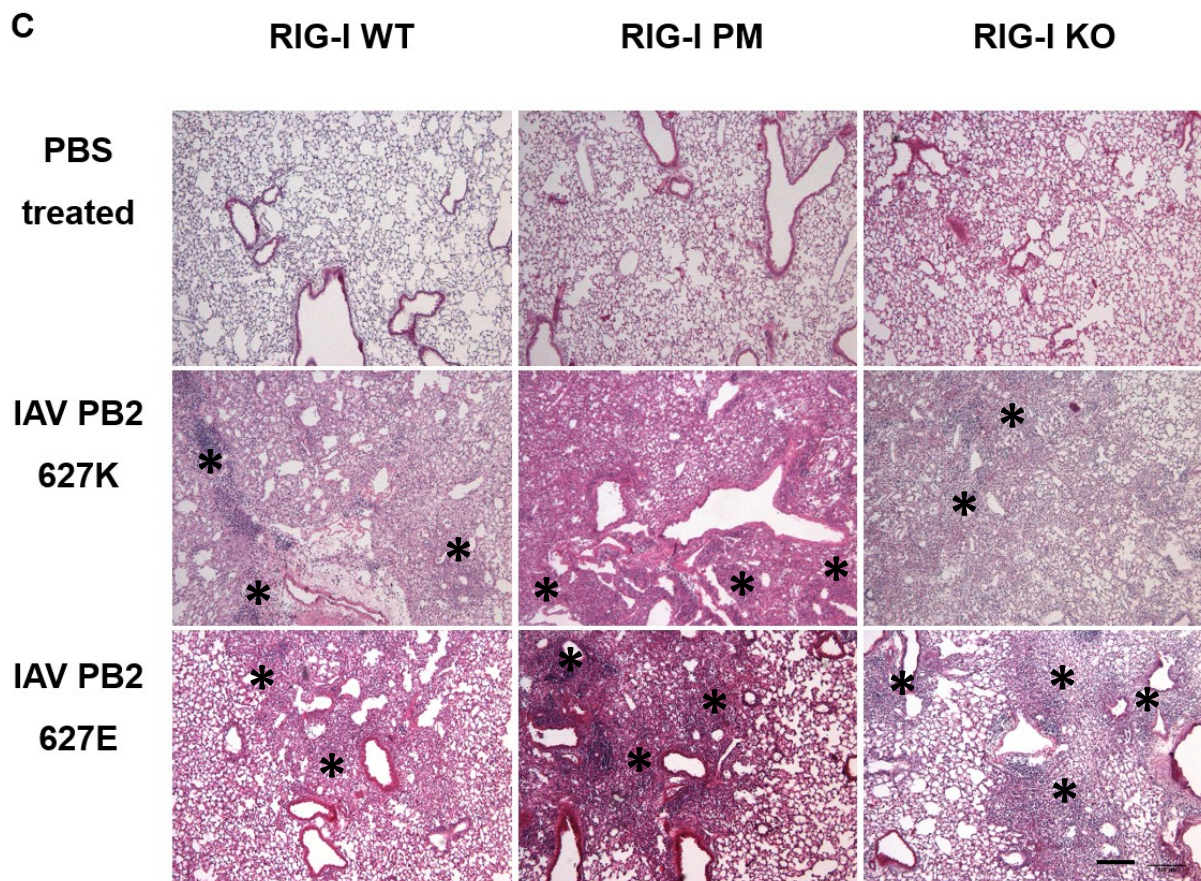
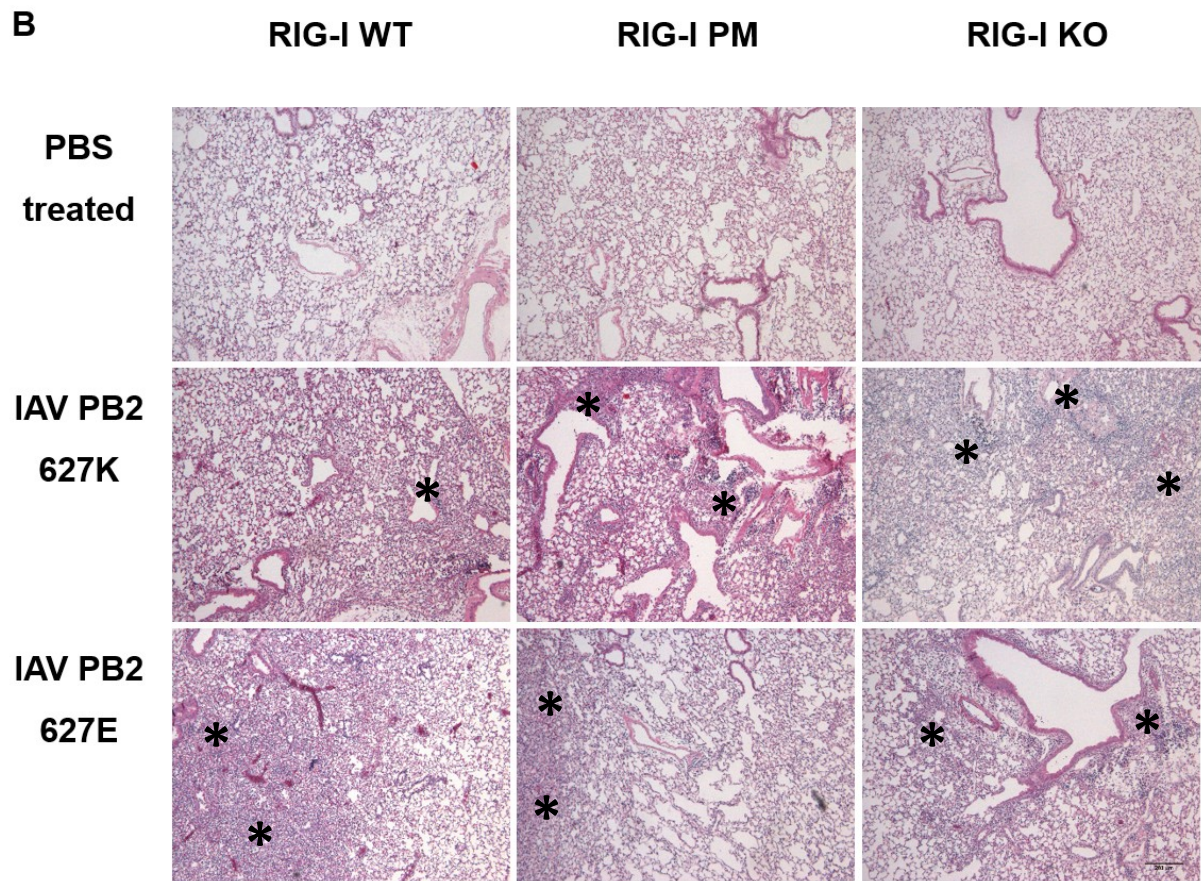
2-Way ANOVA	RIG-I WT vs. PM		RIG-I WT vs. KO		RIG-I PM vs. KO	
source of variation	p value	significance	p value	significance	p value	significance
interaction	0.1630	ns	0.9970	ns	0.0148	*
days p.i.	0.0027	**	<0.0001	****	<0.0001	****
genotype	0.1300	ns	0.8894	ns	0.0240	*

Figure 28: The semi-quantification of viral load in the lung tissue of IAV PB2-627K- and -627E-infected RIG-I WT, PM and KO mice suggests a questionable effect of RIG-I signaling deficiency on the IAV PB2-627E virus titer. RIG-I WT, PM and KO mice were infected either with recombinant IAV PB2-627K (A) or -627E (B). At the indicated day p.i. endpoint, the mice were sacrificed, the lung was fixated and immunohistochemically stained using a primary antibody detecting IAV NP (Thermo scientific, PA532242) and a secondary antibody construct with HRP and a polymer. With a threshold algorithm, the percentage of NP positive lung cells was determined in four lung slides per infection group and the mean was calculated and depicted with the respective standard deviation as histograms. A 2-Way ANOVA was used to determine significant effects of the factors "days p.i." and "RIG-I genotype" on the variable "lung cells infected", as well as the interaction between the factors.

4.4.1.6. An IAV PB2-627K and IAV PB2-627E infection causes infiltration of the lung by mononuclear immune cells

RIG-I WT, PM and KO mice were infected with IAV PB2-627K, -627E or were treated with PBS. To search for immune cell invasion, basal membrane damage and mucus production, tissue samples were stained either with the hematoxylin and eosin (H&E) or the periodic acid-Schiff (PAS) staining. Pictures were taken with a light microscope in 50-fold magnification (c. c. 0). One sector of a representative slide for every infection group was chosen as an example and is depicted (compare Figure 29 day 4 p.i. (A), day 7 p.i. (B), day 10 p.i. (C) and day 14 p.i. (D), females H&E; Figure 30 A-D (females, PAS); Supplementary Figure 4 A-D (males, H&E) and Supplementary Figure 5 A-D (males, PAS)). In the H&E-stained slides from mice infected with either IAV PB2-627K or -627E, an infiltration of the lung tissue by mononuclear immune cells was detectable from day 4 p.i. on, which increased more and more until day 14 p.i., but was not detectable in lung tissue of PBS-treated mice (compare Figure 29 A-D, indicated by asterisks). The invading immune cells formed large cell clusters as cell-rich exudates at day 10 and 14 p.i. (compare Figure 29 C and D, indicated by asterisks). The intensity of immune cell invasion seemed overall comparable in all infection settings, but seemed to be slightly delayed in RIG-I WT females and males at day 4 p.i., compared to PM and KO mice (compare Figure 29 A and Supplementary Figure 4 A).



200 μ m

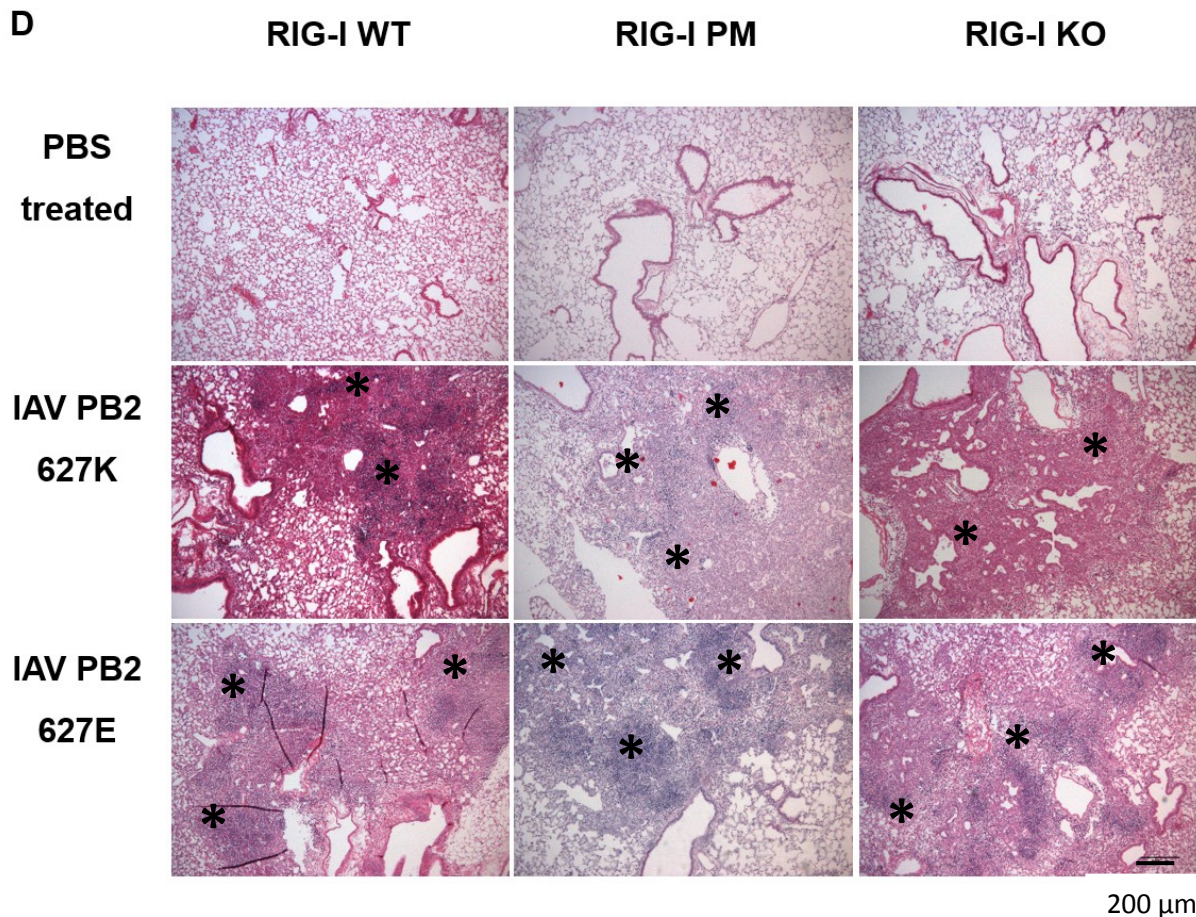
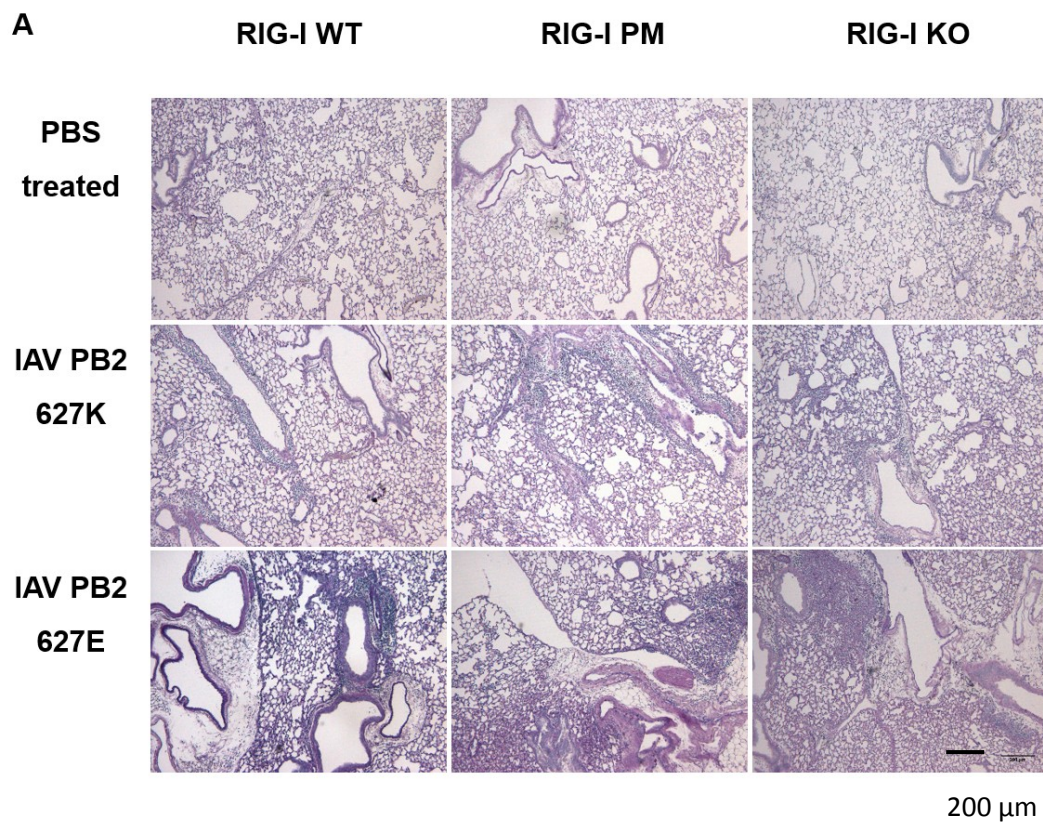


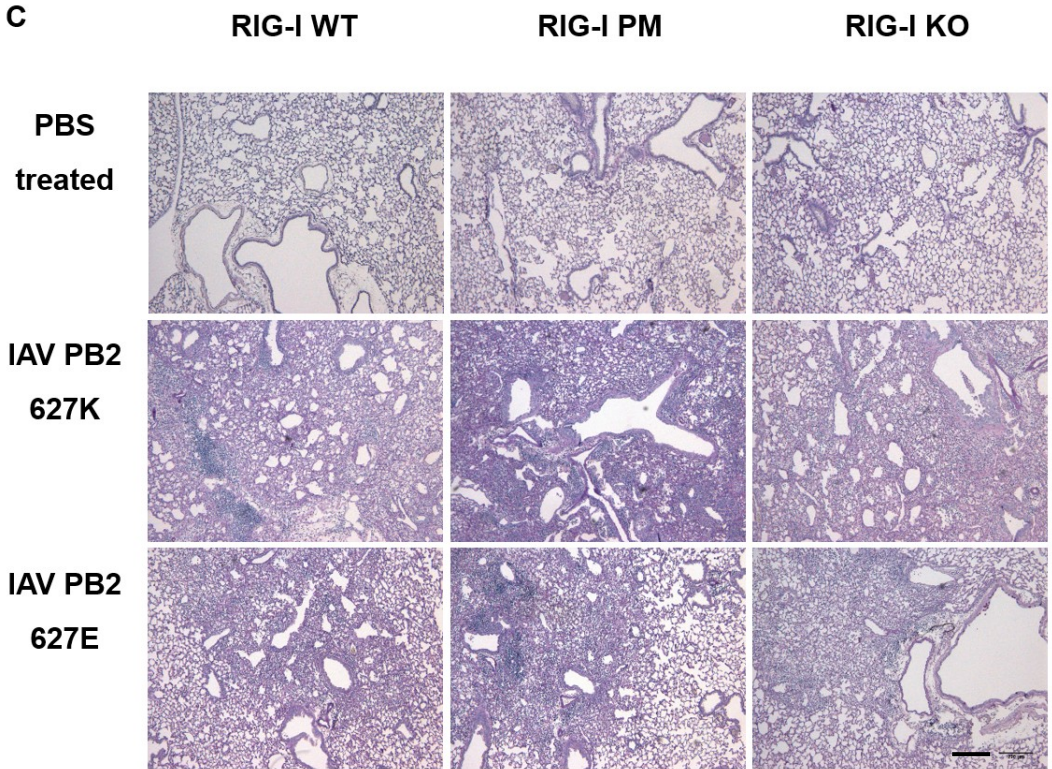
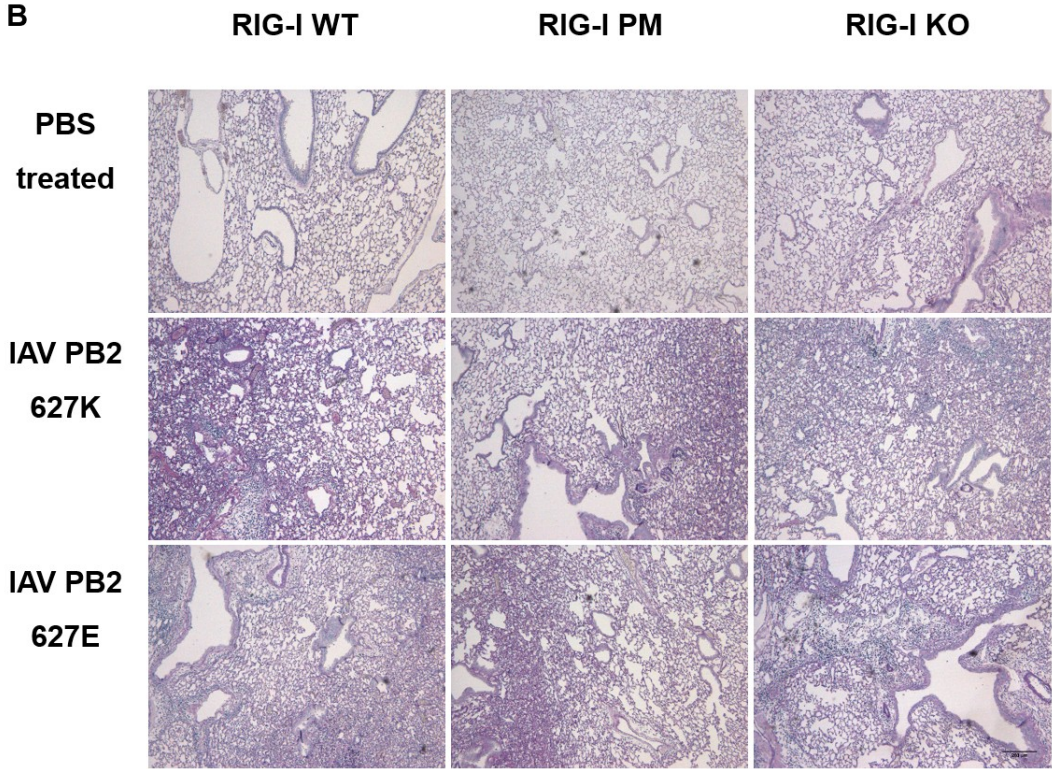
Figure 29: Mononuclear immune cell infiltration of RIG-I WT, PM and KO mouse lungs infected with IAV PB2-627K or -627E results in formation of cellular exudates. RIG-I WT, PM and KO mice were infected with recombinant IAV PB2-627K, -627E or treated with PBS. At day 4 (A), 7 (B), 10 (C) or 14 (D) p.i., the mice were sacrificed. The lung was fixated and stained with H&E to depict general tissue structures (pink) and nuclei (blue). One sector of a slide from a female individual of every infection group was chosen as an example. The asterisks mark infiltration of mononuclear blood cells (A-D) and cell-rich exudates, enrichment zones of these cells (C and D).

Concerning the PAS staining, mice infected with IAV PB2 variants showed no marked mucus production in the lungs. Additionally, there was no marked basal membrane damage detectable in any tissue sample (compare Figure 30 A-D and Supplementary Figure 5 A-D). In both the IAV PB2-627K and -627E infections, the IHC detection of viral NP in the lungs showed virus eradication independent of the RIG-I genotype (compare previous chapter). Since remaining cell-rich exudates and virus particles were still detectable at the latest time point post infection, it was not possible to validate if the healing process will be completed or might transfer into a chronic inflammation process, like postulated by another study (Keeler S. P. 2018).

Taken together, histological analysis of IAV PB2-627K- and -627E-infected lungs with H&E and PAS staining indicates an increasing immune cell invasion from day 4 p.i. until day 14 p.i., resulting in the

formations of cellular exudates. Additionally, an ongoing healing process cleaning the infection was detectable, in consideration of the IHC data, which was not accompanied with detectable mucus production or basal membrane destruction over the time course of observation. Further, no marked differences between the RIG-I WT, PM and KO mice in regard to the observed variables were detectable, except a slight delay of immune cell invasion in RIG-I WT mice at day 4 p.i., in the IAV PB2-627K infections.





200 μm

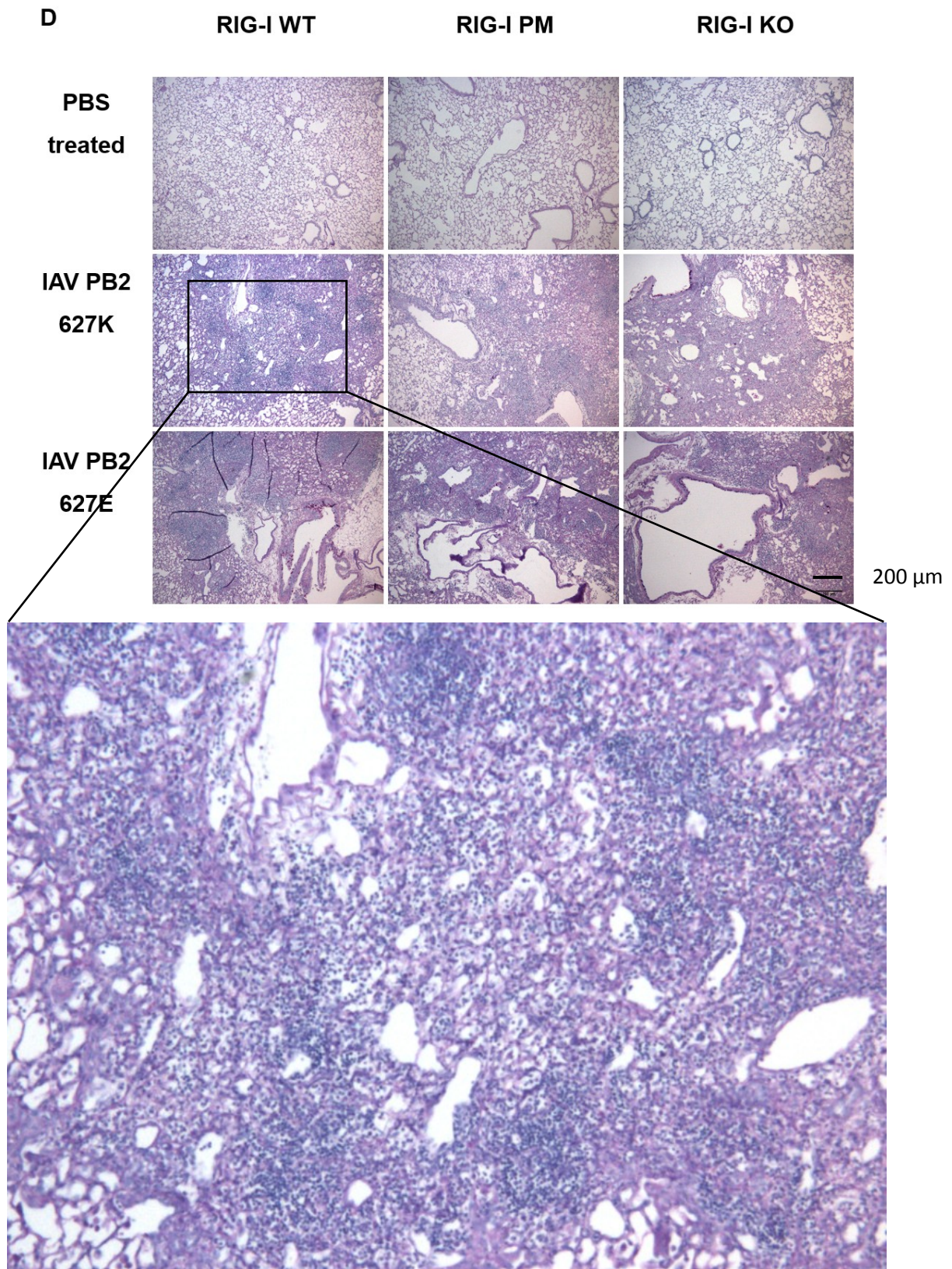


Figure 30: RIG-I WT, PM and KO mice infected with IAV PB2-627K or -627E suffer from an acute lung infection without mucus production and basal membrane damage. RIG-I WT, PM and KO mice were infected with recombinant IAV PB2-627K, -627E, or treated with PBS. At day 4 (A), 7 (B), 10 (C) or 14 (D) p.i., the mice were sacrificed, the lung was fixated and PAS-stained to depict basal membranes and mucus. One sector of a slide from a female individual of every infection group was chosen as an example. The zoomed sector was chosen to make basal membrane integrity visible (D).

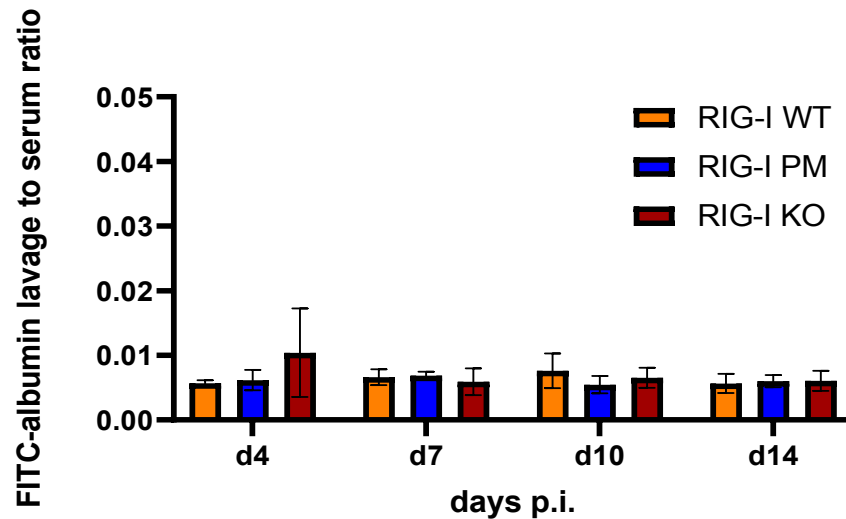
4.4.1.7. Both an IAV PB2-627K and IAV PB2-627E infection cause lung damage, independent of RIG-I variant expression

For the investigation of the integrity of the lung barrier, FITC-labeled albumin can be used to determine the leakage of blood plasma to the alveolar lumen. Therefore, FITC-albumin was applied in the tail vein of mice infected with IAV PB2-627K, -627E or treated with PBS one hour before they were sacrificed. Blood and BALF were harvested and fluorescence emission was measured in duplicates in the serum and cell-free BALF supernatant. After calculation of the mean FITC-albumin lavage to serum ratio with the technical replicates of individual mice (c. c. 3.16.5), the mean was calculated for the infection groups (n = 4) and depicted as histogram, with the respective standard deviation (compare Figure 31). A 2-Way ANOVA was used to determine significant effects of the factors "days p.i." and "RIG-I genotype" on the variable "FITC-albumin lavage to serum ratio", as well as their interaction.

The ANOVA analyses detected no significant effect of the factors "days p.i." or "RIG-I genotype" on the variable, as well as no significant interaction between the factors, in all comparisons between the groups of the PBS-treated control mice. In regard to the IAV PB2-627K and -627E infections, the ANOVA analyses indicated a significant effect of the factor "days p.i." on the variable, in all comparisons between the data groups (p at least 0.0004 in the IAV PB2-627K infections and 0.0214 in the -627E infections). Further, the ANOVA analyses indicate no significant effects of the factor "RIG-I genotype" on the variable, in all comparisons, as well as no significant interaction between the factors (compare Figure 31 A-C). Taken together, these results show that the variable "FITC-albumin lavage to serum ratio", an indicator for lung damage, was significantly increased at day 7 and 10 p.i. in mice infected with the IAV PB2-627K and -627E strain, in comparison to day 4 and 14 p.i. This effect was not detectable in PBS-treated mice (the PBS data set includes one data point in the day 4 p.i. RIG-I KO group, which is higher compared to the other values; this probably results from external tissue damage before BALF harvesting). At first impression, lung damage was accompanied and increased with ongoing virus infection, but the peaks of highest leakage of plasma in the alveolar lumen were delayed in comparison to the peaks of highest virus infestation at day 7 to 8 p.i. (c. c. 4.4.1.4 and 4.4.1.5). Hence, the integrity of the lung barrier might also be disrupted by the activity of invading immune cells. Further, the finding that the FITC-albumin lavage to serum ratio was comparable between PBS-treated and IAV-infected mice at day 4 p.i., suggests, that the lung barrier is still functional at this time point, while it is not completely restored until day 14 p.i. This is in line with the results from the histological and immune histochemical analysis, suggesting that the infections are not completely healed at day 14 p.i. (compare previous chapters). Further, the results

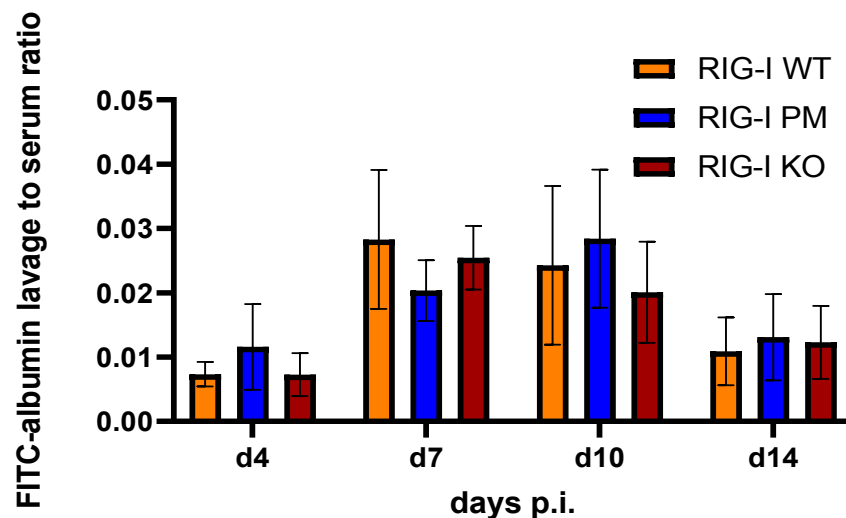
showed a higher lung damage in response to IAV PB2-627K infection compared to -627E infection, which is in line with the previous quantifications.

**A PBS
Treatment**



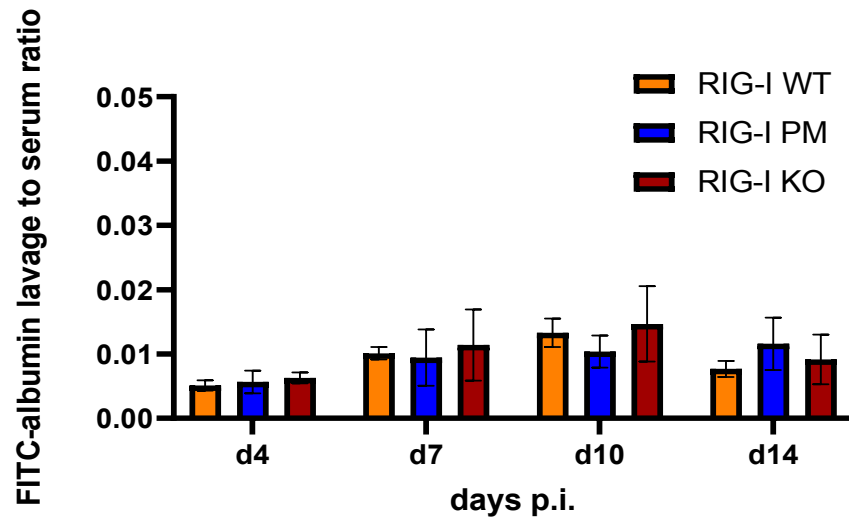
2-Way ANOVA source of variation	RIG-I WT vs. PM		RIG-I WT vs. KO		RIG-I PM vs. KO	
	p value	significance	p value	significance	p value	significance
interaction	0.2319	ns	0.1981	ns	0.2925	ns
days p.i.	0.5183	ns	0.4571	ns	0.3191	ns
RIG-I genotype	0.6138	ns	0.4194	ns	0.2721	ns

**B IAV PB2-627K
infection**



2-Way ANOVA source of variation	RIG-I WT vs. PM		RIG-I WT vs. KO		RIG-I PM vs. KO	
	p value	significance	p value	significance	p value	significance
interaction	0.3990	ns	0.8653	ns	0.2524	ns
days p.i.	0.0004	***	<0.0001	****	0.0002	***
RIG-I genotype	0.8200	ns	0.5876	ns	0.3861	ns

C IAV PB2-627E
infection



2-Way ANOVA source of variation	RIG-I WT vs. PM		RIG-I WT vs. KO		RIG-I PM vs. KO	
	p value	significance	p value	significance	p value	significance
interaction	0.0903	ns	0.9998	ns	0.4072	ns
days p.i.	0.0004	***	0.0004	***	0.0214	*
RIG-I genotype	0.8150	ns	0.2668	ns	0.4321	ns

Figure 31: IAV PB2-627K and -627E infections mediate lung damage formation, independent of RIG-I variant expression. RIG-I WT, PM and KO mice were infected with recombinant IAV PB2-627K, -627E or treated with PBS. At the indicated day p.i., FITC-albumin was injected into the tail vein before the mice were sacrificed; serum and BALF were harvested and analyzed for fluorescence emission. The ratio of the lavage and serum fluorescence levels were calculated. The mean of the FITC-albumin lavage to serum ratio of four mice per infection group was calculated and depicted as histograms with the respective standard deviation, separated by the infection condition (A-C). A 2-Way ANOVA was used to determine significant effects of the factors "days p.i." and "RIG-I genotype" on the variable "FITC-albumin lavage to serum ratio", as well as their interaction.

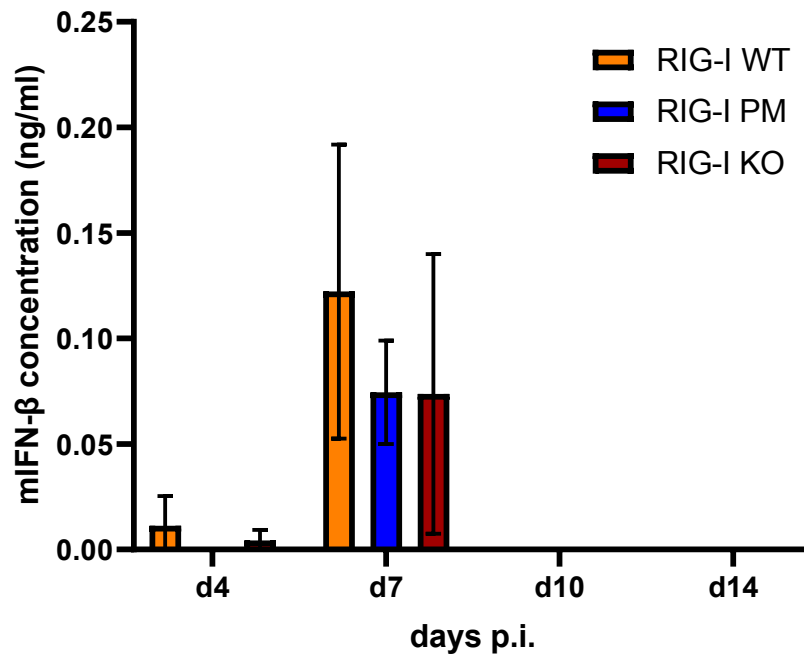
4.4.2. Summary: Primary infection parameters do not markedly differ in dependence of RIG-I variant expression

In the first evaluation step, it was investigated, if the inactivation of RIG-I-mediated signaling alone or the loss of complete RIG-I has a direct effect on the major infection parameters body weight, virus titer in the lung or lung damage. While these parameters were significantly affected by the virus infection, no conclusive pattern of an effect by the RIG-I genotype was detectable, with only differences at several days p.i., depending on the experiment. This finding leads to the conclusion that the infection model is functional and most of the investigated variables could be used to screen for significant effects by factors in general. Nevertheless, none of the different antiviral effects of RIG-I seemed to have a marked effect on the development of the primary infection parameters.

4.4.3. IAV PB2-627K, but not IAV PB2-627E infection causes an induction of IFN- β in RIG-I WT mice, which is reduced in RIG-I PM and KO mice

The investigation of IFN- α levels in RIG-I WT, PM and KO mouse-derived BmdM Φ showed that RIG-I-mediated IFN- α induction was significantly reduced in RIG-I PM and KO mice, compared to RIG-I WT mice (c. c. 4.2.2). To validate the abundance of IFN- α and - β in the BALF of mice infected with IAV PB2-627K or -627E, ELISAs detecting the respective IFN were performed (c. c. 3.7 and 3.17.1). Whereas IFN- α signals were not detectable in BALF samples before high background staining occurred (data not shown), IFN- β was detectable in samples from mice infected with the IAV PB2-627K strain (compare Figure 32), but undetectable after infection with IAV PB2-627E as well as after control treatment with PBS (data not shown). To indicate significant effects of the factors "days p.i." and "RIG-I genotype" on the variable "IFN- β concentration", a 2-Way ANOVA was performed.

The results indicate a significant effect of the factor "days p.i." on the variable in all comparisons between the data groups ($p < 0.0001$). For the factor "RIG-I genotype", the ANOVA analyses indicate no significant effect on the variable, and no significant interaction between the factors was detectable in all comparisons between the groups (compare Figure 32). Taken together, IFN- β was induced only to a low extent at early stages of infection with the IAV PB2-627K virus variant. Remarkably, IFN- β activation *in vivo* upon IAV PB2-627K infection was not significantly different in dependence of the RIG-I genotype, but showed a similar pattern like the *in vitro* IFN- α expression in BmdM Φ upon infection with the IAV/PR/8 Δ NS1 strain, on one hand. On the other hand, infection of BmdM Φ with an IAV/PR/8 PB2-627K strain similar to the one used in the mouse infection study showed no significant induction of IFN- α at all (for both c. c. 4.2.2.2). These findings suggest that the viral NS1 protein hinders RIG-I-mediated IFN-1 expression and that other innate PRRs contribute to the observed IFN- β induction, more than observed in the BmdM Φ .



2-Way ANOVA	RIG-I WT vs. PM		RIG-I WT vs. KO		RIG-I PM vs. KO	
	p value	significance	p value	significance	p value	significance
interaction	0.2526	ns	0.4465	ns	0.9970	ns
days p.i.	<0.0001	****	<0.0001	****	<0.0001	****
genotype	0.1293	ns	0.2651	ns	0.9221	ns

Figure 32: IAV PB2-627K mouse infection causes a significant induction of IFN- β , which is slightly dependent on RIG-I variant expression. Mice with a RIG-I WT, PM or KO background were infected with an IAV PB2-627K strain. BALF was harvested from the mice, the samples of two female or two male mice were pooled. The abundance of IFN- β was measured with an ELISA. The mean IFN- β concentration in two technical replicates of the pooled samples was calculated and depicted in a histogram with the respective standard deviation. A 2-Way ANOVA was used to determine significant effects of the factors "days p.i." and "RIG-I genotype" on the variable "IFN- β concentration", as well as the interaction between the factors.

4.4.4. Proinflammatory and antiinflammatory cytokine expression is enhanced in response to IAV PB2-627K and IAV PB2-627E infection and slightly altered by RIG-I variant expression

To investigate differences in the cytokine profile due to RIG-I variant expression, a multiplex cytokine assay was performed. RIG-I WT, PM and KO mice were infected with IAV PB2-627K, -627E or treated with PBS. The abundance of 23 murine cytokines was measured in the BALF of at least four mice per infection group. Therefore, the BALF of either two female or two male mice per infection group was pooled and analyzed as technical duplicates. The mean of two female and two male mouse replicates was calculated (c. c. 3.17.2). Cytokines with very low abundance were not analyzed (data not shown). For the other cytokines, the means of the different infection groups were depicted in histograms

with the respective standard deviation, separately for the respective infection condition (compare Figure 33 A-N). Of those, the analysis of the data deriving from PBS-treated mice showed a basal abundance or no abundance with low variation, in all cases (data not shown). Further, a subset of the analyzed cytokines, which was considered as less interesting in regard to the results, is depicted in the supplementary data (Supplementary Figure 6 A-F). To determine significant effects of the factors "days p.i." and "RIG-I genotype" on the variable "cytokine concentration", as well as the interaction between the factors, a 2-Way ANOVA was used. Remarkably, subgroups of the data frequently failed the confirmation of a normal distribution of the data, which most likely resulted from sample pooling.

For all the shown cytokines, the ANOVA analyses indicate a significant effect of the factor "days p.i." on the variable "cytokine concentration", in both the IAV PB2-627K and -627E infections, in all of the comparisons between the data groups ($p < 0.0001$). The indication of significant effects of the factor "RIG-I genotype" on the variable are depicted in Table 39 for all of the comparisons between the groups.

Table 39: A summary of the results derived from the multiplex cytokine assay. The differences between RIG-I variant mouse lines in regard to cytokine expression are summarized, for the IAV PB2-627K and -627E infections.

PB2 genotype	IAV PB2-627K			IAV PB2-627E		
	WT vs. PM	WT vs. KO	PM vs. KO	WT vs. PM	WT vs. KO	PM vs. KO
IL-1 β	ns	ns	ns	**	ns	***
IFN- γ	ns	ns	ns	****	*	****
IL-6	ns	ns	ns	**	ns	**
IL-12 p70	ns	ns	ns	*	ns	*
MCP-1	*	ns	ns	**	ns	**
MIP-1 β	ns	ns	ns	**	ns	**
RANTES	*	*	ns	*	ns	***
IL-10	*	ns	ns	**	ns	**
GCSF	ns	ns	ns	ns	ns	ns
KC	ns	ns	ns	ns	ns	ns
MIP-1 α	ns	ns	ns	**	ns	****
IL-17A	ns	ns	ns	*	ns	ns
TNF- α	ns	ns	ns	*	ns	*
IL-4	ns	ns	ns	ns	ns	ns

For the effect of the factor RIG-I genotype on the variable "cytokine concentration", the ANOVA analyses indicate only a few significant differences in the IAV PB2-627K infections. The first difference was detected in the MCP-1 data, showing a significant effect in the comparison between RIG-I WT and PM mice ($p = 0.0159$), as well as a significant interaction between the factors in the same comparison ($p = 0.0038$). The second difference is indicated in the RANTES data, showing a significant effect in the comparison between the RIG-I WT and PM mice ($p = 0.0285$), as well as the RIG-I WT and KO mice ($p = 0.0225$). There was also a significant interaction detectable, for the same comparisons (WT vs. PM $p = 0.0036$ and WT vs. KO $p = 0.0018$). These significant differences were

caused by a higher concentration of the respective cytokine in RIG-I WT mice. Additionally, MIP-1 β showed a comparable, but insignificant difference (compare Figure 33 E, F and G IAV PB2-627K). Since the expression of RANTES is known to be IFN-1 dependent (Lin R. 1999), these findings are consistent with the result that IFN- β was slightly increased in RIG-I WT mice, compared to PM and KO mice upon IAV PB2-627K infection (compare previous chapter). MCP-1 and MIP-1 β (not significant) showed similar patterns like RANTES, but are not known to be IFN dependent. Since these cytokines are linked to chemotaxis of dendritic cells and monocytes (MCP-1) or different types of leucocytes (RANTES and MIP-1 β), the results suggest a contribution of RIG-I to the induction of chemotaxis. There was also a significant difference in the IL-10 data detectable, but this was most likely caused by a high variation in the RIG-I KO day 7 p.i. data (compare Figure 33 H IAV PB2-627K).

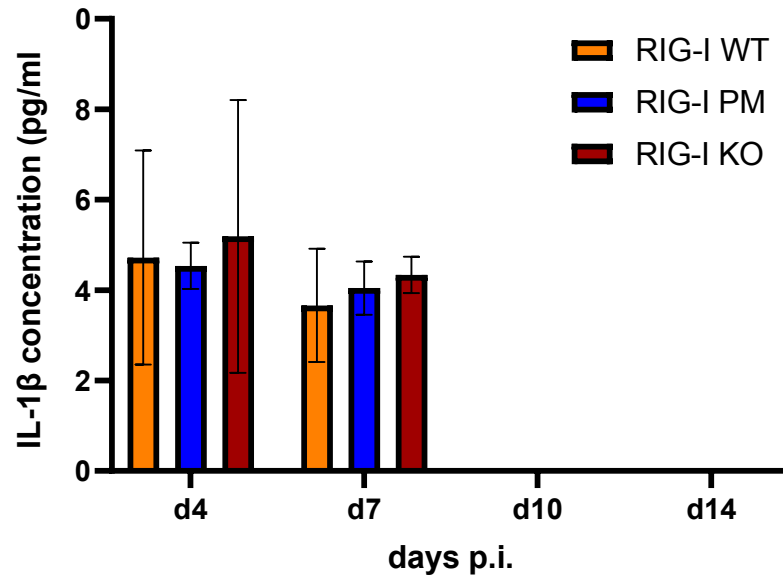
In the context of the IAV PB2-627E infection, some significant effects of the factor "RIG-I genotype" on the variable "cytokine concentration" were detectable, too. Most of the investigated cytokine concentrations seemed to be similar in the RIG-I WT and KO mice, with the only exception of IFN- γ , which was significantly lower in the RIG-I KO mice ($p = 0.0183$). For this comparison, also a significant interaction between the factors was detected ($p = 0.0023$) (compare Figure 33 B IAV PB2-627E). This is an interesting finding, since IFN- γ expression was not known to be dependent on RIG-I activation. Remarkably, the significant difference resulted only from the day 7 p.i. data, while IFN- γ was hardly detectable at the other days. However, the results of the IAV PB2-627K data set showed also a slight reduction in the RIG-I KO mice, compared to the WT and PM mice, which was not significant.

Importantly, for RIG-I PM mice all measured cytokines showed a significantly lower concentration, compared to RIG-I WT and KO mice, especially at day 7 p.i. and in some cases at day 10 p.i., too. There was also a significant interaction between the factors detectable, in all comparisons between RIG-I WT and PM cells and RIG-I PM and KO cells, except for RANTES (only WT and PM) (compare Figure 33 A-H IAV PB2-627E). Compared to the previous results, the virus titer in the BALF and lung tissue of RIG-I PM mice was also lower than in RIG-I WT and KO mice at day 7 and day 10 p.i. in the IAV PB2-627E infections (c. c. 4.4.1.4 and 4.4.1.5). This might explain the lower cytokine responses, since virus titer and cytokine pattern seemed to correlate. These findings came by surprise, since it does not seem reasonable that the infection in mice with full RIG-I functionality (RIG-I WT) and none of the functions available (RIG-I KO) showed the same pattern, while in mice with only RIG-I-IFN signaling deficiency, the intensity of the infection was significantly reduced. Of the additional cytokines depicted in the supplementary data, all showed the same significant differences in the RIG-I PM mice, with GCSF and TNF- α showing a similar tendency and only KC not sharing the pattern

(compare Supplementary Figure 6 A-F). In the end, an infection artifact cannot be excluded as an explanation.

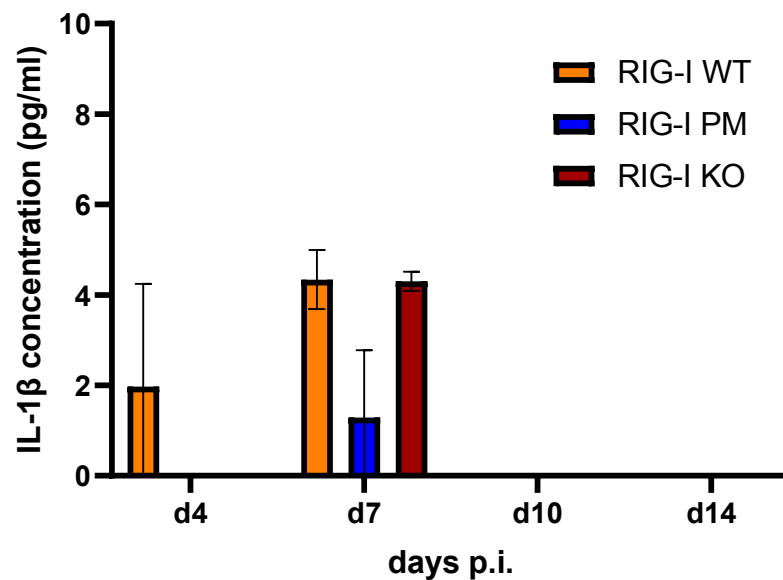
Of special interest is IL-1 β , since RIG-I directly contributes to its bioavailability by activation of the inflammasome and by IFN-1-mediated induction of pro-IL-1 β . The data showed IL-1 β levels at day 4 p.i. only in the RIG-I WT mice infected with the IAV PB2-627E strain. This did not cause a significant effect of the factor "RIG-I genotype" on the variable in the statistical analysis, but a tendency ($p = 0.1042$), in the comparison between RIG-I WT and KO mice. Additionally, the interaction between the factors showed a similar tendency in this comparison ($p = 0.0674$). These findings suggest a RIG-I dependent activation of the inflammasome at very early phases of the inflammation (day 4 p.i.), but the amount of data is thin and carries high variation. At later time points p.i., the pattern was similar to the other proinflammatory cytokines, suggesting that other factors control IL-1 β availability at those stages of the inflammation (compare Figure 33 A IAV PB2-627E). In contrast, the complete lack of an RIG-I effect on the IL-1 β levels in the IAV PB2-627K infections suggests, that either the -627K virus variant is mostly resistant to RIG-I-mediated antiviral effects, or IL-1 β activation is mediated independently of RIG-I during IAV infections.

In summary, the results indicate, that the abundance of proinflammatory cytokines and chemokines (IL-1 β , IFN- γ , IL-6, IL-12 p70, MCP-1, MIP-1 β , RANTES, GCSF, KC, MIP-1 α , IL-17A and TNF- α) significantly rose in both the infections with IAV PB2-627K or -627E at day 4 and day 7 p.i. and decreased until day 10 and 14 p.i. This finding is in line with other results suggesting that the acute phase of the virus-induced inflammation reaches its maximum at day 7 p.i. (c. c. 4.4.1.2 ff.) and is cleared by activation of the adaptive immune responses later on. The decrease of proinflammatory signals at day 10 and day 14 p.i. suggests that no chronic inflammation is ongoing, which is supported by other results suggesting that basal membranes stay intact and lung barrier function is reestablished (c. c. 4.4.1.6 PAS staining and f.). The cytokine profile of the anti-inflammatory cytokine IL-10 and the immune regulatory IL-4 did not show a different pattern compared to the proinflammatory cytokines. This suggests that the regulation is very fast-acting and not delayed. Overall, these findings suggest that pro- and antiinflammatory cytokines show a very similar pattern, which seems to correlate with weight loss and virus titer of the infected mice.

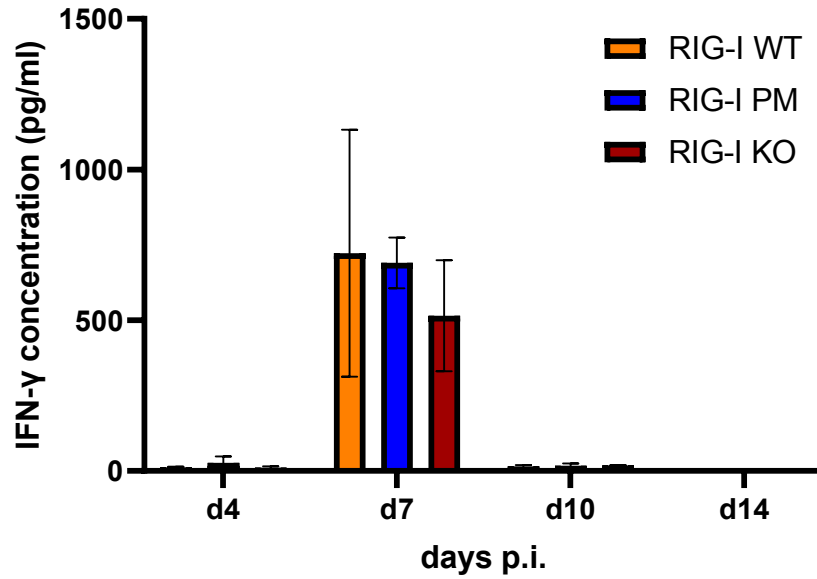
A IL-1 β IAV PB2-627K

2-Way ANOVA	WT vs. PM		WT vs. KO		PM vs. KO	
source of variation	p value	significance	p value	significance	p value	significance
interaction	0.9491	ns	0.9516	ns	0.9251	ns
days p.i.	<0.0001	****	<0.0001	****	<0.0001	****
genotype	0.8858	ns	0.5775	ns	0.5541	ns

IAV PB2-627E

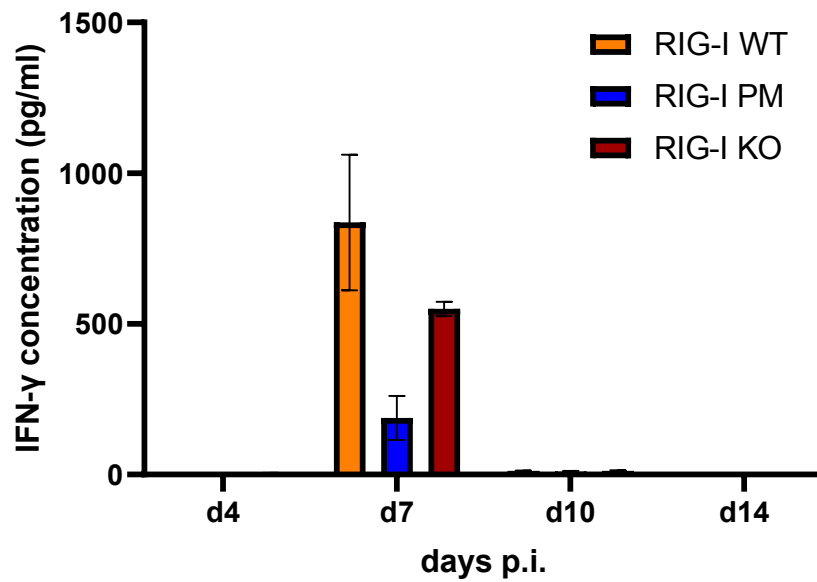


2-Way ANOVA	WT vs. PM		WT vs. KO		PM vs. KO	
source of variation	p value	significance	p value	significance	p value	significance
interaction	0.0102	*	0.0674	ns	<0.0001	****
days p.i.	<0.0001	****	<0.0001	****	<0.0001	****
genotype	0.0015	**	0.1042	ns	0.0005	***

B IFN- γ IAV PB2-627K

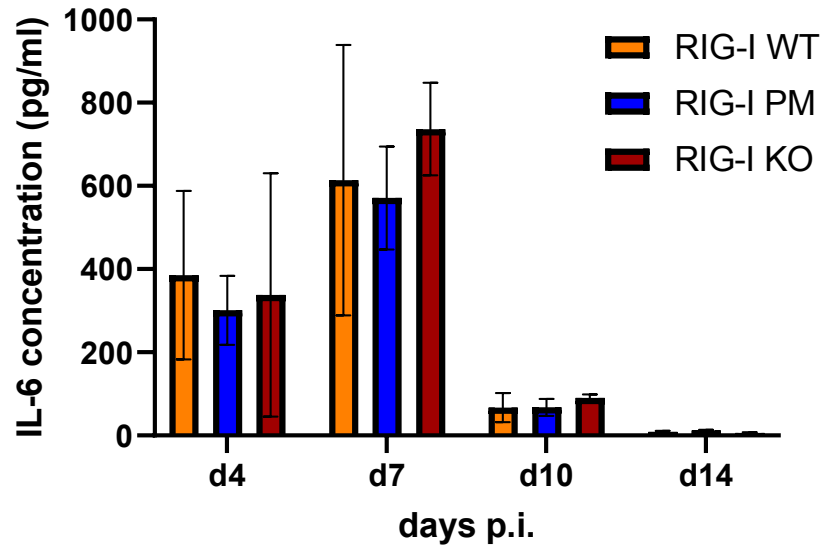
2-Way ANOVA	WT vs. PM		WT vs. KO		PM vs. KO	
source of variation	p value	significance	p value	significance	p value	significance
interaction	0,9906	ns	0,4771	ns	0,0603	ns
days p.i.	<0,0001	****	<0,0001	****	<0,0001	****
genotype	0,9425	ns	0,3676	ns	0,0727	ns

IAV PB2-627E



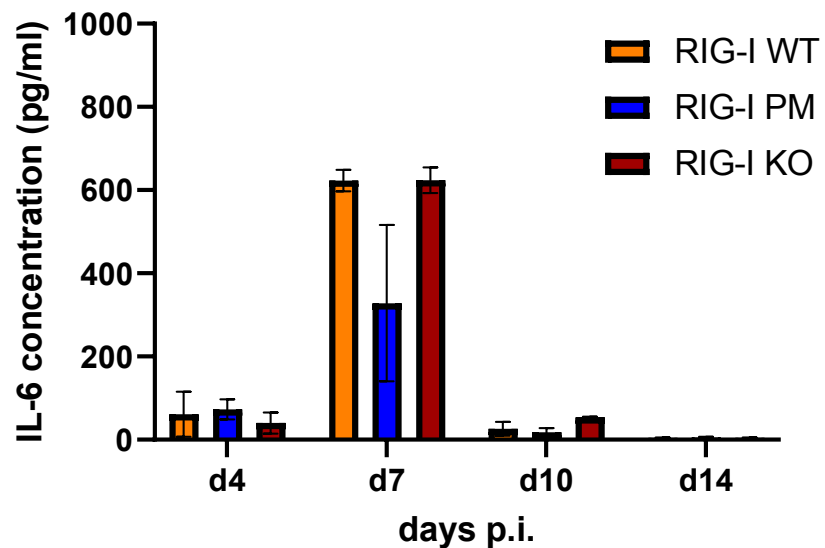
2-Way ANOVA	WT vs. PM		WT vs. KO		PM vs. KO	
source of variation	p value	significance	p value	significance	p value	significance
interaction	<0,0001	****	0,0023	**	<0,0001	****
days p.i.	<0,0001	****	<0,0001	****	<0,0001	****
genotype	<0,0001	****	0,0183	*	<0,0001	****

C IL-6 IAV PB2-627K



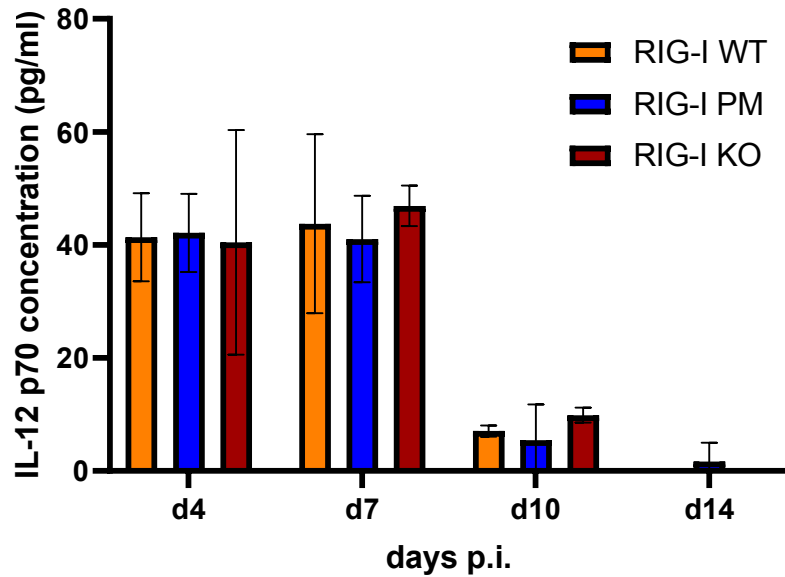
2-Way ANOVA	WT vs. PM		WT vs. KO		PM vs. KO	
source of variation	p value	significance	p value	significance	p value	significance
interaction	0.9213	ns	0.7978	ns	0.5244	ns
days p.i.	<0.0001	****	<0.0001	****	<0.0001	****
genotype	0.5559	ns	0.7009	ns	0.2178	ns

IAV PB2-627E



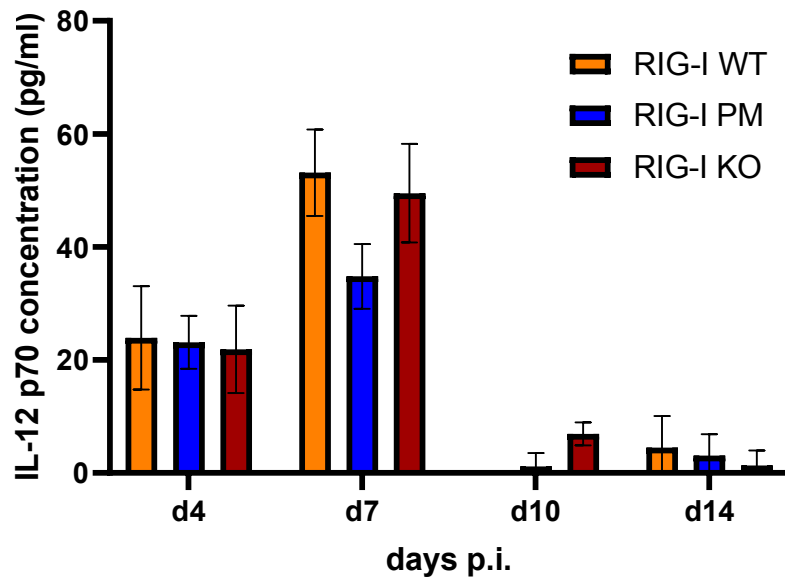
2-Way ANOVA	WT vs. PM		WT vs. KO		PM vs. KO	
source of variation	p value	significance	p value	significance	p value	significance
interaction	0.0004	***	0.3394	ns	0.0002	***
days p.i.	<0.0001	****	<0.0001	****	<0.0001	****
genotype	0.0076	**	0.8448	ns	0.0052	**

D IL-12 p70 IAV PB2-627K



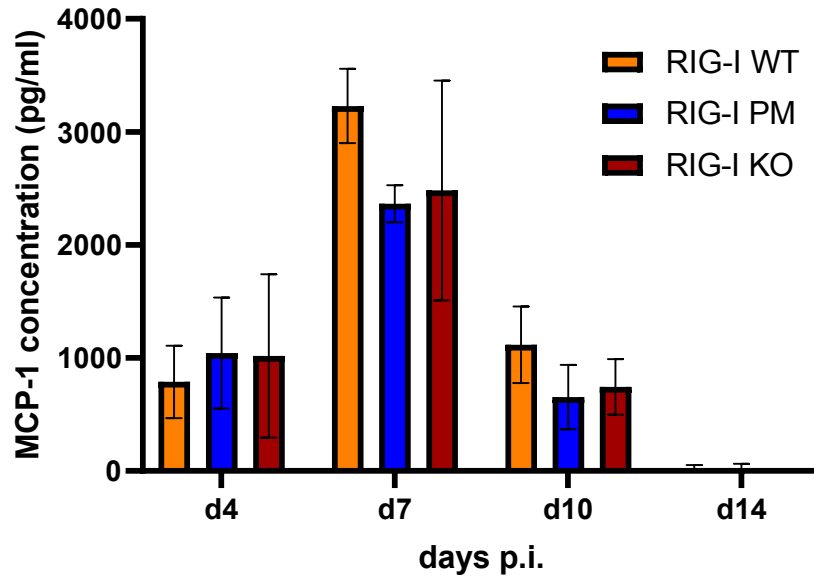
2-Way ANOVA	WT vs. PM		WT vs. KO		PM vs. KO	
source of variation	p value	significance	p value	significance	p value	significance
interaction	0.9345	ns	0.9644	ns	0.7217	ns
days p.i.	<0.0001	****	<0.0001	****	<0.0001	****
genotype	0.8621	ns	0.7109	ns	0.5651	ns

IAV PB2-627E



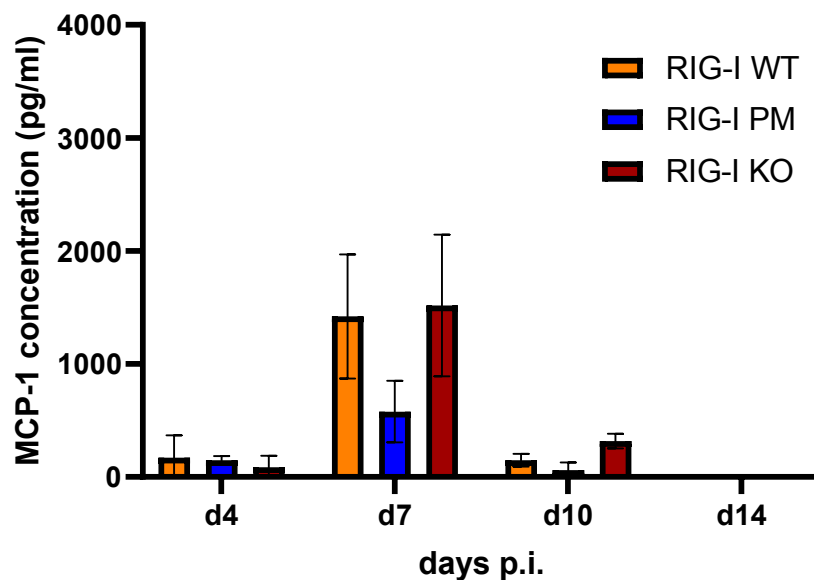
2-Way ANOVA	WT vs. PM		WT vs. KO		PM vs. KO	
source of variation	p value	significance	p value	significance	p value	significance
interaction	0.0059	**	0.3171	ns	0.0146	*
days p.i.	<0.0001	****	<0.0001	****	<0.0001	****
genotype	0.0212	*	0.8307	ns	0.0275	*

E MCP-1 IAV PB2-627K



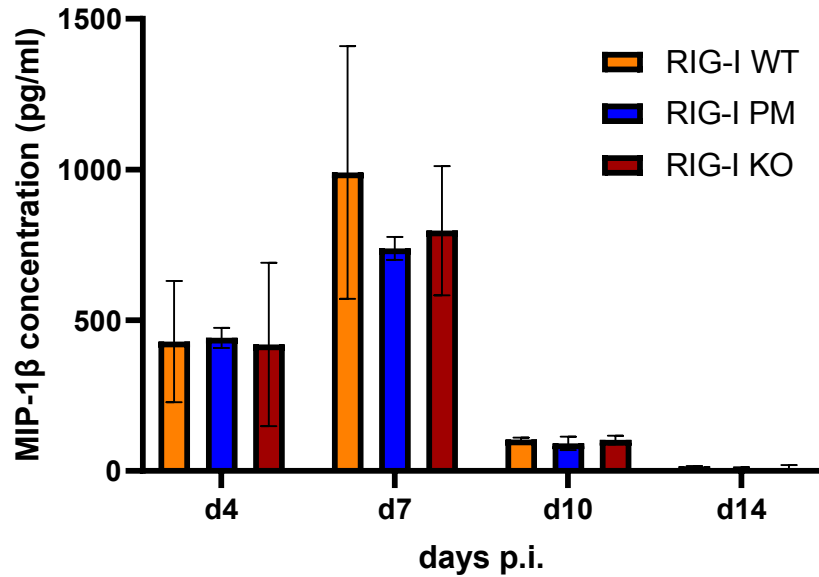
2-Way ANOVA	WT vs. PM		WT vs. KO		PM vs. KO	
source of variation	p value	significance	p value	significance	p value	significance
interaction	0.0038	**	0.2242	ns	0.9861	ns
days p.i.	<0.0001	****	<0.0001	****	<0.0001	****
genotype	0.0159	*	0.1947	ns	0.8185	ns

IAV PB2-627E



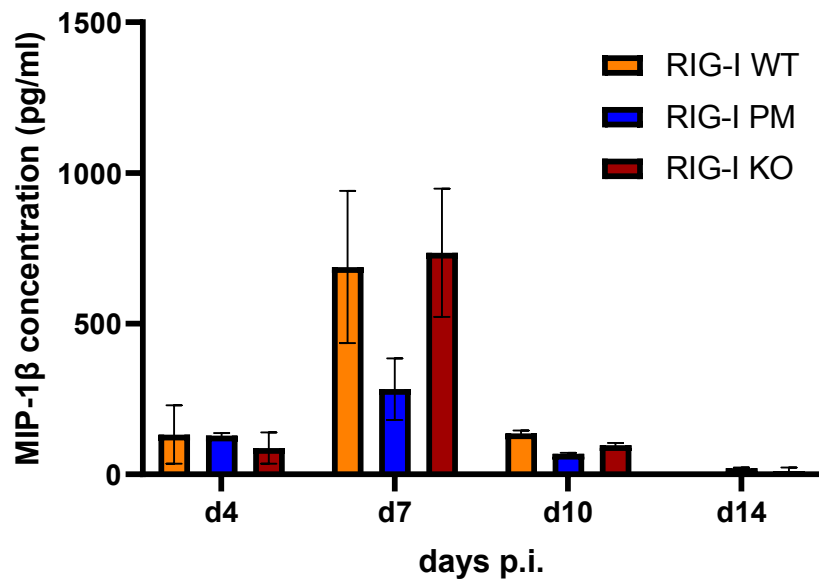
2-Way ANOVA	WT vs. PM		WT vs. KO		PM vs. KO	
source of variation	p value	significance	p value	significance	p value	significance
interaction	0.0030	**	0.8529	ns	0.0016	**
days p.i.	<0.0001	****	<0.0001	****	<0.0001	****
genotype	0.0074	**	0.6790	ns	0.0034	**

F MIP-1 β IAV PB2-627K



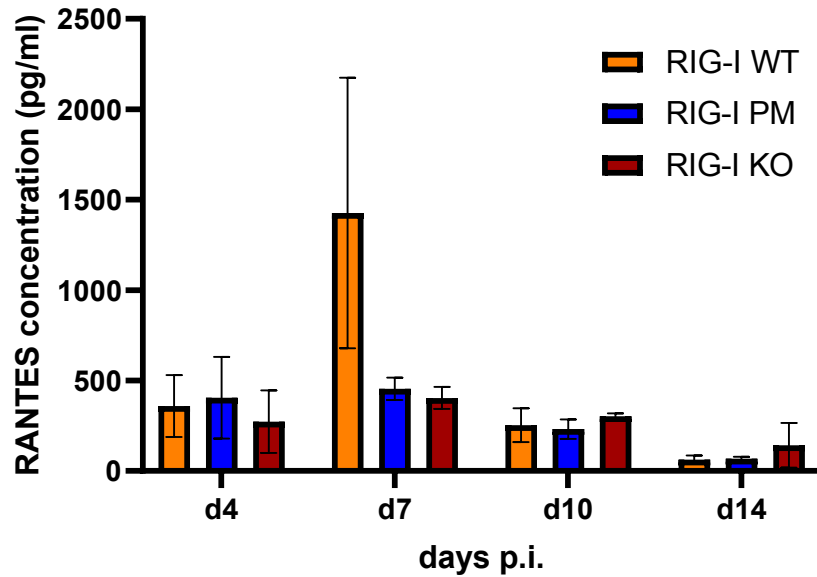
2-Way ANOVA	WT vs. PM		WT vs. KO		PM vs. KO	
source of variation	p value	significance	p value	significance	p value	significance
interaction	0.3549	ns	0.7416	ns	0.9292	ns
days p.i.	<0.0001	****	<0.0001	****	<0.0001	****
genotype	0.2727	ns	0.4747	ns	0.7666	ns

IAV PB2-627E



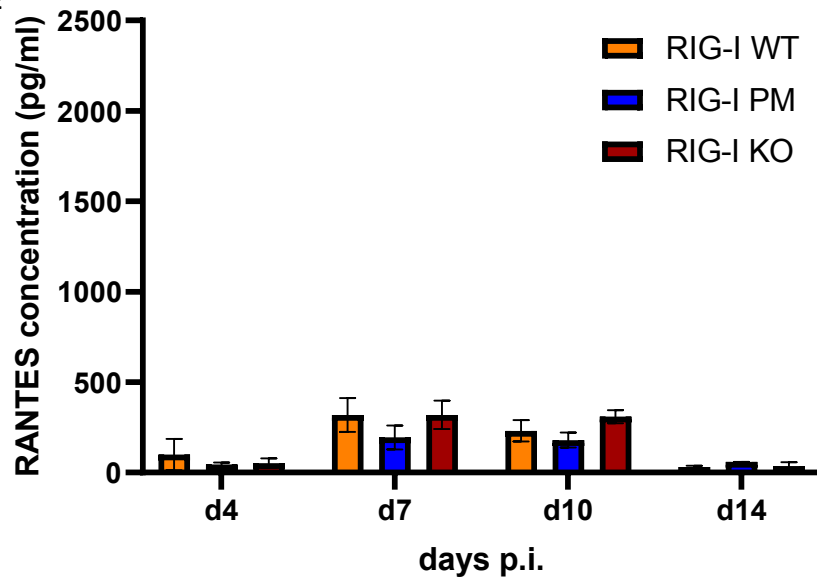
2-Way ANOVA	WT vs. PM		WT vs. KO		PM vs. KO	
source of variation	p value	significance	p value	significance	p value	significance
interaction	0.0011	**	0.8566	ns	<0.0001	****
days p.i.	<0.0001	****	<0.0001	****	<0.0001	****
genotype	0.0043	**	0.8804	ns	0.0016	**

G RANTES IAV PB2-627K



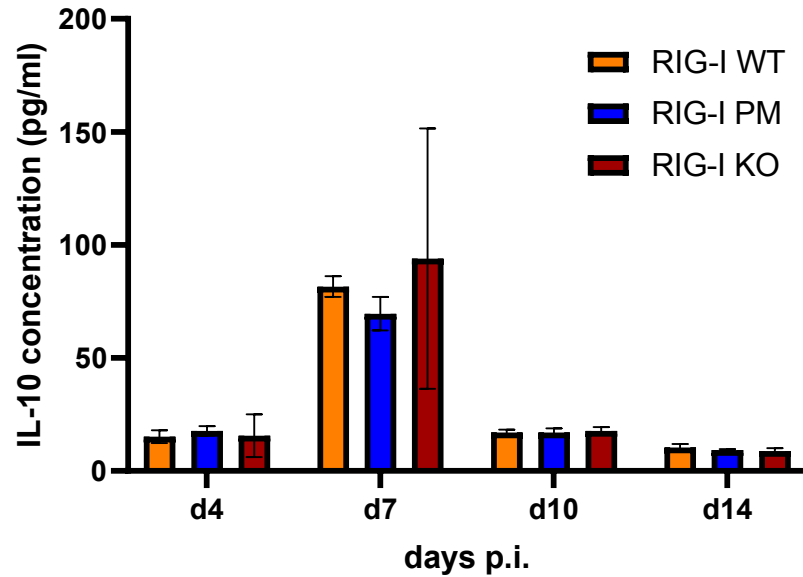
2-Way ANOVA	WT vs. PM		WT vs. KO		PM vs. KO	
source of variation	p value	significance	p value	significance	p value	significance
interaction	0.0036	**	0.0018	**	0.2364	ns
days p.i.	<0.0001	****	<0.0001	****	<0.0001	****
genotype	0.0285	*	0.0225	*	0.8214	ns

IAV PB2-627E



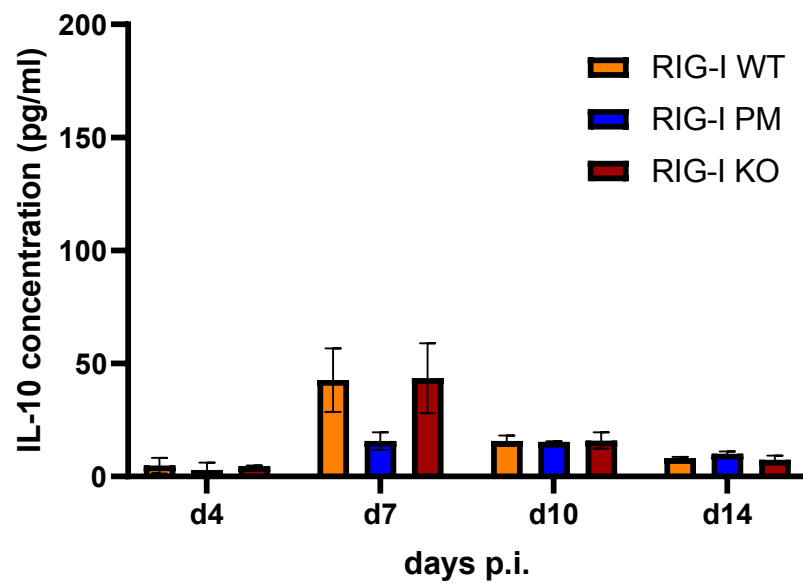
2-Way ANOVA	WT vs. PM		WT vs. KO		PM vs. KO	
source of variation	p value	significance	p value	significance	p value	significance
interaction	0.0957	ns	0.2339	ns	0.0021	**
days p.i.	<0.0001	****	<0.0001	****	<0.0001	****
genotype	0.0189	*	0.6595	ns	0.0006	***

H IL-10 IAV PB2-627K



2-Way ANOVA	WT vs. PM		WT vs. KO		PM vs. KO	
source of variation	p value	significance	p value	significance	p value	significance
interaction	0.0017	**	0.9038	ns	0.5468	ns
days p.i.	<0.0001	****	<0.0001	****	<0.0001	****
genotype	0.0388	*	0.6905	ns	0.4523	ns

IAV PB2-627E



2-Way ANOVA	WT vs. PM		WT vs. KO		PM vs. KO	
source of variation	p value	significance	p value	significance	p value	significance
interaction	<0.0001	****	0.9970	ns	<0.0001	****
days p.i.	<0.0001	****	<0.0001	****	<0.0001	****
genotype	0.0016	**	0.9984	ns	0.0032	**

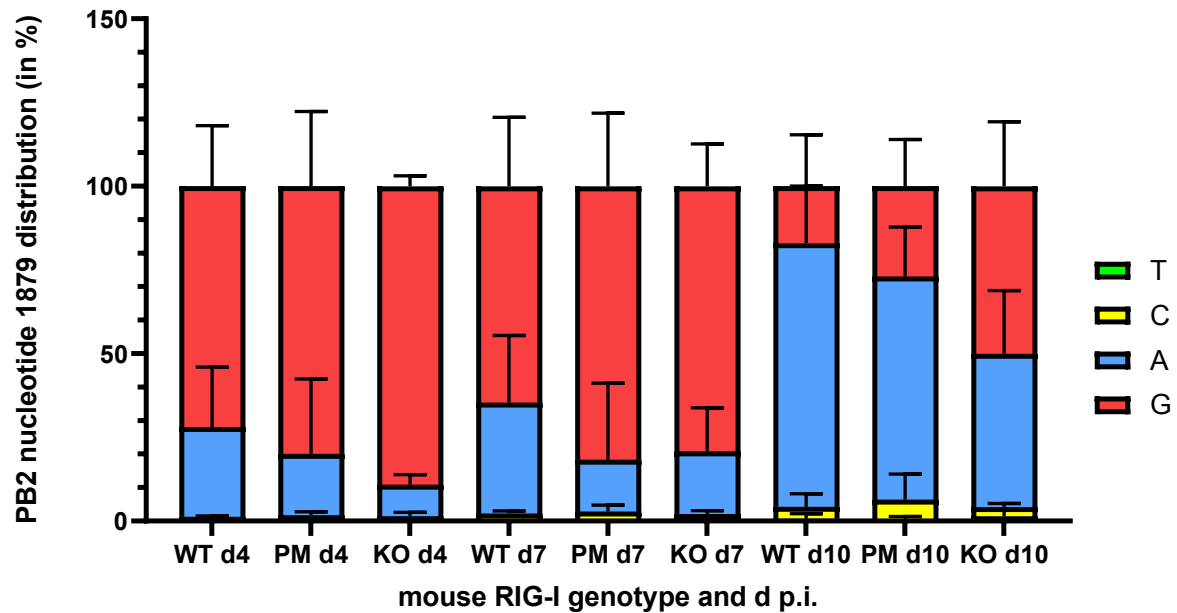
Figure 33: RIG-I variant expression affects the induction of chemokines in an IAV PB2-627K infection and the expression of IFN- γ in an IAV PB2-627E infection. Mice with a RIG-I WT, PM or KO background were infected with either an IAV PB2-627K or -627E strain. BALF was harvested from mice and the samples of two female or two male mice were pooled. The concentrations of IL-1 β (A), IFN- γ (B), IL-6 (C), IL-12 p70 (D), MCP-1 (E), MIP-1 β (F), RANTES (G) and IL-10 (H) were measured with a multiplex cytokine assay (M60009RDPD, Bio-Rad). The mean concentration of two technical replicates of the pooled samples from two female and two male mice was calculated and depicted in histograms with the respective standard deviation. A 2-Way ANOVA was used to determine significant effects of the factors "RIG-I genotype" and "days p.i." on the respective "cytokine concentration" as variable, as well as the interaction between the factors.

4.4.5. The genetic stability of the IAV PB2-627E strain during mouse lung infection is dependent of RIG-I variant expression

In the *in vitro* performed competitive infection experiment, tendencies of differential replication of the IAV PB2-627K and -627E virus strains in dependence of RIG-I variant expression in MEF cells were found (c. c. 4.3.4). Because of the previously found differences in replication and frequently occurring (back) mutations of the IAV PB2-627E virus strain in mammalian cells (c. c. 4.3.2), the genetic stability of the PB2 nt 1879 in BALF samples from mice infected with this strain was verified. Therefore, viral RNA was isolated from BALF of the respective mice, reverse-transcribed to cDNA, multiplied and analyzed by Sanger-sequencing. The mean percentage of the nt distribution at the position 1879 of the viral PB2 gene of four mice of the respective infection group was calculated and depicted with the respective standard deviation in stacked bar plots (compare Figure 34). From the BALF of mice sacrificed at 14 days p.i., not enough virus RNA could be isolated for analysis. For statistical analysis, only the mean percentage abundance of the PB2 nt 1879 G was compared between the infection groups as variable (c. c. 3.18). With a 2-Way ANOVA, significant effects of the factors "days p.i." and "RIG-I genotype" on the variable "PB2 nt 1879 G abundance", as well as their interaction, were analyzed. Unfortunately, the confirmation of normal distribution in the RIG-I WT data set was not successful.

The results of the ANOVAs indicated that the factor "days p.i." had a significant effect on the PB2 nt 1879 G occurrence, for all comparisons between the data groups ($p < 0.0001$). For the factor "RIG-I genotype", the ANOVAs indicated a significant effect on the variable in the comparison between RIG-I WT and KO mice ($p = 0.0038$) and tendencies in the comparisons between RIG-I WT and PM ($p = 0.1490$) and RIG-I PM and KO mice ($p = 0.1662$). Further, the ANOVAs indicated no significant interaction between both factors, in all the comparisons between the data groups (compare Figure 34).

These results show, that the PB2 nt 1879, which was artificially switched from A to G with primer-mediated mutagenesis to generate the IAV PB2-627E strain, was not stable during mouse lung infection. Further, during the course of the IAV PB2-627E infection, the rate of average nt 1879 G to A back mutation significantly increased from day 4 to day 10 p.i. Additionally, the rate of average G to A back mutation was lowest in RIG-I KO mice, intermediate in RIG-I PM mice and highest in RIG-I WT mice. Despite the rate of nt G to A back mutation showed a characteristic pattern, only the difference between RIG-I WT and KO is significant. In conclusion, the results suggest that RIG-I is a factor mediating significant genetic pressure on the IAV PB2-627 codon, favoring the PB2 nt 1879 A variant, which reverts the codon back from aa 627E to 627K. At last, the finding that there was no significant interaction between the factors "RIG-I genotype" and "days p.i.", suggests that the selective pressure is not mediated by RIG-I alone. This finding was also suggested by the results of the competitive infection experiments (c. c. 4.3.4). The additional factor or factors may have a huge impact, since there was an 8.3×10^2 fold difference between the required doses for the IAV PB2-627K and -627E strains to cause similar infection symptoms in mice (c. c. 4.4.1.1). This higher infection titer was not different for RIG-I KO mice, hence RIG-I KO alone did not abolish the effect.



2-Way ANOVA	RIG-I WT vs. PM		RIG-I WT vs. KO		RIG-I PM vs. KO	
source of variation	p value	significance	p value	significance	p value	significance
interaction	0.8837	ns	0.4724	ns	0.3392	ns
days p.i.	<0.0001	****	<0.0001	****	<0.0001	****
RIG-I genotype	0.1490	ns	0.0038	**	0.1662	ns

Figure 34: RIG-I variant expression influences the PB2 nucleotide 1879 G back mutation to A in mice infected with an IAV PB2-627E strain. RIG-I WT, PM or KO mice were infected with an IAV PB2-627E strain. The mice were sacrificed after the indicated time points p.i. and BALF was harvested. The viral RNA was extracted from the BALF, reverse-transcribed into cDNA, multiplied and analyzed by Sanger-sequencing. The mean percentage PB2 nt 1879 distribution with the respective standard deviations of four mice per infection group is depicted as stacked bar diagram. A 2-Way ANOVA was used to indicate significant effects of the factors "days p.i." and "RIG-I genotype" on the variable "PB2 nt 1879 G abundance", as well as their interaction.

5. Discussion

5.1. *Current knowledge and aims of the project*

Today, the arsenal of antiviral therapies gets more and more diverse. Nevertheless, the potential of virus strains to establish new mutations enabling therapy evasion is still impressive. Hence, there is need to unravel virus-host interactions and the antiviral defense mechanisms in detail, with the aim to find new targets for alternative therapies and to predict and understand side effects. RIG-I, one of the PRRs of the innate immune system, plays an important role in the defense against RNA viruses, like IAV and Sendai. The first described antiviral effect of RIG-I is its ability to enhance IFN-1 expression upon RNA binding. Further, it can enhance the level of IL-1 β , another important signaling molecule of the innate immune system (Weber-Gerlach M. 2016a). In the year 2015, Weber *et al.* described a third antiviral function, mediated by binding of RIG-I to the viral RNA itself. This leads to a block of the viral panhandle structures for the access of IAV PB2-627E polymerase variants, which are common in avian-adapted IAV strains (Weber M. 2015).

This project was aimed to show the impact of the several RIG-I-mediated antiviral effects against mammalian- and avian-adapted IAV strains *in vivo* in a mouse system. A special task was to deliver hints for the relevance of the RIG-I-mediated blocking of the viral panhandle structures for the access of the viral polymerase *in vivo*. Therefore, mouse lines expressing completely functional RIG-I (WT), a RIG-I K271A mutant with ATPase dysfunction deficient in signaling (PM) and with complete loss of RIG-I (KO) were generated and validated for their functionality. Furthermore, recombinant IAV/PR/8 PB2-627K and -627E strains, chosen as examples for a mammalian- and avian-adapted strain, were established. Finally, the impact of the different antiviral effects of RIG-I were examined in a mouse infection study using the established mouse lines and IAV strains. In detail, the effect of RIG-I variant expression after infection with the mammalian- or avian-adapted IAV strain was investigated on different infection parameters like weight loss, virus titer in the lung, altered lung epithelial barrier integrity as well as the IFN and the cytokine expression profiles.

5.2. *RIG-I WT, PM and KO mouse lines are not burdened and their immune cells functional corresponding to the genotype*

For the RIG-I PM and KO mouse lines, which were generated using CRISPR/Cas9 technology, no phenotypic alterations, increased susceptibility for diseases or enhanced mortality of puppies were found, which would result in a burden for the respective line. With this finding, both mouse lines were judged as unburdened by the responsible ethics commission. Importantly, the RIG-I PM mouse

line is the first of its kind. Maybe even more important, the RIG-I KO mouse line is the first one that was generated completely unburdened. When the generation of the RIG-I PM and KO mouse was planned, no unburdened RIG-I KO mouse lines were available. Only two RIG-I KO mouse lines had been established so far, showing certain side effects and therefore being categorized as burdened lines. One of these two mouse lines, established by the Wang group, developed colitis (Wang Y. 2007) and was most likely also used by Zhang *et al.*, who found that it shows a tendency to develop progressive myeloproliferative disorders dependent on RIG-I loss (Zhang N.-N. 2008). The other line was established by the Kato group and shows a high rate of embryonal lethality (Kato H. 2005). These burdens may result from side effects due to the applied genetic engineering technique using homology directed repair in combination with a PGK recombination vector targeting RIG-I, in both cases. In the last years, a vital RIG-I KO mouse line was established by intensive crossing of the line described by Kato *et al.* (Wu W. 2018). Hence, it might be an advantage that the RIG-I KO mouse line generated in this project is more similar to the original C57BL6/J line, while the intensively crossed line is less comparable to currently used standard mouse lines.

By verification of the RIG-I protein integrity, it was found that RIG-I protein expression is detectable in RIG-I WT and PM mouse-derived BmdM Φ , while it is not detectable in RIG-I KO mouse cells, as expected (c. c. 4.2.1). Concerning RIG-I-mediated IFN- α induction, it was found that RIG-I PM and KO mouse-derived BmdM Φ are insufficient, in contrast to RIG-I WT mouse-derived cells (c. c. 4.2.2.1). These findings were further validated with IAV/PR/8 dNS1 and Sendai virus infection experiments, indicating a significant induction of IFN- α in response to both infections in RIG-I WT mouse-derived cells, which was significantly lower in RIG-I PM and KO mouse-derived cells. In contrast, the infection with an IAV/PR/8 strain expressing functional NS1 did not induce significant IFN- α production in any cell type, giving a first hint for the high potency of the viral NS1 protein to suppress IFN-1 signaling (c. c. 4.2.2.2). Further, the BmdM Φ from the three mouse lines showed no significant differences in the induction of TLR1, 2, 4 and 9 signaling, as well as cGAS/STING signaling. These findings suggest that there are no significant compensatory up-regulations in response to altered RIG-I expression or unspecific side effects of the genetic engineering in the investigated signaling pathways of the innate immune system, except for RIG-I IFN-1 signaling. In summary, this makes the mouse lines a sufficient model system for the study of RIG-I-mediated functions, with no challenging ethical considerations due to burdening of mice, in contrast to comparable mouse lines.

5.3. The insufficiency of IAV PB2-627E replication in mammalian cells without adaptive mutations highlights the importance of the IAV PB2-627K polymerase adaptation

Using the plasmid-based method to generate recombinant IAV/PR/8 strains (Hoffmann E. 2000), one IAV strain with a mammalian-adapted PB2-627K polymerase (original genotype) and one with an avian-adapted PB2-627E polymerase (PB2 nt 1879 A to G substitution) was generated. The generation and propagation of the IAV PB2-627K strain in mammalian cells caused no problems. In contrast, initial attempts to generate the IAV PB2-627E strain in these cells failed, since there were no virus particles detectable, or sequencing of the PB2 gene indicated the occurrence of unwanted mutations, which in most cases were PB2-627E to -627K back mutations (c. c. 4.3.2). This finding came by surprise, since the validation of the altered plasmid sequence after application of primer-mediated mutagenesis indicated a homogeneous genotype (c. c. 4.3.1). The occurrence of unwanted mutations was a major issue in this project. It is known that IAV PB2-627K variants show at least a partial resistance against RIG-I effects, while -627E variants are susceptible to RIG-I effects (Weber M. 2015). Hence, an IAV PB2-627E strain was important for the study design and intention. In search for alternative host cells for enrichment of an IAV PB2-627E strain, DF-1 chicken cells were chosen, which are established hosts for avian-adapted strains and additionally lack RIG-I, unlike other avian cells (Barber M. R. W. 2010). Both virus strains replicate similar in these cells, which was confirmed by comparison of infectious virus particles, replicating virus particles, hem-agglutination titer, and M protein abundance between the stocks. The finding that RIG-I variant expression of MEF cells only slightly affected the replication advantage of the IAV PB2-627K strain vs. the -627E strain suggests that RIG-I-mediated antiviral effects may not be as potent as initially expected in the chosen model system. On the other hand, the finding that both virus strains did replicate in the MEF cells reduced the risk of generating an IAV PB2-627E virus strain that will not be able to infect mice (c. c. 4.3.4). Cell line experiments do reflect only basic effects of an immune response, so it was decided to take the step into the animal model. As a backup plan, it was considered to generate recombinant IAV strains additionally lacking the NS1 protein, which is known to efficiently inhibit IFN-1 signaling. However, the propagation of an IAV Δ NS1 strain in mammalian cells was also problematic, resulting in the use of chicken eggs (data not shown). Hence, it seemed very likely that an IAV strain lacking two factors enhancing the viral pathogenicity would not be efficient to infect mice.

Importantly, the infection of mice with 100 PFU of the IAV PB2-627K strain or 8.3×10^4 PFU of the IAV PB2-627E strain caused slightly higher percentage in body weight loss by the first despite of the tremendously higher infection dose of the latter (c. c. 4.4.1.1). The range of infection dose between no detectable symptoms and symptoms, which forced a premature abortion of the experiment, was

about the four-fold increase or decrease of the indicated infection titers. The infection inoculum was prepared based on plaque assay titration and not SCIA, to consider fully functional virus particles only. The difference between the required infection titer for IAV PB2-627K and -627E, which is 8.3×10^2 , cannot be explained with the range of infection dose of +/- the four-fold of the indicated amounts. Taken together with the finding that the IAV PB2-627E strain is replicating poorly in mammalian cells, these results strongly suggest a high relevance of the IAV PB2-627K genotype for the virus to replicate efficiently in mammalian cells. However, despite the need of increased infection doses, mice were infected successfully with the avian-adapted IAV strain.

5.4. *Both the recombinant IAV PB2-627K and IAV PB2-627E strain from DF-1 chicken cells are genetically stable*

A contamination of the IAV PB2-627E strain with the -627K variant resulting from the generation of the PB2 vector using primer-mediated mutagenesis technology is very unlikely. This is because both the PCR product and the cleaved vector were purified with agarose-gel electrophoresis after restriction, and the transformed *E. Coli* clones showed no sign of a heterogenic plasmid genotype in Sanger-sequencing (c. c. 4.3.1). Due to the finding that the IAV PB2-627E strain did only replicate in mammalian cells after acquiring additional mutations, which frequently happened (c. c. 4.3.2), the genetic stability of the virus stocks generated in DF-1 cells was validated. Therefore, the complete PB2 RNA gene sequence of the IAV PB2-627K and -627E stock, as well as their previous passages in DF-1 cells, was Sanger-sequenced. In all of the analyzed passages, no mutations were found (c. c. 4.3.5). Additionally, the RNA area flanking the PB2 codon 627 of the stocks was sequenced several times after one additional passage in different MEF cell lines with the same result (c. c. 4.3.4; similar for A549 cells, data not shown). In the competitive infection assay, it was found that the percentage PB2 nt 1879 distribution changed, when MEF cells were infected with a mix of both the IAV PB2-627K and -627E strains, compared to the distribution in the infection mix. This shows that the virus benefits from the IAV PB2-627K genotype, leading to overgrowth of the -627E variant, if both variants are present. Hence, it was concluded that the abundance of PB2-627K copies in the IAV PB2-627E stocks would already lead to a marked change of the background signal during the investigated two passages in DF-1 cells, or at least after another passage in the mammalian MEF cells. Taken together, the findings and considerations suggest, that the recombinant IAV PB2-627K and -627E strains are not cross-contaminated with each other and are genetically stable during the passages in DF-1 cells and during one additional passage in MEF cells with different RIG-I expression status.

5.5. *Competitive infection of MEF cells with both the IAV PB2-627K and IAV PB2-627E strain suggests a slight effect of RIG-I variant expression on virus replication*

To analyze RIG-I effects on the replication of the virus strains, a competitive infection assay was performed, in which calculated and validated ratios between both the IAV PB2-627K and -627E strains were used to infect MEF cells generated from the different RIG-I mouse lines. The results show that the percentage abundance of the IAV PB2-627K genotype increased, while the percentage abundance of the IAV PB2-627E genotype decreased, during infection of MEF cells with both strains simultaneously (c. c. 4.3.4). This shows that the IAV PB2-627K strain did replicate more efficiently in mammalian cells than the IAV PB2-627E strain, which is supported by other observations and consistent with the literature (c. c. 4.3.2) (Weber M. 2015). Interestingly, the IAV PB2-627K replication advantage is slightly, but not significantly, lower in RIG-I KO MEF cells, compared to RIG-I WT and PM cells. This lack of significance suggests that other factors than RIG-I may contribute to the IAV PB2-627K replication advantage and/or that the full potential of WT RIG-I was eventually reduced in the experimental setting. An explanation for the lack of a difference between RIG-I WT and PM cells may deliver the experimental design. It was required to induce RIG-I expression in the MEF cells by IFN- α treatment prior to infection to achieve a difference depending on RIG-I variant expression, but this may also limit the RIG-I-mediated effect, since a high abundance of IFN-1 can mask the potential effect generated by RIG-I-mediated IFN-1 and IL-1 β induction. The lack of a difference between RIG-I WT and PM may also come from the lack of downstream effectors of IFN- α and IL-1 β signaling in the MEF cells and/or that in general *in vitro* based assays are not as meaningful as *in vivo* experiments, since the context of a complete immune system is lacking. Supporting this idea, there is evidence that the C57BL/6J mouse line used in this study lacks the impactful IFN-1 effector MX1, which is a GTPase that inhibits viral transcription and replication (Grimm D. 2007; Verhelst J. 2012; Schwab L. S. U. 2022). Hence, the analysis of these processes should ideally be performed in a mammal with complete RIG-I/IFN/IL-1 β signaling pathways, to have all possible effects involved. In conclusion, the experiments suggest that the RIG-I-mediated signaling functions do not contribute to the positive selection of the PB2-627K polymerase variant, indicated by the lack of differences between PB2 nt 1879 distribution in RIG-I WT and PM MEF cells. Hence, the data suggest an impact of the RIG-I blocking function, which can be mediated by RIG-I WT and PM, but is lacking in RIG-I KO cells.

5.6. *The IAV PB2-627E genotype is not stable during mouse infection and its rate of back mutation is dependent on RIG-I variant expression*

5.6.1. *RIG-I mediates a selective pressure on the IAV PB2-627 codon*

For the generation of the avian-adapted IAV PB2-627E strain, the PB2 nt 1879 was changed from A to G with primer-mediated mutagenesis. Since Sanger-sequencing of three consecutive passages did not indicate alterations in the percentage distribution of the PB2 nt 1879, it was concluded that the generated IAV PB2-627E stocks did not contain any PB2-627K copies (c. c. 4.3.4 and 4.3.5). Surprisingly, the PB2-627E polymerase genotype rapidly reverts to PB2-627K during the mouse infection experiments. However, the finding that the rate of PB2 nt 1879 G to A back mutation was significantly enhanced with the duration of the infection and was higher in RIG-I PM and most pronounced in WT mice, compared to RIG-I KO mice, is very interesting. This observation suggests that WT RIG-I mediates a significant selective pressure to the IAV PB2-627E codon, leading to positive selection and further enrichment of PB2-627K copies, which changes the ratio of nt 1879 distribution from a majority of G to a majority of A in dependence of the time p.i. and the RIG-I genotype (c. c. 4.4.5). Additionally, the finding that the rate of back mutations is lower in the PM mice compared to the WT mice and the lowermost in the KO mice, suggests that at least two antiviral effects of RIG-I still mediate a genetic pressure. Remarkably, this experiment shows in direct and detailed observation, how a virus strain acquires an adaptive mutation in dependence of the functionality of a factor of the host immune system *in vivo*. Further, it greatly illustrates the adaptations and counter adaptations, by which virus and host respond to each other.

These results may also explain the significantly increased weight loss in RIG-I WT mice infected with the IAV PB2-627E strain, in comparison to PM and KO mice (c. c. 4.4.1.2). Since the IAV PB2-627K virus showed more efficient replication in mammalian cells and more pathogenicity in mice (c. c. 4.3.2 and 4.4.1.1) and the highest rate of IAV PB2-627E to -627K back mutation was found in RIG-I WT mice, the higher amount of IAV PB2-627K virus in WT mice may result in a worse course of infection. Remarkably, there was also a slight but insignificant difference between the weight loss of RIG-I PM and KO mice, which further supports this explanation. However, a similar finding was not made for the other investigated primary infection parameters virus titer and lung barrier integrity. Nevertheless, the weight loss data sets are larger than the other sets, which enhances the robustness of the analyses and the likeliness to detect significant differences. The amount of samples might be too low in most of the analyses to indicate the potentially small differences due to RIG-I variant expression.

If the fast accumulation of IAV PB2-627E to -627K back mutation depends on few existing copies of the PB2-627K variant, which are not detectable by Sanger-sequencing of the virus stock preparations, or if the error rate of the viral polymerase of 1:2000 to 1:10000 per bp in combination with an infection dose of 8.3×10^4 PFU is sufficient, remains unknown. The most reasonable explanation is that IAV PB2-627K variants are frequently generated during viral replication and are not negatively selected in the DF-1 cells, suggested by the finding that both the IAV PB2-627K and -627E strains replicate similarly in those cells (c. c. 4.3.5). An explanation why the abundance of PB2-627K copies in the IAV PB2-627E stocks remained undetected in the MEF cells may be, that the required relatively high infection dose of 0.5 MOI prevented extensive virus replication, which might have been required to detect an overgrowth of the PB2-627E genotype by -627K (c. c. 4.3.4). Importantly, the findings also show that the artificial alteration of only one nt in the codon triplet to change an aa in viral proteins is a risky method of model generation due to the high mutation rates of RNA viruses.

Overall, the findings among the IAV PB2-E627K back mutations in different experiments are not described the first time. The PB2-E627K mutation is, next to PB2-D701N and PB2-Q591K, one of the most common and most often described mutations in the IAV PB2 RNA gene, which avian-adapted IAV strains acquire to conquer mammalian hosts successfully (Jagger B. W. 2010; Neumann G. 2014; Elshina E. 2021). These PB2 variations have been described as difference between avian- and mammalian-adapted IAV strains occurring in the nature and have been subject of *in vitro* research. Some examples for similar variations in the PB2 RNA gene are shown in Table 40. Additionally, some studies describe lower replication rates of the IAV PB2-627E strain compared to the -627K variant in mammalian cells (Jagger B. W. 2010; Weber M. 2015). A different study shows that the loss of host immune system components can reduce the selective pressure on a virus, leading to an enhanced occurrence of different mutations, which were not detectable before (Pérez-Cidoncha M. 2014) (c. c. 1.2.6.5). With regard to this report, in this study the genetic stability of the IAV PB2-627K virus strain during mouse infection was not validated in detail, since there was no reason originally. A retrospective sequencing of viral RNA from stored BALF samples may be interesting, to validate if the lack of selective pressure in RIG-I PM and RIG-I KO mice, compared to RIG-I WT mice, is sufficient to support the occurrence of IAV PB2-627K codon mutations. Taken together, the descriptions from the literature make the finding of this study plausible and may question the study concept. Nevertheless, the fast adaptation rate despite of unobtrusive screens for genetic stability of the virus strains were hard to foresee and very surprising in regard to the many similar studies which are known, in which such occurrences were not recognized or not reported.

Table 40: Variations between avian- and mammalian-adapted IAV PB2 RNA genes. The amino acid at the left side refers to the variant common in avians and at the right side to the variant common in mammals. Of the many examples found in the literature, only a subset described in multiple publications is shown.

RNA gene	Variation	Source
PB2	D253N	(Wang C. 2016; Elshina E. 2021)
	I292V	(Neumann G. 2014; Elshina E. 2021)
	Q591K	(Neumann G. 2014; Wang C. 2016; Elshina E. 2021)
	E627K	(Jagger B. W. 2010; Neumann G. 2014; Elshina E. 2021)
	D701N	(Jagger B. W. 2010; Neumann G. 2014; Elshina E. 2021)

5.6.2. RIG-I blocks the access to the panhandle structures for the IAV PB2-627E polymerase

It was found that IFN- α and IFN- β are not detectable in the BALF of mice infected with the IAV PB2-627E strain (data not shown). In contrast, RIG-I-mediated IFN- α induction upon infection with an IAV strain lacking the NS1 protein was significant in BmdM Φ from RIG-I WT mice (c. c. 4.2.2.2). Additionally, the majority of the results suggest a low effect of RIG-I on the IL-1 β level, but the expression of this cytokine may be dependent on RIG-I activation at day 4 p.i. in the IAV PB2-627E infections (c. c. 4.4.4). Taken together, these findings suggest a high, but not complete suppression of RIG-I-mediated IFN-1 and IL-1 β induction by activities of the viral NS1 protein (c. c. 4.4.3 and 4.4.4), which is also supported by the literature (Hale B. G. 2014; Ji Z.-X. 2021). Nevertheless, it cannot be excluded that the ELISAs for IFN-1 were not sensitive enough to detect low protein concentrations in the BALF samples. As already discussed in the previous chapter, it was found that IAV PB2-627E (nt 1879 G) significantly adapts to -627K (nt 1879 A) during 10 days of mouse lung infection and that the rate of adaptation is significantly dependent on RIG-I variant expression (also c. c. 4.4.5). Since the rate of IAV PB2 nt 1879 G to A back mutation differs between RIG-I WT, PM and KO mice, it is suggested that some RIG-I antiviral functions remain intact, despite of the potent effect of the NS1 protein in this infection condition. Hence, the difference between RIG-I WT and PM most likely results from a remaining effect by RIG-I-mediated signaling in the WT mice, with the possibility of RIG-I up-regulation via IFN-1 signaling in a positive feedback loop, which is dysfunctional in the RIG-I PM variant (Yoneyama M. 2004; Pothlichet J. 2013). The remaining effect on the IAV PB2 nt 1879 by RIG-I PM is suggested to be mediated via blocking of the viral panhandle structures by RIG-I, which is not possible in the RIG-I KO mice. This conclusion is further supported by the results of the

competitive infection assay, in which a similar effect was observed for the comparison between RIG-I PM and KO MEFs, while the difference between RIG-I WT- and PM-derived cells was not detectable. This experiment showed that the IAV PB2-627K strain replicated stronger than the -627E strain, with the lowest replication advantage in RIG-I KO cells, which are the only ones lacking all of the RIG-I functions (c. c. 4.3.4 and 5.5). Hence, the results of both experiments suggest that RIG-I-mediated blocking of the viral panhandle structures plays indeed a role in the defense of the murine immune system against avian-adapted IAV strains with a PB2-627E polymerase, as similarly shown by Friedemann Weber in cell culture experiments (Weber M. 2015).

Overall, the results suggest an effect of RIG-I signaling on the rate of back mutation, which is comparable to the suggested effect by blocking the viral panhandle structures. In consideration of the repressive effects by the viral PB2 and NS1 proteins on RIG-I-mediated IFN-1 and IL-1 β induction, the full antiviral potential of the first is assumed to be much higher than the effect of the latter. Nevertheless, the RIG-I blocking function may stay unaffected by the viral NS1 protein effects, while the RIG-I signaling functions do not. Hence, despite of its speculated lower antiviral potential, the RIG-I blocking mechanism may have an important basal barrier function against viruses. For this function, the virus needs a different evasion strategy than for the RIG-I signaling functions. At least one part of this evasion strategy is the adaptation of the PB2-627 codon from E to K, supported by this data and in line with the literature, where the PB2-627K mutation is described to enhance the affinity of the polymerase for the viral NP and the panhandle structure. The replacement of RIG-I by the PB2-627K polymerase at this structure leads to weaker RIG-I-induced signaling (Weber M. 2015). Remarkably, the PB2-627K genotype, which the IAV/PR/8 Δ NS1 most likely has (natural genotype, was not validated), was not sufficient to prevent RIG-I-mediated IFN- α induction alone in an *in vivo* infection of murine BmdM Φ (c. c. 4.2.2.2). On the other hand, substitution of PB2-627K with -627E led to a massive drop in the virus replication capability in mammalian cells (c. c. 4.3.2), which is also described in the literature by similar experiments (Jagger B. W. 2010; Weber M. 2015). Also remarkable, a lack of RIG-I is not sufficient to completely counter the observed effects of better replication of IAV PB2-627K compared to -627E, as well as PB2-627E to 627K back mutation (c. c. 4.3.4 and 4.4.5), also consistent with the literature (Weber M. 2015). This suggests that both the IAV evasion strategies PB2-627E to 627K adaptation and NS1 protein expression are important for the virus and both counteract the functions of RIG-I.

Taken together, these findings suggest that RIG-I is an important gatekeeper against avian-adapted IAV strains, forcing them to keep polymerase variants with high error rates to enable reliable avian to mammalian adaptation and host switches. This may reduce replication efficiency of the virus and

extend the time for the host to establish a sufficient immune response. On the other hand, with the ability of fast genetic adaptation and the NS1 protein, the virus has very potent evasion mechanisms against the innate immune system, which enables it to adapt, replicate and infect new hosts.

5.7. The investigation of cytokine expression upon IAV PB2-627K and IAV PB2-627E infection suggests a differential induction of chemokines and IFN- γ depending on RIG-I variant expression

The infection with either 1×10^2 PFU IAV PB2-627K or 8.3×10^4 PFU IAV PB2-627E virus caused a comparable, significant drop in percentage remaining body weight of the infected mice, a significantly enhanced BALF virus titer, a significantly enhanced virus abundance in the lung and significantly enhanced lung damage (primary infection parameters), while PBS-treatment did not cause any comparable effects (c. c. 4.4.1). The infections additionally caused a characteristic induction pattern of inflammatory cytokines, which seemed to correlate with the detectable virus particles, showing highest values at day 4 and 7 p.i., followed by a decrease until day 10 and 14 in most cases (c. c. 4.4.1.4, 4.4.1.5 and 4.4.4).

5.7.1. The infections with the mammalian-adapted IAV PB2-627K strain

The significant changes in the primary infection parameters upon IAV PB2-627K infection were not significantly different in dependence of the RIG-I genotype, but there might be a delayed infiltration of the lung by immune cells in the RIG-I WT mice at day 4 p.i. (c. c. 4.4.1). In regard to IFN-1 signaling, an IFN- α induction was not detectable, while IFN- β was produced during infection. The IFN- β induction was highest in RIG-I WT mice, but the difference was not significant (c. c. 4.4.3). As discussed in the previous chapter, this finding most likely results from a potent suppression of RIG-I signaling by the PB2-627K polymerase variant and the viral NS1 protein. Nevertheless, there are interesting findings concerning proinflammatory cytokine signaling. Importantly, the IL-1 β expression, which is enhanced by RIG-I-IFN-mediated induction of pro-IL-1 β and RIG-I-mediated activation of the inflammasome (c. c. 1.2.3.8) and (Pothlichet J. 2013), did not differ between RIG-I WT, PM and KO mice. This shows that IL-1 β production is not affected by RIG-I in the IAV PB2-627K infections, supporting the suggestion that the IAV PB2-627K polymerase and the NS1 protein hinder the antiviral potential of RIG-I to unfold.

In contrast, the RANTES concentration in RIG-I WT mice was significantly higher than in PM and KO mice. This seems reasonable, since RANTES expression is known to be IFN-1 dependent (Lin R. 1999)

and also suggests that some remaining IFN induction is RIG-I dependent. This finding is in line with higher IFN- β expression in RIG-I WT mice only. Further, the concentrations of MCP-1 and MIP-1 β were slightly and in some comparisons significantly higher in RIG-I WT mice compared to the PM or KO mice. Hence, an effect related to RIG-I-mediated IFN- β induction is possible. RANTES, MCP-1 and MIP-1 β are linked to chemotaxis of immune cells. This suggests that RIG-I signaling enhances chemokine release in the lung during IAV infection, despite of the reduction of its antiviral potential by viral proteins. This is supported by literature reporting that RIG-I affects immune cell migration, dependent on its CARD domains (Mukherjee A. 2009; Li X.-Y. 2014) (c. c. 1.2.3.10). In contrast, a seemingly lower invasion of lung tissue by immune cells was observed in RIG-I WT mice, compared to RIG-I PM and KO mice (c. c. 4.4.1.6). However, this observation was only made at day 4 p.i. in H&E and PAS stained tissue samples, hence the observation should be validated.

5.7.2. The infections with the avian-adapted IAV PB2-627E strain

Upon the infection with the IAV PB2-627E strain, more significant differences in infection parameters were dependent on RIG-I variant expression. Importantly, the PB2-627E genotype was not stable during the course of infection and underwent a back mutation to the original PB2-627K genotype, which is known as a mammalian adaptation (c. c. 5.6.1) (Weber M. 2015). In consideration of the detected replication differences between IAV PB2-627K and -627E strains in mammalian cell lines and mice (c. c. 4.3.2 and 4.4.1.1), the abundance of different rates of IAV PB2-627K virus in the mouse lungs may have influenced the results gained from the IAV PB2-627E infections, as already suggested for the body weight loss in the RIG-I WT mice (c. c. 5.6.1).

Further, the results of the virus semi-quantification in the lung tissue indicated a significantly lower titer in the lungs of RIG-I PM mice compared to the titer in WT and KO mice. This finding surprised most of all, since no reasonable explanation was found based on the study data. One possible explanation might be that the defect of the RIG-I protein in the PM mouse is compensated by the expression of other PRRs, although no hints for a significantly enhanced stimulation of TLR1/2, 9 and cGAS in BmdM Φ were found. However, there was a very slightly higher but insignificant IFN- α and/or IL-6 induction upon TLR1/2 and 9, as well as cGAS/STING stimulation with a respective ligand in the RIG-I PM BmdM Φ , compared to WT and KO cells (c. c. 4.2.2.4 and 4.2.2.5). Specific ligands for other relevant PRRs like NLRP3, TLR3 and TLR8 were not available and the activation of TLR3 with pl:C, which also activates MDA5, as well as activation of TLR7 with RNA40 were not successful in BmdM Φ (data not shown). Nevertheless, the infections of BmdM Φ with the IAV/PR/8 Δ NS1 or Sendai virus should be sufficient to indicate hints for compensatory up-regulations, but no significant differences between the RIG-I signaling-deficient PM and KO mouse line were found (c. c. 4.2.2.2 and 4.2.2.3). In

contrast, the results of the infections with the IAV/PR/8 strain coding for a functional NS1 protein indicated a significant difference between the PM and KO cells, but the measured IFN- α levels were not significantly dependent on the applied virus dose, unlike in the other infection experiments. This observation leads to the conclusion that the detected significant effect mediated by the RIG-I genotype is based on a different mean background noise and not on a difference in signaling (c. c. 4.2.2.2). Nevertheless, it is still possible that a difference was not detectable in BmdM Φ , while the investigation of other cell types would have indicated a significant difference. However, it seems questionable that a compensation exists in RIG-I PM mice with deficient RIG-I signaling, but not in RIG-I KO mice with complete loss of this protein. The PB2-627E to 627K back mutation also seems to be no reasonable explanation for the low presence of virus in the RIG-I PM mice at day 7 and 10 p.i., because the rate of back mutation seems not to correlate with the patterns of the virus titers and cytokines, if the whole data is compared (c. c. 4.4.1.4, 4.4.1.5 and 4.4.4). Finally, there is also the possibility of an infection artifact, since the application of virus inoculum during short-time narcosis with isoflurane turned out to be error prone. The mice frequently sneezed out a portion of the inoculum, which not always could be prevented successfully. Despite mice showing no symptoms during infection and/ or had an uncharacteristic low BALF virus titer were replaced, some might have been infected with a lower amount of virus than others. In conclusion, it is likely that the number of four mice per group was too low to average out effects due to infection artifacts. To achieve a more accurate infection, a tracheal tube can be used, but this is linked to higher animal burden and requires enhanced skills with narcosis and handling. Since this study was planned as an overview study with the intention to create a follow-up study with higher mouse numbers to draw statistically relevant conclusions, this outcome was a calculated risk from the beginning.

In regard to IFN-1, neither IFN- α nor IFN- β was detectable in the BALF of IAV PB2-627E infected mice (data not shown). This suggests that similar as in the IAV PB2-627K infected mice, RIG-I-mediated signaling is suppressed to its majority by the activity of the NS1 protein. Nevertheless, the complete lack of IFN- α and β expression comes by surprise, since it was expected that the diminished binding of the IAV PB2-627E polymerase enables a high activity of RIG-I-induced by the enhanced binding to the viral panhandle structures. This suggests an even higher IFN-suppressing effect of the NS1 protein than the results from the IAV PB2-627K infections suggest, but it is also possible that the higher infection titer including a much higher initial dose of NS1 protein, combined with the presence of a few copies of the IAV PB2-627K polymerase variant, cause this difference.

The cytokine IL-1 β was detectable in RIG-I WT mice but not in the PM and KO mice at day 4 p.i. In contrast, the concentration did not differ between the mouse lines at the other time points. This

suggests that RIG-I affects IL-1 β production only at early stages of the infection, but since the amount of data is low, it needs to be validated (c. c. 4.4.4). This could be done with detailed *in vitro* experiments and/or an enhanced amount of early time points and more individuals *in vivo*. A similar observation was made for the IFN- γ concentration, which differed significantly between RIG-I WT and KO mice at day 7 p.i. Nevertheless, this observation is very interesting and will be discussed separately in the following section.

5.7.3. IFN- γ may be alternatively induced by a RIG-I dependent positive feedback loop

The finding that the IFN- γ concentration seems to differ significantly between RIG-I WT and KO mice at day 7 p.i. in the IAV PB2-627E infections, while the concentration is very low at the other days, is very interesting. Additionally, there is a non-significant, but similar tendency in the IAV PB2-627K infections. Hence, a hypothesis is suggested (c. c. 4.4.4). The maturation of the precursor pro-IL-18 is dependent on activation of the mammalian inflammasome by NLRP proteins. Additionally, after cleavage, the mature proinflammatory cytokine IL-18 is known to be an inducer of IFN- γ (Gu Y. 1997). Since RIG-I can activate the mammalian inflammasome like members of the NLRP family (Weber M. 2015), it is suggested that RIG-I may contribute to the induction of IFN- γ and may also support prolonged production of this cytokine via a positive feedback loop, since RIG-I regulation in turn is dependent on IFN- γ (Imaizumi T. 2009). Additionally, induction of IFN- γ by IL-12 may also be dependent on RIG-I, since IL-12 is induced upon PRR activation in different immune cells like APCs and neutrophilic granulocytes (Car B. D. 1995; Komatsu T. 1998). Since there is no known literature fully describing this signaling pathway, a detailed investigation might be interesting in a separate study. Since IFN- γ contributes to first line viral responses, unspecific cellular responses (e.g. via NK cells), as well as to the initialization of an adaptive immune response, a good understanding of this signaling network might help in molecular medicine to identify new pharmaceutical targets and to predict and understand therapeutic side effects (Almatrouk S. 2021).

5.8. RIG-I as pharmaceutical target

Different studies suggest to use RIG-I agonists as potential adjuvant candidates for vaccination (Kulkarni R. R. 2014; Ziegler A. 2017). Remarkably, while RIG-I is less often discussed as pharmaceutical target in infectious diseases, there are studies suggesting it as a drug target in cancer therapy, since RIG-I has tumor-suppressive functions (Li X.-Y. 2014; Wu Y. 2017).

As a pharmaceutical target for flu therapy, the study results do not suggest RIG-I as the first option. Direct activation with an agonist during IAV infection may not have a sufficient effect due to the potency of the NS1 protein to inhibit RIG-I-mediated IFN-1 and IL-1 β induction, especially in established infections. Further, IFN-1s are important for the initialization of an immune response, long before symptoms manifest. Nevertheless, a preventive use might be interesting to protect risk groups, but also increase the likeliness to develop a chronic inflammation (Keeler S. P. 2018). On the other hand, the drug Paliperidone, an FDA-approved drug against schizophrenia, has been shown recently to disrupt the binding of the IAV PB2 subunit to the viral NP. Hence, the potential of the IAV/PR/8/1934 polymerase to compete with RIG-I for the access to the panhandle structures is reduced, which should lead to enhanced activation of innate immune signaling by RIG-I (Panagiotidis G. D. 2023). The application of a NS1 antagonist may also be promising, since the results of this study suggest a very high potency of the RIG-I inhibition by this viral protein. Additionally, NS1 seems a very good target due to its manifold effects to inhibit the immune system of the host organism. On the other hand, IAV strains potentially evade such an inhibitor by mutations and establish resistances very fast (Hale B. G. 2014; Weber-Gerlach M. 2016b; Ji Z.-X. 2021). Concerning vaccination, RIG-I agonists seem to be a reasonable target in adjuvant research, since the potent inhibition by the NS1 protein highlights the potency of RIG-I to enhance an innate immune response by inducing IFN-1 and IL-1 β production. Therefore, the recent discovery and detailed description of a natural RIG-I ligand may be of special interest (c. c. 1.2.5.3) (Ziegler A. 2017; Jung S. 2020).

5.9. Conclusion

The mouse study was originally designed to validate the impact of the different RIG-I-mediated antiviral effects: induction of IFN- α and IL-1 β production and block of the viral panhandle structures for the access by the viral polymerase. The intention was to investigate differences in the major infection parameters body weight loss, virus titer and lung barrier integrity, as well as differences in IFN-1 expression and inflammatory cytokine induction, depending on RIG-I variant expression. By this, it was aimed to draw conclusions on the different RIG-I functions. Most of the parameters chosen to validate effects of the virus infections were suitable for this purpose. The results indicated some slight differences in IFN- β induction and chemotaxis in the IAV PB2-627K infections and a difference in body weight loss and cytokine induction were detectable in the IAV PB2-627E infections, dependent on RIG-I variant expression. Interestingly, these findings open the hypothesis that RIG-I activation enhances IFN- γ production in a positive feedback loop, which should be further investigated. Additionally, the results suggest a high repression of RIG-I-induced IFN- α and IL-1 β production by the IAV/PR/8 NS1 and PB2 variant 627K proteins during mouse lung infection. Most

importantly, the validation of the genetic stability of the IAV PB2-627E strain during mouse infection shows, that RIG-I is a factor of the innate immune system that mediates a genetic pressure on the PB2-627 codon, leading to an adaptation from the avian-adapted PB2-627E variant to the mammalian-adapted PB2-627K variant. Further, these results confirm that the RIG-I blocking function, so far only described *in vitro*, also plays a role *in vivo*. The repression of the RIG-I signaling by the viral NS1 and PB2 variant 627K proteins prevents to distinguish between RIG-I IFN and IL-1 β signaling-mediated effects in this study concept and the PB2-627E to 627K back mutation limits the meaningfulness of the data derived from the IAV PB2-627E infections. Nevertheless, the most important drawback of this study is, that the virus titers, as well as inflammatory cytokines, were significantly reduced in the RIG-I PM mice infected with the IAV PB2-627E strain, compared to the WT and KO mice. No explanation for this observation was found in this study, hence larger animal groups, a refined infection procedure and additional experiments are required to validate this data.

5.10. Outlook

Looking at the complete study data, several factors limited the outcome of this study. Hence, for further experiments and studies, different changes and investigations should be considered. For an improved validation of viral stock preparation and the genetic stability, more sensitive sequencing methods like pyro sequencing should be used. To increase the probability of a successful IAV lung infection of mice *in vivo*, application of the inoculum should be performed using tracheal tubes. This may also make the investigation of infection parameters at earlier time points p.i. reasonable, since no validation of successful infection via confirmation of characteristic symptoms would be essential. This would especially be interesting for the study of early responses of the innate immune system. Further, the chosen IAV strains were not the best candidates for the model concept due to high RIG-I inhibition by the viral NS1 protein, the IAV PB2-627K polymerase and fast adaptations of the artificially generated PB2-627E polymerase genotype. Additionally, the lack of the MX1 protein as a potent IFN-stimulated gene in the C57BL/6J based mouse lines is not optimal for the investigation of RIG-I-mediated effects. These factors limit the study concept the most and should be adapted in following studies. For a more detailed and accurate mouse study, for which the actual study was designed to be a basic, the amount of time points can be reduced without the risk of missing important results. The number of individuals per time point should be enhanced, to increase the robustness of the data sets and to increase the probability of statistical analyses to identify significant differences correctly. Furthermore, it may be of interest to investigate differences between female and male mice, which may confirm other studies that are partially controversial

(Vermillion M. S. 2018; Celestino I. 2018; Sabikunnahar B. 2022). The difference between female and male individuals could not be validated in this study due to an insufficient amount of individuals.

The primary aim to validate and compare the antiviral potency of the innate PRR RIG-I was not completely fulfilled, especially in regard to the IFN-1 and IL-1 β signaling potential. Hence, further studies should be planned based on the insights gained in this project. In an *in vitro* analysis, IL-1 β induction upon RIG-I activation should be investigated dependent on RIG-I variant expression. The Sendai virus infection used in RIG-I variant characterization caused induction of IFN- α and IL-6 production, significantly dependent on functional RIG-I. This suggests that this virus could be a good model for studying different RIG-I effects without the counteracting effects of viral proteins. It may also be sufficient to use different IAV strains with less efficient RIG-I evasion mechanisms, as suggested for the IAV/Scotland/20/74 (H3N2) strain, which is described to enhance IFN production efficiently (Pothlichet J. 2008).

Of high interest is the investigation of the hypothesized connection between RIG-I, the inflammasome, IL-18 and IFN- γ . This pathway is not described in detail yet and seems to be important due to connecting key factors of the innate immune system, even reaching out to the initialization of the adaptive immune response. To deepen the understanding of the interactions and connections between the well-described blocks of the innate and adaptive immune systems, a respective study should be planned.

In regard to the slight alterations in chemotaxis, which were found to be dependent on RIG-I variant expression in this study, it might be interesting to look for differences in immune cell invasion to the lung in more detail. Therefore, the invading immune cells could be characterized by IHC with markers like CD4, CD8 and CD20 to analyze differences between the mouse lines, in stored fixated lung tissue samples. The analysis should also get extended by *in vitro* experiments to clarify the inconsistencies found in this study in regard to immune cell migration in the lung (c. c. 5.7.1) and to address observations from the literature concerning potential influences of RIG-I on immune cell migration, phagocytosis, myeloid cells and cancer development (Zhang N.-N. 2008; Li X.-Y. 2014) (c. c. 1.2.3.10). Especially the influence of RIG-I on immune cell migration seems plausible, but not well described by the existing literature (Mukherjee A. 2009; Kandasamy M. 2016).

6. Summary

Influenza A virus infections are common all over the world and cause substantial damage on health and economy by seasonal outbreaks. The infectious disease flu becomes even more life threatening when followed by a secondary bacterial infection, for which especially children and immune-suppressed people are susceptible. Today, the annually adapted influenza vaccination is an important tool to prevent outbreaks of flu. Medical treatments of acute infections are limited with the exceptions of therapeutically targeting the viral proteins neuraminidase and M2. A deeper understanding of the molecular mechanisms of the IAV pathogenicity and antiviral defense mechanisms, as well as their interaction, can help to refine vaccination strategies and direct therapeutic options to generate more target specific and effective antiviral drugs. The pattern recognition receptor RIG-I is one of the most important sensors of the innate immune system to detect foreign RNAs. Upon the binding of RNA ligands like the panhandle structures of influenza A virus, RIG-I amongst others mediates the expression of interferon type 1 and interleukin-1 β in an ATPase dependent manner. Additionally, the binding of RIG-I to the viral panhandle structures is confirmed *in vitro* as another antiviral function by blocking the access for the viral polymerase, as firstly described by Friedemann Weber in the year 2015.

The main aim of this thesis was to investigate the contribution of the different antiviral effects of RIG-I against the influenza A virus in a mouse infection model. Furthermore, additional insights about the RIG-I blocking function should be gained. Therefore, a mouse line deficient in RIG-I signaling and another one lacking RIG-I expression were established with the help of genetic engineering. Additionally, two recombinant influenza strains harboring an adaptation in the viral polymerase gene either to mammalian hosts or to avian hosts (polymerase subunit 2 codon 627K and 627E) were generated. Both virus strains were validated for different quality features. The recombinant virus strains were used to perform an infection study using RIG-I wild type, signaling-deficient and knockout mice. Investigating the effect of RIG-I variant expression on parameters like weight reduction, lung virus titer, loss of lung barrier integrity, interferon and cytokine concentration in response to the influenza A infection, new insights in the antiviral functions of RIG-I were gained.

The established mouse lines expressing signaling-deficient or no RIG-I did not develop any detectable burden by their genotype. The RIG-I-mediated interferon- α induction was found to be abolished in bone marrow derived macrophages of mice with signaling deficiency in RIG-I as well as RIG-I knockout mice while it was intact in RIG-I wild type mouse derived cells, as expected. Hence, an unburdened mouse line with RIG-I signaling deficiency and one with a RIG-I knockout were generated. The RIG-I PM line is the first of its kind. While the generation of a mammalian-adapted

recombinant influenza A strain was successful from the beginning, the generation of the avian-adapted strain was not successful in mammalian cells. A sufficient replication of both strains was achieved in the DF-1 chicken cell line. The received stock preparations showed similar abilities and the stability of their respective genotype was confirmed over several passages in different cell lines. While the infection of mice with the generated recombinant influenza A strains led to a significant change in observed infection parameters and cytokine signaling, only a weak effect of RIG-I variant expression on the infection parameters was detectable. Additionally, the results deliver hints for a RIG-I dependent induction of IFN- γ by RIG-I, which was not described in detail yet. The data also suggest that the antiviral functions of RIG-I may be potentially inhibited by the viral nonstructural protein 1 and the mammalian-adapted polymerase variant. The validation of the genetic stability of the virus strain with the avian-adapted polymerase variant *in vivo* indicates a significant back mutation to the original mammalian-adapted genotype over the course of the infection. This was significantly affected by the time post infection and the type of RIG-I variant expression. A lower rate of back mutation than in RIG-I wild type mice was detected in mice with RIG-I signaling deficiency and the lowest in mice with RIG-I knockout. These findings suggest that both the RIG-I signaling functions and the RIG-I blocking function mediate a selective pressure on the influenza A polymerase subunit 2 codon 627. This conclusion is supported by the results of an *in vitro* competitive infection assay with both virus variants together, showing a replication advantage of the mammalian-adapted polymerase variant over the avian-adapted variant that is affected by the type of RIG-I expression.

Taken together, the results of this study deliver deep insights into the interaction between the innate pattern recognition receptor RIG-I and the influenza A virus. The findings suggest that the presence of RIG-I forces viral polymerase variants common in avian to adapt to a mammalian host. Further, the study delivers additional data confirming a RIG-I-mediated antiviral effect by blocking the access of the viral polymerase to the panhandle structures of viral RNAs. Additionally, the data suggests a high potency of the nonstructural protein 1 and the mammalian-adapted polymerase subunit 2 codon 627K to prevent the effects of RIG-I. The finding that RIG-I may contribute to interferon- γ release could be interesting and should be investigated in future studies, since this interaction is poorly described in the literature, but connects two important features of the innate immune system.

Key words: Influenza A, RIG-I, Virus-host interaction, RIG-I KO mouse, RIG-I K271A mouse, PB2-627K, PB2-627E, virus adaptation, mouse infection, innate immune system, cytokines

7. Zusammenfassung

Das Influenza A Virus ist über die gesamte Welt verbreitet und hat jährlich einen beträchtlichen negativen Einfluss auf die Gesundheit der Bevölkerung und die Wirtschaft. Die sogenannte Grippe, eine Infektionskrankheit, ist vor allem gefährlich, wenn sie mit Sekundärerkrankungen einhergeht. Diese können vor allem für Kinder und immungeschwächte Menschen lebensbedrohlich werden. Durch die jährlich angepasste Gripeschutzimpfung existiert heutzutage eine effektive Präventionsstrategie. Ein wichtiger so genannter *pattern recognition receptor* des angeborenen Immunsystems ist RIG-I. Nach dem Binden an einen seiner Liganden, zum Beispiel die *Panhandle* Struktur der RNAs des Influenza A Virus, kann RIG-I sowohl die Expression der Typ 1 Interferone als auch von Interleukin-1 β induzieren. Außerdem stellt das Binden von RIG-I an die *Panhandle* Struktur der RNA einen kompetitiven Hemmmechanismus für die virale Polymerase dar, da die Bindung blockiert und Transkription und Translation der viralen RNAs negativ beeinträchtigt werden. Ein solcher Effekt wurde erstmals von Friedemann Weber im Jahr 2015 in *in vitro* Versuchen nachgewiesen.

Das Ziel dieser Studie war herauszufinden, in welchem Maße die einzelnen Funktionen des RIG-I *in vivo* zu seinem antiviralen Gesamtpotenzial beitragen. Außerdem sollten weitere Erkenntnisse über den blockierenden Effekt des RIG-I gewonnen werden. Dafür war geplant, eine Mauslinie mit einer *Signaling*-inkompetenten RIG-I Variante und eine weitere mit einem RIG-I *knockout* zu generieren. Für die Infektionen sollten zwei rekombinante Influenzastämme erzeugt werden, von denen der Erste eine genetische Anpassung an einen Säugerwirt und der Zweite eine Anpassung an einen Vogelwirt besitzt (Polymerase Untereinheit 2 Codon 627K und 627E). Im Anschluss sollten die Viren verwendet werden, um eine Influenzainfektion in Mäusen der etablierten Linien zu induzieren. Durch die Untersuchung des Effektes der Expression der RIG-I-Varianten auf Parameter wie Gewichtsverlust, Virustiter in der Lunge, Abnahme der Barriereintegrität des Lungenepithels und die veränderte Expression der Interferone und verschiedener Zytokine in Folge der Influenza A Infektionen sollten neue Einblicke in die antivirale Wirkungsweise von RIG-I gewonnen werden.

Die Ergebnisse zeigten, dass die RIG-I-spezifische Stimulation von *in vitro* differenzierten Makrophagen aus Wildtyp RIG-I Mäusen eine starke Induktion von Interferon- α nach sich zieht, was bei den genetisch veränderten Mäusen nicht der Fall ist. Dies zeigt, dass im Rahmen dieses Projektes eine funktionale und unbelastete Mauslinie mit *Signaling*-defizientem RIG-I oder RIG-I *knockout* erfolgreich etabliert werden konnte. Während es gelang, einen rekombinanten Influenza A Stamm mit einer säugeradaptierten Polymerase-Variante zu erzeugen, war die Erzeugung einer an einen Vogelwirt angepassten Variante in Säugetierzellen nicht möglich. Jedoch konnte eine erfolgreiche

Vermehrung beider Stämme in der DF-1 Hühnerzelllinie erreicht werden. Dabei zeigten beide Stämme vergleichbare Qualitätsmerkmale und waren im Hinblick auf die spezifisch eingefügten genetischen Veränderungen über mehrere Passagen in verschiedenen Zelllinien stabil. Die Infektion von Mäusen der verschiedenen Linien mit den generierten Influenzastämmen führte zu einer signifikanten Veränderung verschiedener Parameter, die zum Nachweis der Infektion untersucht wurden. Weiterhin zeigten sich Veränderungen im *Signaling* des angeborenen Immunsystems. Jedoch zeigte sich auch, dass die Expression der verschiedenen RIG-I Varianten eine sehr geringe Auswirkung auf die beobachteten Effekte hat. Auf der anderen Seite liefern die gewonnenen Daten einen Hinweis für eine noch nicht genauer beschriebene Interaktion zwischen RIG-I und dem Interferon- γ Signalweg. Weiterhin legen die Ergebnisse nahe, dass die antiviralen Funktionen des RIG-I sehr stark durch das virale *Nonstructural protein 1* und die an Säuger angepasste Variante der Polymerase unterdrückt werden. Die Überprüfung der genetischen Stabilität des vogeladaptierten Influenzastammes zeigte, dass eine starke Rückmutation zur originalen Säugeradaption über den Zeitraum der Infektion der Mäuse stattfindet. Dabei ist die Rate der Rückmutation signifikant vom Zeitpunkt nach der Infektion und tendenziell von der Expression der jeweiligen RIG-I Variante abhängig. Diese Daten lassen den Schluss zu, dass sowohl das RIG-I vermittelte *Signaling* als auch seine blockierende Funktion einen selektiven Druck auf das Codon 627 der Influenza A Polymerase Untereinheit 2 ausüben. Diese Schlussfolgerung wird zusätzlich durch die Ergebnisse eines *in vitro* durchgeführten kompetitiven Infektionsexperimentes gestützt. Hierbei zeigt sich bei der gleichzeitigen Infektion mit beiden Virusvarianten ebenfalls ein RIG-I abhängiger Replikationsvorteil des Virusstammes mit der Säugeradaption.

Zusammenfassend liefern die Ergebnisse dieser Studie tiefe Einblicke in die komplexe Interaktion zwischen RIG-I und dem Influenza A Virus. Die Daten zeigen, dass die Präsenz dieses Rezeptors des angeborenen Immunsystems die Adaption der an aviäre Systeme angepassten Polymerase-Varianten in infizierten Säugerwirten erzwingt. Außerdem liefert die Studie wichtige Daten, die den antiviral wirkenden, blockierenden Effekt des RIG-I bestätigen, sowie zahlreiche Hinweise darauf, dass zumindest die verwendeten PR/8 Influenzastämme mit dem *Nonstructural protein 1* und einer säugerangepassten Variante der Polymerase über zwei sehr potente Mechanismen verfügen, um die Funktionen des RIG-I zu blockieren. Den Hinweisen darauf, dass RIG-I den Interferon- γ Signalweg aktiviert, könnte in einer zukünftigen Studie nachgegangen werden. Diese Interaktion ist in der Literatur nicht detailliert beschrieben, sollte aber von großem Interesse sein, da sie eine Verbindung zwischen zwei wichtigen Komponenten des angeborenen Immunsystems darstellt.

Schlüsselwörter: Influenza A, RIG-I, Virus-Wirt Interaktion, RIG-I KO Maus, RIG-I K271A Maus

8. List of citations

- Akira S., Uematsu S., Takeuchi O. 2006. "Pathogen Recognition and Innate Immunity." *Cell*. doi: 10.1016/j.cell.2006.02.015.
- Almatrouk S., Saba I., Abozaid S., Al-Qahtani A. A., Al-Ahdal M. N. 2021. "Virus sensing receptors in cellular infectivity of influenza A virus." *J Infect Dev Ctries* 15 (1):1-8. doi: 10.3855/jidc.13258.
- Bankhead P., Loughrey M. B., Fernandez J. A., Dombrowski Y., McArd D. G., Dunne P. D., McQuaid S., Gray R. T., Murray L. J., Coleman H., G., James J. A., Salto-Tellez M., Hamilton P. W. 2017. "QuPath: Open source software for digital pathology image analysis." *Sci Rep* 7 (1). doi: 10.1038/s41598-017-17204-5.
- Barber M. R. W., Aldridge J. R., Webster R. G., Magor K. E. 2010. "Association of RIG-I with innate immunity of ducks to influenza." *PNAS*. doi: 10.1073/pnas.1001755107.
- Car B. D., Eng V. M., Schnyder B., LeHir M., Shakhov A. N., Woerly G., Huang S., Aguet M., Anderson T. D., Ryffel B. 1995. "Role of Interferon- γ in Interleukin 12-Induced Pathology in Mice." *American Journal of Pathology* 147 (6):1693-707. doi: PMC1869961.
- Celestino I., Checconi P., Amatore D., de Angelis M., Coluccio P., Dattilo R., Alunni Fegatelli D., Clemente A. M., Matarrese P., Torcia M. G., Mancinelli R., Mammola C. L., Garaci E., Vestri A. R., Malorni W., Palamara A. T., Nencioni L. 2018. "Differential Redox State Contributes to Sex Disparities in the Response to Influenza Virus Infection in Male and Female Mice." *Front Immunol* 9:1747. doi: 10.3389/fimmu.2018.01747.
- Chanock R. H., Cockburn W. C., Davenport F. M., Dowdle W. R., Fazekas de St. Groth S., Fukumi H., Kilbourne E. D., Schild G. C., Schulman J. L., Sohler R., Soloviev V. D., Tumova B., Webster R. G., Zakstel L. J., Zdanov V. M. 1972 "A Revised System of Influenza Virus Nomenclature." *Virology* 47:854-6. doi: 10.1016/0042-6822(72)90580-6.
- Chitrakar A., Rath S., Donovan J., Demarest K., Li Y., Sridhar R. R., Weiss S. R., Kotenko S. V., Wingreen N. S., Korennykh A. . 2018. "Real-time 2-5A kinetics suggest that interferons β and λ evade global arrest of translation by RNase L." doi: 10.1073/pnas.1818363116.
- Cooper D. A., Banerjee S., Chakrabarti A., Garcia-Sastre A., Hesselberth J. R., Silverman R. H., Barton D. J. 2015. "RNase L Targets Distinct Sites in Influenza A Virus RNAs." *Journal of Virology*. doi: 10.1128/JVI.02953-14.
- Czudai-Matwich V., Schnare M., Pinkenburg O. 2013. "A simple and fast system for cloning influenza A virus gene segments into pHW2000- and pCAGGS-based vectors." *Springer*. doi: 10.1007/s00705-013-1697-4.
- Devarkar S. C., Wang C., Miller M. T., Ramanathan A., Jiang F., Khan A. G., Patel S. S., Marcotrigiano J. 2016. "Structural basis for m7G recognition and 2'-O-methyl discrimination in capped RNAs by the innate immune receptor RIG-I." *PNAS* 113 (3):596-601. doi: 10.1073/pnas.1515152113.
- Dietert K., Gutbier B., Wienhold S. M., Reppe K., Jiang X., Yao L., Chaput C., Naujoks J., Brack M., Kupke A., Peteranderl C., Becker S., von Lachner C., Baal N., Slevogt H., Hocke A. C., Witzernath M., Opitz B., Herold S., Hackstein H., Sander L. E., Suttrop N., Gruber A. D. 2017. "Spectrum of pathogen- and model-specific histopathologies in mouse models of acute pneumonia." *Plos one*. doi: 10.1371/journal

- Dinareello C. A. 2018. "Overview of the IL-1 family in innate inflammation and acquired immunity. ." *Immunol. Rev.* doi: 10.1111/imr.12621.
- Dou D., Revol R., Östbye H., Wang H., Daniels R. 2018. "Influenza A Virus Cell Entry, Replication, Virion Assembly and Movement." *Frontiers in Immunology.* doi: 10.3389/fimmu.2018.01581.
- Eiz-Vesper B., Schmetzer H. M. 2020. "Antigen-Presenting Cells: Potential of Proven and New Players in Immune Therapies." *Transfusion Medicine and Hemotherapy.* doi: 10.1159/000512729.
- Elshina E., Te Velthuis A. J. W. 2021. "The influenza virus RNA polymerase as an innate immune agonist and antagonist." *Cell Mol Life Sci* 78 (23):7237-56. doi: 10.1007/s00018-021-03957-w.
- Faul F., Erdfelder E., Lang A.-G., Buchner A. 2007. "G*Power 3: A flexible statistical power analysis program for the social, behavioral, and biomedical sciences." *Behavioral Research Methods* 39 (2):175-91. doi: 10.3758/bf03193146.
- Frank K., Paust S. 2020. "Dynamic Natural Killer Cell and T Cell Responses to Influenza Infection." *Frontiers in Cellular and Infection Microbiology.* doi: 10.3389/fcimb.2020.00425.
- Gack M. U., Shin Y. C., Joo C.-H., Urano T., Liang C., Sun L., Takeuchi O., Akira S., Chen Z., Inoue S., Jung J. U. 2007. "TRIM25 RING-finger E3 ubiquitin ligase is essential for RIG-I-mediated antiviral activity." *Nature Letters.* doi: 10.1038/nature05732.
- Graham A. 2021. "Naturalizing mouse models for immunology." *Nature Immunology.* doi: 10.1038/s41590-020-00857-2.
- Grimm D., Staeheli P., Hufbauer M., Koerner I., Martinez-Sobrido L., Solorzano A., Garcia-Sastre A., Haller O., Kochs G. 2007. "Replication fitness determines high virulence of influenza A virus in mice carrying functional Mx1 resistance gene." *Proc Natl Acad Sci U S A* 104 (16):6806-11. doi: 10.1073/pnas.0701849104.
- Gu Y., Kuida K., Tsutsui H., Ku G., Hsiao K., Fleming M. A., Hayashi N., Higashino K., Okamura H., Nakanishi K., Kurimoto M., Tanimoto T., Flavell R. A., Sato V., Harding M. W., Livingston D. J., Su M. S.-S. 1997. "Activation of Interferon- γ Inducing Factor Mediated by Interleukin-1 β Converting Enzyme." *Science* 275 (5297):206-9. doi: 10.1126/science.275.5297.206.
- Hale B. G. 2014. "Conformational plasticity of the influenza A virus NS1 protein." *Journal of General Virology.* doi: 10.1099/vir.0.066282-0.
- Hoffmann E., Krauss S., Perez D., Webby R., Webster R. G. 2002. "Eight-plasmid system for rapid generation of influenza virus vaccines." *Vaccine* 20 (25-26):3165-70. doi: 10.1016/s0264-410x(02)00268-2.
- Hoffmann E., Neumann G., Kawaoka Y., Hobom G., Webster R. G. 2000. "A DNA transfection system for generation of influenza A virus from eight plasmids." *PNAS.* doi: 10.1073/pnas.100133697.
- Hoffmann E., Stech J., Guan Y., Webster R. G., Perez D. R. 2001. "Universal primer set for the full-length amplification of all influenza A viruses." *Archives of Virology* 2001 (146):2275-89. doi: 10.1007/s007050170002.

- Imaizumi T., Tanaka H., Tajima A., Tsuruga K., Oki E., Sashinami H., Matsumiya T., Yoshida H., Inoue I., Ito E. 2009. "Retinoic acid-inducible gene-I (RIG-I) is induced by IFN- γ in human mesangial cells in culture: possible involvement of RIG-I in the inflammation in lupus nephritis. ." *Lupus* 2010 (19):830-6. doi: 10.1177/0961203309360540.
- Jagger B. W., Memoli M. J., Sheng Z. M., Qi L., Hrabal R. J., Allen G. L., Dugan V. G., Wang R., Digard P., Kash J. C., Taubenberger J. K. 2010. "The PB2-E627K mutation attenuates viruses containing the 2009 H1N1 influenza pandemic polymerase." *mBio* 1 (1):1-15. doi: 10.1128/mBio.00067-10.
- Ji Z.-X., Wang X.-Q., Liu, X.-F. 2021. "NS1: A Key Protein in the "Game" Between Influenza A Virus and Host in Innate Immunity." *Front Cell Infect Microbiol* 11:670177. doi: 10.3389/fcimb.2021.670177.
- Jung S., von Thülen T., Yang I., Laukemper V., Rupf B., Janga H., Panagiotidis G.-D., Schoen A., Nicolai M., Schulte L., Obermann H.-L., Weber F., Kaufmann A., Bauer S. 2020. "A ribosomal RNA fragment with 2',3'-cyclic phosphate and GTP-binding activity acts as RIG-I ligand." *Nucleic Acids Research*. doi: 10.1093/nar/gkaa739.
- Kandasamy M., Suryawanshi A., Tundup S., Perez J. T., Schmolke M., Manicassamy S., Manicassamy B. 2016. "RIG-I Signaling Is Critical for Efficient Polyfunctional T Cell Responses during Influenza Virus Infection." *PLoS Pathog* 12 (7):e1005754. doi: 10.1371/journal.ppat.1005754.
- Kato H., Sato S., Yoneyama M., Yamamoto M., Uematsu S., Matsui K., Tsujimura T., Takeda K., Fujita T., Takeuchi O., Akira S. 2005. "Cell type-specific involvement of RIG-I in antiviral response." *Immunity* 23 (1):19-28. doi: 10.1016/j.immuni.2005.04.010.
- Keeler S. P., Agapov E. V., Hinojosa M. E., Letvin A. N., Wu K., Holtzman M. J. 2018. "Influenza A Virus Infection Causes Chronic Lung Disease Linked to Sites of Active Viral RNA Remnants." *J Immunol* 201 (8):2354-68. doi: 10.4049/jimmunol.1800671.
- Kilbourne E. D. 2006. "Influenza Pandemics of the 20th Century." *Emerging Infectious Diseases* 12 (1):9-14. doi: 10.3201/eid1201.051254.
- Kolakofsky D., Kowalinski E., Cusack S. 2012. "A structure-based model of RIG-I activation." *RNA*. doi: 10.1261/rna.035949.112.
- Komatsu T., Ireland D. D. C., Reiss C. S. 1998. "IL-12 and Viral Infections." *Cytokine and Growth Factor Reviews* 9 (3/4):277-85. doi: 10.1016/S1359-6101(98)00017-3.
- Kontaxi C., Piccardo P., Gill A. C. 2017. "Lysine-Directed Post-translational Modifications of Tau Protein in Alzheimer's Disease and Related Tauopathies." *Front Mol Biosci* 4:1-14. doi: 10.3389/fmolb.2017.00056.
- Kopitar-Jerala N. 2017. "The Role of Interferons in Inflammation and Inflammasome Activation." *Front Immunol* 8:873. doi: 10.3389/fimmu.2017.00873.
- Kulkarni R. R., Rasheed M. A., Bhaumik S. K., Ranjan P., Cao W., Davis C., Marisetti K., Thomas S., Gangappa S., Sambhara S., Murali-Krishna K. 2014. "Activation of the RIG-I pathway during influenza vaccination enhances the germinal center reaction, promotes T follicular helper cell induction, and provides a dose-sparing effect and protective immunity." *J Virol* 88 (24):13990-4001. doi: 10.1128/JVI.02273-14.

- Li X.-Y., Guo H.-Z., Zhu J. 2014. "Tumor suppressor activity of RIG-I." *Molecular and Cellular Oncology*. doi: 10.4161/23723548.2014.968016.
- Lin R., Heylbroeck C., Genin P., Pitha P. M., Hiscott J. 1999. "Essential Role of Interferon Regulatory Factor 3 in Direct Activation of RANTES Chemokine Transcription." *Molecular and Cellular Biology* 19 (2):959-66. doi: 10.1128/MCB.19.2.959.
- Long J. S., Giotis E. S., Moncorgé O., Frise R., Mistry B., James J., Morisson M., Iqbal M., Vignal A., Skinner M. A., Barclay W. S. 2016. "Species difference in ANP32A underlies influenza A virus polymerase host restriction." *Nature Letters*. doi: 10.1038/nature16474.
- Lu J., Duan X., Zhao W., Wang J., Wang H., Zhou K., Fang M. 2018. "Aged Mice are More Resistant to Influenza Virus Infection due to Reduced Inflammation and Lung Pathology." *Aging Dis* 9 (3):358-73. doi: 10.14336/AD.2017.0701.
- Malathi K., Dong B., Gale M., Silverman R. H. 2007. "Small self-RNA generated by RNase L amplifies antiviral innate immunity." *Nature Letters*. doi: 10.1038/nature06042.
- Malik G., Zhou Y. 2020. "Innate Immune Sensing of Influenza A Virus." *Viruses* 12 (7). doi: 10.3390/v12070755.
- Min J.-Y., Krug R. M. 2006. "The primary function of RNA binding by the influenza A virus NS1 protein in infected cells: Inhibiting the 2'-5' oligo (A) synthetase/RNase L pathway." *PNAS*. doi: 10.1073/pnas.0602184103.
- Mistry B., Long J. S., Schreyer J., Staller E., Sanchez-David R. Y., Barclay W. 2020. "Elucidating the Interactions between Influenza Virus Polymerase and Host Factor ANP32A." *Journal of Virology*. doi: 10.1128/JVI.
- Mukherjee A., Morosky S. A., Shen L., Weber C. R., Turner J. R., Kim K. S., Wang T., Coyne C. B. 2009. "Retinoic acid-induced gene-1 (RIG-I) associates with the actin cytoskeleton via caspase activation and recruitment domain-dependent interactions." *J Biol Chem* 284 (10):6486-94. doi: 10.1074/jbc.M807547200.
- Nettersheim B. J., Brocks J. J., Schwelm A., Hope J. M., Not F., Lomas M., Schmidt C., Schiebel R., Nowack E. C. M., de Deckler P., Pawlowski J., Bowser S. S., Bobrowski I., Zonneveld K., Kucera M., Stuhr M., Hallmann C. 2019. "Putative sponge biomarkers in unicellular Rhizaria question an early rise of animals." *Nature Ecology and Evolution*. doi: 10.1038/s41559-019-0806-5.
- Neumann G., Macken C. A., Kawaoka Y. 2014. "Identification of Amino Acid Changes That May Have Been Critical for the Genesis of A (H7N9) Influenza Viruses." *Journal of Virology* 88 (09):4877-96. doi: doi:10.1128/JVI.00107-14.
- Noda K., Murakami S., Nakatsu S., Imai H., Muramoto Y., Shindo K., Sagara H., Kawaoka Y. 2018. "Importance of the 1+7 configuration of ribonucleoprotein complexes for influenza A virus genome packaging." *Nature Communications*. doi: 10.1038/s41467-017-02517-w.
- Panagiotidis G. D., Müller C., Binder M., Weber F. 2023. "Influenza A virus strain PR/8/34, but neither HAM/2009 nor WSN/33, is transiently inhibited by the PB2-targeting drug paliperidone." *Arch Virol* 168 (2):63. doi: 10.1007/s00705-022-05696-0.

- Pérez-Cidoncha M., Killip M. J., Oliveros J. C., Asensio V. J., Fernández Y., Bengoechea J. A., Randall R. E., Ortín J. 2014. "An Unbiased Genetic Screen Reveals the Polygenic Nature of the Influenza Virus Anti-Interferon Response." *Journal of Virology* 88 (9):4632-46. doi: 10.1128/JVI.00014-14.
- Peteranderl C., Herold S., Schmoldt C. 2016. "Human Influenza Virus Infections." *Seminars in Respiratory and Critical Care Medicine*. doi: 10.1055/s-0036-1584801.
- Pothlichet J., Chignard M., Si-Tahar M. 2008. "Cutting edge: innate immune response triggered by influenza A virus is negatively regulated by SOCS1 and SOCS3 through a RIG-I/IFNAR1-dependent pathway." *J Immunol* 180 (4):2034-8. doi: 10.4049/jimmunol.180.4.2034.
- Pothlichet J., Meunier I., Davis B. K., Ting J. P.-Y., Skamene E., von Messling V., Vidal S. M. . 2013. "Type I IFN Triggers RIG-I/TLR3/NLRP3-dependent Inflammasome Activation in Influenza A Virus Infected Cells." doi: 10.1371/journal.ppat.1003256.
- Reppe K., Radunzel P., Dietert K., Tschernig T., Wolff T., Hammerschmidt S., Gruber A. D., Suttorp N., Witzenrath M. 2015. "Pulmonary immunostimulation with MALP-2 in influenza virus-infected mice increases survival after pneumococcal superinfection." *Infect Immun* 83 (12):4617-29. doi: 10.1128/IAI.00948-15.
- Russell W. M. S., Burch R. L. 1959. "The Principles of Humane Experimental Technique." *METHUEN & CO LTD* Textbook.
- Sabikunnahar B., Lahue K. G., Asarian L., Fang Q., McGill M. M., Haynes L., Teuscher C., Kremontsov D. N. 2022. "Sex differences in susceptibility to influenza A virus infection depend on host genotype." *Plos one* 17 (9):e0273050. doi: 10.1371/journal.pone.0273050.
- Salaün C., James D. J., Chamberlain L. H. 2004. "Lipid Rafts and the Reegulation of Exocytosis." *PMC*. doi: 10.1111/j.1600-0854.2004.0162.x.
- Schneider W. M., Dittmann Chevillotte M., Rice C. M. . 2014. "Interferon-Stimulated Genes: A Complex Web of Host Defenses." *Annual Review of Immunology*. doi: 10.1146/annurev-immunol-032713-120231.
- Schoggins J. W., Rice C. M. 2011. "Interferon-stimulated genes and their antiviral effector functions." *Curr Opin Virol* 1 (6):519-25. doi: 10.1016/j.coviro.2011.10.008.
- Schwab L. S. U., Villalon-Letelier F., Tessema M. B., Londrigan S. L., Brooks A. G., Hurt A., Coch C., Zillinger T., Hartmann G., Reading P. C. 2022. "Expression of a Functional Mx1 Protein Is Essential for the Ability of RIG-I Agonist Prophylaxis to Provide Potent and Long-Lasting Protection in a Mouse Model of Influenza A Virus Infection." *Viruses* 14 (7). doi: 10.3390/v14071547.
- Steinberg J., Wadenpohl T., Jung S. 2021. "The endogenous RIG-I Ligand is generated in Influenza A-virus infected cells." *Viruses*. doi: 10.3390/vxxxx.
- Swanson K. V., Deng M., Ting J. P.-Y. 2019. "The NLRP3 inflammasome: molecular activation and regulation to therapeutics." *Nature Reviews Immunology*. doi: 10.1038/s41577-019-0165-0.
- Takahashi K., Yoneyama M., Nishihori T., Hirai R., Kumeta H., Narita R., Gale M., Inagaki F., Fujita T. 2008. "Nonself RNA-Sensing Mechanism of RIG-I Helicase and Activation of Antiviral Immune Responses." *Cell Molecular Cell*. doi: 10.1016/j.molcel.2007.11.028.

- van Tuinen M., Hedges S. B. 2001. "Calibration of Avian Molecular Clocks." *Mol. Biol. Evol.* 18 (2):206-13. doi: 10.1093/oxfordjournals.molbev.a003794.
- Verhelst J., Parthoens E., Schepens B., Fiers W., Saelens X. 2012. "Interferon-inducible protein Mx1 inhibits influenza virus by interfering with functional viral ribonucleoprotein complex assembly." *J Virol* 86 (24):13445-55. doi: 10.1128/JVI.01682-12.
- Vermillion M. S., Ursin R. L., Kuok D. I. T., Vom Steeg L. G., Wohlgemuth N., Hall O. J., Fink A. L., Sasse E., Nelson A., Ndeh R., McGrath-Morrow S., Mitzner W., Chan M. C. W., Pekosz A., Klein S. L. 2018. "Production of amphiregulin and recovery from influenza is greater in males than females." *Biol Sex Differ* 9 (1):24. doi: 10.1186/s13293-018-0184-8.
- Wang C., Lee H. H., Yang Z. F., Mok C. K., Zhang Z. 2016. "PB2-Q591K Mutation Determines the Pathogenicity of Avian H9N2 Influenza Viruses for Mammalian Species." *Plos one* 11 (9):e0162163. doi: 10.1371/journal.pone.0162163.
- Wang H., Hu H., Zhang K. 2017. "Overview of Interferon: Characteristics, signaling and anti-cancer effect." *Archives of Biotechnology and Biomedicine* 1 (1):001-16. doi: 10.29328/journal.hjb.1001001.
- Wang Y., Zhang H.-X., Sun Y.-P., Liu Z.-X., Liu X.-S., Wang L., Lu S.-Y., Kong H., Liu Q.-L., Li X.-H., Lu Z.-Y., Chen S.-J., Chen Z., Bao S.-S., Dai W., Wang Z.-G. 2007. "Rig-I^{-/-} mice develop colitis associated with downregulation of G alpha i2." *Cell Res* 17 (10):858-68. doi: 10.1038/cr.2007.81.
- Weber-Gerlach M., Weber F. 2016a. "Standing on three legs: antiviral activities of RIG-I against influenza viruses." *Current Opinion in Immunology, Host Pathogens.* doi: 10.1016/j.coi.2016.05.016.
- Weber-Gerlach M., Weber F. 2016b. "To Conquer the Host, Influenza Virus Is Packing It In: Interferon-Antagonistic Strategies beyond NS1." *Journal of Virology.* doi: 10.1128/JVI.00041-16.
- Weber M., Gawanbach A., Habjan M., Rang A., Borner C., Schmidt A. M., Veitinger S., Jacob R., Devignot S., Kochs G., Garcia-Sastre A., Weber F. 2013. "Incoming RNA Virus Nucleocapsids Containing a 50-Triphosphorylated Genome Activate RIG-I and Antiviral Signaling." *Cell Host Microbe*:336-43. doi: 10.1016/j.chom.2013.01.012.
- Weber M., Sediri H., Felgenhauer U., Binzen I., Bänfer S., Jacob R., Brunotte L., Garcia-Sastre A., Schmid-Burgk J. L., Schmidt T., Hornung V., Kochs G., Schwemmler M., Klenk H.-D., Weber F. 2015. "Influenza virus adaptation PB2-627K modulates nucleocapsid inhibition by the pathogen sensor RIG-I." *Cell Host Microbe*:309-19. doi: 10.1016/j.chom.2015.01.005.
- Weber M., Weber F. 2014. "Segmented negative-strand RNA viruses and RIG-I: divide (your genome) and rule." *Current Opinion in Microbiology.* doi: 10.1016/j.mib.2014.05.002.
- Wu W., Wang X., Zhang W., Tian L., Booth J. L., Duggan E. S., More S., Liu L., Dozmorov M., Metcalf J. P. 2018. "RIG-I Signaling via MAVS Is Dispensable for Survival in Lethal Influenza Infection In Vivo." *Mediators Inflamm* 2018:6808934. doi: 10.1155/2018/6808934.
- Wu Y., Wu X., Wu L., Wang X., Liu Z. 2017. "The anticancer functions of RIG-I-like receptors, RIG-I and MDA5, and their applications in cancer therapy." *Transl Res* 190:51-60. doi: 10.1016/j.trsl.2017.08.004.

-
- Xu L., Wang W., Li Y., Zhou X., Yin Y., Wang Y., de Man R. A., van der Laan L. J. W., Huang F., Kamar N., Peppelenbosch M. P., Pan Q. 2017. "RIG-I Is a Key Antiviral Interferon-Stimulated Gene Against Hepatitis E Virus Regardless of Interferon Production." *HEPATOLOGY* 65 (6). doi: 10.1002/hep.29105.
- Yoneyama M., Kikuchi M., Natsukawa T., Shinobu N., Imaizumi T., Miyagishi M., Taira K., Akira S., Fujita T. 2004. "The RNA helicase RIG-I has an essential function in double-stranded RNA-induced innate antiviral responses." *Nat Immunol* 5 (7):730-7. doi: 10.1038/ni1087.
- Zhang N.-N., Shen S.-H., Jiang L.-J., Zhang W., Zhang H.-X., Sun Y.-P., Li X.-Y., Huang Q.-H., Ge B.-X., Chen S.-J., Wang Z.-G., Chen Z., Zhu J. 2008. "RIG-I plays a critical role in negatively regulating granulocytic proliferation." *PNAS*. doi: 10.1073/pnas.0804895105.
- Ziegler A., Soldner C., Lienenklaus S., Spanier J., Trittel S., Riese P., Kramps T., Weiss S., Heidenreich R., Jasny E., Guzmán C. A., Kallen K.-J., Fotin-Mleczek M., Kalinke U. 2017. "A New RNA-Based Adjuvant Enhances Virus-Specific Vaccine Responses by Locally Triggering TLR-and RLH-Dependent Effects." *The Journal of Immunology*. doi: 10.4049/jimmunol.1601129.

9. Supplementary Figures

A

Version 1.2 / 24.07.2013

ANLAGE 5

Abschlussbeurteilung genetisch veränderter Zuchtlinien

Einrichtung und Adresse: Institut für Immunologie Hans-Meerwein-Str. 2 35043 Marburg					
Beurteilte Linie (internationale Bezeichnung): <small>Angabe erst nach Publikation der Linie notwendig!</small>			Beurteilte Linie (interne Bezeichnung) RIG-I K271A		
Beschreibung der genetischen Veränderung(en) sofern noch nicht in Datenbanken beschrieben ist, was zur Belastungen führt: Punktmutation im murinen RIG-I (DDX58; ATPase/IFN Signaling Funktion)					
Haltungsform der beurteilten Tiere: IVC					
Genorte und Genotyp: Chrom. 9 NC 000009.12 (32455302..32526196, complement), homozygot					
Beurteilte Tiere					
Anzahl: <u>13</u> davon weiblich: <u>7</u> und männlich: <u>6</u>					
durchschnittlicher Untersuchungszeitraum (Wochen): <u>24</u> ±Stabw.: _____					
durchschnittl. Anzahl Untersuchungen /Tier: <u>24</u> ±Stabw.: _____					
Auffälligkeiten im Hinblick auf:	Aufgetreten:	Bei wie vielen Tieren?	Auffälligkeiten im Hinblick auf:	Aufgetreten:	Bei wie vielen Tieren?
Ernährungszustand	ja <input type="checkbox"/> nein <input checked="" type="checkbox"/>		Tumor	ja <input type="checkbox"/> nein <input checked="" type="checkbox"/>	
Körperhaltung	ja <input type="checkbox"/> nein <input checked="" type="checkbox"/>		Hautveränderungen	ja <input type="checkbox"/> nein <input checked="" type="checkbox"/>	
Reaktion auf Handling	ja <input type="checkbox"/> nein <input checked="" type="checkbox"/>		Verletzungen	ja <input type="checkbox"/> nein <input checked="" type="checkbox"/>	
Fell/Körperöffnungen	ja <input type="checkbox"/> nein <input checked="" type="checkbox"/>		Kannibalismus	ja <input type="checkbox"/> nein <input checked="" type="checkbox"/>	
Verhalten	ja <input type="checkbox"/> nein <input checked="" type="checkbox"/>		Rektumprolaps	ja <input type="checkbox"/> nein <input checked="" type="checkbox"/>	
Motorik	ja <input type="checkbox"/> nein <input checked="" type="checkbox"/>		andere: <u>Kiemen</u>		<u>1</u>
Bei weiblichen Tieren:					
Durchschnittliche Anzahl Trächtigkeiten 1.12	Durchschnittliche Aufzuchtverluste (Differenz geb. – abgesetzt ±Stabw) 0.55/Wurf; 7.04% aller Jungtiere bei 9 Würfen		Kolonie-Index (mittlere Anzahl an Nachkommen der Weibchen pro Zeiteinheit)		
Abschließende Beurteilung: (wenn notwendig, bitte Beiblatt verwenden)					
Die Belastungen werden als keine <input type="checkbox"/> gering <input type="checkbox"/> mittel <input type="checkbox"/> schwer <input type="checkbox"/> eingestuft.					
Begründung: Wir konnten keine Auffälligkeiten im Vergleich zu wildtyp-Mäusen feststellen. Lediglich eine geringfügig niedrigere Gewichtszunahme der Männchen ab einem Alter von ca. 12 Wochen im Vergleich zu Werten von Jackson Lab C57BL6 ist zu erwähnen. Die männlichen Mäuse haben im Alter von 20 Wochen ein um 7.9% niedrigeres Durchschnittsgewicht als in den Vergleichswerten von JL. Die beschriebenen Belastungen traten ab einem Alter von _____ Wochen in einer Häufigkeit von _____% der untersuchten Tiere auf.					
Im Falle einer Belastung wird empfohlen, Nachkommen dieser Linie in einem Alter von _____ Wochen zu töten, insoweit der Versuchszweck nicht dagegen spricht. Im Sinne einer Belastungsreduzierung werden folgende Refinementmaßnahmen empfohlen: _____					
Mitglieder des gegebenenfalls mit beurteilenden Tierschutzausschusses: _____					
Ort: <u>Marburg</u> Datum: <u>08.07.20</u> Kenntnis genommen: _____ (Projektleiter und Tierschutzbeauftragter)					

B

Version 1.2 / 24.07.2013

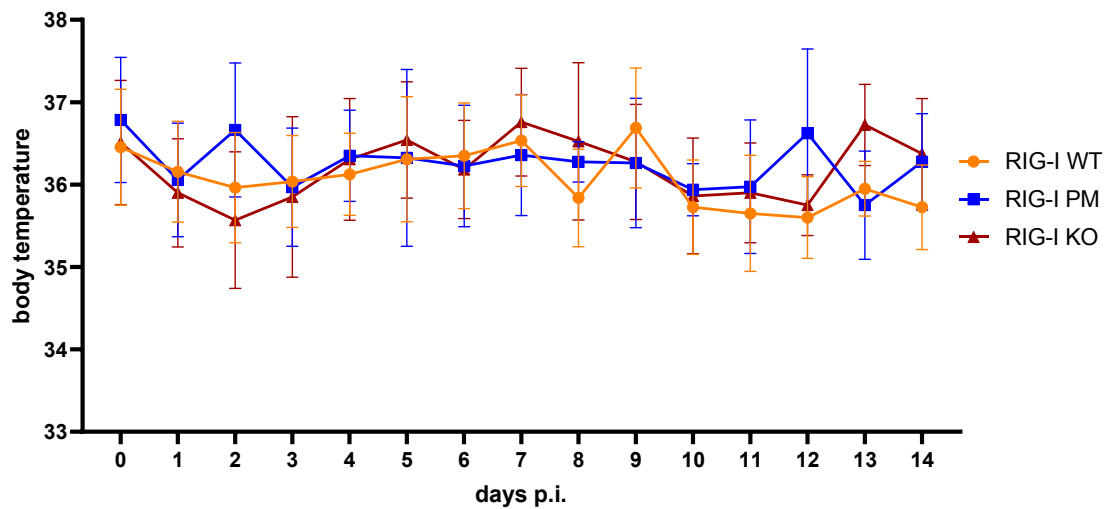
ANLAGE 5

Abschlussbeurteilung genetisch veränderter Zuchtlinien

Einrichtung und Adresse: Institut für Immunologie Hans-Meerwein-Str. 2 35043 Marburg					
Beurteilte Linie (internationale Bezeichnung): <small>Angabe erst nach Publikation der Linie notwendig!</small>			Beurteilte Linie (interne Bezeichnung) RIG-I FS (homozygot)		
Beschreibung der genetischen Veränderung(en) sofern noch nicht in Datenbanken beschrieben ist, was zur Belastungen führt: 5 nt Frameshift im murinen RIG-I (DDX58), Funktionsverlust des Proteins					
Haltungsform der beurteilten Tiere: IVC					
Genorte und Genotyp: Chrom. 9 NC 000009.12 (32455302..32526196, complement), homozygot					
Beurteilte Tiere					
Anzahl: <u>37</u> davon weiblich: <u>16</u> und männlich: <u>21</u>					
durchschnittlicher Untersuchungszeitraum (Wochen): <u>24</u> ±Stabw.: _____					
durchschnittl. Anzahl Untersuchungen /Tier: <u>24</u> ±Stabw.: _____					
Auffälligkeiten im Hinblick auf:	Aufgetreten:	Bei wie vielen Tieren?	Auffälligkeiten im Hinblick auf:	Aufgetreten:	Bei wie vielen Tieren?
Ernährungszustand	ja <input type="checkbox"/> nein <input checked="" type="checkbox"/>		Tumor	ja <input type="checkbox"/> nein <input checked="" type="checkbox"/>	
Körperhaltung	ja <input type="checkbox"/> nein <input checked="" type="checkbox"/>		Hautveränderungen	ja <input type="checkbox"/> nein <input checked="" type="checkbox"/>	
Reaktion auf Handling	ja <input type="checkbox"/> nein <input checked="" type="checkbox"/>		Verletzungen	ja <input type="checkbox"/> nein <input checked="" type="checkbox"/>	
Fell/Körperöffnungen	ja <input type="checkbox"/> nein <input checked="" type="checkbox"/>		Kannibalismus	ja <input type="checkbox"/> nein <input checked="" type="checkbox"/>	
Verhalten	ja <input type="checkbox"/> nein <input checked="" type="checkbox"/>		Rektumprolaps	ja <input type="checkbox"/> nein <input checked="" type="checkbox"/>	
Motorik	ja <input type="checkbox"/> nein <input checked="" type="checkbox"/>		Kümmerer 3 links blind 1	ja <input type="checkbox"/> nein <input checked="" type="checkbox"/>	
Bei weiblichen Tieren:					
Durchschnittliche Anzahl Trächtigkeiten 2,5/Verpaarung		Durchschnittliche Aufzuchtverluste (Differenz geb. – abgesetzt ±Stabw) 0,47/Wurf; 17,8% aller Jungtiere bei 20 Würfen		Kolonie-Index (mittlere Anzahl an Nachkommen der Weibchen pro Zeiteinheit)	
Abschließende Beurteilung: (wenn notwendig, bitte Beiblatt verwenden)					
Die Belastungen werden als keine <input checked="" type="checkbox"/> gering <input type="checkbox"/> mittel <input type="checkbox"/> schwer <input type="checkbox"/> eingestuft. Begründung: Wir konnten keine Auffälligkeiten im Vergleich zu wildtyp-Mäusen feststellen. Lediglich eine geringfügig niedrigere Gewichtszunahme der Männchen ab einem Alter von ca. 12 Wochen im Vergleich zu Werten von Jackson Lab C57BL6 ist zu erwähnen. Die männlichen Mäuse haben im Alter von 20 Wochen ein um 7,0% niedrigeres Durchschnittsgewicht als in den Vergleichswerten von JL, Weibchen 1,7%.					
Die beschriebenen Belastungen traten ab einem Alter von _____ Wochen in einer Häufigkeit von _____ % der untersuchten Tiere auf.					
Im Falle einer Belastung wird empfohlen, Nachkommen dieser Linie in einem Alter von _____ Wochen zu töten, insoweit der Versuchszweck nicht dagegen spricht. Im Sinne einer Belastungsreduzierung werden folgende Refinementmaßnahmen empfohlen: _____ <i>wereiche Kontrolle der Abgabe von Absetzen</i>					
Mitglieder des gegebenenfalls mit beurteilenden Tierschutzausschusses: _____					
Ort: Marburg Datum: <u>7.5.24</u> Prof. Dr. Stefan Bauer Institut für Immunologie, BMFZ Hans-Meerwein-Str. 2 35032 Marburg Ergebnis genommen: _____ (Projektleiter und Tierschutzbeauftragter)					

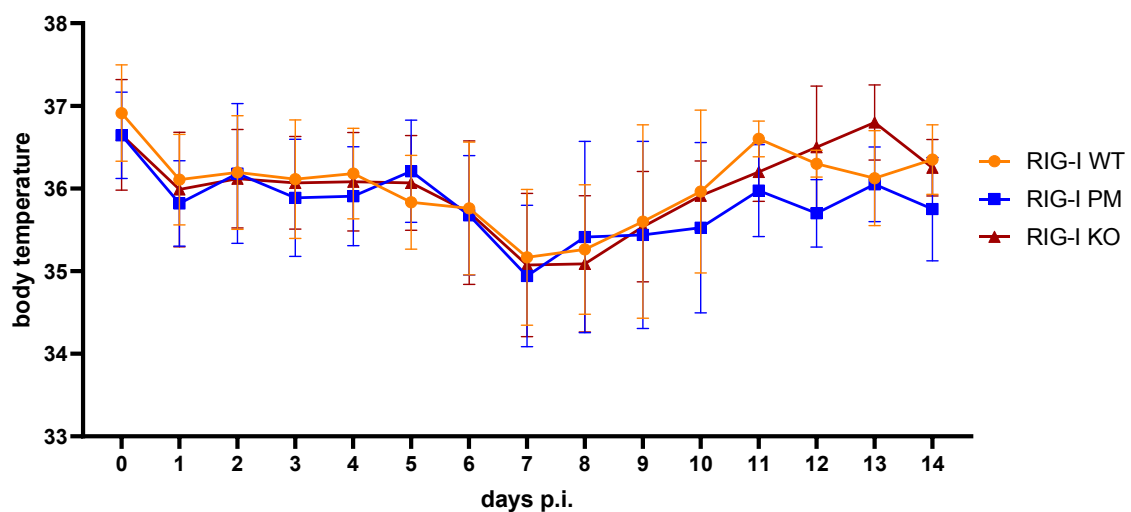
Supplementary Figure 1: A RIG-I PM and RIG-I KO mouse line, generated with CRISPR/Cas9 and homozygous for the respective RIG-I variant, do not develop a burdening phenotype. The final examination documents for A) homozygous RIG-I PM and B) homozygous RIG-I KO mouse lines.

A PBS mock infection



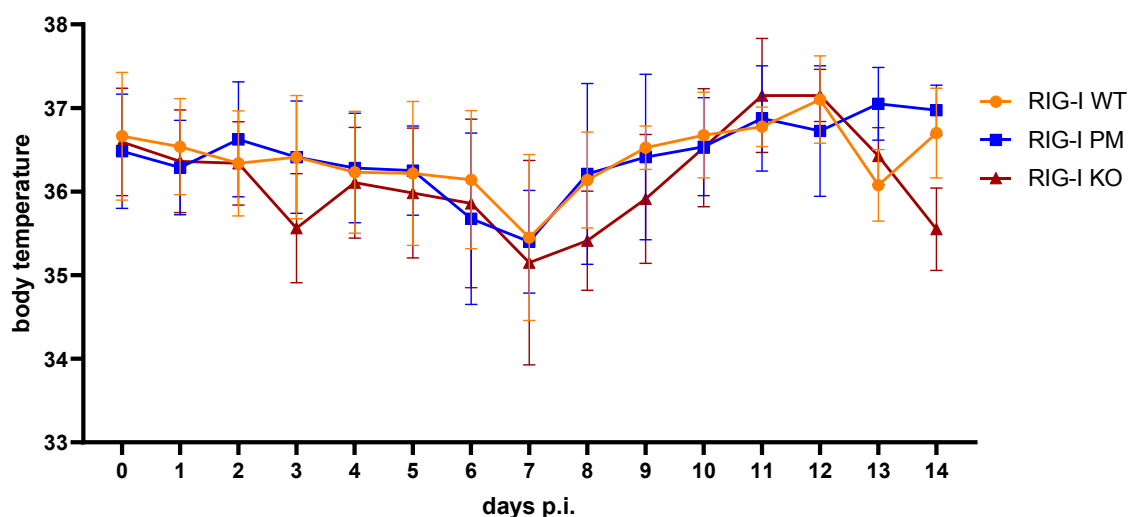
2-Way ANOVA	RIG-I WT vs. PM		RIG-I WT vs. KO		RIG-I PM vs. KO	
source of variation	p value	significance	p value	significance	p value	significance
interaction	0.1800	ns	0.2753	ns	0.0268	*
days p.i.	0.0014	**	<0.0001	****	0.0019	**
RIG-I genotype	0.0416	*	0.1540	ns	0.5818	ns

B IAV PB2-627K infection



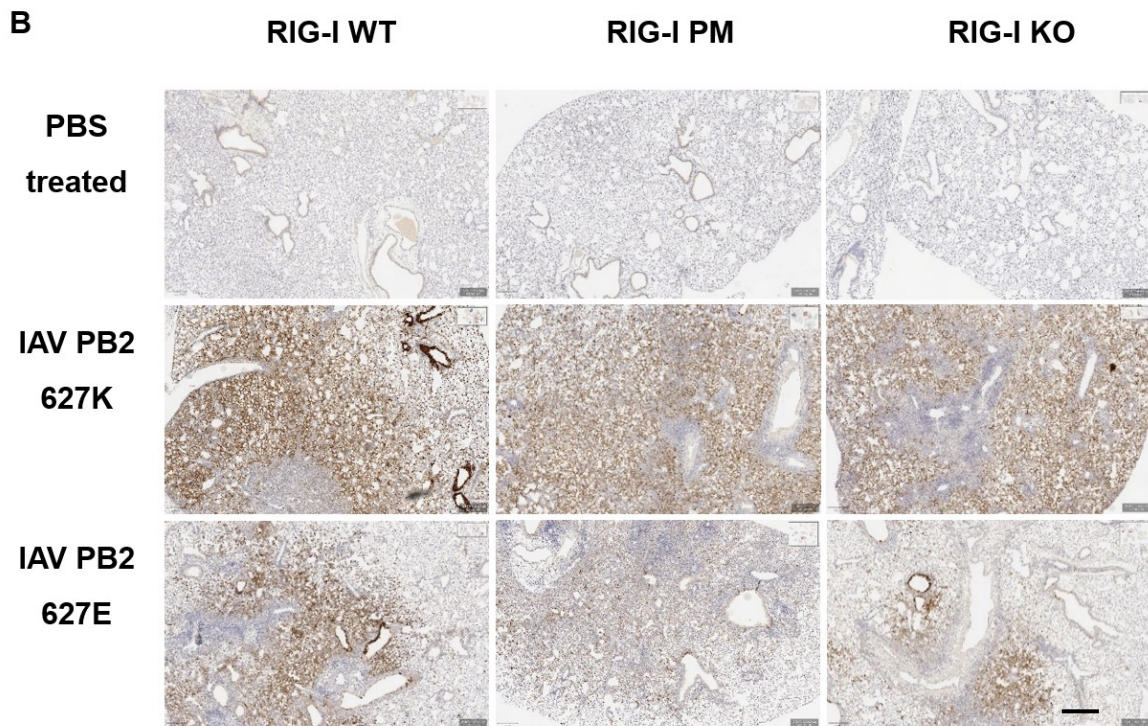
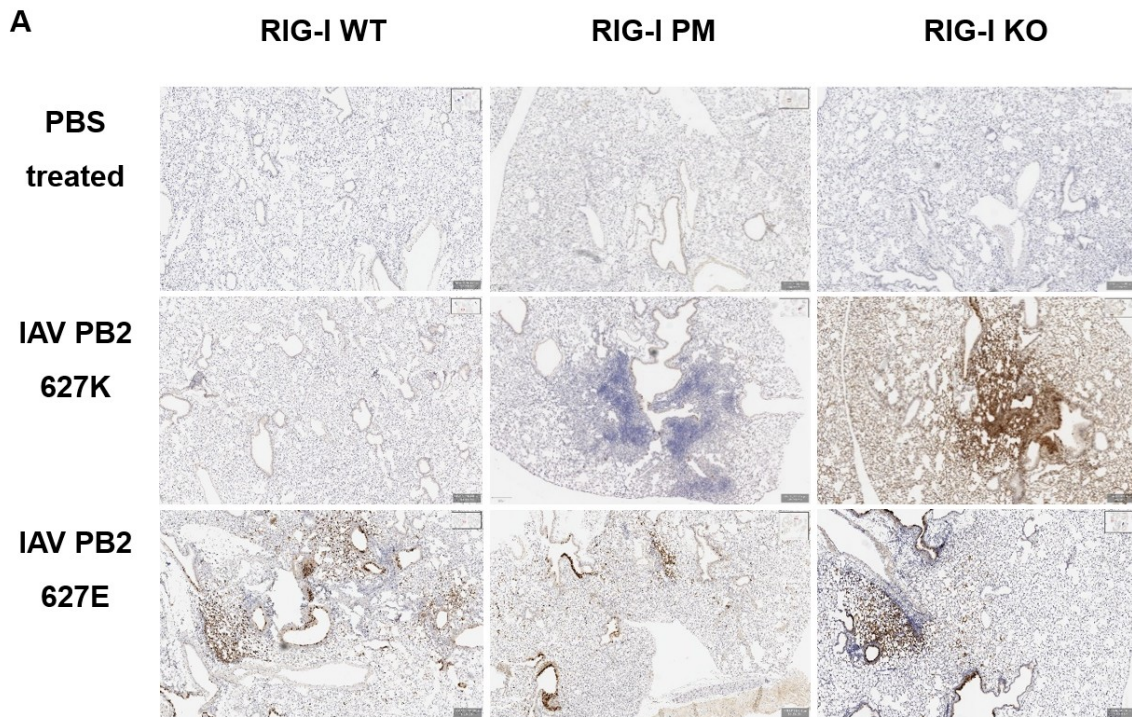
2-Way ANOVA	RIG-I WT vs. PM		RIG-I WT vs. KO		RIG-I PM vs. KO	
source of variation	p value	significance	p value	significance	p value	significance
interaction	0.8857	ns	0.9824	ns	0.8833	ns
days p.i.	<0.0001	****	<0.0001	****	<0.0001	****
RIG-I genotype	0.0195	*	0.7539	ns	0.0356	*

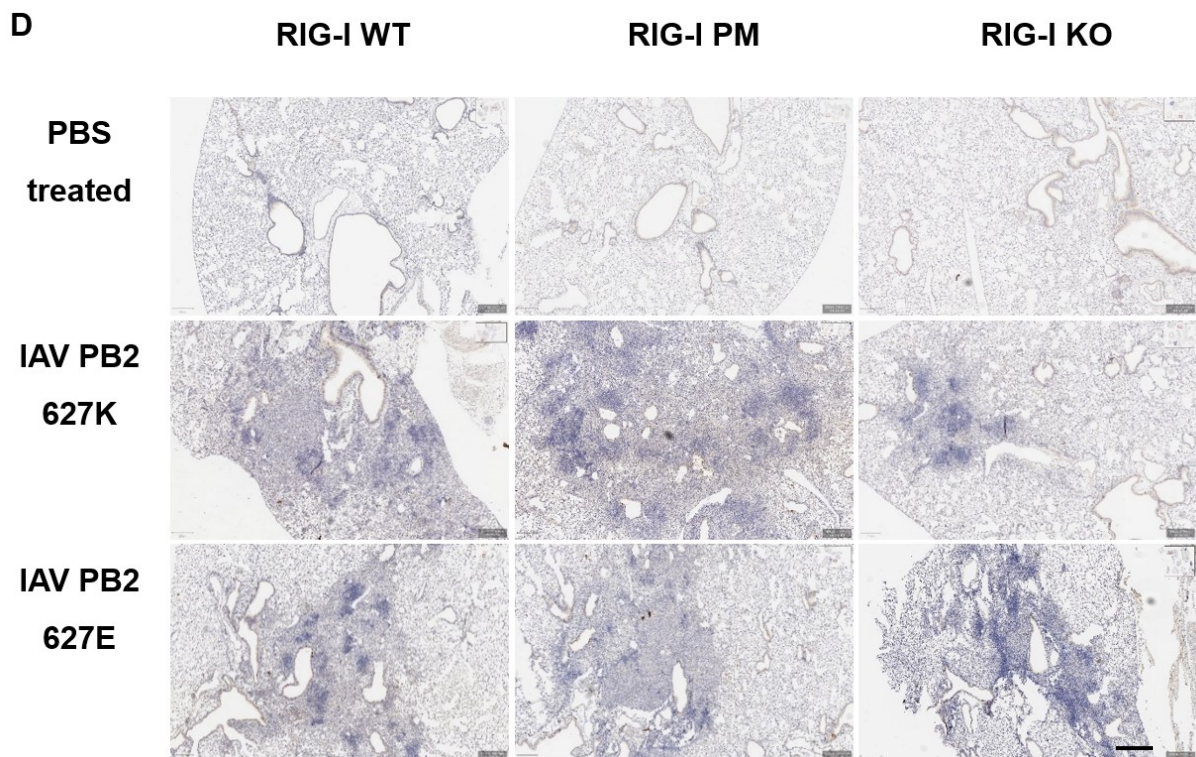
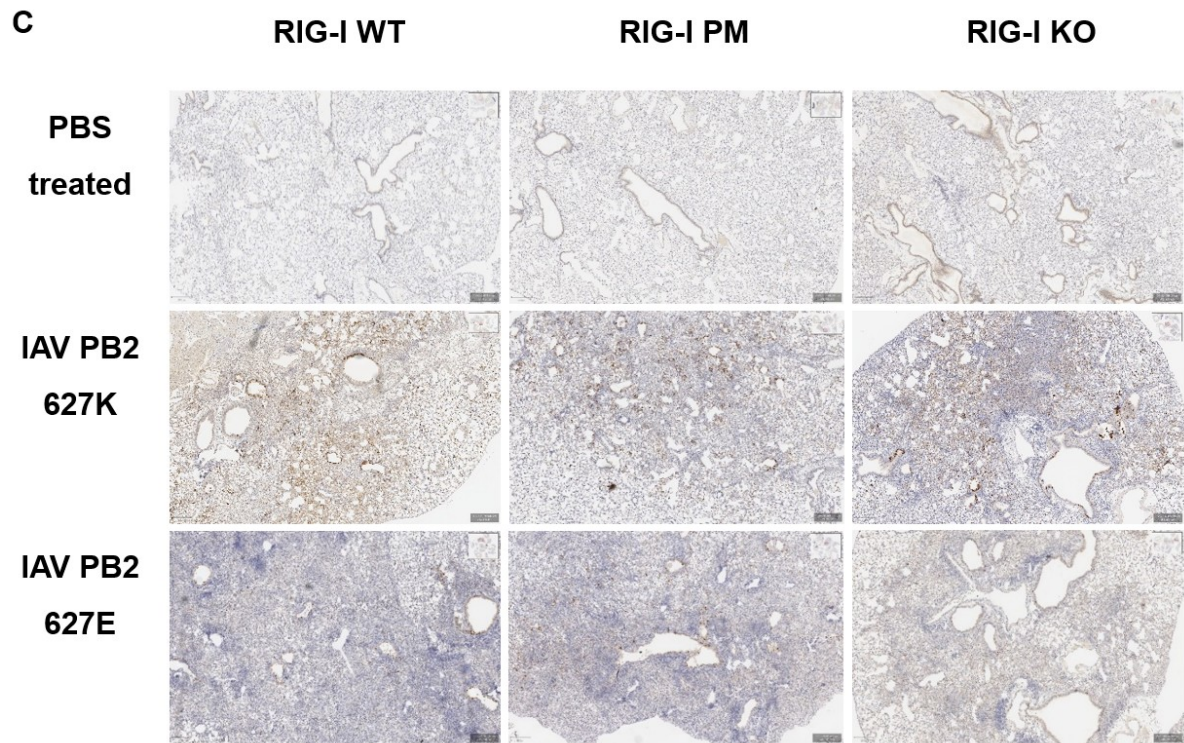
C IAV PB2-627E infection



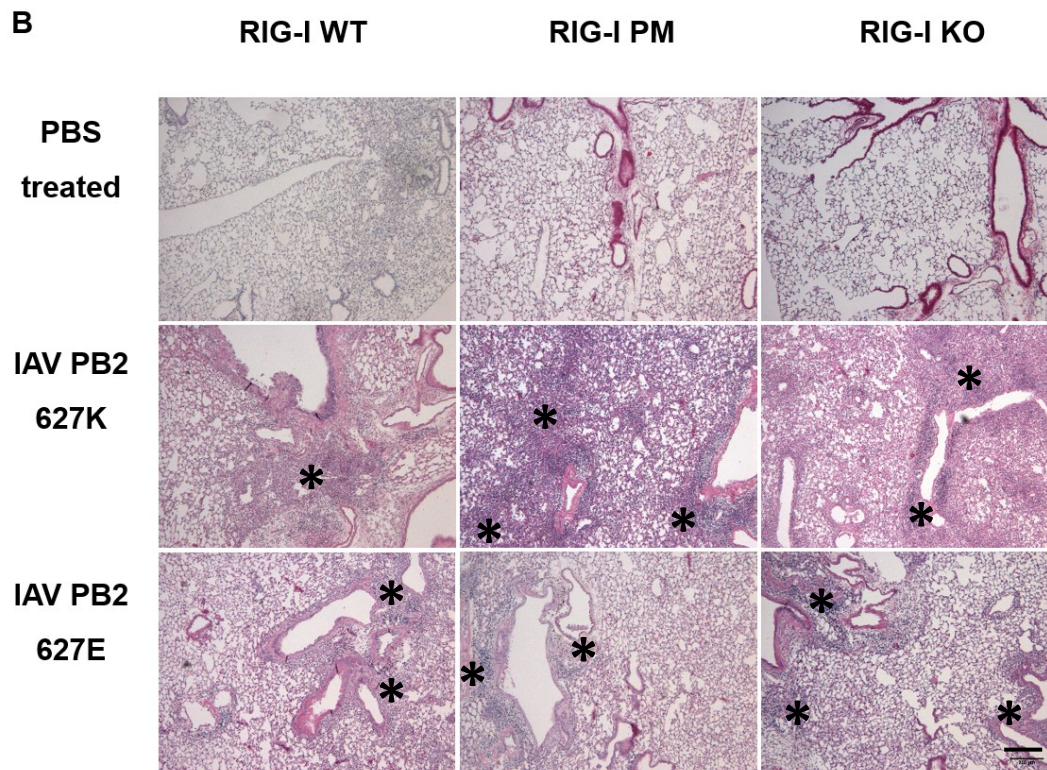
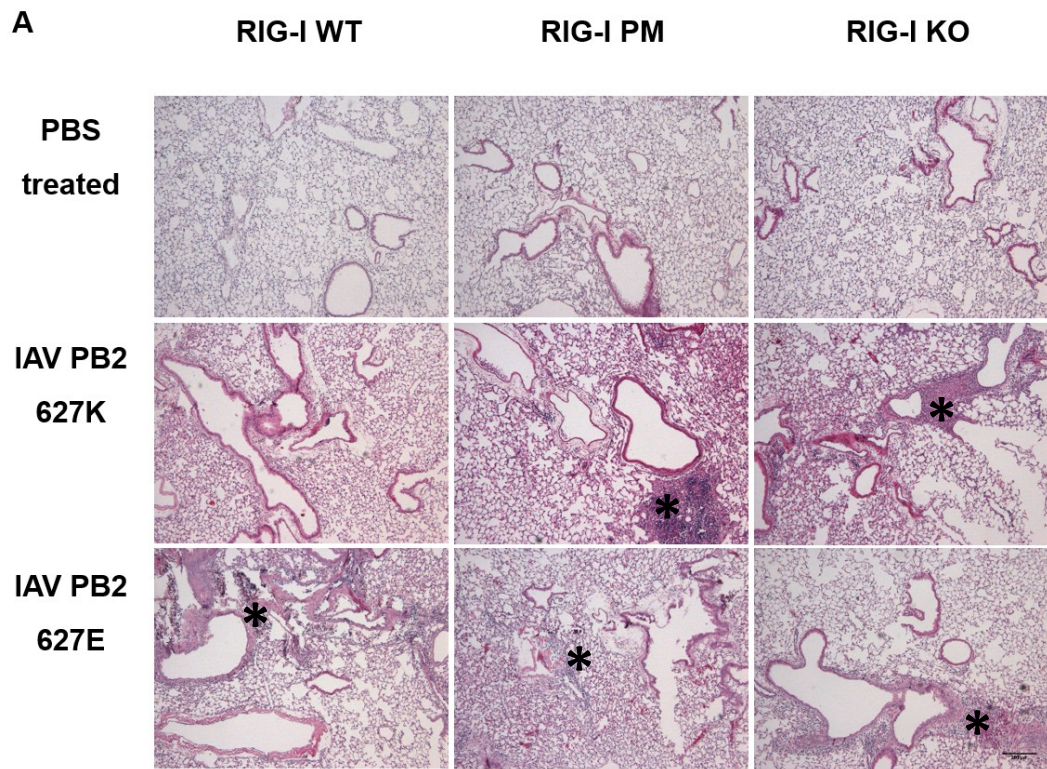
2-Way ANOVA	RIG-I WT vs. PM		RIG-I WT vs. KO		RIG-I PM vs. KO	
source of variation	p value	significance	p value	significance	p value	significance
interaction	0.7327	ns	0.2818	ns	0.0645	ns
days p.i.	<0.0001	****	<0.0001	****	<0.0001	****
RIG-I genotype	0.8731	ns	0.0061	**	0.0041	**

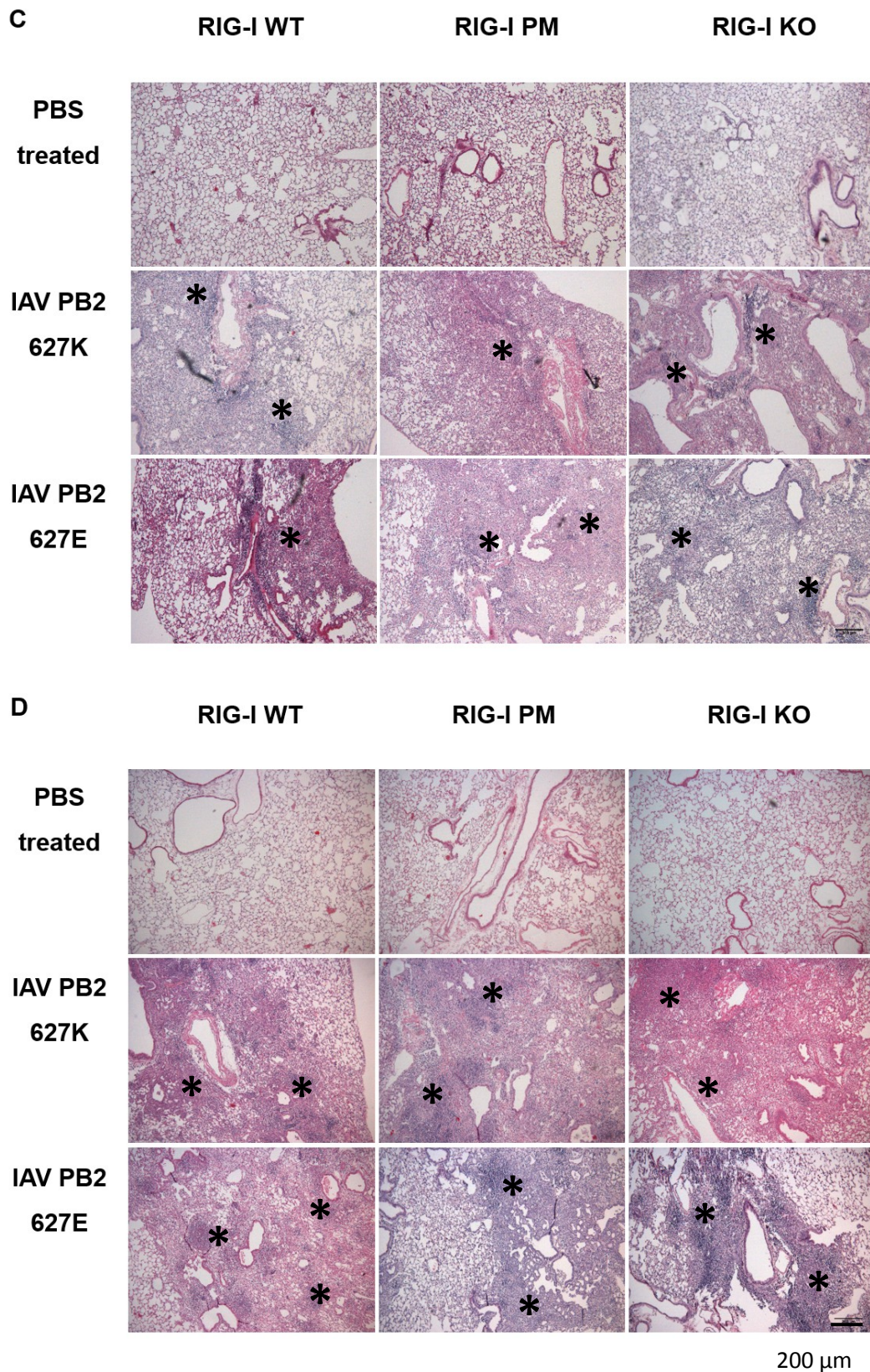
Supplementary Figure 2: The infection of RIG-I WT, PM and KO mice with a recombinant IAV PB2-627K or -627E strain causes a significant drop of the body temperature. RIG-I WT, PM and KO mice were treated with PBS (A) or were infected with a recombinant IAV PB2-627K (B) or -627E (C) strain for a maximum of 14 days p.i. All body temperature data points for the indicated day p.i. of mice included in the study were used to calculate the mean and standard deviation of the body temperature at the respective time point (d0-4: n = 16; d5-7: n = 12; d8-10: n = 8; d11-14: n = 4). A 2-Way ANOVA was used to indicate significant effects of the factors "days p.i." and "RIG-I genotype" on the variable "body temperature", as well as their interaction.

400 μ m

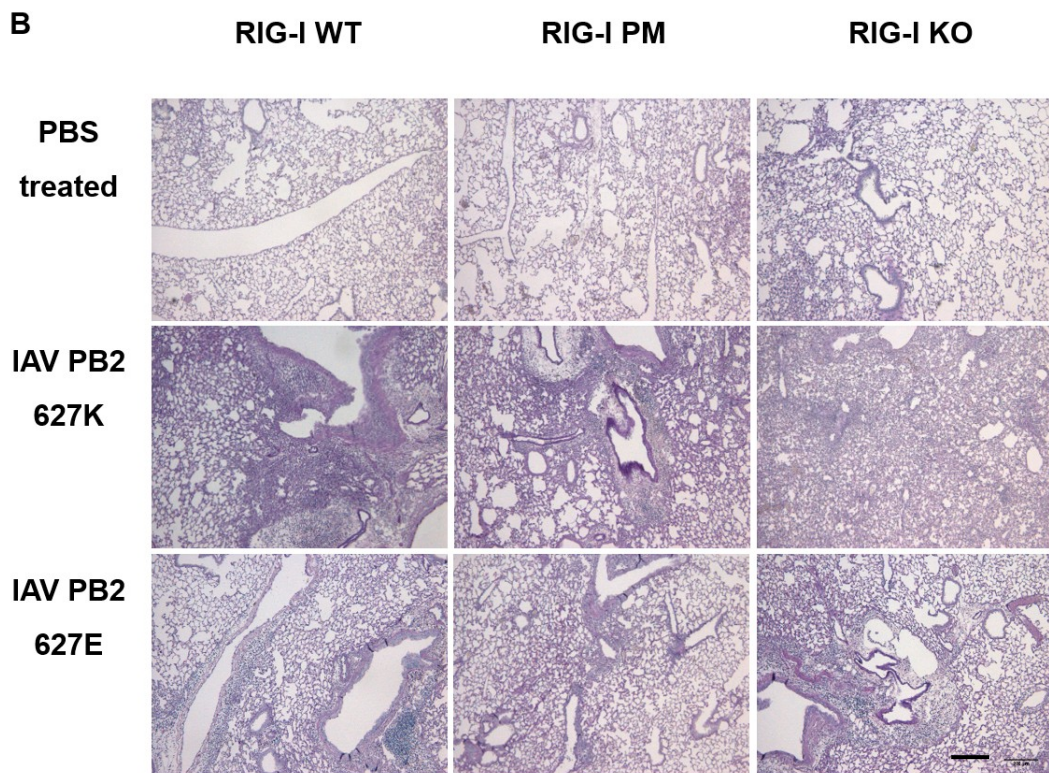
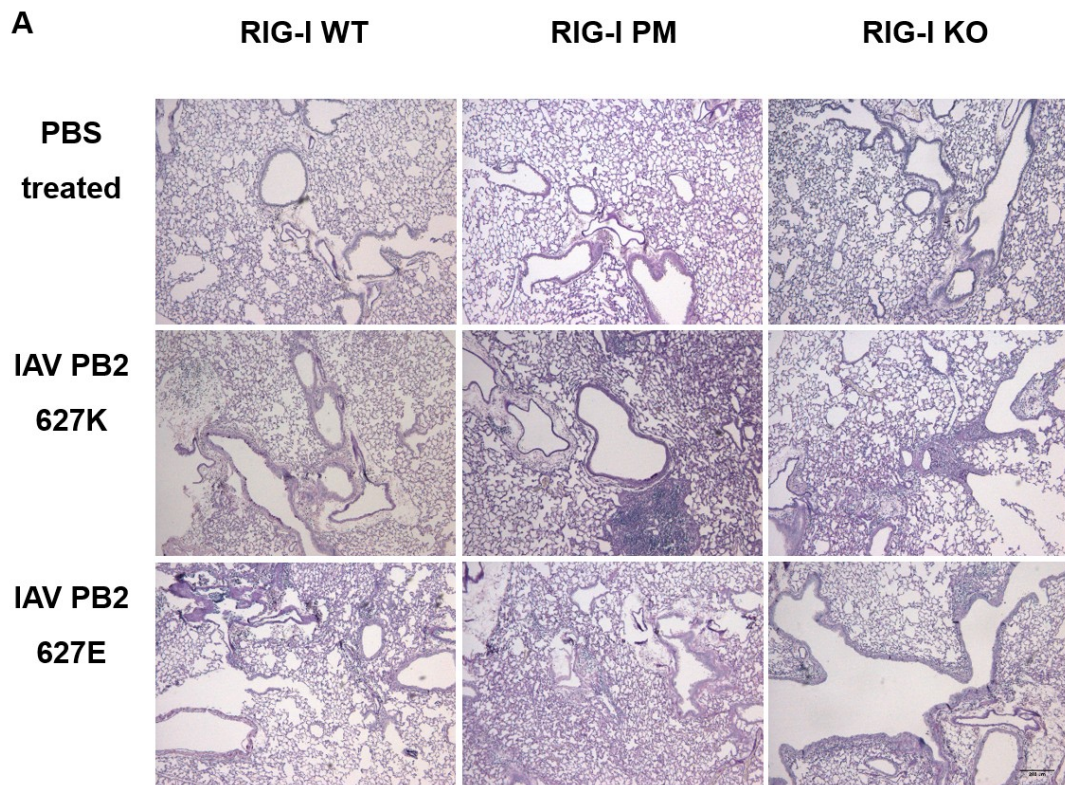
400 μ m

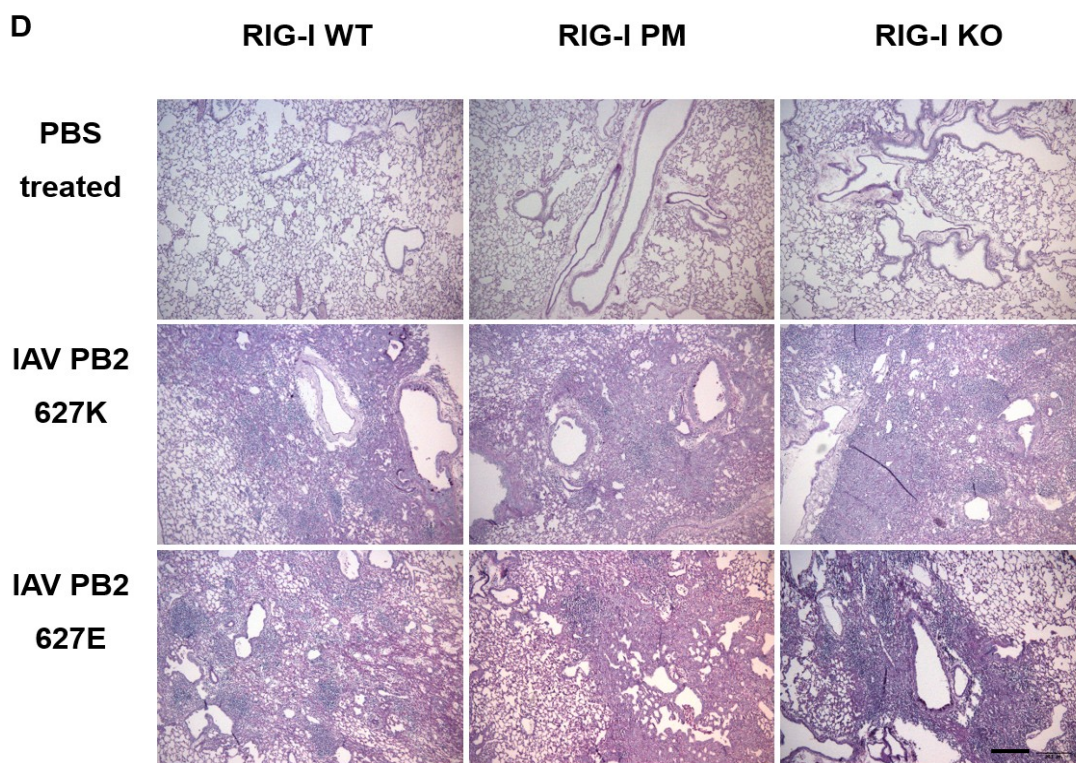
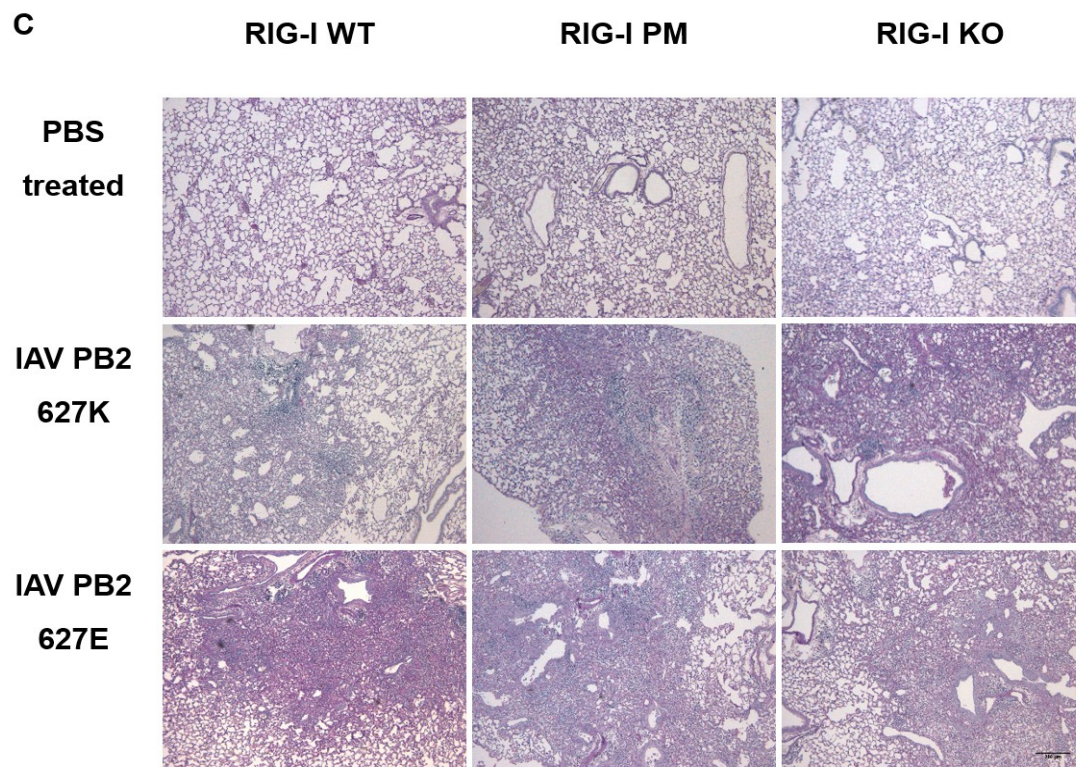
Supplementary Figure 3: The detection of IAV NP protein at different time points p.i. in lung tissue from mice infected with IAV PB2-627K or -627E visualizes the course of the infection. RIG-I WT, PM and KO mice were treated with PBS or infected with the recombinant IAV PB2-627K or the -627E strain for 4 (A), 7 (B), 10 (C) or 14 (D) days. At the indicated day p.i., the mice were sacrificed, the lung was fixated and immune histochemical stained using an antibody detecting IAV NP (Thermo Scientific PA532242). One sector of a slide from a male individual was chosen as an example for any infection group, the pictures were taken in 100-fold magnification.

200 μ m



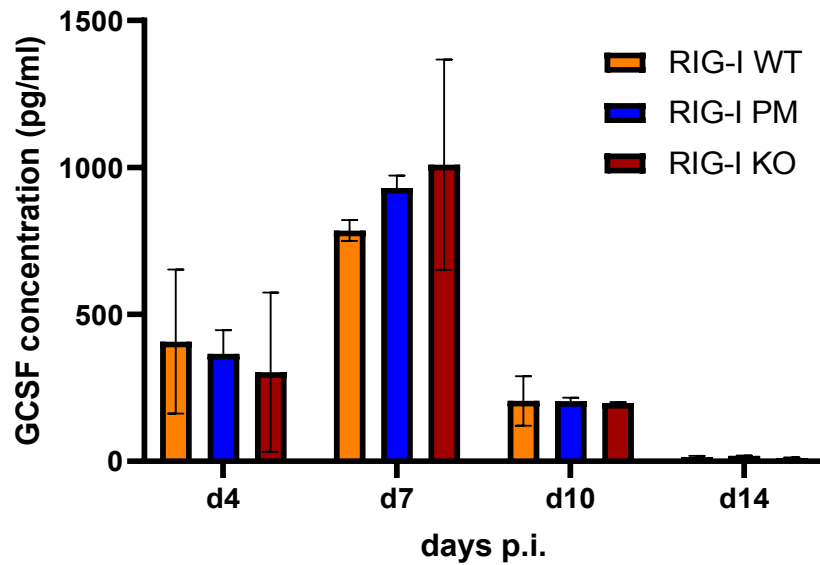
Supplementary Figure 4: Mononuclear immune cell infiltration of RIG-I WT, PM and KO mouse lungs infected with IAV PB2-627K or -627E results in formation of cellular exudates. RIG-I WT, PM and KO mice were infected with recombinant IAV PB2-627K, -627E or were treated with PBS. At day 4 (A), 7 (B), 10 (C) or 14 (D) p.i., the mice were sacrificed, the lung was fixated and stained with a H&E protocol to depict general tissue structures (pink) and nuclei (blue). One sector of a slide from a male individual of any infection group was chosen as an example. The asterisks mark infiltration of mononuclear blood cells (A-D) and cell rich exudates, enrichment zones of these cells (C and D).

200 μ m

200 μ m

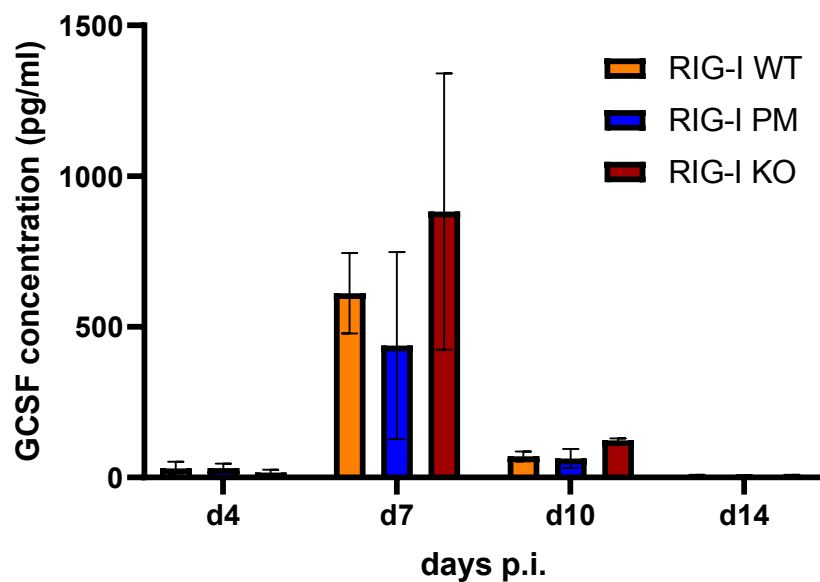
Supplementary Figure 5: RIG-I WT, PM and KO mice infected with IAV PB2-627K or -627E suffer from an acute lung infection without mucus production and basal membrane damage. RIG-I WT, PM and KO mice were infected with recombinant IAV PB2-627K, -627E or were treated with PBS. At day 4 (A), 7 (B), 10 (C) or 14 (D) p.i., the mice were sacrificed, the lung was fixated and stained with a PAS protocol to depict basal membranes and mucus. One sector of a slide from a male individual of any infection group was chosen as an example.

A GCSF IAV PB2-627K



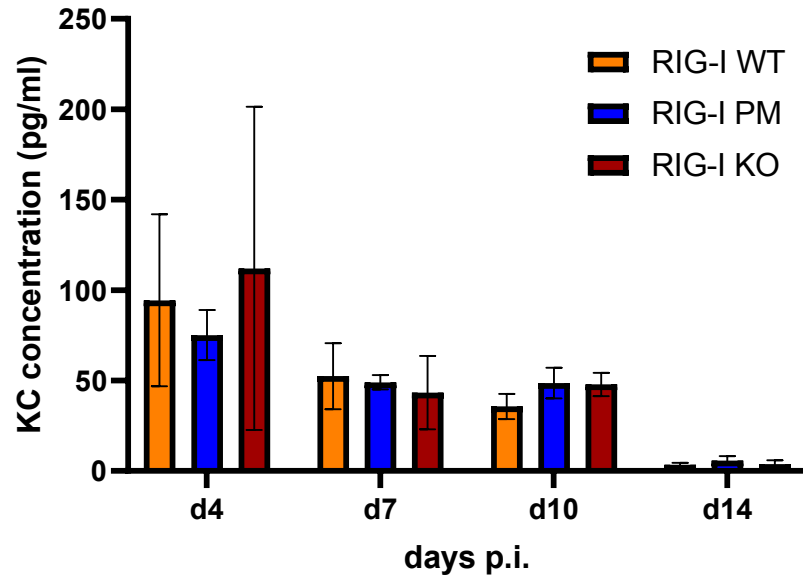
2-Way ANOVA	WT vs. PM		WT vs. KO		PM vs. KO	
source of variation	p value	significance	p value	significance	p value	significance
interaction	0.2699	ns	0.3477	ns	0.8522	ns
days p.i.	<0.0001	****	<0.0001	****	<0.0001	****
genotype	0.4456	ns	0.6773	ns	0.9929	ns

IAV PB2-627E



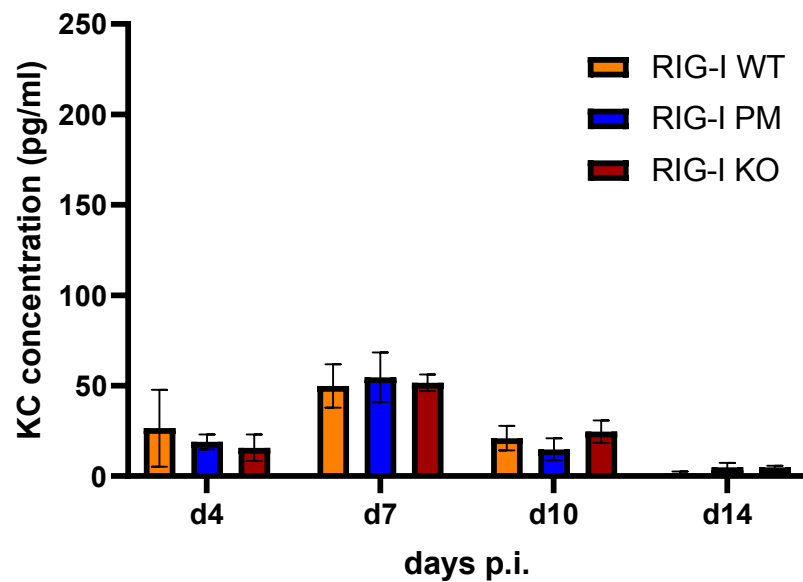
2-Way ANOVA	WT vs. PM		WT vs. KO		PM vs. KO	
source of variation	p value	significance	p value	significance	p value	significance
interaction	0,4023	ns	0,3251	ns	0,0883	ns
days p.i.	<0,0001	****	<0,0001	****	<0,0001	****
genotype	0,3018	ns	0,2047	ns	0,0891	ns

B KC IAV PB2-627K

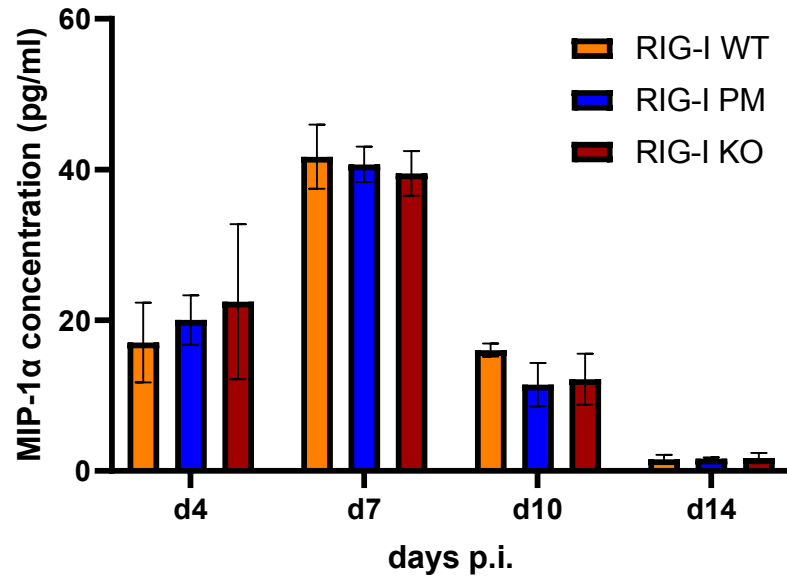


2-Way ANOVA	WT vs. PM		WT vs. KO		PM vs. KO	
source of variation	p value	significance	p value	significance	p value	significance
interaction	0.4193	ns	0.8900	ns	0.5457	ns
days p.i.	<0.0001	****	0.0002	***	0.0002	***
genotype	0.7854	ns	0.6925	ns	0.5471	ns

IAV PB2-627E

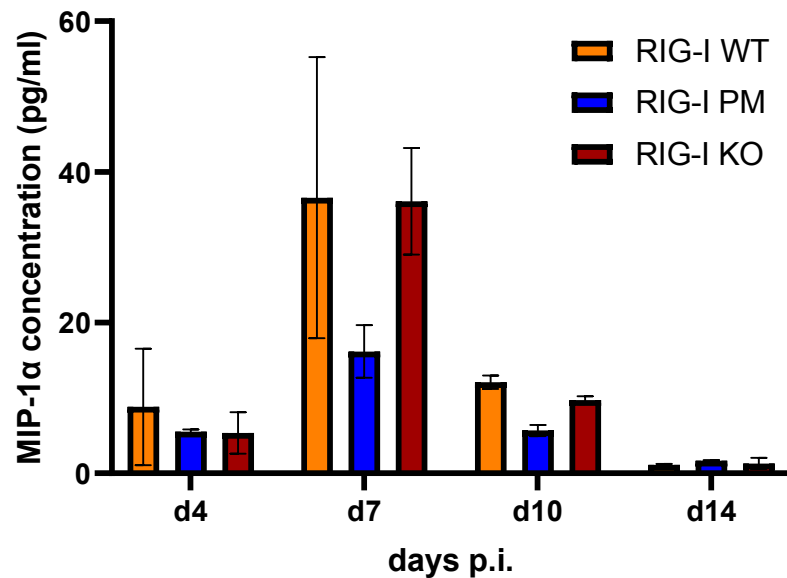


2-Way ANOVA	WT vs. PM		WT vs. KO		PM vs. KO	
source of variation	p value	significance	p value	significance	p value	significance
interaction	0.5552	ns	0.4055	ns	0.2034	ns
days p.i.	<0.0001	****	<0.0001	****	<0.0001	****
genotype	0.7106	ns	0.8789	ns	0.7176	ns

C MIP-1 α IAV PB2-627K

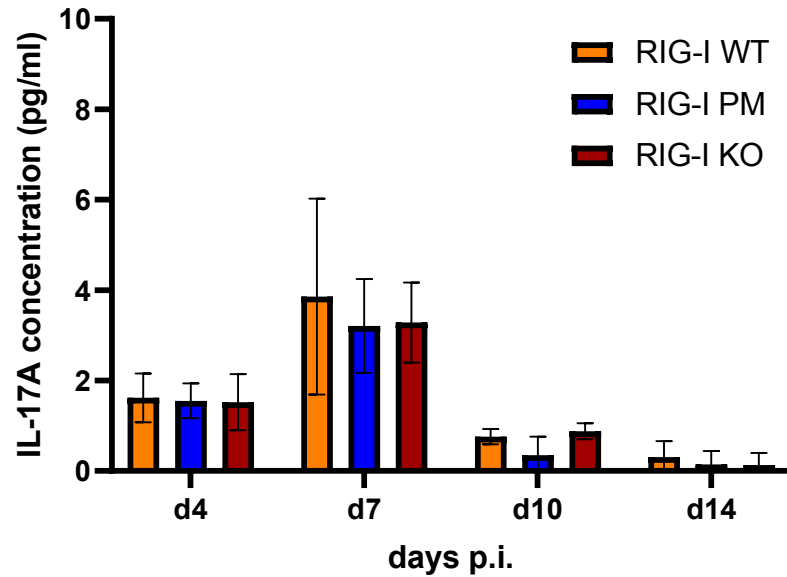
2-Way ANOVA	WT vs. PM		WT vs. KO		PM vs. KO	
source of variation	p value	significance	p value	significance	p value	significance
interaction	0.1151	ns	0.2367	ns	0.8688	ns
days p.i.	<0.0001	****	<0.0001	****	<0.0001	****
genotype	0.5611	ns	0.9393	ns	0.7487	ns

IAV PB2-627E



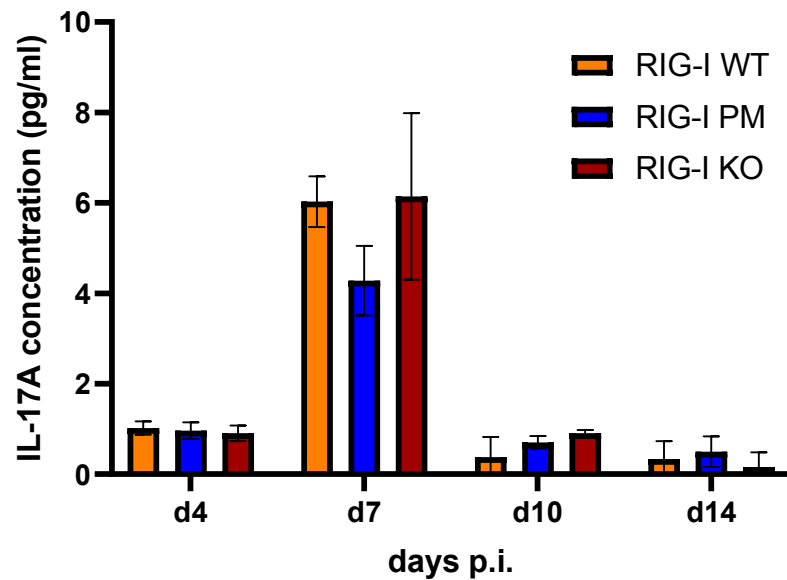
2-Way ANOVA	WT vs. PM		WT vs. KO		PM vs. KO	
source of variation	p value	significance	p value	significance	p value	significance
interaction	0.0427	*	0.9609	ns	<0.0001	****
days p.i.	<0.0001	****	<0.0001	****	<0.0001	****
genotype	0.0082	**	0.5743	ns	<0.0001	****

D IL-17A IAV PB2-627K

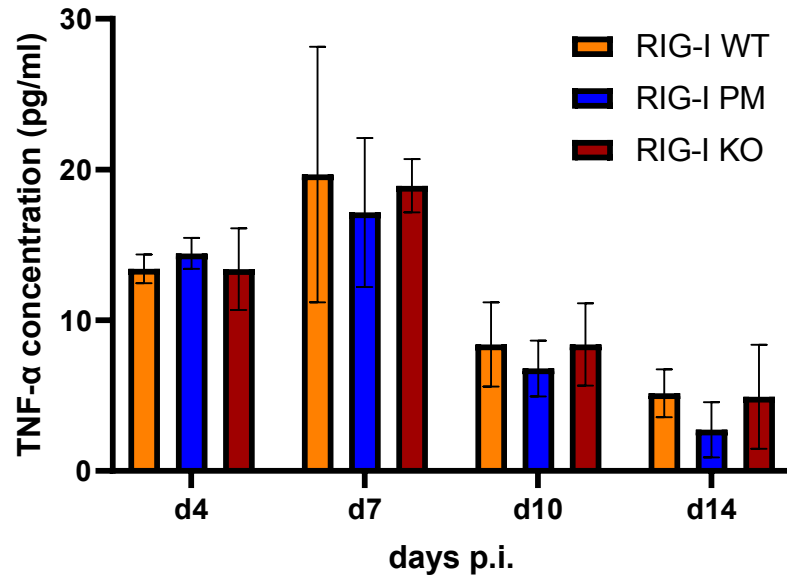


2-Way ANOVA	WT vs. PM		WT vs. KO		PM vs. KO	
source of variation	p value	significance	p value	significance	p value	significance
interaction	0.9191	ns	0.8901	ns	0.7510	ns
days p.i.	<0.0001	****	<0.0001	****	<0.0001	****
genotype	0.3296	ns	0.5708	ns	0.5114	ns

IAV PB2-627E

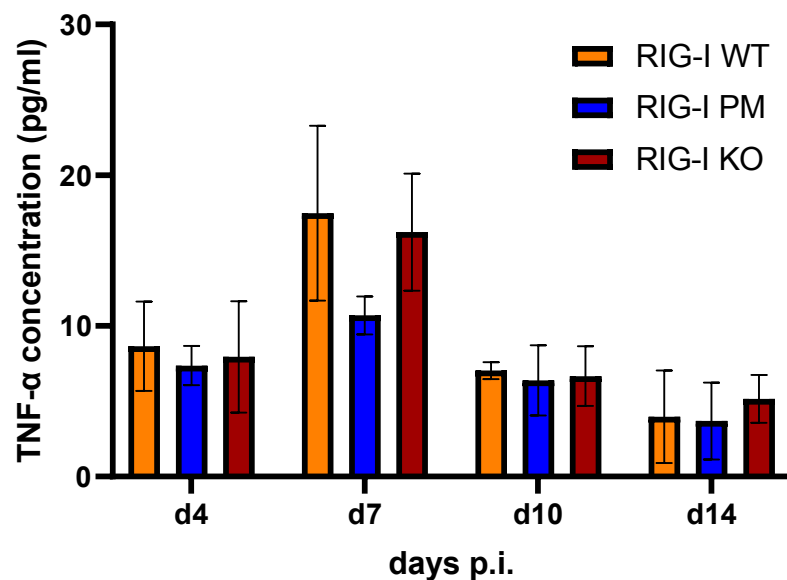


2-Way ANOVA	WT vs. PM		WT vs. KO		PM vs. KO	
source of variation	p value	significance	p value	significance	p value	significance
interaction	0.0002	***	0.7667	ns	0.0270	*
days p.i.	<0.0001	****	<0.0001	****	<0.0001	****
genotype	0.0382	*	0.7362	ns	0.1200	ns

E TNF- α IAV PB2-627K

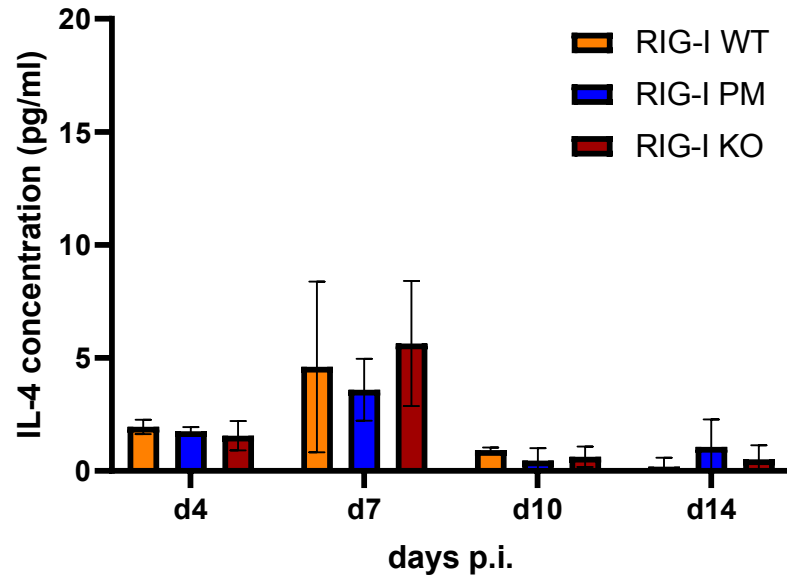
2-Way ANOVA	WT vs. PM		WT vs. KO		PM vs. KO	
source of variation	p value	significance	p value	significance	p value	significance
interaction	0.7687	ns	0.9968	ns	0.6499	ns
days p.i.	<0.0001	****	<0.0001	****	<0.0001	****
genotype	0.3155	ns	0.8524	ns	0.2636	ns

IAV PB2-627E



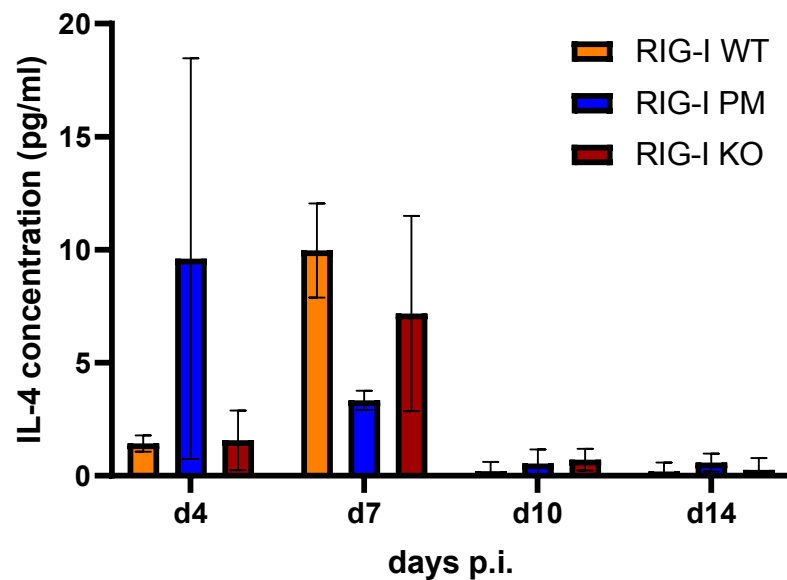
2-Way ANOVA	WT vs. PM		WT vs. KO		PM vs. KO	
source of variation	p value	significance	p value	significance	p value	significance
interaction	0.1124	ns	0.8941	ns	0.1614	ns
days p.i.	<0.0001	****	<0.0001	****	<0.0001	****
genotype	0.0385	*	0.8088	ns	0.0368	*

F IL-4 IAV PB2-627K



2-Way ANOVA	WT vs. PM		WT vs. KO		PM vs. KO	
source of variation	p value	significance	p value	significance	p value	significance
interaction	0.6546	ns	0.8273	ns	0.1881	ns
days p.i.	0.0003	***	<0.0001	****	<0.0001	****
genotype	0.7087	ns	0.7880	ns	0.4142	ns

IAV PB2-627E



2-Way ANOVA	WT vs. PM		WT vs. KO		PM vs. KO	
source of variation	p value	significance	p value	significance	p value	significance
interaction	0.0016	**	0.2514	ns	0.0198	*
days p.i.	0.0005	***	<0.0001	****	0.0070	**
genotype	0.6238	ns	0.4198	ns	0.3925	ns

Supplementary Figure 6: IAV PB2-627E, but not -627K infection-induced cytokine expression varies between the RIG-I mouse lines. Mice with a RIG-I WT, PM or KO background were infected with either an IAV PB2-627K or -627E strain. BALF was harvested from the mice, the samples of two female or two male mice were pooled. The abundance of GCSF (A), KC (B), MIP-1 α (C), IL-17A (D), TNF α (E), and IL-4 (F) were measured with a multiplex-cytokine assay (M60009RDPD, Bio-Rad). The mean of two technical replicates of the pooled samples from two female and two male mice was calculated and depicted as histograms with the respective standard deviation. A 2-Way ANOVA was used to determine significant effects of the factors "RIG-I genotype" and "days p.i." on the respective cytokine concentration, as well as the interaction between the factors.

Lebenslauf

Persönliche Daten

Name	Benjamin Rupf
Geburtstag	25. April 1988
Geburtsort	Karl-Marx-Stadt, heute Chemnitz, in Deutschland
Mail	benjamin.rupf88@gmail.com

Ausbildung

05/2017 bis 12/2022	Doktorand am Institut für Immunologie, Philipps-Universität Marburg; Titel der Abschlussarbeit: "The effect of pattern recognition receptor RIG-I variant expression during mammalian- or avian-adapted influenza A infection and adaptation in the mouse."
10/2014 bis 04/2017	Master of Science Molecular Medicine , Friedrich-Schiller-Universität Jena, Abschlussnote 1,4; Titel der Abschlussarbeit: "Aspects of the interaction between the Wnt/ β -Catenin signaling and the Renin-Angiotensin-Aldosterone system on the post-transcriptional level", Note 1,0
10/2011 bis 09/2014	Bachelor of Science Biochemie/ Molekularbiologie , Friedrich-Schiller-Universität Jena, Abschlussnote 2,1; Titel der Abschlussarbeit: "Androgen regulated expression of genes involved in epithelial-mesenchymal transition in LNCaP cells", Note 1,3
09/2008 bis 08/2011	Berufsausbildung zum Medizinisch-technischen Laboratoriumsassistenten , IFBE Bildungszentrum gem. GmbH Zwickau, Berufserlaubnis 2011
10/2007 bis 06/2008	Grundwehrdienst als Sanitäter, Weißenfels und Frankenberg
09/1999 bis 06/2007	Abitur am Albert-Schweitzer-Gymnasium in Limbach-Oberfrohna

Verzeichnis der akademischen Lehrer

Meine akademischen Lehrer an der Friedrich-Schiller-Universität Jena waren die Damen und Herren:

Arndt, Baniahmad, Berndt, Biskup, Böhmer, Bolz, Chen, Dahse, Damen, Dürst, Englert, Friedrich, Gessner, Große, Heinemann, Heinzel, Heller, Imhof, Jetschke, Jungnickel, Kamradt, Klassert, Krämer, Krause, Kurth, Lehmann, Leistriz, Lupp, Mayerhöfer, Mireskandari, Mittag, Mrowka, Müller, Neuhaus, Petersen, Reuter, Romeike, Rubio, Schiecke, Schmidtke, Schönherr, Schubert, Slevogt, Stumm, Theißen, Wang, Weih, Wesch, Westerhausen, Wetzker, Wöstemeyer und Zipfel.

Danksagung

An erster Stelle danke ich Herrn Prof. Dr. Stefan Bauer für die Möglichkeit, am Institut für Immunologie zu promovieren, für die Bereitstellung des Projektes, die wissenschaftliche Betreuung und die Begutachtung der entstandenen Arbeit.

Als nächstes danke ich Herrn Dr. Andreas Kaufmann für das Teilen von Erfahrungen und die Geduld beim Korrekturlesen.

Weiterhin möchte ich Herrn Prof. Dr. Friedemann Weber und Frau Dr. Michaela Weber-Gerlach danken, die die Grundlagen für das Projekt entdeckt haben und mich mit wichtigen Informationen und Materialien unterstützt haben.

Besonderer Dank geht ebenfalls an Herrn Prof. Dr. Thorsten Buch, Herrn Dr. Johannes vom Berg und Frau Dalila Orniston, mit denen wir in einer kurzen, aber sehr erfolgreichen Zusammenarbeit die RIG-I PM und KO Founder-Mäuse generieren konnten.

Außerdem sei Herrn Dr. Frederik Helmprobst und Herrn Prof. Dr. Axel Pagenstecher, sowie deren Gruppe gedankt, mit deren Hilfe die histologischen Präparate erzeugt und ausgewertet wurden.

Ich danke auch Frau Sonja Dehnert, Frau Stephanie Paul und Frau Sandra Stein für die vielen wichtigen Tipps beim Umgang mit Mäusen und diversen anderen Experimenten. Außerdem danke ich Herrn Prof. Dr. Markus Schnare, Herrn Dr. Philipp Yu und Herrn Prof. Dr. Michael Bacher für anregende Diskussionen nach vielen Progress-Reports und für Unterstützung bei verschiedenen Experimenten. Nicht vergessen sind Frau Gundi Ehm, Frau Marion Kaufmann und Frau Heike Ast, die uns viel organisatorische und bürokratische Arbeit abgenommen haben.

Dank geht in besonderem Maße auch an Frau Prof. Dr. Eva Friebertshäuser und ihr Team, einerseits für die Hilfe und Unterstützung bei verschiedenen Experimenten, für das Bereitstellen von Materialien, eine schnelle Virustitrierung und vor allem das Erstellen des Zweitgutachtens.

Ich möchte an dieser Stelle auch den Mitgliedern des KFO309 danken, vor allem Frau Prof. Dr. Susanne Herold, PD Frau Dr. Chrysanthi Skevaki und Frau Dr. Kathrin Balz, für Anregungen zum Projekt und wichtige Informationen für die Mausinfektionsstudie.

Nicht zuletzt danke ich Frau Marina Nicolai, Frau Judith Icking, Frau Dr. Victoria Bockmann, Frau Eileen Rauch, Herrn Dr. Jens Dorna, Frau Victoria Hunszinger, Frau Lena Soppa, Herrn Francisco Venegas Solis und den anderen zahlreichen temporären Mitgliedern des Instituts für Immunologie für Ihre Hilfe und den wichtigen Austausch von Ideen, Erfahrungen und Informationen.

Zusätzlich danke ich Herrn Dr. Thomas Butterbrodt und Herrn Michael Malysa für die Unterstützung bei wichtigen Experimenten.

Am Ende möchte ich noch Frau Dr. Sina Kreth für das Korrekturlesen und die Verbesserungsvorschläge danken, die einigen Passagen noch den letzten Schliff gegeben haben.